Molecular mechanisms of therapy resistance in HCC

USP29-mediated HIF1α stabilization promotes Sorafenib resistance of hepatocellular carcinoma cells by upregulating glycolysis

and

YAP/TAZ and ATF4 collaboratively drive resistance to Sorafenib therapy in hepatocellular carcinoma by preventing ferroptosis

Inauguraldissertation

Zur Erlangung der Würde eines Doktors der Philosophie vorgelegt der Philosophisch-Naturwissenschaftlichen Fakultät der Universität Basel

Von

Ruize Gao

Basel, 2021

Genehmigt von der Philosophisch-Naturwissenschaftlichen Fakultät auf Antrag von:

Prof. Dr. Gerhard M. Christofori

Prof. Dr. Michael N. Hall

Prof. Dr. Matthias Peter

Basel, den 30.03.2021

Prof. Dr. Marcel Mayor

Dekan

Summary

Primary liver cancer is the 6th most common cancer and 4th leading cause of cancer-related death with over 780,000 new cases annually worldwide. Hepatocellular carcinoma (HCC) represents the most common type of primary malignant liver tumor and accounts for 90% of all liver cancers. But only 30% of all HCC patients are diagnosed at the early stage, most of the HCC patients are diagnosed at very advanced stage, when surgical resection, liver transplantation and percutaneous tumor ablation are not applicable. In 2007, Sorafenib was approved by the FDA as the first-line systemic treatment for advanced HCC patients, however, the prolonged median overall survival is only around 3 months, and resistance to Sorafenib often develops very fast in HCC patients. Therefore, the delineation of the detailed mechanisms of how HCC cells respond to Sorafenib will not only help us to improve the efficacy of Sorafenib therapy in HCC patients, but will also be critical to overcome the development of therapy resistance.

To uncover the molecular mechanisms driving the response and resistance to Sorafenib in HCC cells, we first established Sorafenib-resistant HCC cell lines with treatment of either increasing concentration or constant high concentration of Sorafenib on two Sorafenib-susceptible HCC cell lines Huh7 and Hep3B *in vitro.* Transcriptomic analysis of the established Sorafenib-resistant cells in comparison with their Sorafenib-responsive counterparts were conducted to identify the genes and pathways underlying the development of Sorafenib-resistance in HCC cells.

In a first project, I employed pathway analysis of established Sorafenib-resistant cells and found that HIF1 signaling was upregulated in Sorafenib-resistant HCC cells. As a well-known oncogene, HIF1α has been proved to upregulate drug resistance in many types of cancers, including Sorafenib resistance in HCC. But how HIF1α is regulated and activated in Sorafenib-resistant HCC remains unclear. To uncover the regulation of HIF1α in Sorafenib-resistant HCC, I performed a small-scale siRNA screen targeting different deubiquitylating enzymes (DUBs) in an intrinsic Sorafenib-resistant HCC cell line HLE which identified the DUB USP29 as the potential upstream regulator of HIF1α protein stability in therapy-resistant HCC. Further studies validated that the

regulation of HIF1α by USP29 was through deubiquitylation of HIF1α. As a consequence, USP29-stabilized HIF1α promoted high glycolysis levels in Sorafenib-resistant HCC cells. Together, the results indicate that USP29 could be a potential biomarker for the prediction of therapy response in HCC patients and highlight the USP29-HIF1α-glycolysis regulatory network as an emerging therapeutic target to overcome therapy resistance in HCC patients.

In a second project, I set out to identify potential novel therapeutic targets in HCC to overcome Sorafenib resistance. To achieve this, I performed a shRNA-based genome-wide synthetic lethality screen on Sorafenib-resistant HCC cells. Among several genes, this screen identified the Hippo signaling transcription factor WWTR1, also known as TAZ, as critical in providing Sorafenib-resistant HCC cells with the ability to overcome this therapy. As a functional homologue of TAZ, YAP was also considered as a synthetic lethal gene. Transcriptomic analysis of YAP/TAZ-deficient HCC cells revealed SLC7A11, the gene encoding a cystine importer required for glutathione synthesis, as a potential downstream target of YAP/TAZ transcriptional activity. Gene set enrichment analysis (GSEA) of the expression of YAP/TAZ-deficient cells and the synthetic lethal screening hits indicated that the YAP/TAZ-SLC7A11 axis was activated in Sorafenib-resistant HCC cells to overcome cell death by ferroptosis. Further studies revealed that the regulation of SLC7A11 expression by YAP/TAZ was further regulated by ATF4-dependent and independent mechanisms. Further experimental evidence indicated that a combination treatment of glutathione synthesis inhibitors and Sorafenib was able to re-install ferroptosis in Sorafenib-resistant HCC cells, thus offering a promising new therapeutic approach to overcome Sorafenib resistance in HCC.

In summary, my PhD work generated novel insights into the molecular mechanisms underlying Sorafenib resistance in HCC. 1. As a positive regulator of HIF1α, USP29 promotes its stability and transcriptional activation in HCC, thus conferring high glycolysis levels and resistance to Sorafenib in HCC. 2. YAP/TAZ and ATF4 exert critical roles in the regulation of ferroptosis in Sorafenib-resistant HCC by upregulating SLC7A11 expression which re-installs Sorafenib-induced ferroptosis of HCC cells. The findings thus have direct implications on potential therapeutic approaches of how

to overcome the development of resistance to Sorafenib, one of the main therapies of advanced HCC in patients.

Table of Contents

1. General introduction

1.1 HCC and Sorafenib-resistance

1.1.1 Primary liver cancer and HCC

Primary liver cancer, which is also named primary hepatic cancer, is the 6th most common cancer and 4th leading cause of cancer-related death with over 780,000 new cases annually worldwide [1]. Primary liver cancer is usually caused by chronic liver diseases (chronic inflammation) like cirrhosis and fibrosis. Various risk factors are defined to promote chronic liver diseases, such as hepatitis B virus (HBV) or hepatitis C virus (HCV) infection, abuse of alcohol, metabolic disorders (NAFLD, NASH), liver flukes and intake of toxins (aflatoxin). Chronic inflammation will deteriorate into cirrhosis or fibrosis and finally develop into primary liver cancer if patients were without any proper treatment [2-8] (Figure 1).

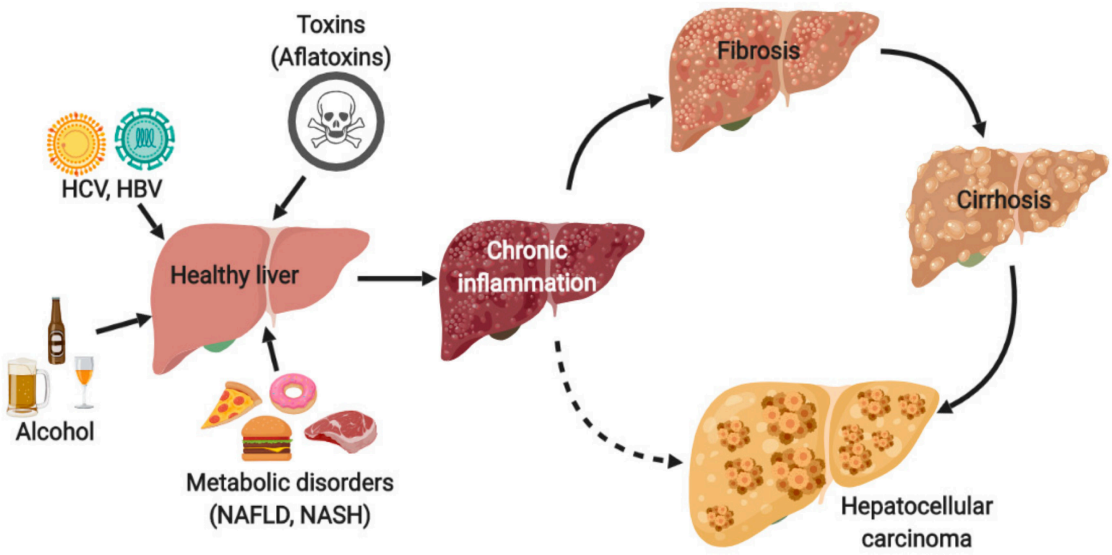

Figure 1. Risk factors and the progression of hepatocellular carcinoma (HCC). Hepatitis C virus, HCV; Hepatitis B virus, HBV; non-alcoholic fatty liver disease, NAFLD; non-alcoholic steatohepatitis, NASH. Adapted from [9].

The most common type of primary liver cancer is hepatocellular carcinoma (HCC), which accounts for around 90% of all primary liver cancers. Cholangiocarcinoma and Cholangiocellular Cystadenocarcinoma usually account for around 6% of primary liver cancers [2]. Carcinosarcomas, teratomas, leiomyosarcoma and rhabdomyosarcoma are fewer common types of liver cancers that come from other structures within the

liver. Hepatoblastoma is another very rare malignant tumor which primarily develops in children, as it is specifically formed by immature liver cells [8,10].

Epidemiology

HCC patients present often with advanced hepatic fibrosis or cirrhosis, which are caused by hepatitis virus B or C (HBV or HCV) infection or abuse of alcohol. Incidence of HCC is closely related to chronic viral hepatitis. Asia and Sub-Saharan Africa have the highest incidences of HCC due to HBV infection [6,7,11]. HCV infection is the leading cause of HCC in America and European countries [4]. Aflatoxin B1 together with HBV infection frequently cause HCC in Africa and South-America. The incidence of HCC is threefold higher in men than in women in most of the regions worldwide. The prevention of HCC is possible due to its well-established risk factors. Moreover, vaccination against HBV has been proved to cut back the incidence of HCC in populations which have a high risk of HBV infection. Reduction of alcohol abuse and Aflatoxin B1could also be efficient ways to prevent chronic liver diseases and HCC [12].

Classification of HCC is routinely done in accordance with the Barcelona Clinic Liver Cancer (BCLC) staging scheme (Figure 2). Less than 30% of HCC are diagnosed at early stages (stage 0 and A), most HCC patients are often diagnosed at advanced stages (stage C) or end stages (stage D) [1,13,14]. Normally, early stage patients are eligible for resection, transplantation or local ablation surgery which could provide survival time of over 60 months, which is more than the natural history survival of 36 months. Patients at intermediate stage (stage B) have a shorter survival time of around 16 months, and chemoembolization treatment is here frequently conducted to reach a median survival of 26 months [15]. The estimated median survival of advanced HCC patients is around 6 months, and patients at this stage could benefit from first-line systemic treatments: Sorafenib or Lenvatinib with a median survival of 10.7- 13.7 months [16-19]. A phase 3 clinical trial of combination of Atezolizumab (PD-L1 inhibitor) and Bevacizumab (VEGF inhibitor) on advanced HCC showed better efficiency than Sorafenib either on median survival or survival without disease progression [20] (Figure 2).

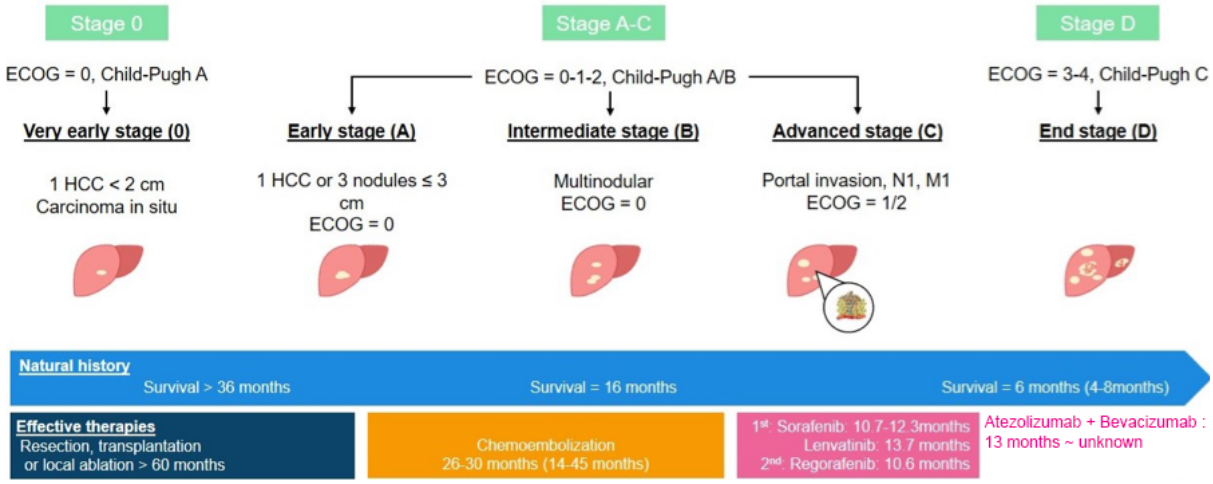

Figure 2. Classification and treatments of HCC
Adapted from Llovet JM. Harrison's Principles of Medicines, 20th edition, 2018

Molecular mechanisms of HCC

The development of HCC is a multistep process that is closely related to the pathologies of chronic liver diseases like fibrosis and cirrhosis [21-23]. Like other types of tumors, HCC is also caused by the genomic alterations and cancer-related driver genes which contribute to tumorigenesis as initiation, progression and metastasis [22,24-26]. *TERT* (telomerase reverse transcriptase) promoter mutations have been uncovered in HCC initiation with promoting chromosomal instability and additional mutations [27-29]. Alterations of many driver genes, including like Lysine(K)-specific methyltransferase 2B (KMT2B or MLL4), Lysine(K)-specific methyltransferase 2D(KMT2D), cyclin E1 (CCNE1), cyclin A2 (CCNA2), tumor necrosis factor superfamily member 10 (TNFSF10), SUMO1/sentrin-specific peptidase 5 (SENP5), TP53, ARID1A, and PKD1, could also induce hepato-carcinogenesis. Changes in DNA methylation in the promoters of CDKL1, FOXE 3, SEPT 9 have also been reported to promote the initiation of HCC [30,31].

Several pathways have been uncovered in the regulation of HCC progression. Activation of the WNT/β-catenin pathway occurs in around 11-37% of HCC patients. Mutations of AXIN1, APC, ZNRF3 are frequent and may induce the hyperactivation of WNT/β-catenin signaling [32-34]. Inactivation and alteration of the classic tumor suppressor p53 is also present in HCC patients, especially in the patients which are

related to HBV infection [30,35]. As a newly discovered tumor suppressor, the protein histidine phosphatase LHPP is found with inactivating mutations in HCC patients [36]. PI3K-AKT-mTOR and MAPK pathways are also frequently activated in HCC. Activation of PI3K-AKT-mTOR pathway is caused by mutations of PTEN (phosphatase and tensin homologue). Mutations of RAS are rarely found to activate MAPK signaling, but inactivation of RPS6KA3 (ribosomal protein S6 kinase a3) are often identified to activate RAS-MAPK signaling in HCC. Moreover, mutations in the TERT promoter contribute to tumor progression in around 60% of HCC patients [29]. Other cancer drivers, such as CCND1(Cyclin D1), FGF19, and VEGFA, have also been identified with high-level amplifications in HCC and represent potential therapeutic targets [37-39] (Figure 3).

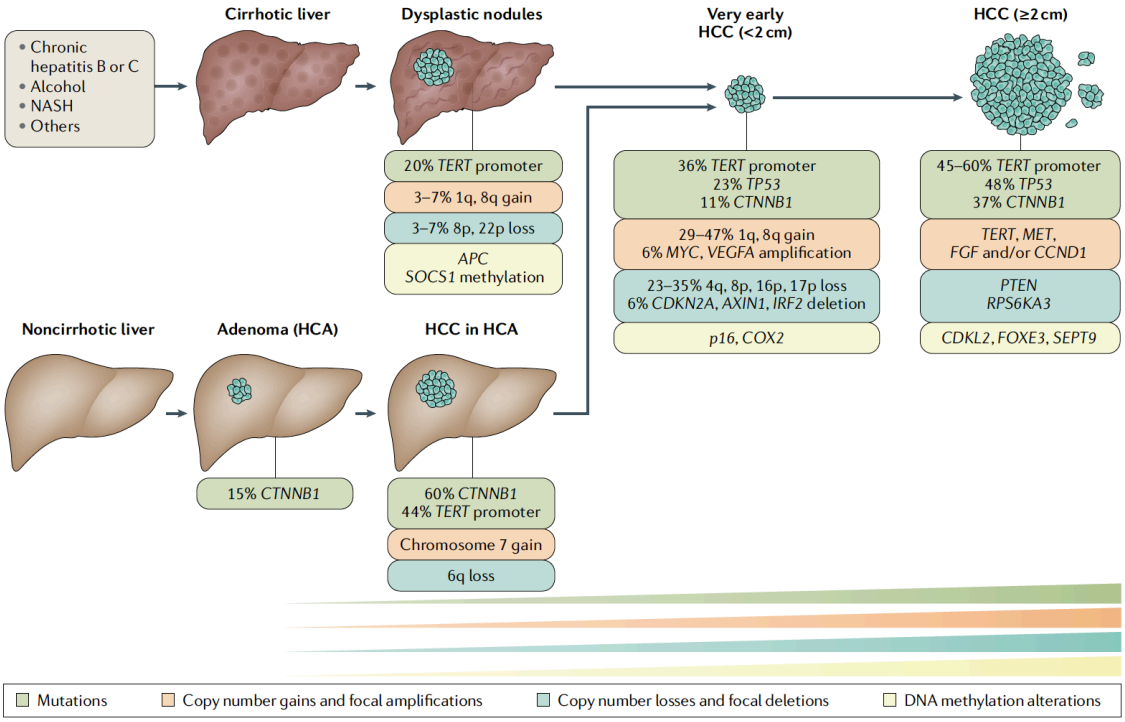

Figure 3. Hepato-carcinogenesis. Over 90% of hepatocellular carcinomas (HCCs) arise on the background of chronic liver diseases. Genetic alterations are detectable in dysplastic nodules and HCC. TERT promoter mutations occur in every stage of dysplastic nodules and HCC, TP53 and CTNNB1 mutations are found in early and late HCC and thought to function as drivers of HCC progressions. Other mutations like MYC, VEGFA amplifications, CDKN2A, AXIN1, IRF2 deletions are also thought to promote HCC progression. Adapted from [40].

1.1.2 Sorafenib and Sorafenib resistance in HCC

Sorafenib

Sorafenib (Nexavar, Bayer HealthCare Pharmaceuticals-Onyx Pharmaceuticals) is an oral multi-kinase inhibitor approved as a treatment for advanced renal cell carcinoma (RCC), advanced hepatocellular carcinomas (HCC) and thyroid cancer [41,42]. As a multi-kinase inhibitor, Sorafenib can suppress tumor cell proliferation via blocking the activity of RAF kinases and the MEK/ERK signaling pathway. Moreover, vascular endothelial growth factor receptor (VEGFR), platelet-derived growth factor receptor (PDGFR), hepatocyte factor receptor(c-Kit), Fms-like tyrosin E kinase (FLT-3) are also inhibited by Sorafenib, thus repressing angiogenesis [43,44].

Sorafenib was also found to induce apoptosis in tumor cells by downregulating the anti-apoptotic protein myeloid cell leukemia sequence 1 (MCL1) and caspase-independent mechanism, induced by the inhibition of ERK-independent activities of RAF [45,46]. Additionally, Sorafenib has been also identified as an inhibitor of cystine/glutamate antiporter xCT (SLC7A11) to induce lipid peroxidation and ferroptosis [47-49] (Figure 4).

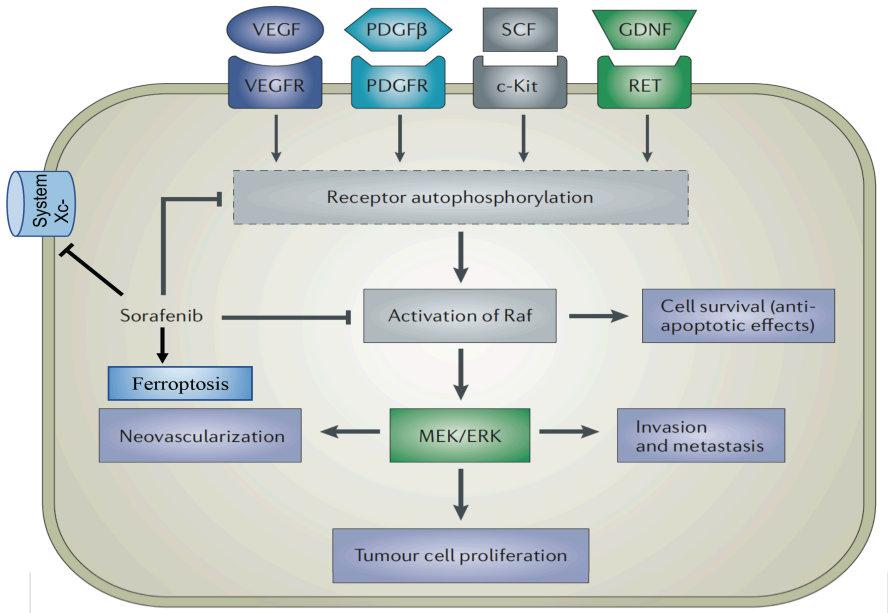

Figure 4. Sorafenib Targets. Sorafenib suppresses VEGFR, PDGFR, c-Kit, RET and System Xc- and blocks downstream Raf to prevent tumor survival and growth through anti-apoptotic, antiproliferative effects and induction of Ferroptosis. (ERK, extracellular signal-regulated kinase; GDNF, glial-derived neurotrophic factor; MEK, mitogen-activated protein kinase; PDGFR, platelet-derived growth factor receptor; SCF, stem cell factor; VEGFR, vascular endothelial growth factor receptor.) Adapted from [16].

Sorafenib resistance in HCC

Sorafenib was approved by the FDA as the first systemic treatment of HCC in 2007, and the SHARP (Sorafenib HCC Assessment Randomized Protocol) trial result was published in the *New England Journal of Medicine* in 2008 [17]. Results showed that advanced hepatocellular carcinoma patients with Sorafenib treatment had a 3-month median survival benefit than placebo-treated patients. Given the lack of adequate therapeutic options for advanced HCC patients, Sorafenib was recommended and approved as the first-line treatment of advanced HCC. However, Sorafenib also induced some side effects in HCC patients, such as weight loss, diarrhea and hand/foot skin reactions. Therapy resistance frequently occurred once HCC patients were treated with Sorafenib, either with primary resistance or acquired resistance.

Some HCC patients have no response to Sorafenib treatment because of the genetic heterogeneity of HCC, which is termed primary resistance. Anomalous expression or activation of EGFR, ERK, c-Jun N-terminal kinase (JNK), and VEGFR have been associated with the sensitivity of HCC to Sorafenib [50,51]. Besides primary resistance, like with other types of tumors HCC patients often develop acquired resistance during treatment with Sorafenib [52]. Alterations in the regulation of transport processes, programmed cell death, tumor microenvironment and epithelial-mesenchymal transition (EMT) have been reported to contribute to Sorafenib resistance [53].

Transport processes contribute to drug resistance in most types of cancers. Sorafenib resistance in HCC also involves changes in transport processes. For example, ATP-binding cassette (ABC) transporters are the main families of membrane transporters to pump out sorafenib from HCC cells [54]. Members of the ABCB, ABCC, and ABCG2 families were reported to be associated with chemotherapy resistance: ABCG2 (BCRP) was reported to pump out Sorafenib, and the combination treatment of Sorafenib and ABCG2 inhibitor could significantly induce HCC cell death, ABCC2(MRP2) was also found to contribute to the Sorafenib resistance in several another studies [55] [56] [57] [58]. The human solute carrier (SCL) superfamily is another key family of transporter that can regulate drug resistance. SLC22A1(Organ cation transporter) has been reported to be involved in the uptake of Sorafenib, and methylation or aberrant expression of SLC22A1 have been uncovered the association with the poor survival

in HCC patients treated with Sorafenib [59]. SLC46A3 is catabolizes transporter that exerts opposite effect on Sorafenib resistance [60].

Sorafenib-resistant HCC presents less apoptosis in response to Sorafenib treatment, and several pathways have been uncovered to regulate apoptosis and drug resistance. Morgensztern *et al.* reported that inhibition of PI3K/AKT/mTOR pathway could sensitize cells in response to Sorafenib treatment [61]. Aberrant activation of JAK/STAT pathway was also found to contribute to Sorafenib resistance in HCC [62]. Autophagy is another process that has been found to regulate Sorafenib resistance. Shimizu *et al.* found that Sorafenib could induce autophagy and autophagic flux in HCC [63]. Autophagy is a self-protective mechanism, and excessive autophagy could also induce programmed cell death. Thus, on one side, Sorafenib treatment somehow promotes HCC cell survival via autophagy to resist Sorafenib anti-cancer effects, but on the other side, excessive autophagy also induces HCC cell death in response to Sorafenib treatment. Therefore, the therapeutic modulation of autophagy levels to convert HCC cell survival to cell death could possibly decline Sorafenib resistance in HCC. Ferroptosis is another type of cell death that could be induced by Sorafenib in HCC, but the mechanism of Sorafenib's anti-cancer effect in HCC is complex: on one hand, Sorafenib can directly target SLC7A11 to induce ferroptosis [47-49], yet on the other hand, Sorafenib itself can also promote the expression of SLC7A11 and to overcome ferroptosis and thus to facilitate Sorafenib resistance.

Epithelial-mesenchymal transition (EMT) is a process where epithelial cells transform into mesenchymal cells by losing cell polarity, cell-cell adhesion and by gaining invasive properties [64]. EMT is essential for developmental processes and also in physio-pathological processes like wound healing and cancer metastasis. Due to the changes in cell characteristics during EMT, cancer cells turn to be more insensitive to anti-cancer drugs. Several studies also revealed that EMT contributed to Sorafenib resistance in HCC [53]. Van Malenstein *et al.* reported that cultured Sorafenib-resistant HCC cell lines showed mesenchymal features, including the loss of E-cadherin, high expression of vimentin, and resistant cells became more invasive and aggressive [52]. However, the exact mechanistic connections between EMT and Sorafenib resistance remain unclear, warranting further investigations into the role of EMT in Sorafenib resistance.

It is now well established that the tumor microenvironment also plays a key role in tumor initiation and progression. Hypoxia is a well-known factor to affect the tumor microenvironment, for example via upregulating the transcriptional activity of hypoxia inducible factor-1α (HIF1α) [65]. Several pathways and cell processes are regulated by hypoxia and by HIF1α in tumor initiation and progression, including metabolic reprogramming, angiogenesis, anti-apoptotic mechanisms, metastasis and chemotherapy resistance [66,67].

1.2 Hypoxia, HIF1α and DUBs

1.2.1 General introduction of Hypoxia and HIF1α

Hypoxia is the situation where tissues and cells are deprived of oxygen, it has been known for many years that hypoxia is a feature of solid tumors. Due to the rapid growth of tumor cells, blood supply could not reach all the cells, thus the inner portions of solid tumors form the hypoxic regions with lower oxygen than the normal tissues. To survive from the hypoxic microenvironment, tumor cells change a number of molecular and cellular processes to adapt to the situation, including metabolism, extracellular matrix, metastatic behavior and drug sensitivity [68,69].

Cellular responses to hypoxia are mainly mediated by changes in gene expression, and hypoxia-inducible factors (HIFs) are the responsible transcriptional factors that mediate these processes [70,71]. HIFs consist of an alpha and a beta subunit which form heterodimeric complexes and bind to the hypoxia response elements (HREs) in the promoters of over 200 different genes encoding proteins or RNAs that regulate angiogenesis, cell survival, anti-apoptosis in response to hypoxia [72]. HIFs belong to the PER-ARNT-SIM (PAS) subfamily of the basic helix-loop-helix (bHLH) family of DNA binding factors. Unlike the stable feature of the beta subunit, the alpha subunit of HIFs is oxygen-liable and sensitive to oxygen [73]. There are three different forms of HIF-alpha (HIF1α, HIF2α, HIF3α) [71,74,75], and HIF1α is the best-studied and universally expressed in different cells and tissues upon hypoxia.

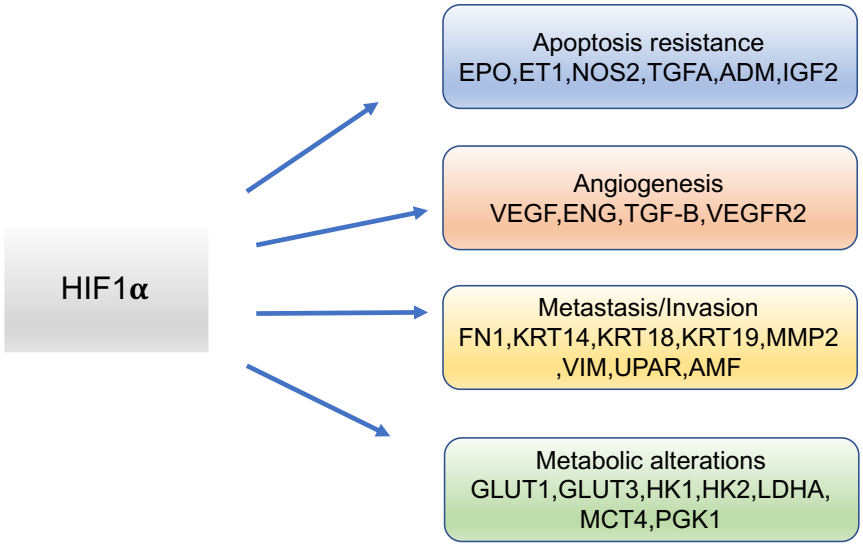

Figure 5. Targets of HIF1α in cancer cells. Cancer cells that express high HIF1α protein levels exhibit high apoptosis resistance, angiogenesis, metastasis and a change in metabolism. The regulations of the processes are mediated by the upregulation of HIF1α's transcriptional targets.

HIF1 and Glycolysis

Aerobic glycolysis (Warburg effect) is a general metabolic feature of malignant tumors. Activation of HIF1 has been proved to upregulate the glycolytic energy production in tumor cells. Several glycolysis-related genes have been reported as the downstream targets of HIF1, such as GLUT1/3, HK1/2, LDHA, PGK1, MCT4 [76,77]. Glycolysis is a linear process, and many glycolysis-related enzymes are regulated by HIF1. Thus, HIF1 not only regulates glucose uptake, glucose phosphorylation, conversion of pyruvate to lactate, but also lactate removal [77].

HIF and angiogenesis

Rapid growth of cancer cells results in a hypoxic microenvironment in solid tumors, since blood supply cannot provide enough nutrient to the inner portions of cancer cells. In response to this extreme situation, hypoxic cancer cells induce the formation of new blood vessels by angiogenesis. VEGFA has been identified as the key target of HIF in the process of angiogenesis. Other factors, including VEGFR, TGFβ, and FGF, are also upregulated by HIF to promote angiogenesis. [68,78-82]

HIF and extracellular matrix, metastasis

Hypoxia and the hypoxic extracellular matrix (ECM) play crucial roles in mediating metastasis of cancer. Hypoxic cells are known to be more aggressive and invasive.

Mechanistically, hypoxia and HIF regulate the migratory behavior of cancer cells by the induction of epithelial-mesenchymal transition (EMT) [78,83]. The expression of E-cadherin, vimentin, N-cadherin, smoot muscle actin (SMA), CXCR4 and β-catenin have been reported to be regulated by hypoxia and HIF in the progression of EMT [84] [85]. TGFβ, which is a well-known master regulator of EMT, is also upregulated by HIF to activate downstream transcriptional factors like Snail, Slug, Twist and Smads [85] [86]. Hypoxia and HIF can also upregulate lysyl oxidases (LOX), which are extracellular enzymes that modify collagens to promote cell migration and to form a "pre-metastatic niche" in distant organs [87].

HIF and therapy resistance

It is well established that hypoxia promotes the resistance to radiotherapy, since upon insufficient oxygen supply free radicals fail to react with oxygen and lead to irreversible DNA damage. The mediation of drug resistance by hypoxia and HIF is a multiple factors' process, and proliferation, angiogenesis, metabolism, anti-cell death all contribute to it. HIF also regulates drug efflux by inducing expression of the multidrug resistance (MDR) gene [88]. Several anti-apoptotic factors, such as Bak, Bax, Bcl-2, Mcl-1, NF-kb, and p53, have been identified as downstream targets of HIF in the regulation of anti-apoptosis processes [89-91] (Figure 5).

1.2.2 Hypoxia and HCC Sorafenib resistance

Hypoxia and HCC

The tumor microenvironment plays a pivotal role in tumor development. Hypoxia is a common feature of solid tumors including hepatocellular carcinoma (HCC). In HCC, HIFs have been also reported to regulate many genes that are involved in proliferation, glucose metabolism, angiogenesis, and metastasis. Both HIF1α and HIF2α have been reported to be highly expressed and considered as biomarkers of poor prognosis in HCC [92,93].

Hypoxia, HIF and Sorafenib resistance

Hypoxia and HIFs also contribute to drug resistance in HCC as observed for most of the other solid tumors. Yingjian *et al.* have reported that HIF1α exhibits higher levels in Sorafenib-resistant HCC patients as compared to Sorafenib-sensitive HCC patients [94]. Even though Sorafenib can inhibit HIF1α protein synthesis and VEGF expression to suppress tumor angiogenesis, hypoxic HCC cells appear to survive from Sorafenib exposure as a result of selection, limiting the efficiency of Sorafenib treatment. High expression of VEGFA, MDR, GLUT1, HK2 highly correlate with HIF1α levels in Sorafenib-resistant HCC. Li *et al.* have reported that the inhibition of GLUT1 and HK2 increases Sorafenib efficiency on HCC [95]. Moreover, higher expression of MDR, encoding for a P-glycoprotein which can reduce the intracellular concentration of Sorafenib, further promotes Sorafenib resistance in HCC [88]. Upregulated ADRB2 signaling also occurs to suppress autophagy in Sorafenib-resistant HCC, thus to help the resistant cells to escape from Sorafenib exposure [96]. Additionally, HIF2α has also been reported to maintain Sorafenib resistance via activating TGFα/EGFR pathway [97]. Thus, combination treatment of Sorafenib and HIF inhibitors could possibly be a potential therapeutic strategy to treat Sorafenib non-responders.

1.2.3 Regulations of HIF1α

HIF1 (Hypoxia-inducible factor 1) was discovered by Gregg L. Semenza and Guang Wang in 1995 [98]. HIF1α protein synthesis is regulated by phosphatidylinositol 3-kinase (PI3K) and MAPK pathways, whereas the stability of HIF1α protein is regulated by the ubiquitin proteasome system (UPS) [99,100].

HIF1α remains unstable in normoxia condition owing to ubiquitin-mediated degradation, but turns to be stable in hypoxia. In normoxic condition, prolines 402 and 564 of HIF1α are hydroxylated by prolyl hydroxylases (PHDs) [101], and hydroxylated HIF1α is then recognized and ubiquitinated by VHL, and degraded by the proteasome [102]. PHDs take oxygen as a low-affinity substrate, thus HIF1α is not hydroxylated by PHDs in hypoxia condition. VHL is an E3 ligase which is named as von Hippel-Lindau tumor-suppressor protein, with its loss of function in renal cancers resulting in the constitutive stability of HIF1α and tumorigenesis [103,104]. Asparagine hydroxylase factor 1 (FIH1) is another hydroxylase that mediates HIF1α's

hydroxylation at asparagine (Asn)-803 to inhibit the interaction between HIF1α and the transcriptional coactivators p300 and CBP and thus suppresses HIF1α's activity [100].

In addition to VHL, several de-ubiquitinases (DUBs) have been reported to diminish the levels of HIF1α ubiquitination by removing ubiquitin from ubiquitinated-HIF1α. USP8, USP28 and UCHL1 have been reported to stabilize HIF1α under normoxia [105] [106,107]. DUBs thus prevent proteasomal degradation to stabilize HIF1α (Figure 6).

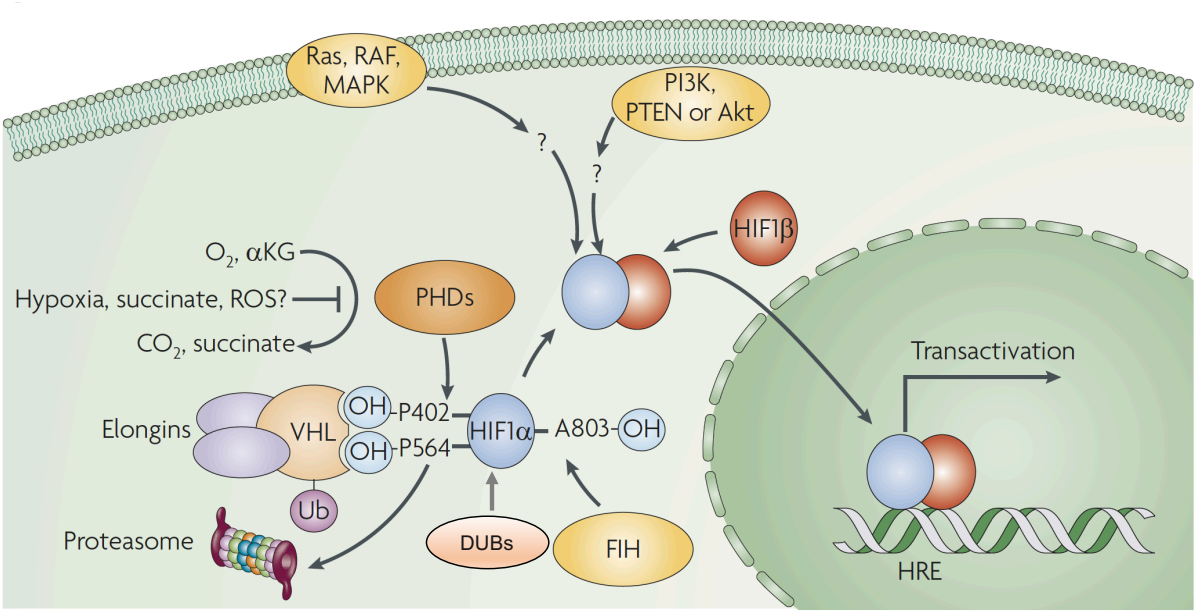

Figure 6. Regulation of HIF1α. Hydroxylation at P402 and P564 of HIF1α by PHDs in response to oxygen exposure or the hydroxylation at A803 by FIH lead to binding of HIF1α to the VHL complex and hence mediate HIF1α's proteasomal degradation. In contrast, DUBs remove ubiquitin from HIF1α leading to its stabilization. Activation of the Ras-RAF-MAPK or the PI3K-AKT pathways promotes HIF1α's stability via unknown mediators. (PHDs: prolyl hydroxylase domain enzymes; VHL: von Hippel-Lindau disease tumor suppressor; HRE: Hypoxia response element) Adapted from [108].

1.2.4 Ubiquitin-specific peptidase 29 (USP29)

USP29 is a highly conserved DUB which belongs to the PH_USP37_like family. The PH_USP37_like family plays important roles in cell proliferation and cancer growth. It consists of three members: USP26, USP29 and USP37, of which USP26 is a positive regulator of Androgen Receptor in prostate cancer cells [109], and USP37 directly deubiquitinates and stabilizes c-Myc in lung cancer [110]. USP29 has been identified

as a regulator of the checkpoint adaptor Claspin [111]. Qian *et al.* have recently reported that USP29 could promote gastric cancer cell migration by cooperating with phosphatase SCP1 [112]. Snail has also been reported to be regulated by USP29 to enhance chemotherapy-induced stemness in non-small cell lung cancer in response to oxidative stress [113].

However, the functional contribution of USP29 to tumorigenesis and therapy resistance has remained unexplored.

1.3 Hippo pathway

1.3.1 General introduction to the Hippo pathway

Hippo signaling pathway

The Hippo pathway is a highly conserved signaling pathway that was initially identified in *Drosophila melanogaster* as a key regulator of tissue growth and organ size. In recent years, studies in mammals have revealed the important role of Hippo signaling in multiple processes, such as proliferation, cell survival, differentiation, tissue homeostasis and tumorigenesis [114-116].

In *Drosophila*, the first four identified Hippo core proteins are the NDR family protein kinase Warts (Wts), WW domain-containing protein Salvador (Sav), Ste20-like protein kinase hippo (Hpo) and adaptor protein Mob-as-tumor-suppressor (Mats), these four components form the kinase cascade where Hpo-Sav phosphorylates and activates Wts-Mats which finally suppress the transcriptional coactivator Yorkie (Yki) to inhibit cell growth in *Drosophila* [117-120].

The mammalian homologues of Hippo signaling pathway have been subsequently identified and found to control tissue growth in development and regeneration, as well as in pathological processes like tumorigenesis[121-123] . The core components are the serine/threonine kinases, sterile 20-like kinase 1/2 (MST1/2) and the large tumor suppressor 1/2 (LATS 1/2), which together with Salvador homolog 1 (SAV1) and MOB

kinase activator 1A/B (MOB1A/B) phosphorylate and suppress the transcriptional effectors Yes-associated protein (YAP) and PDZ-binding motif (TAZ or WWTR1) [122]. Phosphorylation of YAP and TAZ inhibits their activity through the interaction with 14-3-3 protein to mediate the cytoplasmic retention of YAP/TAZ [124]. Moreover, phosphorylation of YAP/TAZ leads to their proteasomal degradation via binding to the E3-liagse beta-TrCP [125,126]. Suppression of the Hippo pathway will activate YAP/TAZ transcriptional activity and the expression of their target genes, but also promote the activity of several other transcription factors, including TEADs, SMADs, RUNX1/2 and TBX5. As a result, target genes are activated which promote cell proliferation and tumorigenesis, such as CTGF, CYR61, ANKRD1 and AXL [127-129]. Neurofibromin 2 (NF2 or Merlin) have also been identified as the upstream regulator of Hippo by activating Mst1/2 and SAV1 to inhibit YAP/TAZ activity [130] (Figure 7).

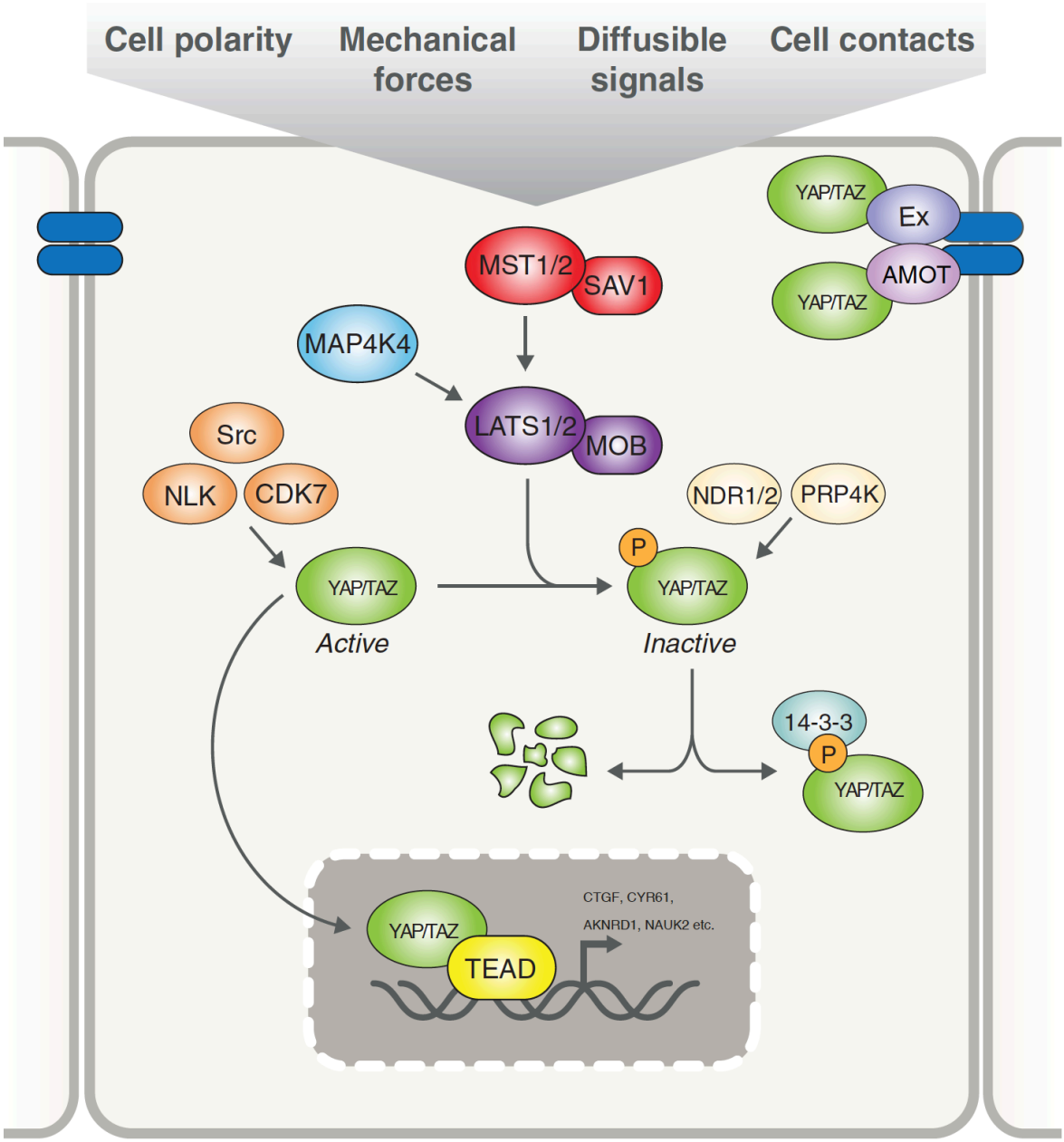

Figure 7. Hippo pathway. MST1/2 and MAP4K4 act as upstream inducers of Hippo signaling, by activation of LATS1/2 to mediate YAP/TAZ phosphorylation and proteasomal degradation. Src, NLK, CDK7 upregulate the activity of YAP/TAZ to promote the nuclear localization of YAP/TAZ which then act as transcriptional activators of the DNA binding factor TEAD to promote the expression of *CTGF,CYR61,ANKRD1,NAUK2* and others. Adapted from [131] .

Hippo pathway in cancer

Mutations of Hippo or excessive expression and activation of YAP/TAZ are associated with cell proliferation, metastasis, metabolism and drug resistance in many types of cancer. In solid tumors, frequent amplification of YAP/TAZ and mutations of LATS1/2

frequently occur. Additionally, aberrant expression of YAP/TAZ and TEADs correlates with cancer malignancy and poor prognosis [132]. Other signaling pathways have also been reported to regulate YAP/TAZ activity. For example, PI3K has been identified to facilitate YAP nuclear localization and activation by repressing Hippo [133,134]. WNT and GPCR signaling pathway are also known to regulate YAP/TAZ in a variety of cellular processes [135].

Proliferation

YAP overexpression in mice has been reported to cause excessive proliferation of several tissues, including liver and heart. Yang *et al.* reported that CDK1 could phosphorylate YAP/TAZ during the G2-M phase of the cell cycle to promote cell proliferation and neoplastic transformation and thus to facilitate cell migration and invasion [136]. Hyperactivation of YAP/TAZ by NF2/MST/LATS loss of function mutations also facilitates proliferation of cancer cells [130].

Metastasis

Dysregulation of the Hippo signaling pathway has a positive clinical correlation with cancer metastasis. Low MST1 levels are associated with LN metastasis in colorectal and gastric cancers. LATS1/2 have also been reported to be expressed at very low levels in advanced-stage ovarian, breast, colorectal, gastric, lung, renal cancers and to promote metastasis [137-139].

As downstream effectors of Hippo signaling, hyperactivation of YAP/TAZ plays a critical role in the promotion of metastasis. Corresponding to low levels of MST/LATS, YAP/TAZ exhibit increased transcriptional activities in advanced stage cancers, such as colon cancer, hepatocellular carcinoma, NSCLC and breast cancer.

Besides the dysregulation of the Hippo pathway, YAP/TAZ are also regulated by other proteins to facilitate cancer metastasis. Ras association domain family 1 isoform A (RASSF1A) has been reported to downregulate YAP and, thus, downregulation of RASSF1A promotes tumor metastasis via the activation of YAP [140]. Abelson tyrosine protein kinases (ABL) has also been reported to promote metastasis formation of breast cancer via TAZ [141].

Metabolism

The Hippo signaling pathway also affects cancer metabolism, for example glycolysis. Glucose transporter 1 and 3 (GLUT1, GLUT3) have been identified as the downstream targets of YAP to promote the extent of cancer cell glycolysis by increasing glucose uptake [142,143]. Increased YAP activity also induces the expression of Hexokinase 2 (HK2), another glycolysis-related gene, and thus promotes lactate production [144]. YAP also affects insulin signaling to upregulate glucose metabolism, and YAP has been found to have a positive correlation with the expression of insulin receptor substrate2 (IRS2) in HCC [145].

Drug resistance

A correlation between drug resistance and activated Hippo signaling has been amply confirmed. High expression of YAP/TAZ or depletion of LATS1/2 have been reported to promote Taxol resistance in many types of cancer cells. Resistance to other chemotherapeutic agents, including doxorubicin and 5-FU, has also been found to correlate with high YAP/TAZ activity. Moreover, YAP has been identified as the critical player in bypassing pathway-targeted therapies. Ghiso *et al.* have reported that YAP-dependent AXL overexpression mediates resistance to EGFR inhibitors in NSCLC [129]. Kapoor *et al.* have found that YAP1 activation enables pancreatic cancer cells to bypass K-Ras addiction [146]. Finally, Lin *et al.* have reported that YAP promotes resistance to RAF- and MEK-targeted cancer therapies [147].

1.3.2 Hippo and HCC

Hippo and HCC

The Hippo signaling pathway effectors YAP/TAZ have been identified as oncogenes in different cancer types, including hepatocellular carcinoma (HCC). High expression of YAP/TAZ has been reported in HCC patients by immunohistochemical staining of tumor tissue compared with normal liver tissue [148]. Liver-specific depletion of NF2 or MST1/2 in mouse models has also demonstrated that the activation of YAP/TAZ promotes the development and progression of HCC, which has also been observed in transgenic mice expressing activated YAP in hepatocytes [130,149].

Several key transcriptional targets of YAP/TAZ have been identified as regulators of HCC progression. Connective tissue growth factor (CTGF) has been reported to regulate liver fibrosis and thus to promote the progression of HCC [150]. Extracellular matrix protein CCN1 (CYR61) is another target of YAP/TAZ and has been reported to regulate Fas-mediated apoptosis in HCC cells [151]. Recently, Yuan *et al.* have found that sucrose nonfermenting (SNF1)-like kinase (SNARK/NUAK2) is also a critical YAP target which contributes to hepatomegaly and HCC progression [152].

Hippo and Sorafenib resistance

Besides the connection with HCC progression, the Hippo pathway has also been reported to participate in the regulation of Sorafenib resistance in HCC. Gao *et al*. have reported that YAP is involved in the development of Sorafenib resistance in HCC cells [153]. Zhou *et al.* have found that the inactivation of YAP overcomes the hypoxic resistance to Sorafenib in HCC cells. They report that the combined treatment of statins (inhibitors of hydroxymethylglutaryl-CoA reductase which can restrict YAP activity) and Sorafenib has significantly suppressed the growth of Sorafenib-resistant HCC cells [148].

Moreover, Verteporfin, another YAP1 inhibitor which disrupts YAP-TEAD complex formation and thus suppresses the oncogenic transcriptional activity of YAP, has also been shown to potentiate the effect of Sorafenib in HCC [154,155]. Finally, Tang *et al.* have reported that LATS1 maintains Sorafenib resistance in a kinase-independent manner by restricting lethal autophagy. By interacting with the autophagy core-machinery component Beclin1, LATS1 promotes the inactive dimer formation of Beclin1 and thus inhibits autophagy in HCC cells [156]. However, the detailed mechanisms of how Hippo signaling directly regulates Sorafenib resistance still remains in HCC remains largely unknown.

1.4 Ferroptosis

General introduction of ferroptosis

Ferroptosis is a new type of regulated and non-apoptotic form of cell death dependent on intracellular iron and characterized by the accumulation of lipid peroxides and reactive oxygen species (ROS). As a newly discovered form of cell death, the phenotype of ferroptosis has been known for several years, but only by 2012, the process of ferroptosis has been characterized and classified in a systematic and comprehensive manner by Brent Stockwell and co-workers [157]. They have found that the RAS-selective lethal (RSL) compounds Erastin and RSL3 induce a new type of cell death without the classic features of apoptosis, such as mitochondrial cytochrome c release, activation of caspases and chromatin fragmentation. Rather, in this type of programmed cell death intracellular reactive oxygen species (ROS) levels significantly increase, and this can be prevented by iron chelation or lipophilic antioxidants. Due to the differences in cell morphology and in biochemical and genetic features of ferroptosis with the other types of regulated cell death, they have termed this unique iron-dependent form of non-apoptotic cell death ferroptosis [157].

1.4.1 Mechanism of ferroptosis

Ferroptosis was first defined based on studies with the RSL compounds and their induction of non-apoptotic and peroxidation-driven cell death. Thereby, the initiation and execution of ferroptosis are affected by iron, amino acid, and lipid metabolism and also by signaling pathways such as the MAPK pathway [158].

The trans-sulfuration pathway has been recognized to regulate ferroptosis by Hayao *et al.* in 2016. Employing a genome-wide siRNA screen they have identified that knocking down of cysteinyl-tRNA synthetase (CARS) promotes the synthesis of cysteine from methionine and thereby facilitates cells' resistance to Erastin-induced ferroptosis [159]. As a glutamate-cystine transporter and as part of antioxidant pathways, system Xc- also restricts ferroptosis by suppressing cysteine synthesis. System Xc- is composed of two subunit proteins, SLC7A11 and SLC3A2, and it can exchange cystine and glutamate in and out of cells, respectively, at a ratio of 1:1. Intracellular cystine is essential for the synthesis of cysteine and subsequently of glutathione (GSH). Hence, inhibition of system Xc- restricts the synthesis of GSH, leading to an increased ROS levels, lipid peroxidation and, finally, to ferroptosis [160].

Sensitivity to ferroptosis is also regulated by iron metabolism. Transferrin and its receptor are essential for the uptake of iron into cells. Depletion of IREB2 (which is the master regulator of iron metabolism) reduces cells' sensitivity to ferroptosis [157]. Additionally, transferrin receptor has also been identified as a marker of ferroptosis. Ferritin, NCOA4, HSPB1 and CISD1 have also been reported to regulate ferroptosis sensitivity via impacting iron metabolism [158,161,162]. The transcription factor BTB domain and CNC homolog 1 (BACH1), a regulator of iron and heme metabolism, has also been found to promote ferroptosis by repressing the transcription of a subset of ferroptosis-protective genes [163].

The regulation of lipid metabolism is also closely connected to ferroptosis. Polyunsaturated fatty acids (PUFAs) have been found to be sensitive to lipid peroxidation, a process central and essential to ferroptosis. However, PUFAs must be esterified into membrane phospholipids and by oxidation to become PUFA-PEs (phosphatidylethanolamines which contains arachidonic acid (C20:4) or adrenergic acid (C22:4), and then to initiate ferroptosis [164,165]. LPCAT3 and ASCL4 are reported to be involved in this process, and depletion of these genes leads to diminished lipid peroxidation of their substrates and thus to a repression of ferroptosis [166]. Lipoxygenases (LOXs) are also reported to facilitate ferroptotic peroxidation by catalysis of PUFA-PEs [167].

Ferroptosis is also regulated by several other pathways [168]. Coenzyme Q10 (CoQ10) is an endogenous inhibitor of ferroptosis by reducing lipid peroxidation in cells. The inducer of ferroptosis FIN56 restricts both CoQ10 and GPX4 to promote ferroptosis. As an essential reductant to eliminate lipid hydroperoxides, NADPH has been identified as a biomarker of ferroptosis in several cancer cell lines. Selenium is also important for anti-oxidation as an essential co-factor of GPX4. 4-hydroxynonenal (4-HNE) and malondialdehyde (MDA) are also used as biomarkers of oxidative stress and as potential biomarkers of ferroptosis in tissue sections. Several other genes have also been implicated in the ferroptotic process. The transcription factor NRF2 mediates the expression of several ferroptosis-related genes, such as AKR1C, SLC7A11, GCLC/GLCM, GSS, and GPX4, to regulate the levels of key proteins in iron metabolism and glutathione synthesis and thus to restrict ferroptosis [169]. Another

transcription factor, ATF4, is also able to upregulate the expression of SLC7A11 and HSPA5 to confer resistance to ferroptosis [170,171].

Inducers of ferroptosis

More and more small molecular compounds are identified which induce ferroptosis by targeting xCT, GSH synthesis and GPX4 [172]. Erastin and the analogs, such as piperazine erastin and imidazole ketone erastin, inhibit the activity of xCT to suppress the synthesis of GSH [173]. Other drugs like Sorafenib and Sulfasalazine also inhibit xCT directly, and high extracellular levels of glutamate also inhibit the activity of xCT [48] [174]. BSO is another known drug which targets GCL to restrict GSH synthesis, thus to facilitate ferroptosis [172,175].

Direct inhibition of GPX4 can also induce ferroptosis in cells, and several reagents containing electrophilic chloroacetamide can suppress GPX4 activity. RSL3, and DPI7/ML162 can interact with the active site of GPX4 to repress its activity and to induce ferroptosis. Degradation of GPX4 induced by FIN56 also promotes the activation of ferroptosis [168]. Organic peroxides are also reported to induce ferroptosis in murine and human cells by producing free radicals and oxidative damage. Tert-butyl hydroperoxide (t-BuOOH) was first reported as a ferroptosis inducer, and FINO2 is another organic peroxide that not only induces iron oxide but also indirectly inhibits GPX4 activity [176,177].

Inhibitors of ferroptosis

A common strategy to prevent cells from undergoing ferroptosis is to restrict lipid peroxidation and the formation of lipid peroxides. Ferrostatin-1 and liproxstatin-1 are two classical ferroptosis inhibitors which restrict lipid peroxidation levels via scavenging chain-carrying radicals [157]. N-acetyl cysteine (NAC), CoQ10 and Vitamin E are reported to act against oxidative cell death and to protect cells from ferroptosis. Some inhibitors protect GPX4 from degradation and thus are also functional in suppressing ferroptosis, including the ACAC inhibitor TOFA and the HSP90 inhibitor 2-amino-5-chloro-N,3-dimehtylbenzamide (CDDO) [178,179] (Figure 8).

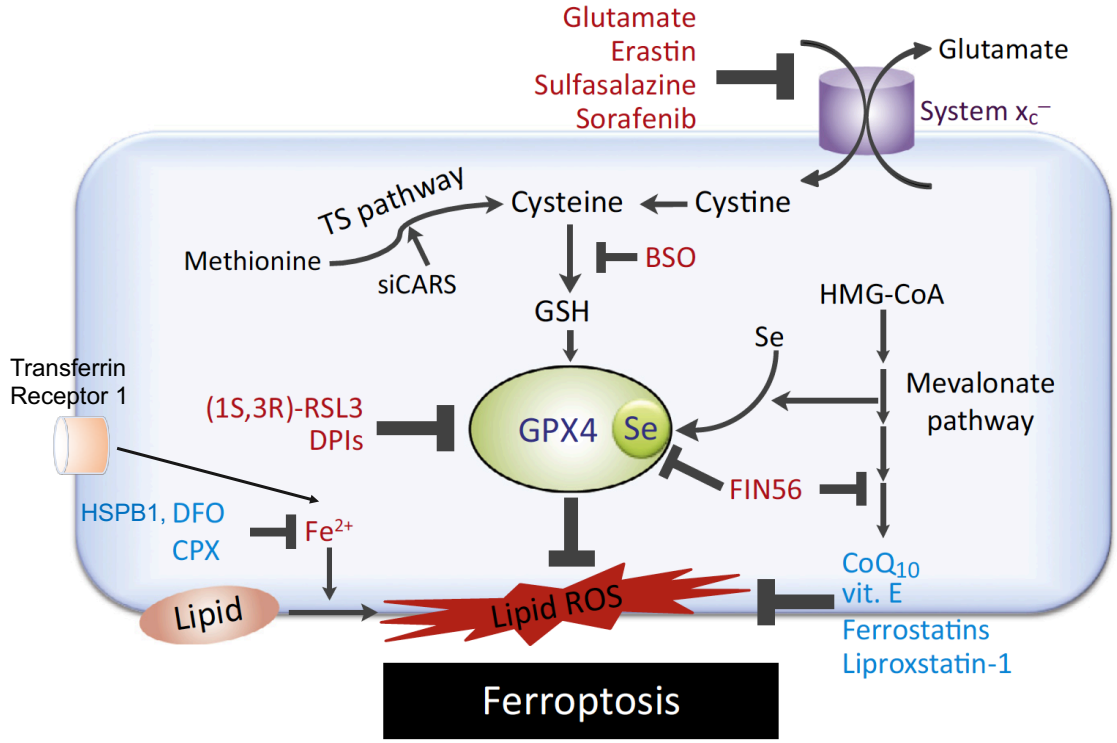

Figure 8. Ferroptosis. Ferroptosis is a non-apoptotic cell death induced by the accumulation of lipid ROS. Small molecules like glutamate, Erastin, Sulfasalazine, and Sorafenib block GSH synthesis via inhibiting system Xc-. BSO blocks GSH synthesis from Cysteine. Other Ferroptosis inducers like (1S,3R)-RSL3, DPIs and FIN56 block GPX4 directly to induce lipid ROS. Inhibitors of ferroptosis include CoQ10, Vitamin E, Ferrostatin, Liproxstatin-1, DFO, CPX, and HSPB1. They reduce lipid ROS and protect cells from ferroptosis. Adapted from [175].

Ferroptosis and disease

Ferroptosis has been reported to play a role in several different cell processes and pathological conditions. Degenerative diseases like Alzheimer, Parkinson and Huntington have been reported to involve ferroptosis, and it appears to play a critical role also in a variety of other diseases, including kidney degeneration, traumatic brain injury, stroke and also carcinogenesis. Accordingly, inhibitors of ferroptosis, such as ferrostatins, have been shown to be protective in mouse models of degenerative diseases. Ischemic injury of liver, brain and heart could also be improved the inhibition of ferroptosis suppression in mouse models.

Carcinogenesis is another key pathological process which appears to be regulated by ferroptosis. Yang *et al.* have reported that the ferroptosis inducer RSL3 could induce

cell death in 177 different cancer cell lines by targeting GPX4 [172]. In lung tumors, the iron sulfur cluster biosynthetic enzyme (NFS1) has been shown to protect cells from ferroptosis, when the cells acquired large amounts of ROS. Conversely, the tumor suppressor p53 can downregulate SLC7A11 and thus promoting the accumulation of ROS and leading to ferroptosis in A549 cells, a process which could be further enhanced by the treatment with Erastin [180]. However, Xie *et al.* have found that P53 can inhibit Erastin-induced ferroptosis in colorectal cancer via inhibiting dipeptidyl-peptidase 4 (DPP4) [181]. In addition, the cancer stem cell marker CD44v was also reported to form a complex with SLC7A11 to restrict ferroptosis in breast cancer [182]. Finally, inhibition of GSH synthesis in clear cell renal cell carcinoma (ccRCC) has been found to induce ferroptosis [183].

Hence, ferroptosis has been reported to exist in different types of cancers and, as a new form of regulated cell death, ferroptosis may be a new adequate target for cancer therapy.

1.4.2 Ferroptosis in HCC and Sorafenib resistance

Ferroptosis has also been identified to regulate liver fibrosis and HCC progression, and the p62 - Kelch-like ECH-associated protein 1 (Keap1) - nuclear factor erythroid 2-related factor 2 (NRF2) pathway was reported to prevent Ferroptosis in HCC cells [169]. Sigma 1 receptor (S1R) is another protein that was recognized to protect against ferroptosis in HCC cells [184].

Several genes have also been reported to regulate ferroptosis that is induced by Sorafenib in HCC. As the first-line systemic treatment in HCC, Sorafenib was first reported to induce ferroptosis in HCC cell lines in 2013 and 2014 [48,49]. Afterwards, Sorafenib has been shown to induce ferroptosis via the direct inhibition of xCT, yet not by its anti-kinase activities [47].

NRF2 is a well-known regulator of antioxidant response. But whether and how NRF2 regulates ferroptosis remained unclear until Sun *et al.* had found that in HCC cells, upon exposure to ferroptosis inducers (Erastin, Sorafenib, buthionine sulfoximine), p62 could prevent NRF2 degradation and promote NRF2 nuclear accumulation via

restricting KEAP1 [169]. Moreover, several antioxidants, such as quinone oxidoreductase 1 (NQO1), heme oxygenase-1 (HO-1) and ferritin heavy chain 1 (FIH1), are also upregulated by NRF2 to resist ferroptosis. Additionally, Metallothionein-1G (MT-1G) has also been identified as a critical negative regulator of ferroptosis upon exposure to Sorafenib. The expression of MT-1G is induced by Sorafenib via the transcriptional activity of NRF2. Depletion of MT-1G increases glutathione depletion and lipid peroxidation, indicating that MT-1G could be a potential therapeutic target to offset Sorafenib resistance [185].

Loss of function of the retinoblastoma (Rb) protein is a common genetic event underlying HCC. Upon loss of Rb, HCC cells exhibit a two- to threefold increase in cell death upon Sorafenib treatment, and Rb-negative HCC cells show higher levels of ferroptosis upon exposure to Sorafenib as compared with Rb-positive HCC cells [186].

Although first important insights into Sorafenib-induced ferroptosis and of Sorafenib-resistance in HCC have been provided, the detailed molecular mechanisms still remain largely unknown. Understanding ferroptosis in HCC seems to be warranted to develop efficacious therapy against HCC and to overcome Sorafenib resistance.

2. Aim of the Study

Sorafenib is approved as the first-line systemic treatment of HCC for around 15 years. Even though some new drugs and combined treatments have been approved for the first or second-line treatments of HCC, Sorafenib is still the standard therapy on advanced HCC patients. However, despite significant improvements on the median survival of HCC patients, Sorafenib resistance frequently occurs in HCC patients and most patients succumb to the disease. Therefore, a better understanding of the molecular mechanisms underlying Sorafenib resistance is urgent needed to identify new therapeutic targets that may help to overcome Sorafenib resistance in HCC patients. In the past years, several genes and pathways have been identified as regulators of Sorafenib resistance, but the detailed mechanisms of their mode of action and their druggabilities have not been delineated.

With my PhD studies, I have aimed at the better understanding of molecular mechanisms of Sorafenib resistance in HCC. To achieve this, we have established Sorafenib-resistant HCC cell lines *in vitro,* and through transcriptomic analysis combined with siRNA screening and synthetic lethal shRNA screening, we successfully identified several potential therapeutic targets which may allow to improve the therapy response to Sorafenib treatment in HCC:

1. USP29-mediated HIF1α stabilization promotes Sorafenib resistance of hepatocellular carcinoma cells by upregulating glycolysis

2. YAP/TAZ and ATF4 collaboratively drive resistance to Sorafenib therapy in hepatocellular carcinoma by preventing ferroptosis

3. Results

3.1 USP29-mediated HIF1α stabilization promotes Sorafenib resistance of hepatocellular carcinoma cells by upregulating glycolysis

Ruize Gao[1*], David Buechel[1], Ravi K.R. Kalathur[1], Marco F. Morini[1], Mairene Coto-Llerena[2], Caner Ercan[2], Salvatore Piscuoglio[2], Qian Chen[1,3] Tanja Blumer[1,3], Xueya Wang[1,3], Eva Dazert[4], Markus H. Heim[1,3], Michael N. Hall[4], Fengyuan Tang[1*] and Christofori Gerhard[1*]

[1]Department of Biomedicine, University of Basel, Basel, Switzerland
[2]Institute of Pathology, University Hospital Basel, Basel, Switzerland
[3]University Hospital Basel, Basel, Switzerland
[4]Biozentrum, University of Basel, Basel, Switzerland

[*]**Corresponding authors:**
Ruize Gao, Fengyuan Tang and Gerhard Christofori
Department of Biomedicine, University of Basel
Mattenstrasse 28, CH-4058 Basel, Switzerland
Tel. +41 61 207 35 62
Fax. +41 61 207 35 66
E-mail: ruize.gao@unibas.ch; fengyuan.tang@unibas.ch;
gerhard.christofori@unibas.ch

Manuscript in revision with 'Oncogenesis'

3.1.1 Abstract

Understanding the mechanisms underlying evasive resistance in cancer is an unmet medical need to improve the efficacy of current therapies. In hepatocellular carcinoma (HCC), aberrant expression of hypoxia inducible factor 1 α (HIF1α) and increased aerobic glycolysis metabolism represent drivers of the development of resistance to therapy with the multi-kinase inhibitor Sorafenib. However, it has remained unknown how HIF1α is activated and how its activity and the subsequent induction of aerobic glycolysis promotes Sorafenib resistance in HCC. Here, we report the ubiquitin-specific peptidase USP29 as a new regulator of HIF1α and of aerobic glycolysis during the development of Sorafenib resistance in HCC. In particular, we have identified USP29 as a critical deubiquitylase (DUB) of HIF1α, which directly deubiquitinates and stabilizes HIF1α and, thus, promotes its transcriptional activity. Among the transcriptional targets of HIF1α is the gene encoding for hexokinase 2 (HK2), a key enzyme of the glycolytic pathway. The absence of USP29, and thus of HIF1α transcriptional activity, reduces the levels of aerobic glycolysis and reinstalls the sensitivity to Sorafenib treatment in Sorafenib-resistant HCC cells *in vitro* and in xenograft transplantation mouse models *in vivo*. Notably, the absence of USP29 and high HK2 expression levels correlate with the response of HCC patients to Sorafenib therapy. Together, the data demonstrate that, as a DUB of HIF1α, USP29 promotes Sorafenib resistance in HCC cells by upregulating glycolysis, thereby opening new avenues for therapeutically targeting Sorafenib-resistant HCC in patients.

3.1.2 Introduction

Liver cancer is the second leading cause of cancer-related death world-wide. Hepatocellular carcinoma (HCC) represents the most common type of primary malignant liver tumor, accounting for 90% of all liver cancers [187]. Unfortunately, only 30% of HCC patients are diagnosed at an early stage of carcinogenesis. Most of the patients are diagnosed at advanced stages, where surgical resection, allogeneic liver transplantation or percutaneous tumor ablation are not applicable. Sorafenib, a multi-kinase inhibitor, is the standard of care treatment for advanced HCC patients, yet it prolongs the median overall survival and radiological progression by only ~3 months [17]. Comparable to many other targeted therapies, evasive resistance to Sorafenib is

invariably observed in HCC patients. Therefore, a detailed understanding of how HCC cells respond to Sorafenib will not only help to improve the efficacy of Sorafenib therapy in HCC patients, but it will also be critical to overcome the development of therapy resistance.

HIF1 (Hypoxia-inducible factor 1) is a well-known key regulator of cellular adaptive responses to hypoxia. Furthermore, it is a highly oncogenic transcription factor which promotes tumor growth via regulating global transcriptomic networks involved in tumor angiogenesis, metabolism and therapy resistance [188]. Hypoxia and HIF1α play important roles in HCC development and relapse after chemotherapy [189]. HIF1α is also found at high protein levels in tumors of HCC patients which are resistant to Sorafenib treatment [94]. As a heterodimeric transcription factor composed of HIF1α and HIF1β (ARNT), HIF's transcriptional activity is mainly regulated at HIF1α's protein level. Thereby, the protein stability of HIF1α is regulated by the Ubiquitin-Proteasome System (UPS). Under normoxic conditions, HIF1α is hydroxylated by oxygen-dependent proline hydroxylases (PHDs), which makes it a substrate of the ubiquitin E3 ligase von Hippel-Lindau (VHL), and after ubiquitylation it is degraded by the proteasome. Under hypoxic conditions, PHDs are not active, and HIF1α is not hydroxylated and ubiquitylated and, thus, stabilized to exert its transcriptional activities [190-194]. Recent studies have indicated that HIF1α can also be stabilized by deubiquitinating enzymes (DUBs) not only under hypoxic but also under normoxic conditions [190].

Aerobic glycolysis (Warburg effect) is a general metabolic feature of malignant tumors [195]. Aberrant glycolysis levels, including increased glucose uptake and lactate production, seem to be central for the malignant progression of solid tumors, and HIF1α also has been implicated in the regulation of genes responsible for aberrant glycolysis [108]. Excessive glycolysis has also been reported to contribute to Sorafenib resistance in HCC cells [196,197]. However, it has remained unclear how glycolysis is upregulated in Sorafenib-resistant HCC cells.

Ubiquitin-specific peptidase 29 (USP29) is a highly conserved DUB which belongs to the PH_USP37_like family. The PH_USP37_like family plays important roles in cell proliferation and cancer growth. It consists of three members: USP26, USP29 and USP37, of which USP26 is a positive regulator of Androgen Receptor in prostate cancer cells [109], USP37 directly deubiquitinates and stabilizes c-Myc in

lung cancer [110], and USP29 has been recognized as a regulator of the checkpoint adaptor Claspin [111]. In particular the functional contribution of USP29 to tumorigenesis and therapy resistance has remained unexplored.

Here, we report the identification of USP29 as a new regulator of HIF1α in HCC cells. Our data indicate that the USP29-HIF1α axis regulates Sorafenib resistance by promoting glycolysis in HCC cells. The findings highlight USP29 and HIF1α as biomarkers for Sorafenib resistance in HCC and the USP29-HIF1α-glycolysis regulatory cascade as a potential therapeutic target to overcome Sorafenib resistance in HCC patients.

3.1.3 Results

3.1.3.1 Identification of HIF1α as a biomarker of Sorafenib-resistance

To uncover the molecular mechanisms underlying Sorafenib resistance of HCC, we first determined the IC50 values for Sorafenib in repressing the growth of patient-derived HCC cell lines (Suppl. Fig.1a). Of this list, we selected two of the most Sorafenib-susceptible cell lines (Huh7 and HepG2) to establish cellular models of Sorafenib resistance by treating the cells with either increasing concentrations (IR) or a consistently high concentration (CR) of Sorafenib (Suppl.Fig.1b). These treatments generated the Sorafenib-resistant cell lines Huh7-IR and Huh7-CR and Hep3B-IR and Hep3B-CR with IC50 values of 10.7μM, 10.8μM, 7.2μM and 8.3μM, respectively, which are close to the clinically relevant concentration of 10μM Sorafenib (Suppl. Fig. 1c).

Next, we performed whole transcriptomic analysis of Sorafenib-responsive Huh7 and Hep3B parental cells and of the various Sorafenib-resistant cells, and genes differentially expressed between the parental cell lines and the Sorafenib-resistant cell lines were determined (Suppl. Fig. 1d; Suppl. Table I). KEGG pathway analysis of the genes specifically expressed in Sorafenib-resistant cells identified hypoxia inducible factor (HIF)-mediated signaling as a major signaling pathway activated in Sorafenib-resistant cells (Fig. 1a). HIF1α is known to regulate a global adaptive transcriptional response to hypoxia and, as such, it is a critical oncoprotein in promoting tumor growth via regulating transcriptomic networks involved in angiogenesis, metabolism and therapy resistance. To assess whether HIF1α and its transcriptional target genes were contributing to Sorafenib resistance, we first identified the HIF1α target genes highly

expressed in Sorafenib-resistant HCC cells (Fig. 1b). Indeed, quantitative RT-PCR analysis validated the high expression of a selection of prototype HIF1α target genes in Sorafenib-resistant Huh7-IR and CR cells as compared to Huh7-parental cells (Fig. 1c). Consistent with the increased expression of its target genes, HIF1α was found increased at the protein level in the Sorafenib-resistant cells as compared to their parental Huh7, notably even under normoxic culture conditions (Fig.1d).

To assess the functional role of HIF1α in driving Sorafenib resistance, we performed colony formation assays with Huh7-IR and Huh7-CR cells with and without siRNA-mediated depletion of HIF1α expression and in the presence of different concentrations of Sorafenib (Fig. 1e-h). In line with a previous study showing a critical role of HIF1α in Sorafenib-naïve cells, the results demonstrated that HIF1α was critically required for the maintenance of Sorafenib resistance in patient-derived HCC cell lines. HIF2α is another family member of hypoxia-inducible factors known to promote tumorigenesis. However, siRNA-mediated depletion of HIF2α in both Huh7-IR and Huh7-CR cells had no impact on sorafenib resistance in HCC cells (Suppl. Fig. 2a-d).

Together, these results suggest that HIF1α, but not HIF2α, sustains the resistance of HCC cells to sorafenib therapy.

Figure 1, Gao et al.

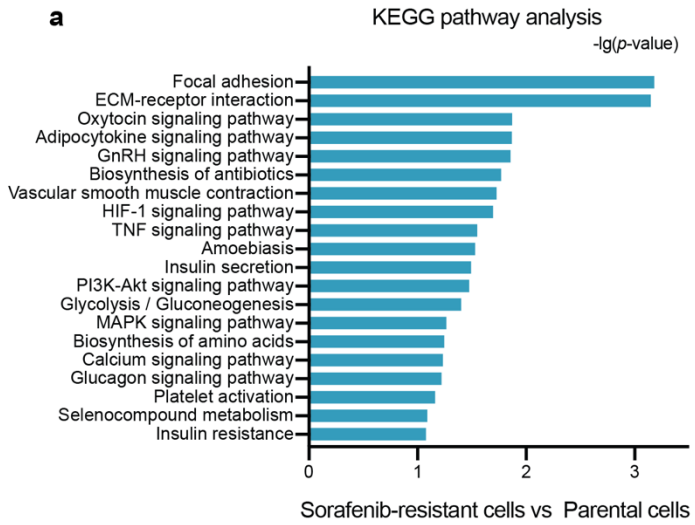

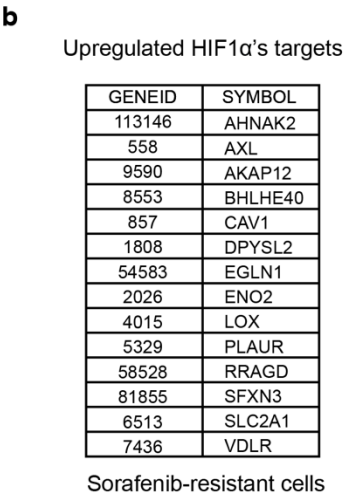

GENEID	SYMBOL
113146	AHNAK2
558	AXL
9590	AKAP12
8553	BHLHE40
857	CAV1
1808	DPYSL2
54583	EGLN1
2026	ENO2
4015	LOX
5329	PLAUR
58528	RRAGD
81855	SFXN3
6513	SLC2A1
7436	VDLR

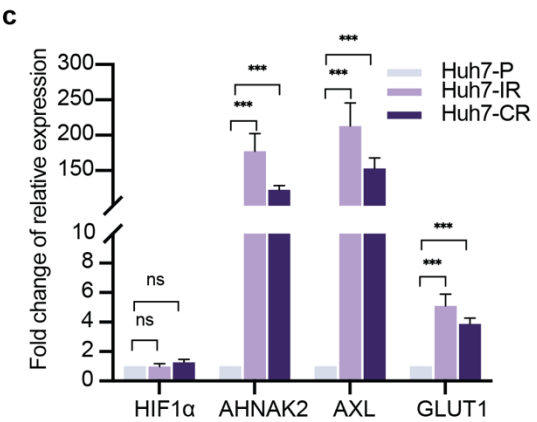

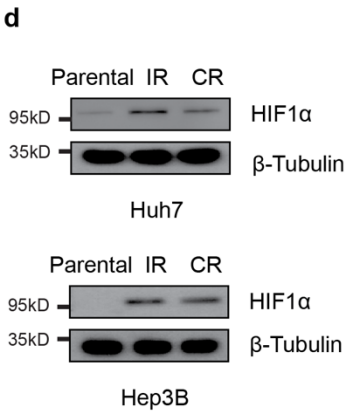

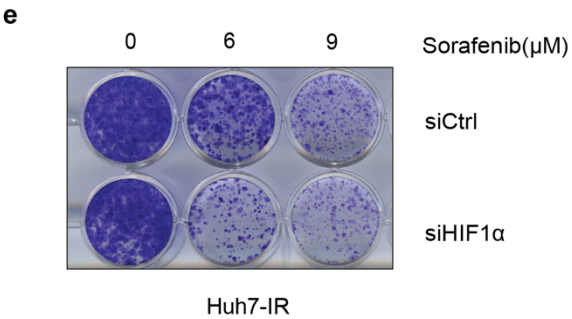

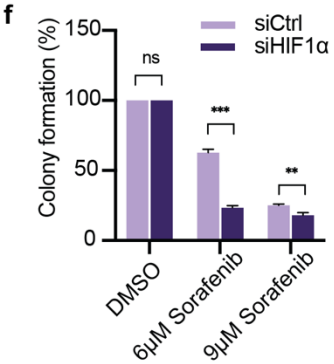

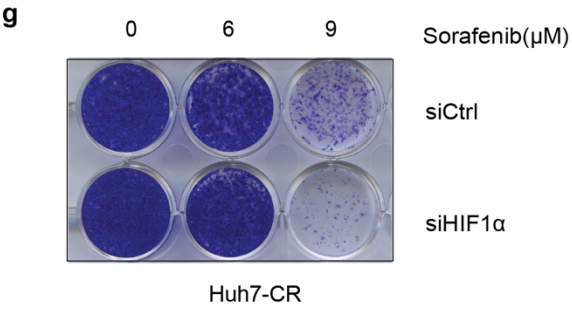

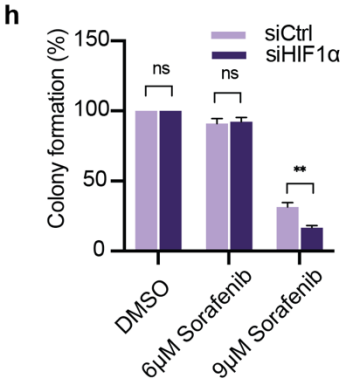

Figure 1. Identification of HIF1α as a biomarker of Sorafenib-resistance.

(a) KEGG pathway analysis of the genes specifically upregulated in their expression in Sorafenib-resistant cells. The HIF-1 signaling pathway was identified as an upregulated pathway. **(b)** Top list of HIF1α target genes highly expressed in Sorafenib-resistant cells. **(c)** Huh7-IR and Huh7-CR cells expressed high mRNA levels of HIF1α target genes *HIF1α*, *AHNAK2*, *AXL* and *GLUT1*. The transcripts of selected HIF1α target genes were quantified by quantitative RT-PCR. Fold increases are shown (n = 2 independent replicates). ns = not significant; *, P < 0.05; **, P < 0.01; *** P < 0.001; Student's t-test. **(d)** Higher HIF1α protein levels were detected in Sorafenib-resistant Huh7(Hep3B)-IR and Huh7(Hep3B) -CR cells as compared to Huh7(Hep3B) parental cells. Immunoblotting for β-Tubulin was used as loading control. **(e-h)** Loss of HIF1α in Sorafenib-resistant Huh7-IRand Huh7-CR cells induced cell death upon Sorafenib treatment. Colony formation assays were performed with Huh7-IR (d) and Huh7-CR (f) cells with either siCtrl or siHIF1α transfection and treatment with different concentrations of Sorafenib (0 μM, 6μM, 9μM) for 2 weeks. Colony formation was quantified by crystal violet staining (f, h). n = 3 independent replicates. ns = not significant; **, P < 0.01; *** P < 0.001; Student's t-test.

3.1.3.2 USP29 stabilizes HIF1α

Next, we sought to examine how the activity of HIF1α is regulated in Sorafenib-resistant HCC cells. As a transcriptional factor, HIF1α's stability and activity are predominantly regulated at the post-transcriptional level, namely by the Ubiquitin-Proteasome System (UPS). In normoxia, the E3 ligase and tumor suppressor gene Von Hippel Lindau (VHL) is well known to ubiquitylate HIF1α and thereby to earmark it for proteasomal degradation. On the other hand, deubiquitylating enzymes (DUBs), such as USP8, USP28 and UCHL1, are known to stabilize HIF1α under normoxia. Given that the HIF1α mRNA levels were not changed in the Sorafenib-resistant HCC cells, yet its protein levels were increased, we hypothesized that HIF1α protein levels were stabilized by a tight regulation of its levels of ubiquitination.

We thus performed a small-scale functional siRNA screen of the Sorafenib-resistant HCC cell line HLE against a panel of DUBs implicated in the regulation of HIF1α, including USP8, USP28, USP29, USP36, USP37, and UCHL1. Among these, siRNA-mediated ablation of USP29 had the strongest effect on HIF1α protein levels, indicating that USP29 might be a key DUB in promoting HIF1α protein stability in Sorafenib-resistant HCC cells (Suppl. Fig. 3a, b). To further validate the role of USP29 in HIF1a stability, we analyzed the effect of two unique siRNAs against USP29 with differential knock-down efficacy on HIF1α protein levels in Sorafenib-resistant HLE and SNU398 cells. Indeed, the efficiency of USP29 depletion of the two different siRNAs correlated with the extent of HIF1α protein loss (Fig. 2a; Suppl. Fig. 3c). Moreover, transfection of an increasing amount of plasmid expressing USP29 resulted

in an increasing stabilization of HIF1α in HLE cells (Fig. 2b). Moreover, transfection of a siRNA-refractory cDNA encoding for USP29 efficiently reinstalled the stabilization of HIF1α protein levels upon USP29 deficiency in HLE and HEK-293T cells (Fig. 2c; Suppl. Fig. 3d), supporting a general role of USP29 in stabilizing HIF1α in HCC and HEK cells.

We further determined the robustness of USP29-mediated stabilization of HIF1α in a hypoxia-reoxygenation assay in Sorafenib-resistant HLE cells. While HIF1α levels were found high under hypoxic culture conditions, upon reoxygenation HIF1α protein levels were diminished over time in siControl-transfected cells (Fig. 2d). Notably, upon siRNA-mediated depletion of USP29, loss of HIF1α was substantially accelerated, further supporting a direct role of USP29 in stabilizing HIF1α.

As a transcription factor, HIF1a has to translocate to the nucleus for mediating its transcriptional outputs. We thus investigated the functional impact of USP29-mediated stabilization of HIF1α by analyzing its nuclear localization and transcriptional activity. Firstly, immunofluorescence microscopy analysis of HLE cells revealed an increase in the nuclear localization of HIF1α by the forced expression of USP29 (Fig. 2e) and a reduction of nuclear HIF1α upon siRNA-mediated depletion of USP29 expression (Fig. 2f; Suppl. Fig 3e). Secondly, the expression of HIF1α target genes was significantly increased upon the forced expression of USP29, while the mRNA levels of HIF1α remained unaffected (Fig. 2g). Conversely, siRNA-mediated depletion of USP29 expression in HLE cells resulted in the reduced expression of HIF1α target genes (Fig 2h). Thirdly, in line with the observed effects of USP29 on the expression of HIF1α target genes, the loss of USP29 directly reduced HIF1α transcriptional activity, as determined by a hypoxia response element (HRE)-driven luciferase reporter assay (Fig 2i).

Together, these findings suggest USP29 as a potent positive regulator of HIF1α protein stability and transcriptional activity in Sorafenib-resistant HCC cells.

Figure 2, Gao et al.

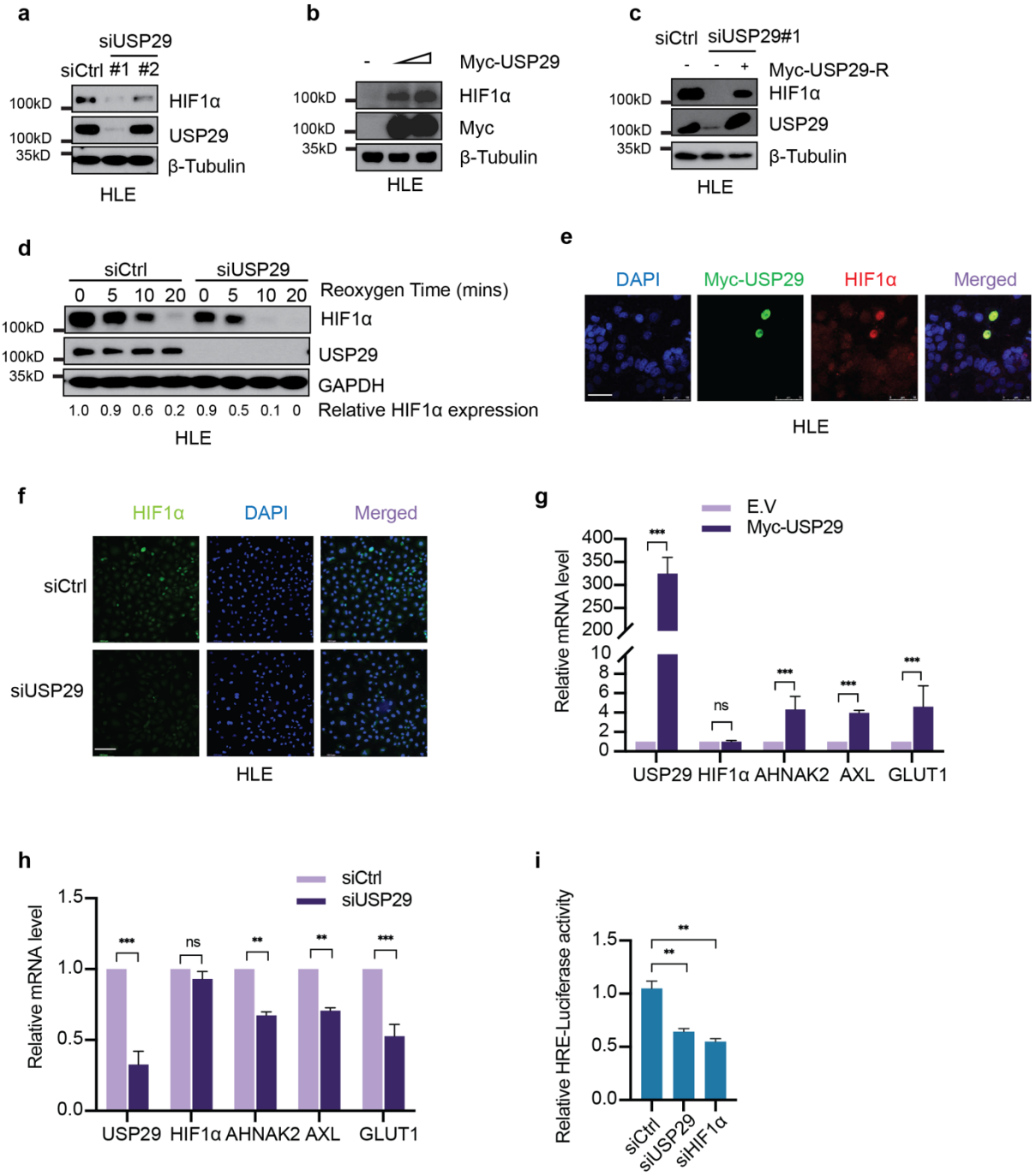

Figure 2. USP29 stabilizes HIF1α and promotes HIF1α's transcriptional activity.

(a) Depletion of USP29 diminished HIF1α protein levels in Sorafenib-resistant HLE cells. Two different siRNAs against USP29 (siUSP29#1 and siUSP29#2) were transfected into cells for the depletion of USP29. siUSP29#1 had a more effective knockdown efficiency than siUSP29#2. **(b)** USP29 promotes HIF1α protein stability. Myc-tagged USP29 was transfected into HLE cells, and endogenous HIF1α protein level was measured by immunoblotting. Immunoblotting for β-Tubulin was used as loading control. **(c)** Expression of a RNAi-resistant USP29 (Myc-USP29-R) rescued USP29 deficiency-induced instability of HIF1α. THLE cells were first transfected with siUSP29#1 and 24 hours later with Myc-USP29-R or Empty-Vector. USP29 and HIF1α protein levels were determined by immunoblotting. β-Tubulin was used as loading control. **(d)** USP29 deficiency induces HIF1α protein

degradation. HLE cells transfected with siCtrl or siSUP29#1 were incubated in a hypoxia chamber (1% O2, 94% N2, 5% CO2) for 6 hours and then moved to normoxia for 0 min, 5 mins, 10 mins and 20 mins. Immunoblotting was used to visualize the kinetics of HIF1α degradation. Immunoblotting for USP29 was used to validate the knockdown efficiency and GAPDH as loading control. **(e)** USP29 promotes HIF1α stability and nuclear localization. A plasmid encoding for Myc-tagged USP29 was transfected into HLE cells and Myc-tagged USP29 and endogenous HIF1α were visualized by immunofluorescence microscopy analysis. Staining with DAPI was used to visualize nuclei. Scale bars, 50µm. **(f)** Loss of USP29 expression reduces HIF1α stability and nuclear localization. HLE cells were transfected with siCtlr or siUSP29, and HIF1a was visualized by immunofluorescence microscopy for staining of endogenous HIF1α. DAPI staining was used to visualize nuclei. Scale bars, 132.5µm. **(g)** USP29 promotes HIF1α transcriptional activity. Expression of the HIF1α target genes *AHNAK2, AXL, GLUT1* was examined in HKLE cells transfected with a plasmid encoding for Myc-tagged USP29, and mRNA levels were determined by quantitative RT-PCR. Relative mRNA expression is shown. n=2 independent replicates. ns = not significant; ***, P < 0.001; Student's t-test. **(h)** USP29 deficiency reduces HIF1α transcriptional activity. HLE cells were transfected with siCtlr or siUSP29, and the expression of a panel of HIF1α transcriptional target genes was analyzed by quantitative RT-PCR. Relative mRNA expression is shown. n=2 independent replicates. ns = not significant; **, P < 0.01; ***, P < 0.001; Student's t-test. **(i)** Loss of USP29 expression reduces HIF1α transcriptional activity. HLE cells were transfected with siCtrl, siUSP29, and siHIF1α and 24 hours later with plasmids carrying a HIF responsive element (HRE) driving the expression of *Firefly* luciferase (pGL4.42) and CMV promoter-driven *Renilla* luciferase (pRL-CMV) in a 10:1 mass ratio. Relative luciferase activities were measured by a dual-luciferase reporter assay. Results represent three independent experiments. **, P < 0.01; Student's t-test.

3.1.3.3 USP29 interacts with and deubiquitinates HIF1α

We next sought to investigate the molecular mechanisms underlying USP29-mediated regulation of HIF1α protein stability. We hypothesized that USP29, as a DUB, could specifically deubiquitinate HIF1α, thereby preventing its proteasomal degradation. To this end, we first determined the physical interaction between USP29 and HIF1α. Indeed, we found that USP29 can bind to HIF1α and vice versa when expressed at high levels in HEK293-T cells (Fig. 3a, b). We also found that exogenously expressed USP29 also physically interacted with endogenous HIF1α (Fig. 3c). Unfortunately, the analysis of endogenous USP29 was hampered by a lack of suitable antibodies.

Next, we assessed the functional consequence of the interaction between USP29 and HIF1α by focusing on the ubiquitination status of HIF1α. Interestingly, we observed a reduction of ubiquitination on HIF1α by the expression of USP29 in a dose-dependent manner (Fig. 3d). The removal of ubiquitin on HIF1α seemed to be directly catalyzed by the DUB activity of USP29, since a catalytically inactive form of USP29 (CA) failed to reduce ubiquitination of HIF1α (Fig. 3e) and, as a consequence, the CA form of USP29 was unable to stabilize HIF1α.

Together, these results demonstrate that USP29 interacts with HIF1α to catalyze the de-ubiquitination of HIF1α and, thereby, to stabilize it.

Figure 3, Gao et al.

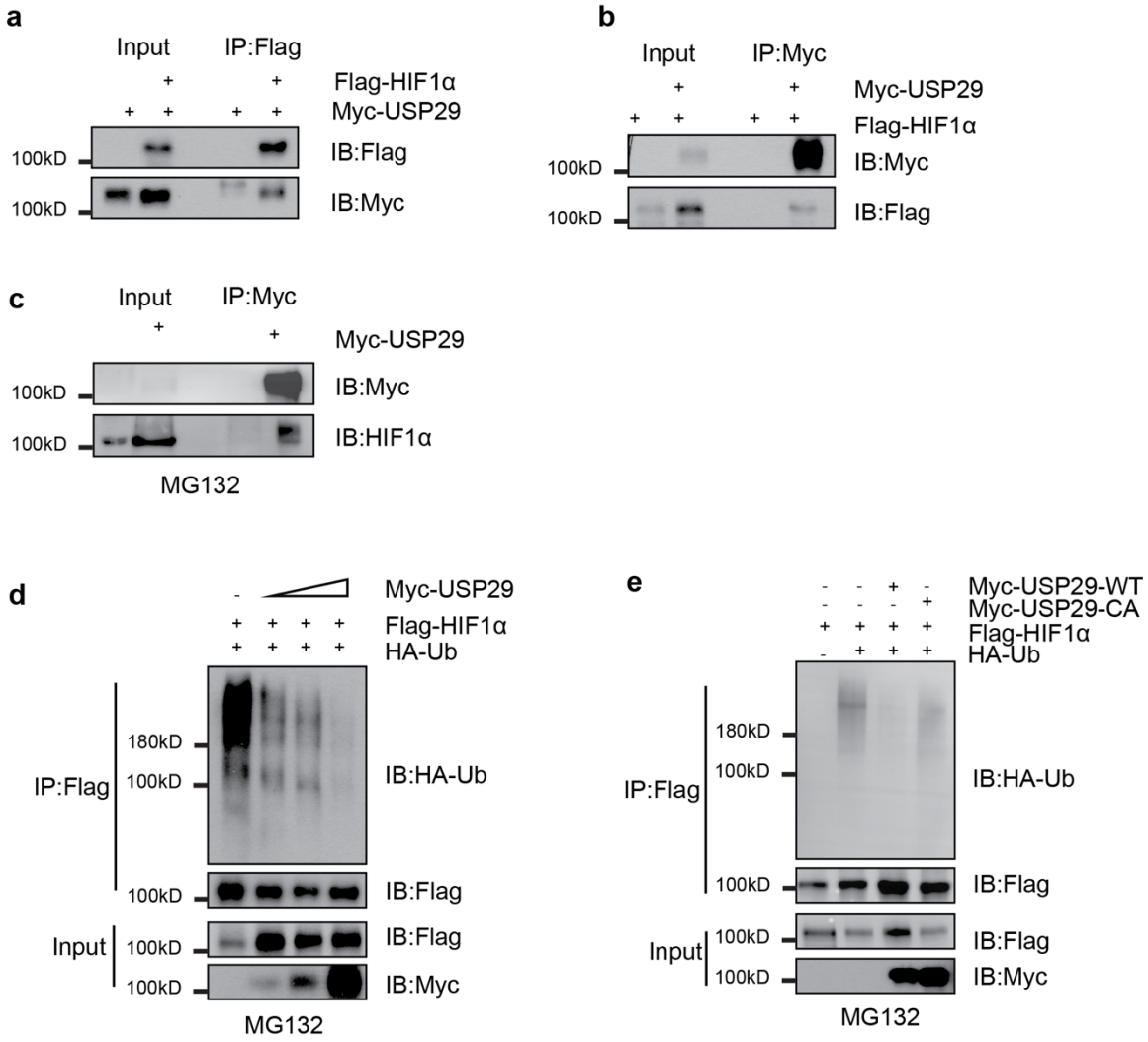

Figure 3. USP29 interacts with and deubiquitinates HIF1α.

(a) Myc-tagged USP29 binds Flag-tagged HIF1α. Plasmids encoding for Flag-tagged empty vector or for Flag-HIF1α were transfected into HEK-293T cells together with a plasmid encoding for Myc-USP29. Anti-Flag antibody and Protein A/G beads were used to precipitate (IP) Flag-tagged HIF1α, and the immunoprecipitates were immunoblotted (IB) for Flag (Flag-HIF1α) and for Myc (Myc-USP29). Input represents 1/10 of the lysate used for the immunoprecipitations. **(b)** Flag-tagged HIF1α binds Myc-tagged USP29. Plasmids encoding for Myc-tagged empty vector or for Myc-tagged USP29 were transfected into HEK-293T cells together with Flag-tagged HIF1α. Anti-Myc antibody and Protein A/G beads were used to precipitate (IP) Myc-tagged USP29, and the immunoprecipitates were immunoblotted (IB) for Myc (Myc-USP29) and for Flag (Flag-HIF1α). Input represents 1/10 of the lysate used for the immunoprecipitations. **(c)** Myc-tagged USP29 binds endogenous HIF1α. Plasmids encoding for Myc-tagged empty vector or for Myc-tagged USP29 were transfected into HEK-293T cells. Anti-Myc

antibody and Protein A/G beads were used to precipitate (IP) Myc-tagged USP29, and the immunoprecipitates were immunoblotted (IB) for Myc (Myc-USP29) and for endogenous HIF1α. Input represents 1/10 of the lysate used for the immunoprecipitations. **(d)** USP29 removes poly-ubiquitin from HIF1α. Increasing amounts of a plasmid encoding for Myc-USP29 were transfected together with Flag-HIF1α and HA-tagged ubiquitin (HA-Ub) into HEK-293T cells. HIF1α was then immunoprecipitated (IP) with anti-Flag antibody, and the precipitates were immunoblotted (IB) for HA (HA-Ub) and for Flag (Flag-HIF1α). USP29 reduced the poly-ubiquitination level of HIF1α. Input represents 1/10 of the lysate used for the immunoprecipitations. MG132 was added into the culture medium 8 hours before harvest to prevent proteasomal degradation. **(e)** The catalytic activity of USP29 is required to remove poly-ubiquitin from HIF1α and to stabilize it. Plasmids encoding for Myc-tagged wildtype USP29 or Myc-tagged CA-mutant USP29 were transfected together with Flag-HIF1α and HA-tagged ubiquitin (HA-Ub) into HEK-293T cells. HIF1α was then immunoprecipitated (IP) with anti-Flag antibody, and the precipitates were immunoblotted (IB) for HA (HA-Ub) and for Flag (Flag-HIF1α). USP29 reduced the poly-ubiquitination level of HIF1α. Input represents 1/10 of the lysate used for the immunoprecipitations. MG132 was added into the culture medium 8 hours before harvest to prevent proteasomal degradation.

3.1.3.4 Identification of USP29 as a regulator of Sorafenib-resistance

The above results prompted us to further delineate the functional contribution of the USP29-HIF1α axis to Sorafenib resistance in HCC cells. We first tested whether the depletion of well-known DUBs for HIF1α, including USP8, USP28, USP29, USP36, USP37, and UCHL1, would exert a synthetic lethal effect on Sorafenib-resistant HLE cells in the absence or presence of Sorafenib. As a functional readout we monitored the levels of cancer cell apoptosis by immunoblotting for cleaved PARP. In line with our findings described above, we found that the siRNA-mediated ablation of USP29 expression led to highest levels of cell death in combination with Sorafenib treatment as compared to the ablation of the expression of other DUBs and to the absence of Sorafenib (Fig. 4a). Importantly, the effect of USP29 on sorafenib resistance was specific, as the siRNA targeting USP29 with poor efficacy failed to induce comparable Sorafenib-induced cell death in Sorafenib-resistant HLE cells (Fig. 4b). Similar results were obtained with Hep3B and Huh7 cells, indicating that USP29 exerts a critical and general role in in mediating Sorafenib resistance in HCC cells (Suppl. Fig. 4a, b).

To further explore the impact of USP29 in Sorafenib-resistant cells, we performed long-term colony formation assays with Huh7-IR and Huh7-CR cells. Indeed, we found that the siRNA-mediated ablation of USP29 reverted the acquired Sorafenib resistance in Huh7-IR and Huh7-CR cells and also the intrinsic Sorafenib resistance in HLE and SNU398 cells (Fig. 4c-f; Suppl. Fig. 4c-f), suggesting that USP29 exerts a critical role in the maintenance of acquired and intrinsic resistance of

HCC cells to Sorafenib therapy. Analysis of the expression of USP29 in Sorafenib-resistant cells by immunoblotting revealed an increase of USP29 protein levels in Sorafenib-resistant Huh7 and Hep3B cells. Consequently, an upregulation of the expression of HIF1α and HIF1α transcriptional target genes was also observed (Fig. 4g, h).

To assess whether in the regulation of Sorafenib resistance USP29 acted epistatically to HIF1α, we performed colony formation assays with Sorafenib-resistant Huh7-IR and Huh7-CR cells with and without depletion of USP29 under hypoxia culture conditions, which was well-known to activate HIF1α transcriptional output. Interestingly, while siRNA-mediated ablation of USP29 led to decreased colony numbers under normoxia, the effect of USP29 depletion was minimal under hypoxic conditions, indicating that another type of HIF1α protein stabilization could promote Sorafenib resistance and that HIF1α acts downstream of USP29 in mediating Sorafenib resistance (Fig. 4c-f; Suppl. Fig.4 g-j).

Together, the results demonstrate a general role of the USP29-HIF1α axis in driving Sorafenib resistance in HCC cells.

Figure 4, Gao et al.

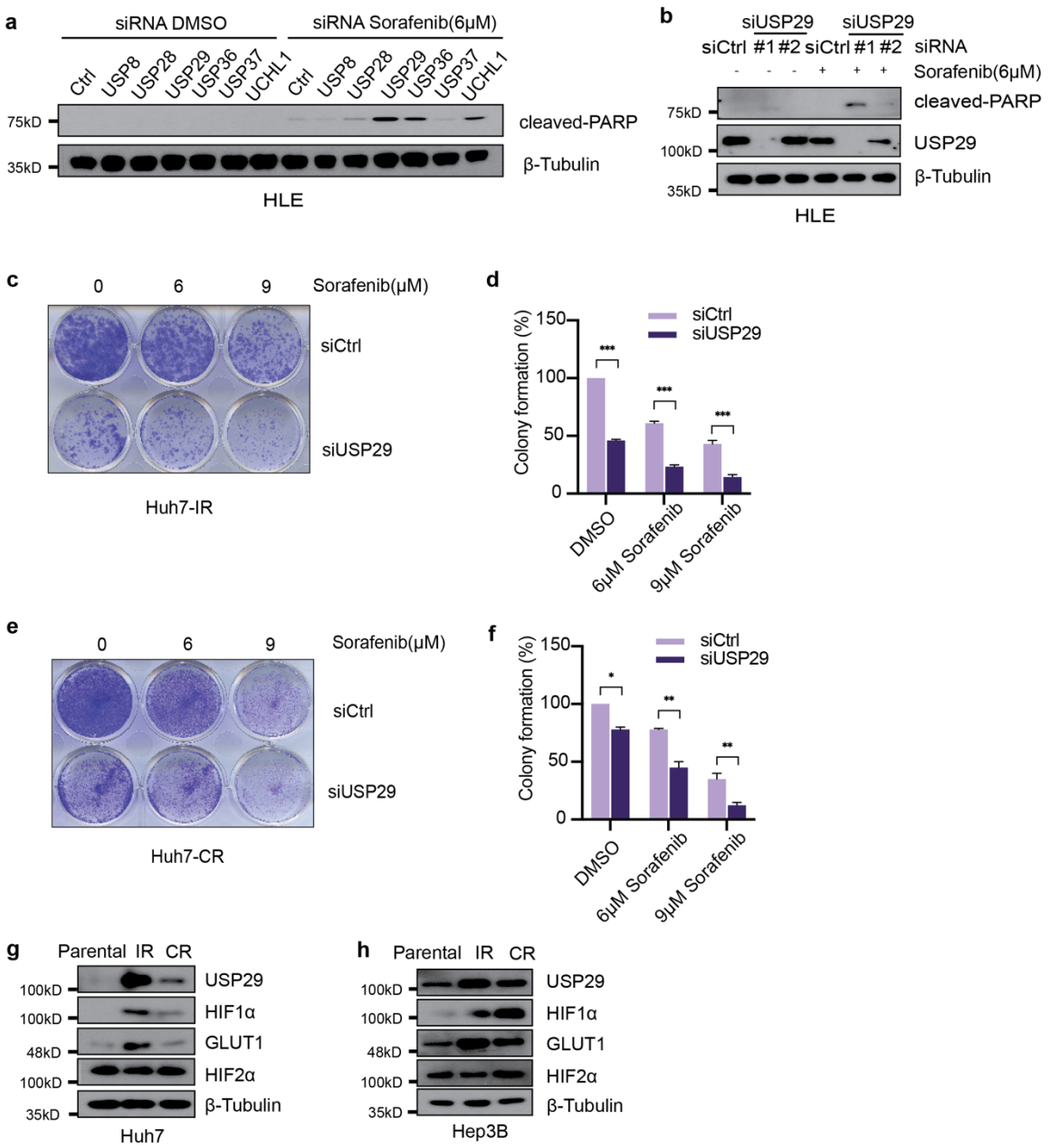

Figure 4. USP29 is a regulator of Sorafenib resistance in HCC.

(a) siRNA mini-screen to identify DUBs required for cell survival. USP29 deficiency induces the highest levels of HLE cell apoptosis in response to short-term Sorafenib treatment. ON-TARGET siRNAs against selected DUBs were transfected into HLE cells, and the cells were treated with DMSO or with Sorafenib, respectively, for 18 hours. Immunoblotting for cleaved PARP shows that the depletion of USP29 induced he highest levels of apoptosis compared with other siRNAs. Immunoblotting for β-Tubulin was used as loading control. **(b)** Two distinct siRNAs against USP29 (siUSP29#1 and siUSP29#2) were transfected into HLE cells, and the cells were treated with DMSO or Sorafenib, respectively, for 18 hours. Immunoblotting shows that siUSP29#1 has more knock down efficiency than siUSP29#2, and that the extent of cleaved PARP as measure for apoptosis increased with the knockdown efficiency. Immunoblotting for β-Tubulin was used as loading control. **(c-f)** USP29 deficiency represses cell growth in Sorafenib-resistant cells. Colony formation assays were performed with Huh7-IR cells (c) and Huh7-CR cells (e) transfected with either siCtrl or siUSP29 and treated with increasing concentrations of Sorafenib (0μM,

3μM, 6μM, 9μM) for two weeks. Colony formation was quantified by crystal violet staining (d,f). n = 3 independent replicates. ns = not significant; *, P < 0.05; **, P < 0.01; ***, P < 0.001; Student's t-test. **(g,h)** Immunoblotting analysis revealed that USP29 and HIF1α and its target gene GLUT1 were specifically expressed in Sorafenib-resistant Huh7-IR and Huh7-CR cells (g) and Hep3b-IR and Hep3B-CR cells (h), as compared to their parental Sorafenib-responsive cells, while HIF2α was not. Immunoblotting for β-Tubulin was used as loading control.

3.1.3.5 The USP29-HIF1α axis induces glycolysis to mediate Sorafenib resistance

Besides hypoxia regulation, the transcriptomic analysis of Sorafenib-resistant cells also revealed pathways involved in cellular metabolism (Fig. 1a). In this context, we observed that the color of the culture medium of Sorafenib-resistant cells quickly changed to yellow even when cultured under Sorafenib-free condition as compared to Sorafenib-responsive cells at same cell numbers (Fig. 5a). These observations suggested a general acidification caused by increased glycolysis and production of lactate. Indeed, pH determination revealed lower pH values in the medium of Sorafenib-resistant Huh7-IR and Huh7-CR cells as compared to the parental cells (Fig. 5b). To demonstrate that sorafenib resistance is coupled to glycolysis, we firstly measured glucose uptake and lactate production in sorafenib-resistant Huh7-IR and Huh7-CR and in Sorafenib-responsive parental Huh7 cells. Indeed, we observed higher glucose uptake and lactate production in resistant cells in comparison to the parental cells (Fig. 5c, d). In line with the transcriptomic analysis, a subset of glycolytic gene transcripts was found specifically upregulated in Sorafenib-resistant cells (Fig. 5e). These results indicate a glycolytic shift in sorafenib-resistant cells.

It is widely recognized that glycolysis is an adaptive metabolic response driven by various stresses, such as hypoxia and therapy resistance [198,199]. HIF1α is one of the pivotal regulators of glycolysis by directly transcriptional regulation of key glycolytic genes. Our findings of USP29-HIF1α axis regulating sorafenib resistance motivated us to investigate the functional connection between glycolysis and USP29-HIF1α-driven Sorafenib resistance. To this end, we first assessed the functional contribution of USP29-HIF1α to the acidification of culture medium. In comparison to siControl-transfected cells, siRNA-mediated depletion of USP29 or of HIF1α in Sorafenib-resistant Huh7-IR and Huh7-CR cells prevented culture medium color change and acidification (Fig. 5f-i) and reduced glucose uptake and lactate production (Fig. 5j-m).

We next assessed whether key glycolytic network gene transcripts were changed upon depletion of the USP29-HIF1α pathway in Sorafenib-resistant cells. Interestingly, the expression of *GLUT1, HK2, PDK1, MCT3 and MCT4* was significantly down-regulated in Sorafenib-resistant Huh7-IR and Huh-CR cells upon siRNA-mediated depletion of USP29 and HIF1α, as compared to siControl-transfected cells (Suppl. Fig. 5a, b).

To assess whether Sorafenib resistance is coupled to abnormal glycolysis regulation in HCC of patients, we analyzed the whole proteome of needle biopsies from tumors of Sorafenib responders in comparison to non-responders. Consistent with our *in vitro* analysis, Sorafenib non-responders showed high protein levels of HK2 in contrast to responders, indicating a potential upregulation of glycolysis in Sorafenib-resistant HCC of patients (Fig. 5n).

Altogether, these findings demonstrate that the USP29-mediated stabilization of HIF1α and its transcriptional output promote glycolysis and thus Sorafenib resistance in HCC cells.

Figure 5, Gao et al.

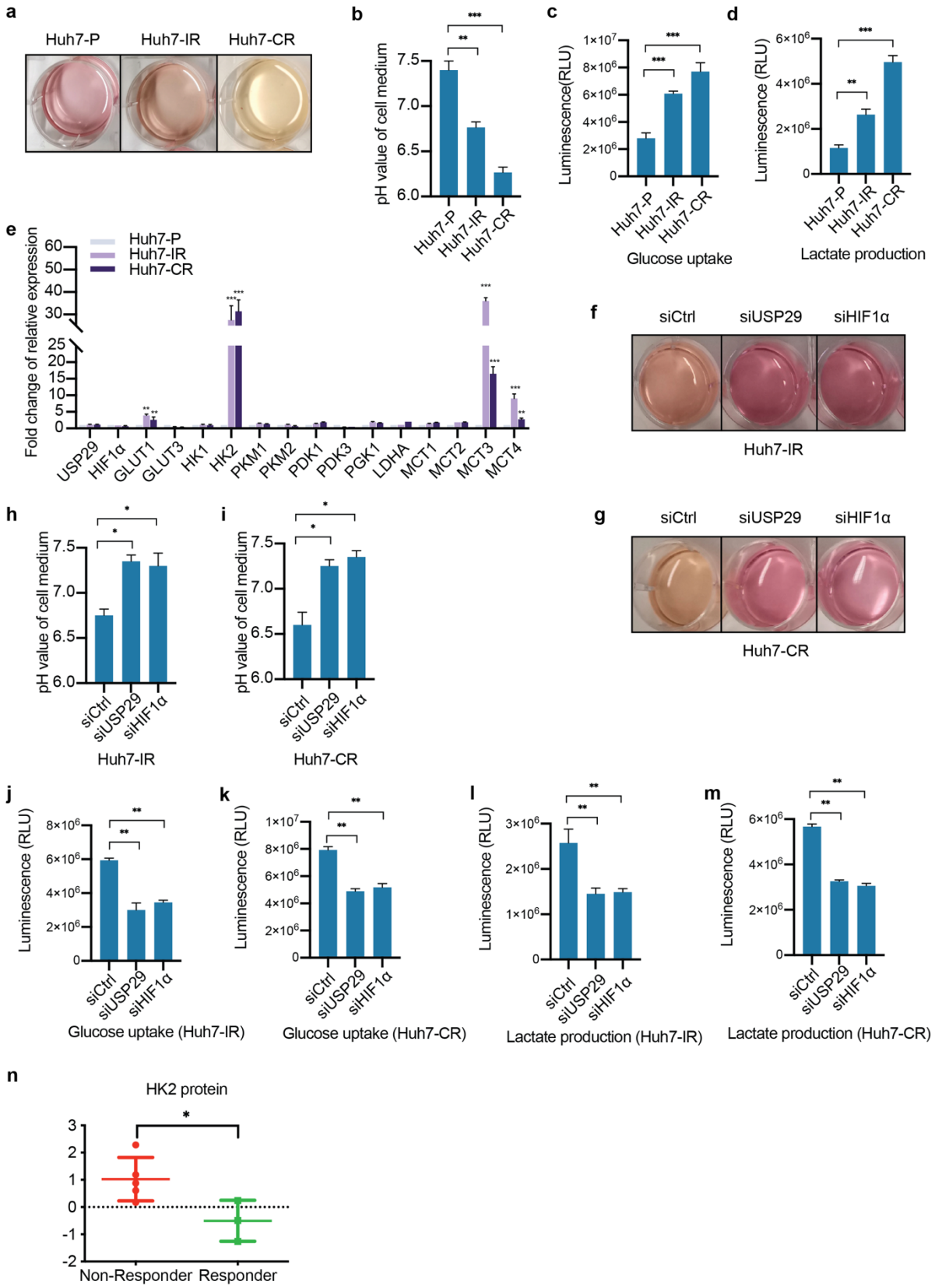

Figure 5. USP29/HIF1α axis in regulation of glycolysis.

(a,b) Huh7-IR/CR cells present increased acidification of cell medium. (a) Cells were plated at same numbers, and color changes of the culture medium were recorded 24 hours after the seeding. (b) pH values of the culture media were directly measured. n=3 independent replicates. **, P < 0.01; ***, P < 0.001; Student's t-test. **(c,d)** Sorafenib-resistant cells present high glycolysis levels. Glucose uptake (c) and lactate production (d) were determined in Sorafenib-responsive Huh7 parental cells and in Sorafenib-resistant Huh7-IR and Huh7-CR cells. Normalized to cell numbers, Huh7-IR/CR cells showed higher glucose uptake and lactate production levels than Huh7 parental cells. n=2 independent replicates. **, P < 0.01; ***, P < 0.001; Student's t-test. **(e)** The mRNA levels of selected subset of glycolysis-related genes were determined by quantitative RT-PCR in Sorafenib-responsive Huh7 parental cells and in Sorafenib-resistant Huh7-IR and Huh7-CR cells. High transcriptional levels of *GLUT1, HK2, MCT3, MCT4* are found in the Sorafenib-resistant cells. Expression of *USP29, HIF1A* was unchanged between Huh7 parental cells and Huh7-IR/CR cells. n = 2 independent replicates). ns = not significant; **, P < 0.01; ***, P < 0.001; Student's t-test. **(f- i)** Depletion of USP29 or HIF1α diminishes the acidification of the culture medium in Sorafenib-resistant cells. Huh7-IR (f) and Huh7-CR (g) cells were plated at the same cell numbers 24 hours after the transfection with siCtlr or siRNAs against USP29 and HIF1α. Color changes were recorded 24 hours later (f,g). pH values of the culture medium were directly measured in Huh7-IR (h) and Huh7-CR (i) cells. n=3 independent replicates. *, P < 0.01; Student's t-test. **(j-m)** USP29 or HIF1α deficiency reduces glycolysis metabolism in Sorafenib-resistant cells. Huh7-IR (j,l) and Huh7-CR (k,m) cells were plated at the same cell numbers and transfected with siCtlr or siRNAs against USP29 and HIF1α. Glucose uptake (j,k) and lactate production (l,m) were examined by determining relative luminescence (RLU) levels 24 hours after siRNA transfection and normalized to cell numbers. n=2 independent replicates. **, P < 0.01; Student's t-test. **(n)** The protein levels of hexokinase 2 (HK2), a major enzyme of the glycolytic pathway, were determined in a database of the whole proteomic analysis of needle biopsies from patients with HCC who responded to Sorafenib treatment (responder) or did not respond (non-responder).

3.1.3.6 USP29 promotes sorafenib resistance in vivo

We next determined whether USP29 is required for Sorafenib resistance *in vivo*. Towards this goal, Sorafenib-resistant SNU398 HCC cells were transfected to stably express a control shRNA against luciferase and a shRNA against USP29. These cells were then implanted into the flanks of immunodeficient NSG mice, which were then treated or not with Sorafenib, and tumor growth was monitored over time. In line with our *in vitro* observations, tumor growth was significantly delayed and tumor weights were found significantly reduced at the end of the experiment upon USP29 knockdown and treatment with Sorafenib (Fig. 6a-c). The results indicate that the ablation of USP29 re-sensitizes Sorafenib-resistant HCC cells to Sorafenib therapy in a preclinical mouse model of HCC *in vivo*. Immunohistochemical staining of tumor sections for USP29 and HIF1α confirmed that the siRNA-mediated ablation of USP29 not only efficiently depleted USP29 but also reduced HIF1α levels (Fig. 6d). Immunohistochemical staining of tumor sections for cleaved Caspase 3 and subsequent quantification revealed that the extent of cancer cell apoptosis was

already increased by Sorafenib treatment but that it was even higher in combination with the depletion of USP29 (Fig. 6d, e).

Finally, to explore whether an increased activity of the USP29-HIF1α axis would also correlate with Sorafenib expression in patient samples, we analyzed their expression in patient-derived xenotransplanted (PDX) tumors which were previously classified as either sensitive or resistant to Sorafenib treatment. Indeed, immunoblotting analysis revealed high protein levels of USP29, HIF1α and its transcriptional target GLUT1 in Sorafenib-resistant PDX tumors as compared to Sorafenib-sensitive PDX tumor (Fig. 6f). Notably, the levels of these proteins were also increased in Sorafenib-sensitive tumors upon acute Sorafenib treatment, while the levels were already very high even without Sorafenib treatment in Sorafenib-resistant tumors.

In conclusion, these data uncovered USP29 as a new regulator of HIF1α transcriptional activity which is critical to maintain Sorafenib-resistance in HCC cells by promoting glycolysis. Hence, the USP29-HIF1α axis represents a potential therapeutic target to overcome Sorafenib resistance in HCC.

Figure 6, Gao et al.

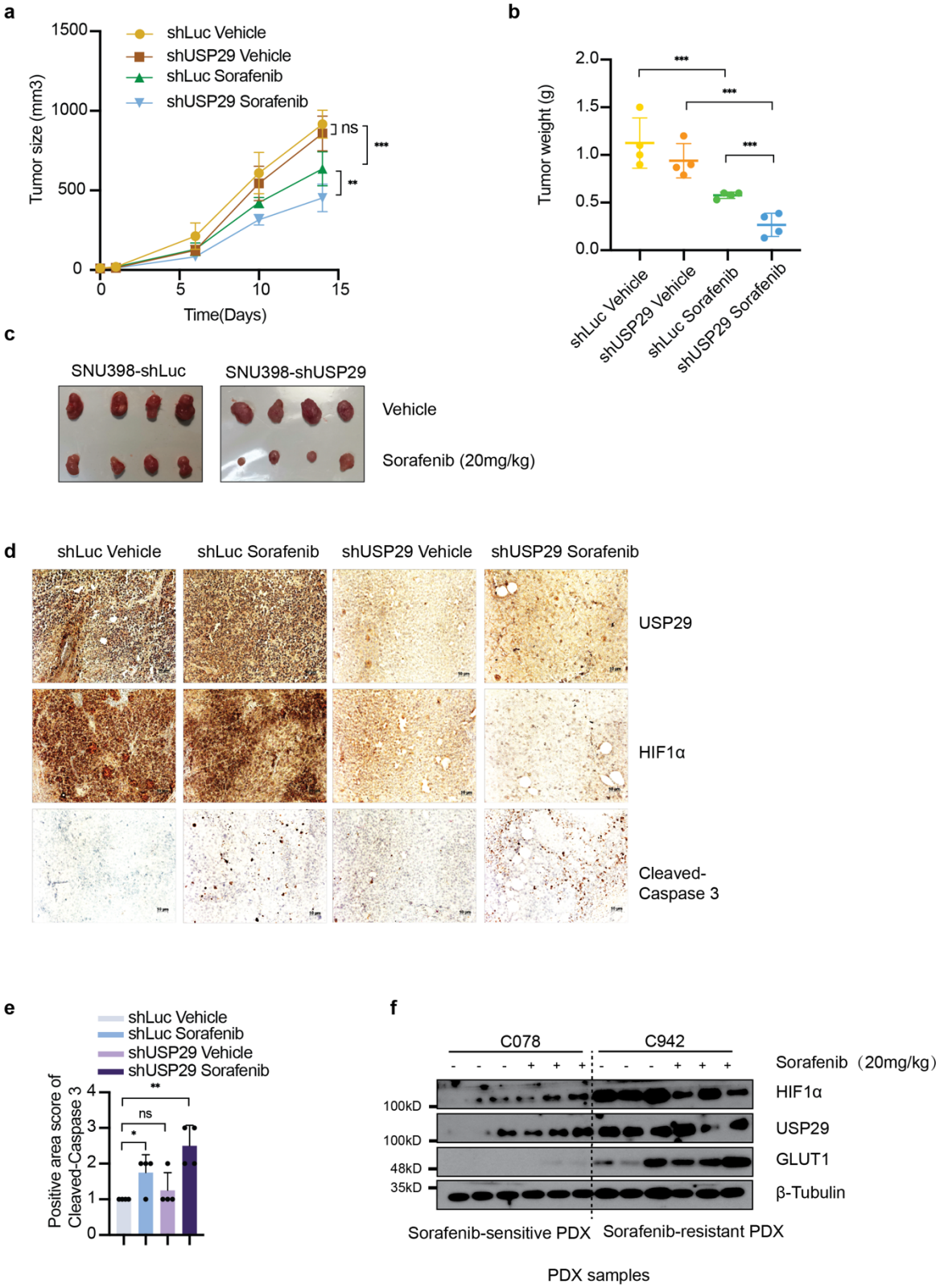

Figure 6. USP29 regulates tumor growth in response to Sorafenib treatment *in vivo.*

(a-c) Xenotransplanted HCC is re-sensitized to Sorafenib treatment upon depletion of USP29. Sorafenib-resistant SNU398 cells expressing either a control shRNA (shLuc) or a shRNA against USP29 (shUSP29) were implanted into the flanks of immunodeficient NSG mice and treated with vehicle solution or Sorafenib, respectively. Tumor

growth curves over time (a) and tumor weights at the time of sacrifice (b) were determined. Images of the tumors at the time of sacrifice are shown in (c). ns = not significant; **, P < 0.01; ***, P < 0.001; Two-way ANOVA. **(d,e)** USP29-deficient tumors exhibit higher rates of apoptosis upon Sorafenib treatment. Histological sections of the tumors described in (a-c) were immunostained for USP29 and HIF1α (d). Immunostaining for cleaved Caspase 3 was used to quantify apoptosis (d, e). **(f)** Sorafenib-resistant PDX tumors present high USP29, HIF1α, and GLUT1 protein levels. Tumor pieces of HCC patient-derived xenotransplanted (PDX) mice which have been previously classified as Sorafenib-responsive or Sorafenib-resistant were analyzed by immunoblotting for the expression of HIF1α, USP29 and GLUT1. Immunoblotting for β-Tubulin was used as loading control.

3.1.4 Discussion

Sorafenib, a small molecule multi-kinase inhibitor, targets Raf-1, B-Raf, vascular endothelial growth factor receptors (VEGFRs) [17,200] and PDGFR-β (platelet-derived growth factor receptor β) involved in cancer cell proliferation, angiogenesis and invasion in a wide range of cancer cells [44,201]. It is the first line of standard therapy that has been approved by the FDA in 2007 for the treatment of advanced HCC patients. However, based on the sobering observation that the targeted therapy with Sorafenib has only a moderate and temporal effect on HCC progression and fails to cure HCC patients, the delineation of the molecular mechanisms underlying Sorafenib resistance and the design and development of alternative therapies overcoming Sorafenib resistance are pivotal medical goals.

Several factors and signaling pathways have been previously reported to contribute to Sorafenib resistance, including the PI3K-AKT, JAK-STAT and ERK2 signaling pathways, epithelial-mesenchymal transition and hypoxia-induced signaling [202,203]. Previous results from our laboratory have identified LATS1 as a regulator of Sorafenib resistance in mediating a cross-talk between Hippo signaling and autophagy [156]. In spite of these meaningful findings, the actual mechanisms of the establishment of Sorafenib resistance and potential therapeutic targets to overcome it still remain widely elusive.

Here we have identified the deubiquitylating enzyme (DUB) USP29 as one critical player in the establishment and maintenance of Sorafenib resistance in HCC cells. USP29 deubiquitylates HIF1α resulting in its stabilization and activation of its transcriptional output. Hypoxia is a key microenvironmental factor promoting cancer progression, including the induction of Sorafenib resistance in several different cancer types [204,205]. As a frequent feature of solid tumors, hypoxia is promoting cancer cell proliferation, tumor angiogenesis, metastasis and metabolic changes which

altogether may cause therapy resistance. Hypoxia inducible factors (HIFs) are transcription factors which execute the progresses in response to oxygen change. HIF1α and HIF2α have been reported highly expressed in HCC and that both contribute to Sorafenib resistance [97,206]. However, we found that HIF1α and not HIF2α is highly in Sorafenib-resistant HCC cells. Moreover, depletion of HIF1α resulted into cell death of Sorafenib-resistant cells, while depletion of HIF2α did not, indicating that HIF1α was the critical player in maintaining Sorafenib resistance in HCC cells. These results are consistent with previous reports suggesting that HIF1α confers Sorafenib resistance in HCC patients [94,207]. However, the actual mechanisms by which HIF1α activity is regulated in Sorafenib-resistant HCC cells and patients has remained unclear.

HIF1α protein stability is regulated by its quality and quantity of ubiquitination. In the presence of sufficient oxygen, it is ubiquitylated by the E3 ligase VHL and then rapidly degraded by the Ubiquitin Proteasome System (UPS) [190-194]. On the other hand, DUBs like USP8, USP28, UCHL1 have been previously identified to stabilize HIF1α by removing the polyubiquitin of HIF1α under either hypoxia or normoxia and thus regulating tumorigenesis and cilia growth [105,106,190]. Employing a functional mini-screen on a selected subset of DUBs we identified USP29 as the most critical DUB in the stabilization and activation of HIF1α and in conferring Sorafenib resistance to HCC cells.

The contribution of DUBs to tumor progression and therapy resistance is not without precedence. For example, USP28 has been reported to stabilize MYC and present high expression levels in colon and breast cancers [208]. USP36 and USP37 have been reported to regulate tumorigenesis by preventing MYC degradation in breast and lung cancer [110,209]. USP7 could stabilize MDM2 to prevent degradation of the tumor suppressor p53 [210,211], and USP8 has been reported a novel target for overcoming Gefitinib resistance in lung cancer [212]. In the context of HCC, it has been reported that USP10 promotes HCC cell proliferation and metastasis by deubiquitylating and stabilizing YAP and TAZ, the effector transcription factors of the Hippo signaling pathway and SMAD4, the major signaling effector of TGFβ signaling [213,214]. As a consequence, first small molecular inhibitors have been developed to interfere with DUB functions. P5091 (inhibitor of USP7) and b-AP15 (inhibitor of USP14/UCHL5) have been reported to repress the growth of bortezomib-resistant

multiple myeloma [215,216]. The USP8 inhibitor 9-ethyloxyimino-9H-indeno (1,2-b) pyrazine-2,3-dicarbonitrile has been shown to suppress the growth of non-small cell lung carcinoma (NSCLC) cells [212]. Here we report by proof-of-concept experiments that the depletion of USP29 is sufficient to re-sensitize HCC cells to Sorafenib therapy *in vitro* and *in vivo*, suggesting USP29 as a novel and suitable target for overcoming Sorafenib resistance in HCC.

Consistent with previous reports [217,218], our transcriptomic analysis of Sorafenib-resistant HCC cells identified glycolysis as highly upregulated metabolic pathway in Sorafenib-resistant cells. Our study demonstrates that USP29 is intimately associated with glycolysis through HIF1α, including glucose uptake and lactate production. Depletion of USP29 reduces glucose homeostasis and lactate production significantly. Downregulations of *GLUT1, HK2, MCT3, MCT4* with USP29 knockdown further support the link between USP29 and glycolysis.

A high level of glycolysis has been proven to contribute to therapy resistance of different types of cancer cells. Along these lines, our laboratory has previously reported that resistance to anti-angiogenic therapy relies on a glycolytic shift which establishes a metabolic symbiosis between hypoxic, glycolytic and lactate-producing tumor cells and normoxic, lactate-importing tumor cells which use lactate and oxygen for oxidative phosphorylation [219]. In these experiments, interference with lactate transport or with glycolysis has overcome therapy resistance, suggesting that also in HCC interference with glycolytic pathways may contribute to overcoming Sorafenib resistance, a notion that warrants further investigation.

In summary, our study identifies USP29 as a novel DUB that stabilizes HIF1α and promotes its transcriptional activity in HCC. This USP29-HIF1α axis induces a glycolytic shift in HCC cells which is coupled with sorafenib resistance. Our study also indicates that USP29 and HIF1α represent translational biomarkers for the prediction of therapy response in HCC patients, highlighting the USP29-HIF1α-glycolysis regulatory network as an emerging therapeutic target to overcome therapy resistance in HCC patients.

3.1.5 Materials and Methods

DNA Constructs, siRNAs and antibodies

A cDNA construct encoding for Flag-HIF1α was amplified from a cDNA library and cloned into pcDNA4.0, and Myc-USP29 was amplified from a cDNA library and cloned into pcDNA4/TO/myc-His B. To generate Myc-USP29-CA, Myc-USP29 was mutated at C294S and H831N. pGL4.42 and pRL-CMV were purchased from Promega. On-target siRNAs were purchased from Dharmacon. siUSP29#1, siUSP29#2 were ordered from Microsynth and list at supplementary table 1. Myc-USP29-R was mutated on Myc-USP29 to be resistant to siUSP29#1, primers are list at supplementary table 1. The Sequences of siRNAs are presented in Suppl. Table I, antibodies used are listed in Suppl. Table II, and oligonucleotides are listed in Suppl. Table III.

Cell culture, transfection and reagents

HEK-293T, SNU398 were obtained from American Type Culture Collection (ATCC), Huh7, HLE, Hep3B were gifts from Dr. Luca Quagliata. All cell lines used in this study were tested for the absence of Mycoplasma contamination every two weeks.

Plasmids transfection into HEK293T cells were carried out using PEI (Polyethylenimine, Linear, MW 25000, Polysciences Catalog No. 23966-1), plasmids transfection into HCC cells were carried out with Lipofectamine 3000 (Invitrogen). siRNA transfections were carried out with Lipofectamine RNAiMAX (Invitrogen) according to the manufacturer's instructions. pBabe-retro-puro or pSuper-retro-puro constructs were used for establishing stable knock-down and stable overexpressing cell lines, Platinium-A cells were used for retrovirus production, infections were performed using 8μg/ml Polybrene.

Dual-Luciferase report assay

Cells were seeded into 24-well plates, transfections of siRNAs were performed once cell confluence had reached 60%. Medium was changed after 8 hours. 24 hours later, pGL4.42 and pRL-CMV were transfected together into cells in a 10:1 mass ratio, and medium was changed after 8 hours. Cells were washed with PBS twice, and *Firefly* luminescence and *Renilla* luminescence were measured using Dual-Luciferase report Assay Kit (Promega E1980) and a (Berthold Centro LB 960).

Glucose uptake assay

Cells were seeded into 96-well plates (5000 cells per well), treated with DMSO or 6µM Sorafenib, respectively, 18 hours later cells were washed with PBS twice and Glucose uptake levels were measured using Glucose Uptake-Glo™ Assay Kit (Promega J1341) and a Berthold luminometer (Berthold Centro LB 960).

L-Lactate assay

Cells were seeded into 96-well plate (5000 cells per well), treated with DMSO or 6µM Sorafenib, respectively, 18 hours later the medium was collected, and cells were washed with PBS twice, and the Lactate levels of cell medium and cells were measured by using Lactate-Glo™ Assay Kit (Promega J5021) and a Berthold luminometer (Berthold Centro LB 960).

Colony formation assay

Cells were seeded into 12-well plates (5000 cells per well) and cultured for 2 weeks, siRNAs were transfected every other day, culture medium with either DMSO or Sorafenib was exchanged every 24 hours. 2 weeks later cells washed with PBS and fixed with 4% Paraformaldehyde for 30 minutes at room temperature, washed with PBS again and stained with crystal violet (1mg/ml dissolved into 10% Ethanol) for 30 minutes at room temperature. After washing with PBS, plates were left to dry and cells stained with crystal violet were counted using Fiji (NIH Image).

Tumor transplantation

SNU398-shLuc or SNU398-shUSP29 cells (1*10^6 in 100µl PBS) were implanted into the left flanks of immuno-deficient NOD/SCID; common γ receptor-/- (NSG) mice. When tumors were palpable, vehicle solution or Sorafenib (20mg/kg) was applied daily via gavage for 3 weeks. Tumor width and length were measured twice a week, tumor volumes were calculated using the formulation of volume = length * width^2*0.52. All animal experiments were performed according the Swiss Federal Animal Welfare Law under approval number 2839 by the Veterinary Office of the Canton Basel Stadt.

Protein lysis, immunoprecipitation, ubiquitination assay

For immunoblotting analysis, cells were washed with 1x PBS twice and lysed with RIPA lysis buffer (Sigma R0278). Cell lysates were centrifuged and the pellets were removed before protein concentration measurement and immunoblotting analysis.
For immunoprecipitation, cells were washed with 1x PBS twice and lysed with CST lysis buffer (CST9803) supplemented with protease inhibitors (Sigma P2714) at 4°C, then centrifuged at 13000rpm for 10 minutes, and pellets were removed. 1/10 of the cell lysate was taken as input, the rest of the cell lysate were incubated with specific antibodies and protein A/G-Sepharose overnight at 4 °C. After 5 times washing with CST lysis buffer, the precipitated proteins were eluted with SDS-loading buffer and analyzed by immunoblotting.
For the ubiquitination assay, cells transfected with plasmids were lysed with RIPA buffer supplemented with additional 0.1% SDS to a final concentration of 0.2% SDS, followed by standard immunoprecipitation protocols.
For immunoblotting analysis, protein samples were fractionated by SDS-PAGE gels and transferred to PVDF membranes, then membranes were blocked with 5% skimmed milk in TBST, and antibodies were incubated with the membranes overnight at 4 °C. Membranes were washed with TBST 3x10 minutes and incubated with the secondary antibodies for 2 hours at room temperature, then washed for 3x10 minutes with TBST. Chemiluminescence was detected with X-Ray films or Fusion machine (Analis) once the membranes were incubated with chemiluminescent HRP substrate (Millipore WBKLS0500). Fiji software was used to quantify the immunoblots by densitometry (NIH Image). Information on the antibodies used is presented in Suppl. Table III.

RNA extraction and real-time PCR

RNA samples were extracted with TRIZOL reagent (Sigma T9424), reverse transcription PCR was performed with Reverse Transcriptase kit (Promega A3803), real-time PCR was performed using Powerup SYBR Green PCR master mix (A25743) and a Step-One Plus real-time PCR machine (Applied Biosystems). Human RPL19 expression was used for normalization. Sequences of primers are list at Suppl. Table IV.

Immunofluorescence

Cells were cultured on coverslips, washed with PBS twice and fixed with 4% Paraformaldehyde for 10 minutes, and then washed twice PBS. Cells were permeabilized with 0.1% Triton (DAPI was also diluted into Triton at 100ng/ml to stain the nucleus) on ice for 10 mins. After three times wash with PBS, cells were blocked with 5% goat serum for 1 hour at room temperature, then incubated with diluted antibodies (in 5% goat serum) overnight at 4°C. Cells were washed with PBS three times then incubated with secondary antibody (1:200 dilution) at room temperature for 1 h. Then cells were washed with PBS three times, and mounting medium was added to mount coverslips to glass slides. Immunofluorescence staining was visualized on Leica DMI 4000/6000 microscope.

Immunohistochemistry

Tumor sections were deparaffinized with 3x10 minutes Roticlear, 2x5 minutes 100% EtOH, 1x10 minutes 90% EtOH, 1x5 minutes 80% EtOH, 1x5 minutes 70% EtOH, 1x5 minutes 30% EtOH, 3x10 minutes PBS. Antigen-retrieval was performed in 10mM pH6.0 citrate buffer in a pressure-cooker, wash 3x10 minutes with 0.3% Trition-100 in PBS. Quench peroxidase with 3% H_2O_2 for 10 minutes, wash 3x10 minutes PBS, then block with 2.5% goat serum for 30 minutes at room temperature. Incubation with primary antibody (diluted into 2.5% goat serum) was at 4 °C overnight, followed by washing 3x10 minutes with PBS, incubation with secondary antibody (Vector MP-7541-50) at room temperature for 30 minutes, washing 3x10 minutes with PBS, incubation with peroxidase substrate (Vector SK-4105) at room temperature for 5 minutes and washing with water for 5 minutes. Counterstaining with Hematoxylin was done for 1 min to stain nuclei, followed by washing with water for 5 minutes, and dehydration with 50% EtOH, 70% EtOH and 95% EtOH for 5 minutes each, then 2x10 minutes 100% EtOH, and clearing with 2x10 minutes xylene. Coverslip were mounted with 2 to 3 drops mounting media (Thermo Fisher Scientific Cytoseal™ XYL mounting media 8312-4) and let try overnight. Slides were imaged with a Zeiss brightfield microscope (Zeiss Axioskop 2 Plus) and analyzed with Fiji (NIH Image). Positive area scores were defined as: 1: 0-25% positive area, 2: 26%-50% positive area, 3: 51%-75% positive area, 4: 76%-100% positive area.

RNA sequencing analysis

RNA was extracted in biological triplicates using miRNeasy Mini kit (Qiagen) according to the manufacturer's instructions. RNA quality control was performed using a fragment analyser and the standard or high-sensitivity RNA analysis kits (Labgene; DNF-471-0500 or DNF-472-0500). RNA concentrations were measured using the Quanti-iTTM RiboGreen RNA assay Kit (Life Technologies/Thermo Fisher Scientific). A total of 200ng of RNA was utilized for library preparation with the TruSeq stranded total RNA LT sample prep Kit (Illumina). Poly-A + RNA was sequenced with HiSeq SBS Kit v4 (Illumina) on an Illumina HiSeq 2500 using protocols defined by the manufacturer.

Single-end RNA-seq reads (81-mers) were mapped to the human genome assembly, version hg19 (GRCh37.75), with RNA-STAR [220], with default parameters except for allowing only unique hits to genome (outFilterMultimapNmax=1) and filtering reads without evidence in spliced junction table (outFilterType="BySJout"). Expression levels per gene (counts over exons) for the RefSeq mRNA coordinates from UCSC (genome.ucsc.edu, downloaded in December 2015) were quantified using qCount function from QuasR package (version 1.12.0). The differentially expressed genes were identified using the edgeR package (version 3.14.0). Genes with p-values smaller than 0.05 and minimum log2-fold changes of +/-0.58 were considered as differentially regulated and were used for downstream functional and pathway enrichment analysis.

Functional enrichment analysis

We performed functional enrichment analysis of differentially expressed genes for biological processes or pathways in R using several publicly available Bioconductor resources including org.Hs.eg.db (version 3.3.0), GO.db (version 3.4.1), GOstats (version 2.42.0) [221], KEGG.db (version 3.2.3) and ReactomePA (version 1.16.2) [222]. The significance of each biological processes or pathways identified was calculated using the hypergeometric test (equivalent to Fisher's exact test) and those with p values ≤0.05 were considered significant.

Gene set enrichment analysis (GSEA)

The GSEA analysis was performed using the JAVA application of the Broad Institute version 3.0 (http://www.broadinstitute.org/gsea). The gene sets used for the analysis were derived from gene ontology annotations, and pathways were obtained from the

Kyoto Encyclopedia of Genes and Genomes (KEGG) (http://www.genome.jp/kegg/) databases.

Patient material and ethics

All relevant ethical regulations were strictly followed in this study. All the analysis using human tissue samples reported in this study were approved by the ethics commission of Northwestern Switzerland (EKNZ, approval No.361/12).

Statistical analysis

All statistical tests were two-sided. Data are presented as mean. Bar plots with error bars represent mean ± standard derivation (SD). Statistical significance is defined as *, $P<0.05$; **, $P<0.01$; ***, $P<0.001$. All analyses were performed using Prism 8.0 (Graphpad Software, Inc., La Jolla, CA).

Data availability

The RNA sequencing files are deposited on GEO database with an accession number GSE158458.

3.1.6 Supplementary Information

Supplementary Figures

Suppl. Figure 1, Gao et al.

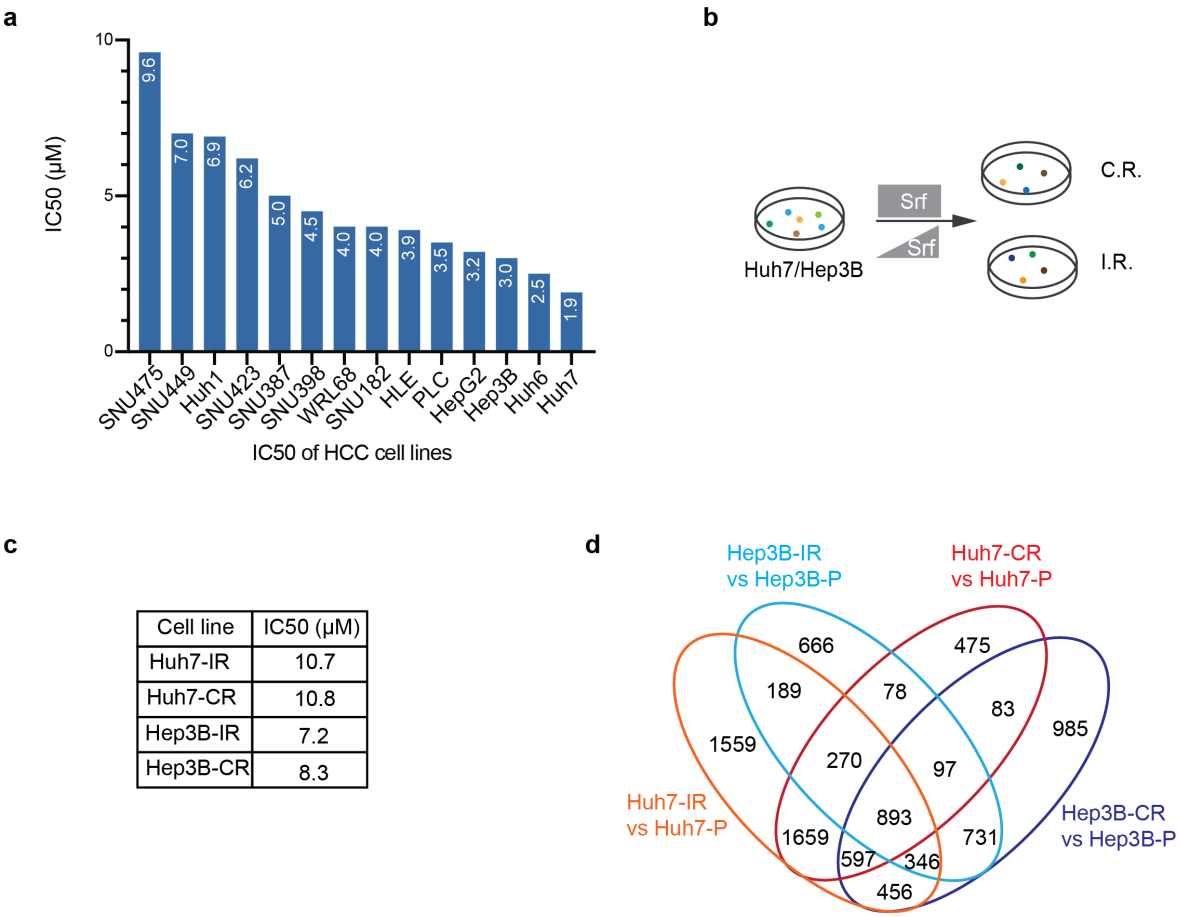

Cell line	IC50 (μM)
Huh7-IR	10.7
Huh7-CR	10.8
Hep3B-IR	7.2
Hep3B-CR	8.3

Supple. Figure 1. Establishment of Sorafenib-resistant cell lines and RNA sequencing.
(a) IC50 for Sorafenib responsiveness of different HCC cell lines. Different patient-derived HCC cell lines were treated with increasing doses of Sorafenib, and the IC50 values for cell growth inhibition by Sorafenib were determined. Hep3B and Huh7 were selected as two Sorafenib-responsive and HLE and SNU398 as moderate Sorafenib-resistant HCC cell lines. **(b)** Schematic representation of the establishment of Sorafenib-resistant derivatives of HUH7 and Hep3B HCC cell lines. Huh7 or Hep3B cells were treated with increasing or with consistently high concentration Sorafenib to establish acquired Sorafenib-resistant cell lines. **(c)** Sorafenib IC50 values of Huh7-IR, Huh7-CR and Hep3B-IR and Hep3B-CR. These IC50 values are fairly close to Sorafenib's clinically relevant concentration of 10μM. **(d)** Differential gene expression between the four Sorafenib-resistant cell lines and their Sorafenib-responsive ancestors. The Venn diagram shows the numbers of genes that are differentially expressed between individual parental and Sorafenib resistant cells and the number of genes which are changing with Sorafenib in several or all of the cell lines.

Suppl. Figure 2, Gao et al.

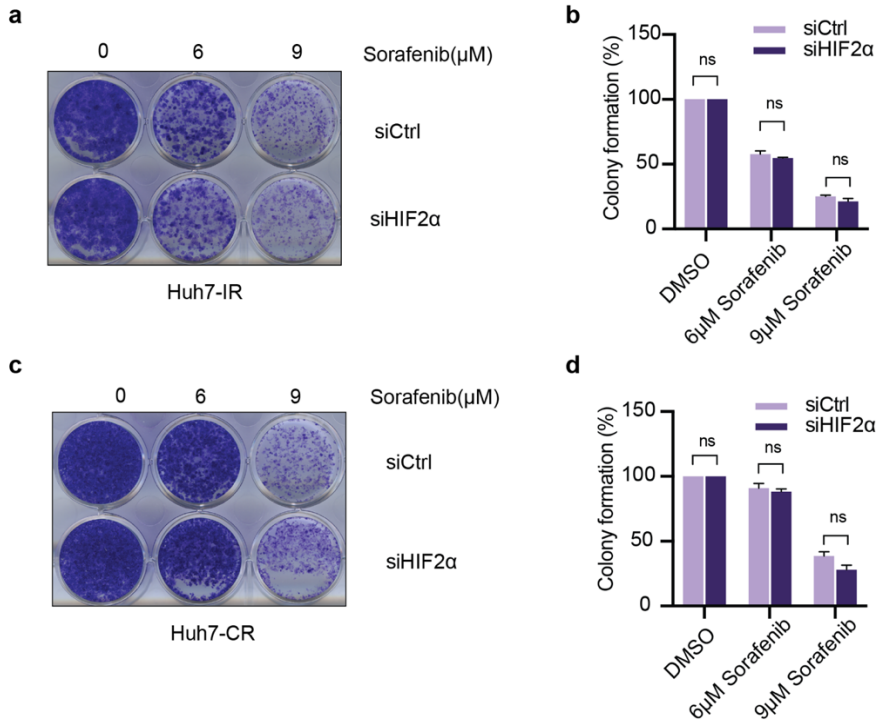

Suppl. Figure 2. HIF2α is not required for Sorafenib resistance.

(a-d) HIF2α's loss of function has no effect on cell death with Sorafenib treatment.

Huh7-IR (a, b) or Huh7-CR (c, d) cells were transfected with siCtrl or siHIF2α and treated with DMSO or with 6μM or 9μM Sorafenib for 2 weeks. Colony formation assays (a, c) and quantification of colony formation by crystal violet staining (b, d) did not revealed any effect on colony formation by the siRNA-mediated depletion of HIF2α.

Suppl. Figure 3, Gao et al.

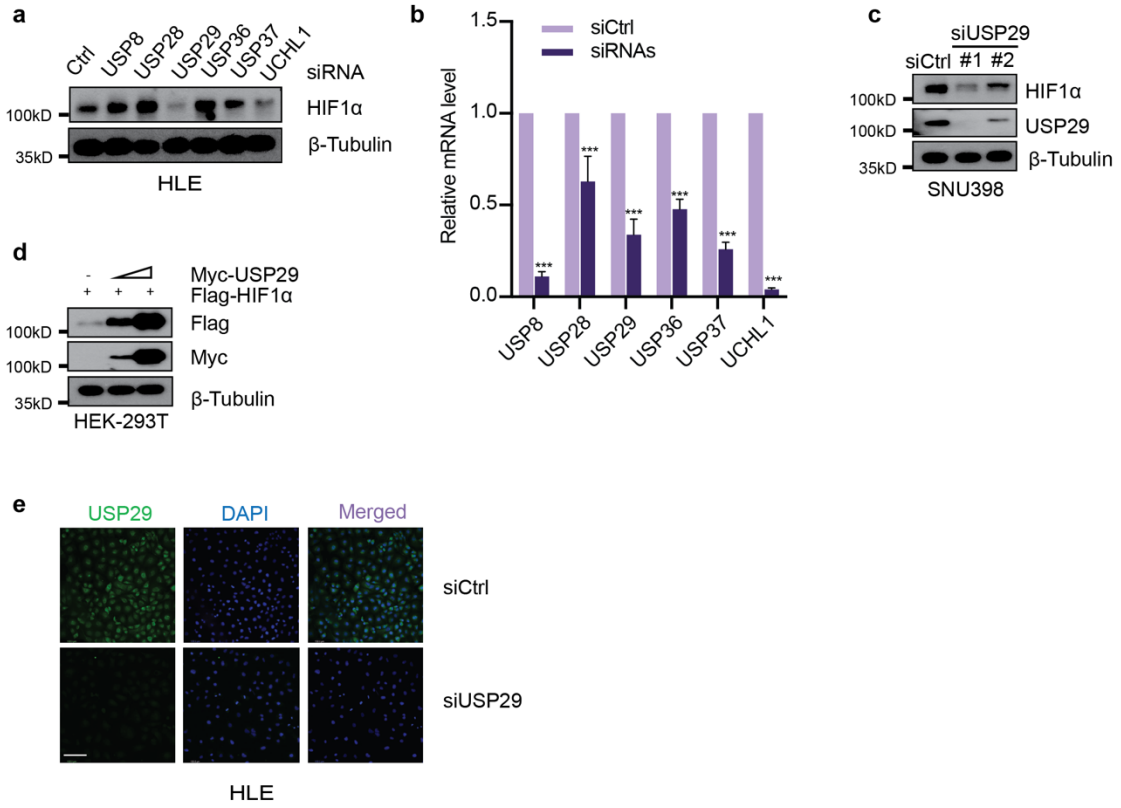

Suppl. Figure 3. USP29 has a positive correlation with HIF1α.

(a) Identification of USP29 as a DUB of HIF1α. A mini-screen with siRNAs against a selected panel of DUBs in Sorafenib-resistant HLE cells revealed that USP29 is one of the most critical players in stabilizing HIF1α protein, as revealed by immunoblotting for HIF1α. Immunoblotting for β-Tubulin was used as loading control. **(b)** Knock down efficiencies of the siRNAs used in (a). Different siRNAs targeting USP8, USP28, USP29, USP36, USP37, UCHL1 were transfected into HLE cells, quantitative RT-PCR analysis were conducted to determine knock down efficiencies. **(c)** Loss of USP29 results in instability of HIF1α protein in Sorafenib-resistant SNU398 cells. Two distinct siRNAs against USP29 (siUSP29#1 and siUSP29#2) were transfected into SNU398 cells and the protein levels of HIF1α, and USP29 was determined by immunoblotting analysis. Immunoblotting for β-Tubulin was used as loading control. **(d)** USP29 stabilizes HIF1α. HEK293T cells were transfected with a plasmid encoding for Flag-HIF1α together with increasing amounts of plasmid encoding for Myc-USP29. HIF1A and USP29 protein levels were determined by immunoblotting against Flag (Flag-HIF1α) and Myc (Myc-USP29). Immunoblotting for β-Tubulin was used as loading control. **(e)** Knockdown efficiency of siUSP29. HLE cells were transfected with siCtrl and siUSP29 and the expression and localization of USP29 was monitored by immunofluorescence microscopy analysis. DAPI was used to visualize nuclei. Scale bars, 132.5μm.

Suppl. Figure 4, Gao et al.

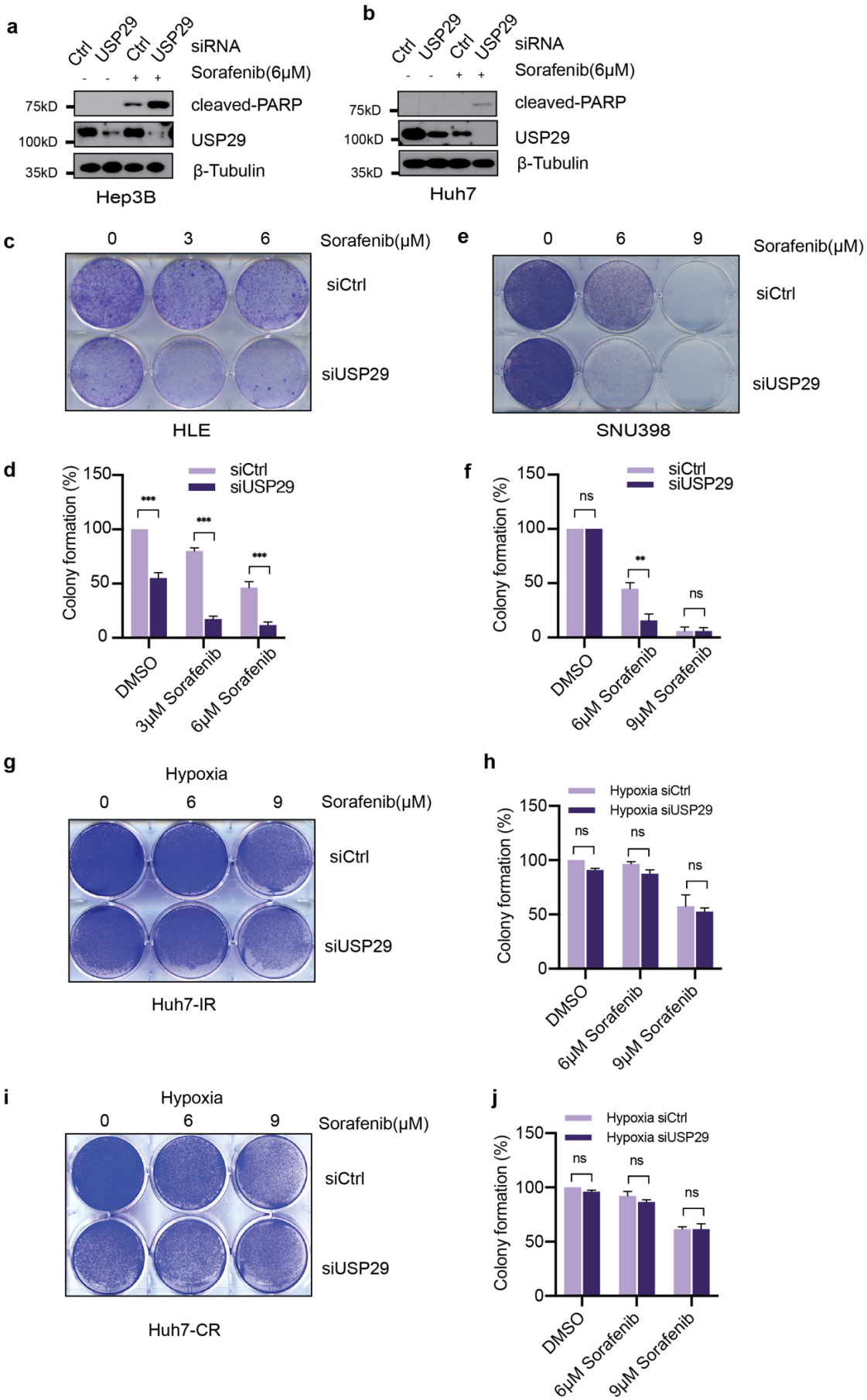

Suppl. Figure 4. USP29 deficiency promotes Sorafenib-induced cell death which can be overcome by hypoxia.

(a,b) Loss of USP29 induces cell death upon Sorafenib treatment in Hep3B and Huh7 cells. Hep3B and Huh7 cells were transfected with siCtrl or siUSP29 and treated with Sorafenib for 18 hours. Immunoblotting for cleaved PARP visualizes the levels of apoptosis. **(c-f)** USP29 deficiency diminishes cell survival in Sorafenib-resistant cell lines. Sorafenib-resistant cell lines HLE (c, d) and SNU398 (e,f) were transfected with siCtrl or siUSP29 and plated for colony formation assays (c,e) under treatment with different concentrations of Sorafenib for 2 weeks. Quantification of colony formation by crystal violet staining (d, f) revealed decreased cell survival upon loss of USP29 expression and Sorafenib treatment in comparison with controls. n = 3 independent replicates. ns = not significant; *, $P < 0.05$; **, $P < 0.01$; ***, $P < 0.001$; Student's t-test. **(g-j)** Hypoxia treatment rescues cell death induced by USP29 deficiency and Sorafenib treatment. Colony formation assays were conducted on Huh7-IR (g, h) and Huh7-CR (i,j) cells, cells were transfected with siCtrl or siUSP29 and cultured under normoxia or hypoxia condition together with different concentrations of Sorafenib treatment for 2 weeks in a colony formation assay (g,i). Quantification of colony growth by crystal violet staining (h,j) revealed the cell death induces by loss of USP29 expression and Sorafenib treatment under normoxic culture conditions could be overcome by culturing the cells in hypoxia. n = 3 independent replicates. ns = not significant; *, $P < 0.05$; **, $P < 0.01$; ***, $P < 0.001$; Student's t-test.

Suppl. Figure 5, Gao et al.

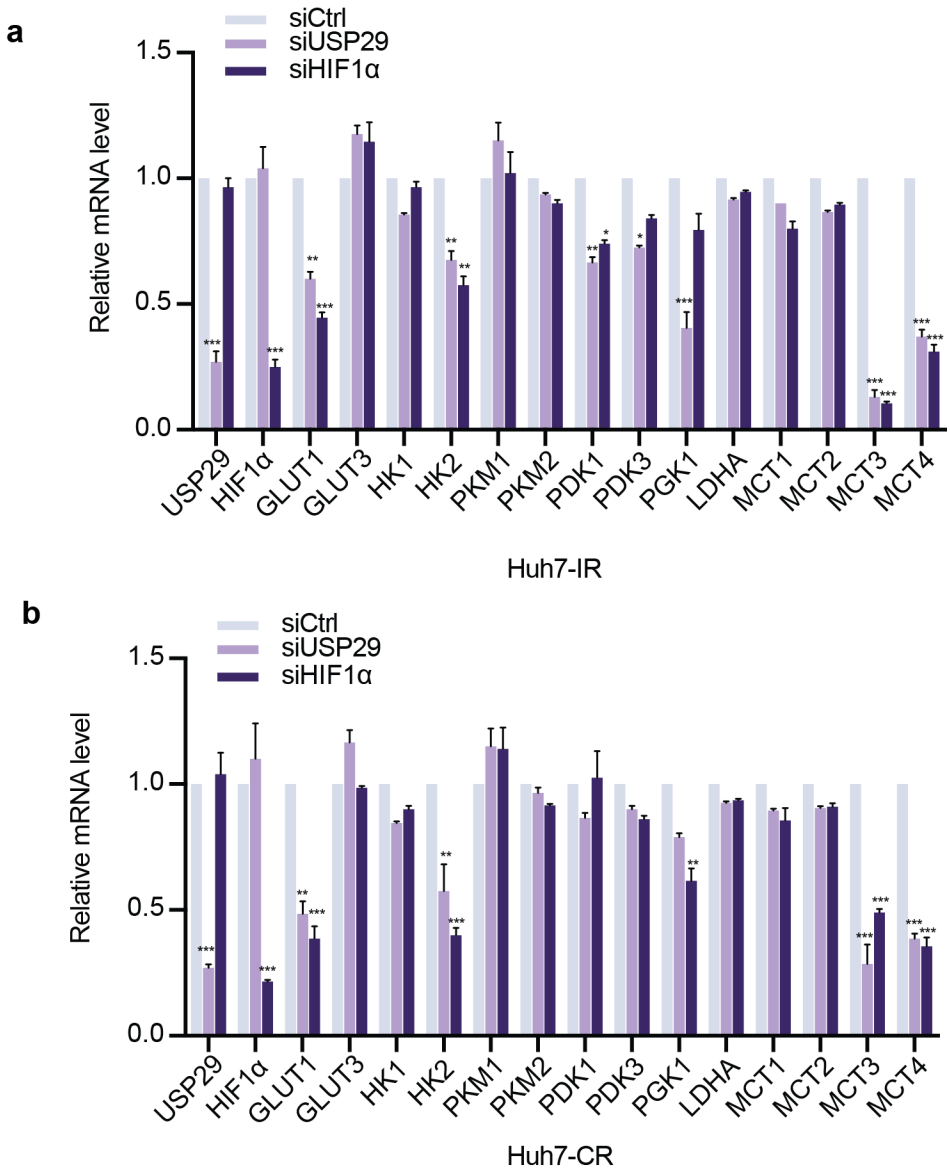

Suppl. Figure 5. The USP29-HIF1α axis regulates glycolysis in Sorafenib resistant cells.

(a,b) Knockdown of USP29/HIF1α diminishes the expression of glycolysis-related genes in Sorafenib resistant Huh7-IR (a) and Huh7-CR (b) cells. Transcriptions of glycolysis metabolism were measured by quantitative RT-PCR with siRNA-mediated depletion of either USP29 or HIF1α. The expression *GLUT1, HK2, PDK1, PDK3, PGK1, MCT3, MCT4* showed decreased mRNA levels upon depletion of USP29 or HIF1α. n = 2 independent replicates). ns = not significant; *, P < 0.05; **, P < 0.01; ***, P < 0.001; Student's t-test.

Suppl. Table I. siRNAs used in the study.

	SOURCE/Sequence (5' --- 3')
siUSP8	ON-TARGET plus Human USP8 (9101)
siUSP28	ON-TARGET plus Human USP28 (57646)
siUSP29	ON-TARGET plus Human USP29 (57663)
siUSP36	ON-TARGET plus Human USP36 (57602)
siUSP37	ON-TARGET plus Human USP37 (57695)
siUCHL1	ON-TARGET plus Human UCHL1 (7345)
siHIF1α	ON-TARGET plus Human HIF1A (3091)
siHIF2α	ON-TARGET plus Human EPAS1 (2034)
siUSP29#1	CCCAUCAAGUUUAGAGGAUdTdT
siUSP29#2	GGAAUAUGCUGAAGGAAAUdTdT
shUSP29-Forward	GATCCCCCCATCAAGTTTAGAGGATTTCAAGAGAAT CCTCTAAACTTGATGGGTTTTTGGAAA
shUSP29-Reverse	AGCTTTTCCAAAAACCCATCAAGTTTAGAGGATTCTC TTGAAATCCTCTAAACTTGATGGGGG
Myc-USP29-RNAi-resistant-Forward	GGAAGAACCCTTCTAGCCTCGAAGACTTAGAAAAAGATA
Myc-USP29-RNAi-resistant-Reverse	TATCTTTTTCTAAGTCTTCGAGGCTAGAAGGGTTCTTCC

Suppl. Table II. Antibodies used in the study.

Antibodies	SOURCE	IDENTIFIER
HIF1α	Novus	NB100-449
HIF2α	Novus	NB100-122
USP29	Eurogentec	Peptide:1810359-1479
GAPDH	Abcam	ab9485
β-Tubulin	CST	2128
GLUT1	Abcam	ab652
Flag tag	Sigma	F1804
Myc tag	CST	2276

HA tag	CST	2362
Cleaved-PARP	CST	5625
Histone 3	Abcam	ab1791
Cleaved-caspase3	CST	9661

Suppl. Table III. Oligonucleotides used in the study.

Oligonucleotides	5' --- 3'
hRPL19, forward primer	GATGCCGGAAAAACACCTTG
hPRL19, reverse primer	TGGCTGTACCCTTCCGCTT
HIF1α, forward primer	GAACGTCGAAAAGAAAAGTCTCG
HIF1α, reverse primer	CCTTATCAAGATGCGAACTCACA
USP29, forward primer	GGTGCCTCTTGACTCTCATTC
USP29, reverse primer	TGGGACACCTTGAGTGAGTAAG
GLUT1, forward primer	TTGCAGGCTTCTCCAACTGGAC
GLUT1, reverse primer	CAGAACCAGGAGCACAGTGAAG
GLUT3, forward primer	CAGAACCAGGAGCACAGTGAAG
GLUT3, reverse primer	TTGAACACCTGCATCCTTGA
HK1, forward primer	GCCACGATGAACCAAGGAATGG
HK1, reverse primer	GACAATG TGATCAAACAGCTC
HK2, reverse primer	GAGTTTGACCTGGATGTGGTTGC
HK2, forward primer	CCTCCATGTAGCAGGCATTGCT
PKM1, forward primer	CTATCCTCTGGAGGCTGTGC
PKM1, reverse primer	CGCACAAGTTCTTCAAACAGC
PKM2, forward primer	CTATCCTCTGGAGGCTGTGC
PKM2, reverse primer	GTGGGGTCGCTGGTAATG
LDHA, forward primer	GGATCTCCAACATGGCAGCCTT
LDHA, reverse primer	AGACGGCTTTCTCCCTCTTGCT
PDK1, forward primer	CATGTCACGCTGGGTAATGAGG
PDK1, reverse primer	CTCAACACGAGGTCTTGGTGCA
PDK3, forward primer	TGGAAGGAGTGGGTACTGATGC
PDK3, reverse primer	GGATTGCTCCAATCATCGGCTTC
MCT1, forward primer	TTGTTGGTGGCTGCTTGTCAGG

MCT1, reverse primer	TCATGGTCAGAGCTGGATTCAAG
MCT2, forward primer	TGCTGGCTGTTATGTACGCAGG
MCT2, reverse primer	TGCTGGCTGTTATGTACGCAGG
MCT3, forward primer	TGCAGTTCGAGGTGCTCATGGC
MCT3, reverse primer	GTTCTTCAACACATCCACCAGGC
MCT4, forward primer	CGTTCTGGGATGGGACTGAC
MCT4, reverse primer	ATGTGCCTCTGGACCATGTG
AXL, forward primer	GTTTGGAGCTGTGATGGAAGGC
AXL, reverse primer	CGCTTCACTCAGGAAATCCTCC
AHNAK2, forward primer	GAGAAGGAGGACACGGATGTTGC
AHNAK2, reverse primer	CCCCGCTTGCTCTTTATGGATTG
VEGFA, forward primer	AGGGCAGAATCATCACGAAGT
VEGFA, reverse primer	AGGGTCTCGATTGGATGGCA
USP8, forward primer	TTCCATTCAATACTTGGACCTGG
USP8, reverse primer	CCAAAGAGCCTTTAGCCAATGT
USP28, forward primer	CACTGTTGCTACAGAACCATCT
USP28, reverse primer	TGGGAGACTCCAGTAGACTCA
USP36, forward primer	TCTGCCAAGAAGGTCCTTTTACA
USP36, reverse primer	TGGCGACTAGCTCCCTCTG
USP37, forward primer	CCAGTGGAGCGAAACAAAGC
USP37, reverse primer	CCTCTGCATCCTTACTTGGTACT
UCHL1, forward primer	CCTGTGGCACAATCGGACTTA
UCHL1, reverse primer	CATCTACCCGACATTGGCCTT

3.1.7 Acknowledgements

We thank C. Beisel and the Genomics Facility Basel for RNA-sequencing. E. Antoniadis, U. Schmieder and the DBM animal core facility for the support with animal experiments, and P. Lorentz and the DBM microscopy facility for imaging.

3.1.8 Author contributions

R.G, F.T. and G.C conceived this study. R.G. and F.T. designed and performed the experiments, analyzed the data and wrote the manuscript. G.C. designed the

experiments and wrote the manuscript. D.B, F.T. and M.F.M established the cell lines. R.K.R.K analyzed the RNA-sequencing data. Q.C. and M.H. established the PDX model and provided the samples. E.D. and M.N.H. analyzed the proteome of patient samples.

3.2 YAP/TAZ and ATF4 collaboratively drive resistance to Sorafenib therapy in hepatocellular carcinoma by preventing ferroptosis

Ruize Gao[1], Ravi K.R. Kalathur[1], Mairene Coto-Llerena[2], Caner Ercan[2], David Buechel[1], Song Shuang[4], Salvatore Piscuoglio[2], Michael T. Dill[3], Fernando D. Camargo[3], Gerhard Christofori[1*]and Fengyuan Tang[1*]

[1]Department of Biomedicine, University of Basel, Basel, Switzerland;
[2]Institute of Pathology, University Hospital Basel, Basel, Switzerland;
[3]Stem Cell Program, Boston Children's Hospital, Boston, MA 02115, USA; Department of Stem Cell and Regenerative Biology, Harvard University, Cambridge, MA 02138, USA.
[4]Friedrich Miescher Institute for Biomedical Research, Basel, Switzerland

[*]**Corresponding authors:**
Fengyuan Tang and Gerhard Christofori
Department of Biomedicine, University of Basel
Mattenstrasse 28, CH-4058 Basel, Switzerland
Tel. +41 61 207 35 62
Fax. +41 61 207 35 66

Manuscript is in revision with “EMBO Molecular Medicine”

3.2.1 Abstract

Understanding the mechanisms underlying evasive resistance in cancer is an unmet medical need to improve the efficacy of current therapies. In this study, a combination of shRNA-mediated synthetic lethality screening and transcriptomic analysis revealed the transcription factors YAP/TAZ as key drivers of Sorafenib resistance in hepatocellular carcinoma (HCC) by repressing Sorafenib-induced ferroptosis. Mechanistically, in a TEAD-dependent manner YAP/TAZ induce the expression of SLC7A11, a key transporter maintaining intracellular glutathione homeostasis, thus enabling HCC cells to overcome Sorafenib-induced ferroptosis. At the same time, YAP/TAZ sustain the protein stability, nuclear localization and transcriptional activity of ATF4 which in turn cooperates to induce SLC7A11 expression. Our study uncovered a critical role of YAP/TAZ in the repression of ferroptosis and thus in the establishment of Sorafenib resistance in HCC, highlighting YAP/TAZ-based rewiring strategies as potential approaches to overcome HCC therapy resistance.

3.2.2 Introduction

Liver cancer is the second leading cause of cancer-related mortality in patients. Hepatocellular carcinoma (HCC) represents about 90% of all cases of primary liver cancer [187,223]. Although cancer therapies have substantially improved clinical outcome [224,225], patients invariably experience cancer relapse. Thus, understanding the mechanisms underlying evasive resistance of HCC is an unmet medical need.

Ferroptosis is an emerging type of cell death induced by metal iron and reactive oxygen species and driven by lipid peroxidation [226,227]. Among the core regulatory components, the cystine-glutamate antiporter known as system Xc- or xCT (SLC7A11, encoded by the gene *SLC7A11*) imports cystine for the *de novo* synthesis of the important anti-oxidant peptide glutathione (GSH). GSH, among many functions, is also used as a substrate of Phospholipid-Hydroxyperoxid-Glutathione-Peroxidase (GPX4) to catalyze the detoxification of phospholipid hydroperoxides [228]. Hence, ferroptosis can be potently induced by cysteine deprivation and GPX4 inhibition. Small pharmacological inhibitors, including the GPX4 inhibitor RSL3, and Erastin and

Sorafenib as direct inhibitors of xCT-mediated import function, are widely used for the induction of ferroptosis [226,228].

YAP/TAZ are well characterized transcriptional effectors of Hippo signaling involved in a variety of physio-pathological processes, including tumorigenesis and tissue regeneration [229,230]. Previous studies have suggested the Hippo-YAP/TAZ pathway is a key driver of ferroptosis in epithelial tumors [231,232]. Here, we aimed at dissecting the molecular drivers of Sorafenib resistance in HCC and identified YAP/TAZ as negative regulators of ferroptosis. In a TEAD- and ATF4-dependent manner, YAP/TAZ induce the expression of SLC7A11, thus assisting cells in overcoming Sorafenib-induced ferroptosis. Moreover, the data suggest YAP/TAZ as key chaperones in stabilizing ATF4 protein and sustaining its nuclear transcriptional activity. Our study thus highlights YAP/TAZ as novel repressors of ferroptosis and, thus, as attractive therapeutic targets to overcome therapy resistance.

3.2.3 Results

3.2.3.1 Identification of YAP/TAZ as key drivers of Sorafenib resistance

To identify the molecular mechanisms underlying therapy resistance in HCC, we had previously established Sorafenib-resistant HCC cell lines, called Huh7-IR and Huh7-CR and Hep3B-IR and Hep3B-CR, as compared to their Sorafenib-sensitive parental cell lines Huh7 and Hep3B [233]. Global transcriptomic analysis between the Sorafenib-sensitive parental cells and their Sorafenib resistant derivates revealed that, in addition to changes in various signaling pathways, cellular metabolism pathways had dynamically shifted in HCC cells upon the establishment of Sorafenib resistance, including amino acid metabolism (**Suppl. Figure 1a; Suppl. Table I**).

To functionally identify intrinsic drivers of Sorafenib resistance in HCC cells, we performed a genome-wide shRNA-mediated synthetic lethality screen in Sorafenib resistant HCC cells (**Figure 1a**). Notably, we turned our focus on the identification of factors and pathways involved in the establishment of adaptive resistance to Sorafenib, as opposed to the factors and pathways activated during an acute response to Sorafenib treatment. Huh7-IR and Huh7-CR cells were transfected with a shRNA library selected to target all genes known to play a role in cell signaling and covering each gene with at least 8 independent shRNA sequences. Cells were then cultured for 4 weeks under selection conditions in the presence of Sorafenib. Then, genomic

DNA was extracted, and shRNA barcodes were amplified for next-generation sequencing to identify shRNAs and their target genes which have been lost during long-term culture, indicating that these genes may be critical for the maintenance of Sorafenib resistance. shRNAs which had dropped out in parental Huh7 cells upon acute treatment with Sorafenib were subtracted from the list, to only enrich for the genes critical for the maintenance of Sorafenib resistance, a total of 1072 genes were identified (**Supple. Figure 1b; Supple. Table II**). We also reasoned that critical drivers of Sorafenib resistance were deregulated at a transcriptional level during the adaptive reprogramming. Thus, we overlaid the hits from the synthetic lethal screen with the list of genes differentially regulated during the establishment of therapy resistance. This analytical combination revealed a total of 38 significant hits, among which eight genes were retrieved by more than three independent shRNA sequences and their gene regulation was highly significant (**Figure 1b; Suppl. Table III**). Interestingly, among these eight top candidate genes was the Hippo pathway transducer WWTR1 (also known as TAZ).

The mammalian Hippo pathway has been previously implicated in tumorigenesis and therapy response in liver cancers [230], and YAP and TAZ are well established Hippo transducers sharing redundant functional read-outs [234]. Thus, we next focused our analysis on examining the expression of YAP and TAZ in Sorafenib-sensitive and resistant HCC cell lines. Indeed, we found high expression of YAP and TAZ in Sorafenib-resistant cells as compared to their sensitive counterparts (**Figure 1c**). Importantly, shRNA-mediated ablation of YAP and TAZ expression revealed that they were required to maintain the acquired resistance to Sorafenib, as determined by a colony formation assay (**Figure 1d**).

Together, these data indicate that YAP and TAZ represent critical drivers of acquired resistance to Sorafenib in HCC cells.

3.2.3.2 YAP/TAZ promote resistance by antagonizing Sorafenib-induced ferroptosis

To investigate the molecular mechanisms underlying YAP/TAZ-driven Sorafenib resistance, we analyzed the global transcriptomic changes upon loss of YAP and TAZ in intrinsically Sorafenib-resistant HLE cells by RNA sequencing. Interestingly, among the deregulated pathways, the genes involved in the regulation of lipid peroxidation, a hallmark of ferroptosis, were found to be significantly enriched (**Figure 1e**). Notably, Sorafenib is known to potently promote ferroptosis by blocking SLC7A11-mediated

cellular cystine import[235]. We thus sought to validate the role of YAP and TAZ in the regulation of Sorafenib-induced lipid reactive oxygen species (ROS). Indeed, loss of YAP and TAZ resulted in upregulated basal levels of ROS (**Figure 1f**). Moreover, loss of function of YAP and TAZ resulted in increased lipid peroxidation not only at a basal level (**Figure 1g**), but also under treatment with Sorafenib or H_2O_2 (**Suppl. Figure 1c**). Furthermore, Ferrostatin-1, a specific inhibitor of ferroptosis [226], prevented YAP/TAZ deficiency-induced lipid peroxidation. Consistent with these notions, intracellular GSH levels were decreased upon downregulation of YAP and TAZ (**Suppl. Figure 1d**).

Based on these observations, we hypothesized that YAP and TAZ promoted Sorafenib-resistance by detoxifying Sorafenib-induced ferroptosis. We thus assessed whether Ferrostatin-1 can prevent the cell death induced by Sorafenib upon loss of YAP and TAZ. Indeed, Ferrostatin-1 fully restored the viability of YAP/TAZ-deficient cells in the presence of Sorafenib, as determined by a colony formation assay (**Figure 1h**). We further asked whether YAP/TAZ were able to antagonize ferroptosis in a general manner, not only Sorafenib-induced ferroptosis. To this end, we treated HLE cells with Erastin, a well-known inducer of ferroptosis [226], and observed that Erastin induced ferroptosis in shLuc-transfected cells, which was further enhanced upon shRNA-mediated ablation of YAP and TAZ. In both conditions, cell death could be blocked by treatment with Ferrostatin-1, indicating that cell death was due to ferroptosis (**Suppl. Figure 1e**).

Altogether, the results demonstrate that YAP and TAZ act as general inhibitors of ferroptosis, thereby promoting Sorafenib resistance.

Figure 1. Gao et al

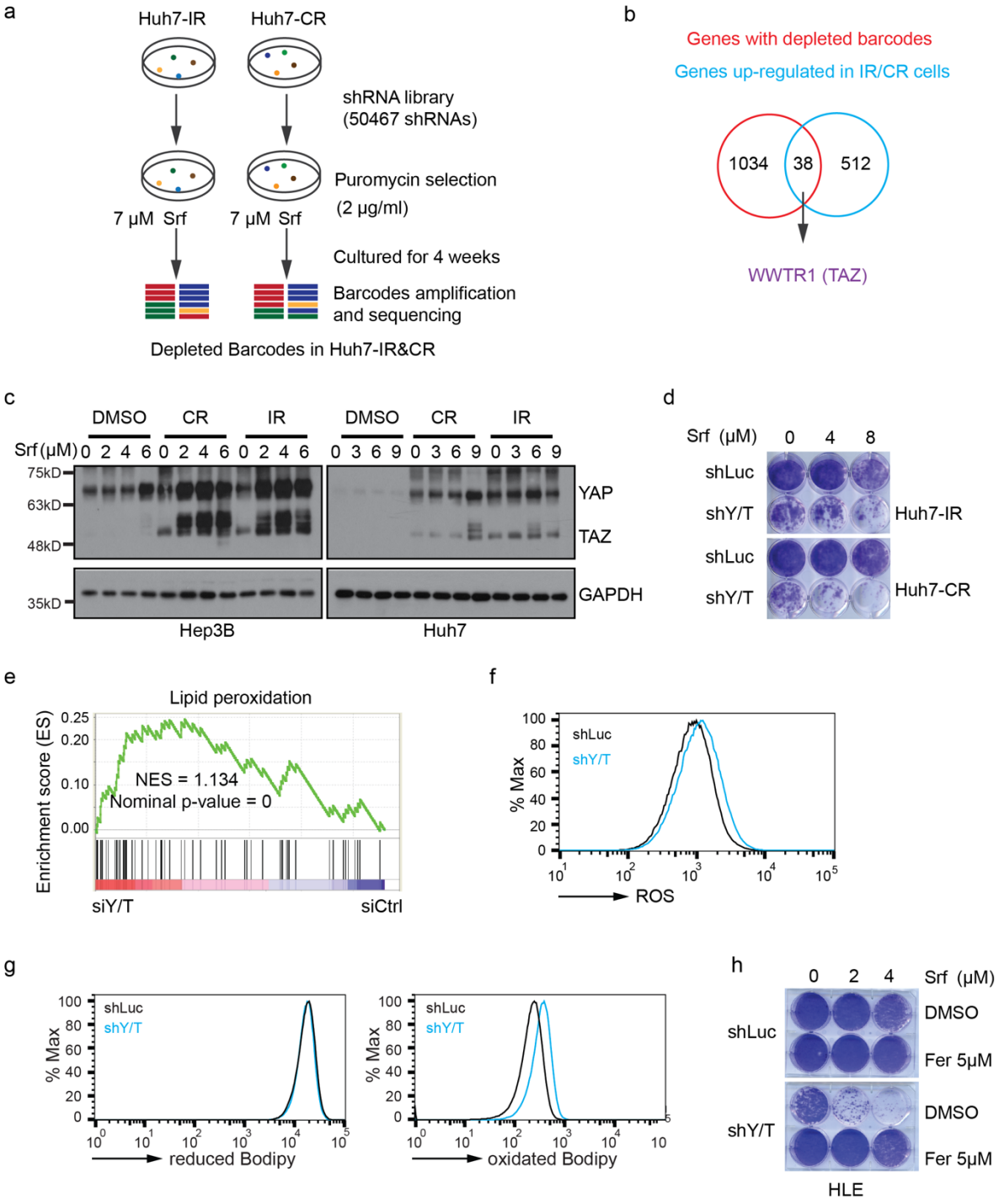

Figure 1. YAP/TAZ are key drivers of Sorafenib resistance by inhibiting ferroptosis.

(a) Scheme of shRNA-mediated synthetic lethal screening. Huh7- IR and CR cells were infected with lentiviral virus (MOI=0.5) expressing the shRNA library (human genome-wide pooled lentiviral shRNA library module 1, Vector: pRSI16cb, Cellecta) and cultured with 2μg/ml Puromycin for the selection of shRNA-expressing cells plus 7μM Sorafenib. After 4 weeks of culture, genomic DNA was extracted and shRNA barcodes were amplified for next-generation sequencing to uncover the critical genes for Sorafenib resistance. **(b)** Combinatorial analysis of genes differentially expressed between Sorafenib-sensitive and resistant cells and genes with depleted barcodes in Huh7-IR and CR cells. 38 common genes were identified, among which was *WWTR1* coding for TAZ. **(c)** Huh7-parental,

IR and CR, and Hep3B-parental, and I.R and C.R cells were treated with different concentrations of Sorafenib (0, 3, 6, 9μM) for 18 hours before harvest. Protein levels of YAP and TAZ were determined by immunoblotting illustrating higher protein levels of YAP/TAZ in Sorafenib-resistant cells. GAPDH served as loading control. **(d)** Colony formation assay showing that shRNA-mediated depletion of YAP/TAZ leads to increased cell death in response to Sorafenib treatment. Huh7 IR and CR cells either expressing a control shRNA (shLuc, non-targeting shRNA) or shRNA against both YAP and TAZ (shY/T) were treated with different concentrations of Sorafenib (0, 4, 8μM) for 2 weeks and colonies were visualized by crystal violet staining. Results represent three independent experiments. **(e)** Gene Set Enrichment Analysis (GSEA) of the genes differentially expressed between YAP/TAZ-deficient (siY/T) and control siRNA (siCtrl)-transfected HLE cells showed an enrichment for genes involved in the regulation of lipid peroxidation. **(f)** Basal reactive oxygen (ROS) levels increased upon loss of YAP/TAZ. HLE-shLuc and HLE-shY/T cell lines were stained with CellROX™ Green Flow Cytometry Assay Kit, ROS levels were measured by flow cytometry using a 488 nm laser. **(g)** Basal lipid peroxidation levels increased with the loss of function of YAP/TAZ. HLE-shLuc and HLE-shY/T cells were stained with C11-BODIPY 581/591. Reduced-Bodipy was measured by flow cytometry using a 488 nm laser, and oxidized-Bodipy was measured with a 561 nm laser. A significant shift of oxidized-Bodipy occurred upon depletion of YAP/TAZ. **(h)** Colony formation assay demonstrating that the ferroptosis inhibitor Ferrostatin-1 (Fer) could reverse Sorafenib-induced cell death in YAP/TAZ-deficient HCC cells. HLE-shLuc and shY/T cells were treated with different concentrations of Sorafenib (0, 4, 8μM) plus either DMSO or Ferrostatin-1 (Fer; 5μM) for 2 weeks. Results represent three independent experiments.

3.2.3.3 YAP/TAZ transcriptionally upregulate SLC7A11

To further investigate how the transcription factors YAP/TAZ restrict ferroptosis, we set out to identify their transcriptional target genes in the context of Sorafenib resistance of HCC cells. To this end, we overlaid the list of genes down-regulated in their expression in YAP/TAZ-depleted HLE cells and the list of genes upregulated in Sorafenib-resistant cells, which led to the identification of 56 genes (**Suppl. Table IV**). Of note, SLC7A11, coding for the cystine-glutamate antiporter known to regulate ferroptosis, was among these genes (**Figure 2a**).

As a key regulator of lipid peroxidation and ferroptosis, we confirmed the functional importance of SLC7A11 in Sorafenib resistance in HCC cells. Loss of SLC7A11 resulted in an increase of intracellular ROS levels (**Suppl. Figure 2a**) as well as of lipid peroxidation (**Suppl. Figure 2b**). Moreover, cystine uptake was inhibited by siRNA-mediated depletion of SLC7A11 (**Suppl. Figure 2c**) and, as a consequence, the levels of intracellular GSH were diminished (**Suppl. Figure 2d**). Finally, the depletion of SLC7A11 resulted in increased cell death in a colony formation assay which was fully rescued by Ferrostain-1 (**Suppl. Figure 2e, f**). These results confirm SLC7A11 as a key regulator of ferroptosis in response to Sorafenib.

We further explored the expression of SLC7A11 in HCC. Of note, SLC7A11 mRNA was highly upregulated in primary HCC tumors. Further, immunohistochemical analysis of HCC tumor sections revealed that SLC7A11 was upregulated in HCC of patients as compared with adjacent liver parenchyma (**Suppl. Figure 2g**). Statistical analysis using multi-tissue arrays with non-tumor and tumor tissues confirmed its high expression in HCC (**Suppl. Figure 2h**). Interestingly, SLC7A11 protein significantly correlated with the worse differentiation of HCC samples, as classified by Edmonson grades III and IV (**Suppl. Figure 2i**). Even more important, using the expression data retrieved from the TCGA liver dataset 15 we observed that SLC7A11 expression predicted patient survival, with high expression of SLC7A11 significantly correlating with poor clinical outcome (**Suppl. Figure 2j**).

We next sought to validate whether YAP/TAZ directly affected SLC7A11 gene expression. Indeed, knock-down of both YAP/TAZ together resulted in a significant down-regulation of SLC7A11 at both mRNA level and protein level (**Suppl. Figure 3a; Figure 2b, c**). Moreover, overexpression of a constitutive active form of YAP induced an up-regulation of SLC7A11 (**Suppl. Figure 3b**). The transcriptional activity of YAP/TAZ was best known to be regulated by cell-cell contact, and we thus further explored whether SLC7A11 was also sensitive to changes in cell density. Indeed, the expression of SLC7A11 was significantly down-regulated with increasing cell density (**Suppl. Figure 3c**).

To determine whether YAP/TAZ directly regulated SLC7A11 gene expression, we first analyzed the transcriptional activity of a SLC7A11-promoter luciferase reporter construct in dependence on YAP/TAZ activities. Indeed, we observed that the SLC7A11 promoter was fully responsive to the absence or presence of YAP/TAZ (**Figure 2d**). Moreover, analysis of the SLC7A11 promoter sequence identified a potential TEAD binding motif approximately 400 bps upstream of the transcriptional start site (**Figure 2e**). Chromatin immunoprecipitation with specific antibodies to YAP or TAZ followed by quantitative PCR (ChIP-qPCR) demonstrated a direct binding of YAP or TAZ to the TEAD motif in the promoter of the SLC7A11 gene (**Figure 2f**).

To functionally validate the critical role of YAP/TAZ-mediated SLC7A11 expression in Sorafenib resistance, we asked whether the cystine-glutamate antiporter SLC7A11 acted downstream of YAP/TAZ in overcoming Sorafenib-induced ferroptosis and whether it could replace YAP/TAZ activities. Interestingly, knock-down of YAP/TAZ resulted in impaired cystine uptake (**Figure 2g**). Moreover, the forced

expression of SLC7A11 in YAP/TAZ knock-down cells was able to prevent loss of YAP/TAZ-induced cell death in response to Sorafenib (**Figure 2h, Suppl. Figure 3d**).

To assess the functional connection of YAP/TAZ and SLC7A11 expression in patients, we explored the correlation of YAP and SLC7A11 expression in HCC samples from patients. In fact, a significant positive correlation was observed between YAP and SLC7A11 protein levels in HCC patient samples, suggesting YAP as one of the key regulators of SLC7A11 gene expression during HCC development (**Figure 2i, j**).

Together, the results show that SLC7A11, as a direct transcriptional target of YAP/TAZ, is upregulated in HCC and, as mRNA or protein, is a prognostic factor of HCC aggressiveness and of clinical outcome. Importantly, SLC7A11 acts epistatically downstream of YAP and TAZ to drive Sorafenib resistance in HCC.

Figure 2. Gao et al

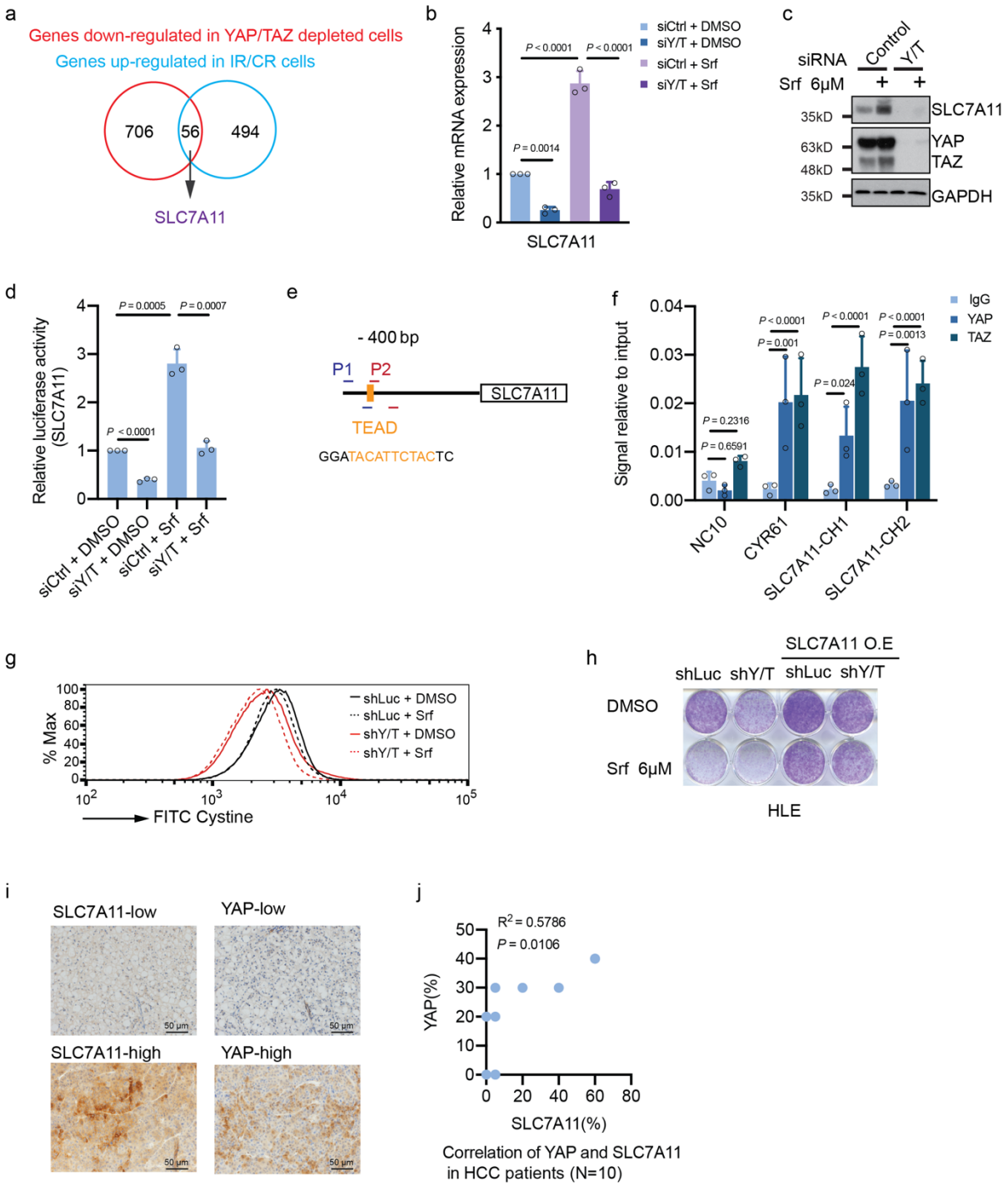

Figure 2. YAP/TAZ transcriptionally upregulate *SLC7A11* expression.

(a) Combinatorial analysis of the genes up-regulated in Sorafenib-resistant cells and the genes down-regulated upon YAP/TAZ depletion uncovered 56 common genes, among which was *SLC7A11*. **(b)** Quantitative RT-PCR analysis confirmed the dependency of *SLC7A11* gene expression on YAP/TAZ. HLE cells were transfected with control siRNA (siCtrl) or siRNA against YAP/TAZ (siY/T) and cultured with DMSO or 6μM Sorafenib for 18 hours. RNA was extracted and analyzed by quantitative RT-PCR. Statistical significance was calculated using one-way ANOVA. **(c)** SLC7A11 protein levels were downregulated by siRNA-mediated depletion of YAP/TAZ, yet upregulated by the exposure to Sorafenib. HLE cells were transfected with siCtrl or siY/T and cultured with DMSO

or 6μM Sorafenib for 18 hours before harvest, followed by immunoblotting for YAP/TAZ and SLC7A1. GAPDH served as loading control. Results represent three independent experiments. **(d)** siRNA-mediated ablation of YAP/TAZ significantly reduced SLC7A11 promoter activity, as determined by SLC7A11-promoter-luciferase reporter assay. HLE cells were transfected with *SLC7A11*-promoter *firefly* luciferase-reporter construct and a constitutive-active *Renilla* luciferase reporter construct (pRL-CMV) and with siCtrl or siY/T. Relative luciferase activity was measured using the Dual-Luciferase report Assay Kit (Promega E1980). Statistical significance was calculated using one-way ANOVA. **(e)** A potential TEAD binding motif was predicted at - 400bp within the promoter region of *SLC7A11.* PCR primers SLC7A11-CH1 (P1) and SLC7A11-CH2 (P2) were designed to examine the potential binding of transcription factors to the TEAD binding motif. By chromatin immunoprecipitation (ChIP). **(f)** Binding of YAP and TAZ to the TEAD binding motif in the *SLC7A11* promoter. ChIP was performed on HLE cell lysate with antibodies against YAP and TAZ and rabbit IgG as control. DNA fragments were amplified using the primers specific for TEAD binding motif in the *SLC7A11* promoter region shown in (e). The non-coding region NC10 served as negative control, and the bona fide TEAD target gene *CYR61* served as positive control. Statistical significance was calculated using one-way ANOVA. **(g)** Knockdown of YAP/TAZ impairs cystine uptake either with or without Sorafenib treatment, and cystine uptake decreased with the exposure to Sorafenib. HLE-shLuc and HLE-shY/T cells were cultured with DMSO or 6μM Sorafenib for 18 hours, cystine-FITC was added to cells and after incubation at 37°C for 30 minutes intracellular Cystine-FITC levels were measured by flow cytometry using a 488 nm laser. Results represent three independent experiments. **(h)** Colony formation assay showing that stable overexpression of SLC7A11 could reverse Sorafenib-induced cell death in YAP/TAZ-deficient HCC cells. HLE-shLuc and HLE-shY/T were or were not transfected to overexpress SLC7A11 (SLC7A11 OE) and treated with DMSO or 6μM Sorafenib for 2 weeks as indicated. Results represent three independent experiments. **(i)** Representative images of immuno-histochemical staining of SLC7A11 and YAP proteins in HCC samples from patients. Scale bar, 50μm.**(j)** Quantification of the immunohistochemical stainings in (i) showed a positive correlation of YAP and SLC7A11 expression, N=10. Statistical significance was calculated using Pearson correlation analysis.

3.2.3.4 ATF4 regulates SLC7A11 in response to Sorafenib treatment

Our study revealed YAP/TAZ as novel regulators of *SLC7A11* gene expression. Interestingly, Sorafenib can potently induce *SLC7A11* expression, while it does not boost YAP/TAZ activity [235]. This promoted us to investigate alternative key factors driving *SLC7A11* expression in response to Sorafenib treatment. It is well-known that stress-induced *SLC7A11* expression can be controlled by the ROS sensor NRF2 [236] and the stress regulator ATF4 [237]. Therefore, we tested the contribution of these two transcription factors by siRNA-mediated loss-of-function studies (**Figure 3a, b**). Surprisingly, we observed that ATF4, rather than NRF2, was a predominant driver of SLC7A11 expression in HCC cells at both protein and mRNA levels. Interestingly, ATF4 itself was upregulated in response to Sorafenib, most probably due to Sorafenib-induced ER-stress [235,238]. Sorafenib-induced ATF4 activity in return increased *SLC7A11* promoter activity in a luciferase reporter assay, suggesting that ATF4 directly regulated *SLC7A11* gene expression in response to Sorafenib (**Figure 3c**).

We next investigated the functional consequences of increased ATF4 activity on HCC cell survival and found that loss of ATF4 resulted in increased ROS levels as well as lipid peroxidation (**Figure 3d, e**). Moreover, cystine uptake and intracellular GSH level were down-regulated upon ATF4 depletion (**Suppl. Figure 4a, b**). Consequently, loss of ATF4 resulted in decreased cell viability in a colony formation assay, which was fully blocked by the ferroptosis inhibitor Ferrostatin-1 (**Figure 3f; Suppl. Figure 4c**). In addition, the forced expression of SLC7A11 in ATF4-deficient cells also restored cell viability (**Figure 3g**), suggesting that ATF4 was a key transcriptional factor for the repression of ferroptosis by inducing *SLC7A11* gene expression.

We further explored the expression of ATF4 in HCC patient samples and found that ATF4 was upregulated in tumor tissues in comparison to adjacent liver parenchyma (**Figure 3h**). Quantification of ATF4 levels in a multi-tissue arrays of patient samples further revealed that ATF4 was highly expressed in HCC tumors (**Figure 3i**). Finally, the significant correlation of ATF4 and SLC7A11 protein levels suggested that these two proteins were co-expressed in HCC of patients (**Figure 3j, k**).

Together, our study reveals that ATF4 is a key regulator of SLC7A11 expression and, thus, prevents Sorafenib-induced ferroptosis in HCC.

Figure 3. Gao et al

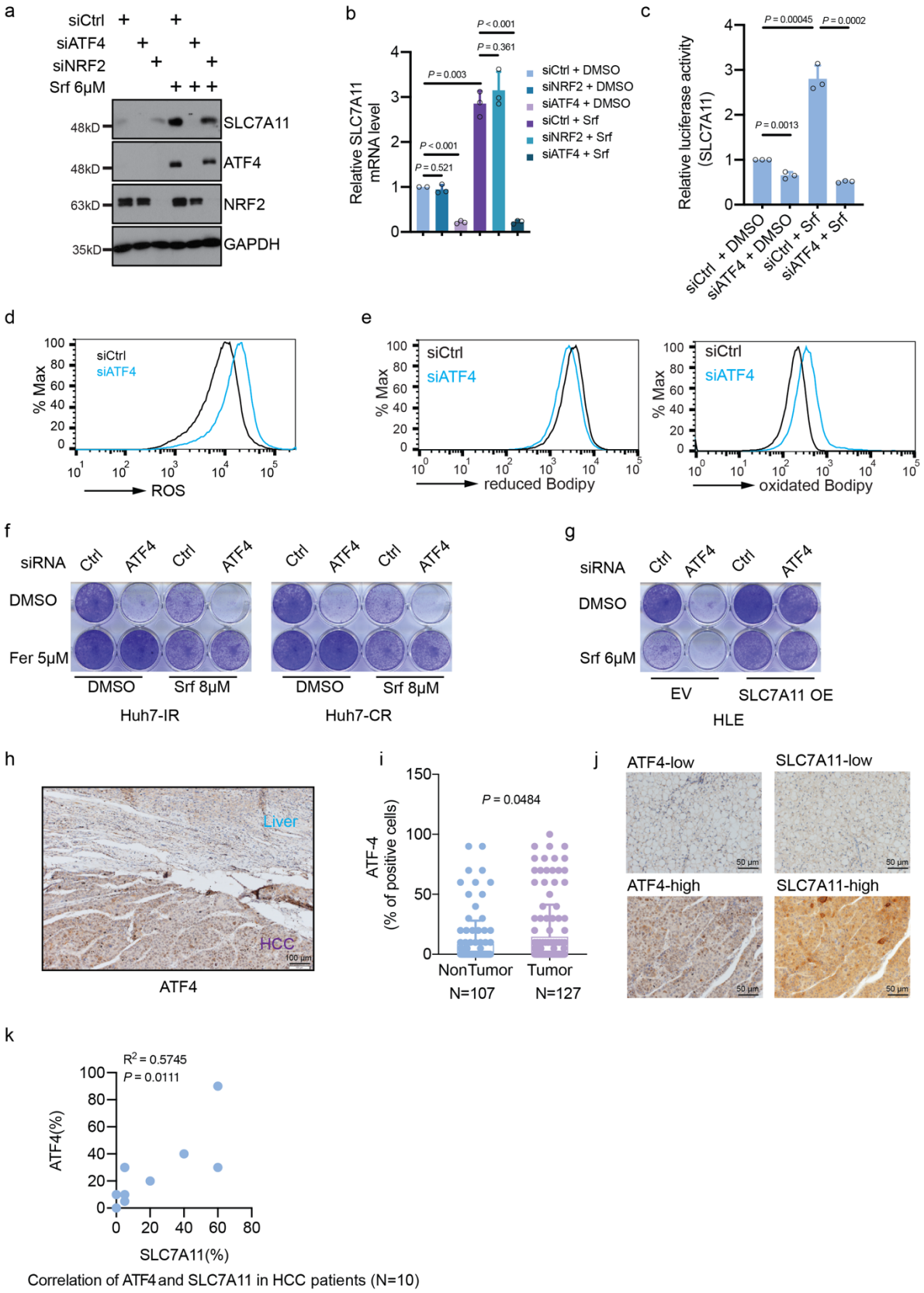

Figure 3. ATF4 regulates SLC7A11 in response to Sorafenib treatment.

(a) SLC7A11 protein levels decreased upon siRNA-mediated depletion of ATF4 but not of NRF2 either with or without Sorafenib treatment, and Sorafenib promoted the expression of ATF4. HLE cells were transfected with

siCtrl, siATF4 or siNRF2 and treated with or without 6μM Sorafenib for 18 hours. The expression of SLC7A11, ATF4 and NRF2 was determined by immunoblotting. GAPDH served as loading control. Results represent three independent experiments. **(b)** *SLC7A11* mRNA levels were decreased upon ATF4 depletion but not NRF2 depletion. HLE cells were transfected with siCtrl, siATF4 or siNRF2 and cultured with DMSO or 6μM Sorafenib for 18 hours. Quantitative RT-PCR was used to determine *SLC7A11* mRNA levels. Statistical significance was calculated using one-way ANOVA. **(c)** siRNA-mediated ablation of ATF4 significantly reduced SLC7A11 promoter activity, as determined by SLC7A11-promoter-luciferase reporter assay. HLE cells were transfected with *SLC7A11*-promoter *firefly* luciferase-reporter construct and a constitutive-active *Renilla* luciferase reporter construct (pRL-CMV) and with siCtrl or siATF4 and treated or not with 6μM Sorafenib. Relative luciferase activity was measured using the Dual-Luciferase report Assay Kit (Promega E1980). Statistical significance was calculated using one-way ANOVA. **(d)** Basal reactive oxygen (ROS) levels increased upon loss of ATF4. HLE cells were transfected with siCtrl or siATF4 and cultured for 36 hours were stained with CellROX™ Green Flow Cytometry Assay Kit, ROS levels were measured by flow cytometry using a 488 nm laser. Results represent three independent experiments. **(e)** Basal lipid peroxidation levels increased with the loss of ATF4. HLE cells were transfected with siCtrl or siATF4 and cultured for 36 hours were stained with C11-BODIPY 581/591. Reduced-Bodipy was measured by flow cytometry using a 488 nm laser, and oxidized-Bodipy was measured with a 561 nm laser. A significant shift of oxidized-Bodipy occurred upon depletion of ATF4. Results represent three independent experiments. **(f)** Colony formation assay demonstrating that the ferroptosis inhibitor Ferrostatin-1 (Fer) could reverse Sorafenib-induced cell death in ATF4-deficient HCC cells. HLE cells transfected with siCtrl or siATF4 were treated with Sorafenib (8μM) or DMSO plus either DMSO or Ferrostatin-1 (Fer; 5μM) for 2 weeks. Results represent three independent experiments. Results represent three independent experiments. **(g)** The forced expression of SLC7A11 rescued cell death induced by ATF4 ablation. HLE cells were transfected with a construct coding for SLC7A11 (SLC 7A11 OE) or empty vector (EV) and with siCtrl or siATF4 every other day. Cells were then treated with either DMSO or 8μM Sorafenib for 2 weeks. Colony formation was visualized by crystal violet staining. Results represent three independent experiments. **(h)** Immunohistochemical staining of ATF4 in HCC and adjacent non-neoplastic areas from patients. Tumor tissues showed a higher expression of ATF4. Scale bar, 100μm. **(i)** Quantification of ATF4-positive cells in tumor and non-tumor samples showed that HCC tumors present higher ATF4 levels. Statistical significance was calculated using unpaired t-test. **(j)** Representative images of immuno-histochemical staining of ATF4 and SLC7A11 proteins in HCC samples from patients. Scale bar, 50μm.**(k)** Quantification of the immunohistochemical stainings in (j) showed a positive correlation of ATF4 and SLC7A11 expression, N=10. Statistical significance was calculated using Pearson correlation analysis.

3.2.3.5 YAP/TAZ stabilize and direct ATF4 into the nucleus

Our study thus far revealed YAP/TAZ and ATF4 as novel regulators of *SLC7A11* gene expression. The fact that ATF4 was up-regulated by Sorafenib and simultaneously regulated *SCL7A11* expression promoted us to investigate a potential crosstalk of YAP/TAZ with ATF4 in the regulation of *SLC7A11* expression.

We first assessed whether YAP/TAZ and ATF4 affected each other's expression levels in response to Sorafenib. Indeed, YAP/TAZ deficiency resulted in a marked down-regulation of Sorafenib-induced ATF4 expression at the protein level (**Figure 4a**). Subcellular localization by immunofluorescence microscopy analysis as

well as cellular fractionation and immunoblotting revealed that loss of YAP/TAZ resulted into a reduction of nuclear ATF4 in HCC cells (**Figure 4b-d**). Moreover, high cell density culture resulted in the expected deactivation of YAP/TAZ, but also in decreased ATF4 expression in HCC cells (**Figure 4e**).

To further explore how YAP/TAZ regulates ATF4 protein levels, we next asked whether YAP/TAZ affected ATF4 protein stability and/or whether YAP/TAZ directly induced ATF4 transcriptional activation. Protein levels can be regulated by proteasome-mediated degradation or auto-lysosomal-driven turnover. Thus, we treated HCC cells with the proteasome inhibitor MG132 and we found that it efficiently blocked the down-regulation of ATF4 induced by the siRNA-mediated depletion of YAP/TAZ (**Suppl. Figure 5a**). In contrast, treatment with Chloroquine (CQ) as an inhibitor of lysosomal degradation had no effect on ATF4 protein levels. Proteasomal degradation is generally preceded by protein ubiquitination. We thus analyzed the influence of YAP/TAZ expression on the ubiquitination of ATF4. Indeed, the loss of YAP/TAZ resulted in increased ubiquitination of ATF4 (**Suppl. Figure 5b**). These results suggested that YAP/TAZ promoted ATF4 function by restricting ATF4 poly-ubiquitination and thus stabilizing ATF4.

It is well-known that the shuttling of YAP/TAZ between cytoplasm and nucleus enables them to act as core-chaperones and to facilitate the subcellular translocation of specific factors, such as β-catenin [239]. Therefore, we asked whether YAP/TAZ directed ATF4 to the nucleus. Analysis of a direct protein-protein interaction by co-immunoprecipitation revealed that ATF4 indeed physically bound to YAP and TAZ (**Figure 4f**). To study the active role of TAZ in translocating ATF4 to the nucleus, we transfected HLE HCC cells with plasmid constructs coding for wildtype TAZ, constitute-active TAZ, or constitutive-active TAZ lacking the nuclear localization signal (NLS), and analyzed ATF4 subcellular localization by immunofluorescence microscopy. Notably, while wildtype TAZ and in particular constitutive-active TAZ increased nuclear ATF4, constitutive-active TAZ lacking the NLS failed to translocate ATF4 into the nucleus (**Figure 4g**). Since TEADs have been shown to promote the nuclear import of YAP/TAZ [240], we also assessed whether TEADs indirectly affected ATF4 nuclear localization. Indeed, siRNA-mediated ablation of all TEADs resulted in a loss of nuclear ATF4 and also in a substantial reduction of ATF4 protein levels (**Suppl. Figure 5c-e**).

We further explored the correlation of YAP and ATF4 expression in HCC of patients. Intriguingly, a significant positive correlation was observed in HCC patient samples, suggesting YAP as a key regulator of ATF4 expression in HCC (**Figure 4h, i**).

Together, the data indicate that YAP/TAZ interact with ATF4 and together with TEADs promote its nuclear import to prevent its ubiquitylation and proteasomal degradation in the cytoplasm.

Figure 4. Gao et al

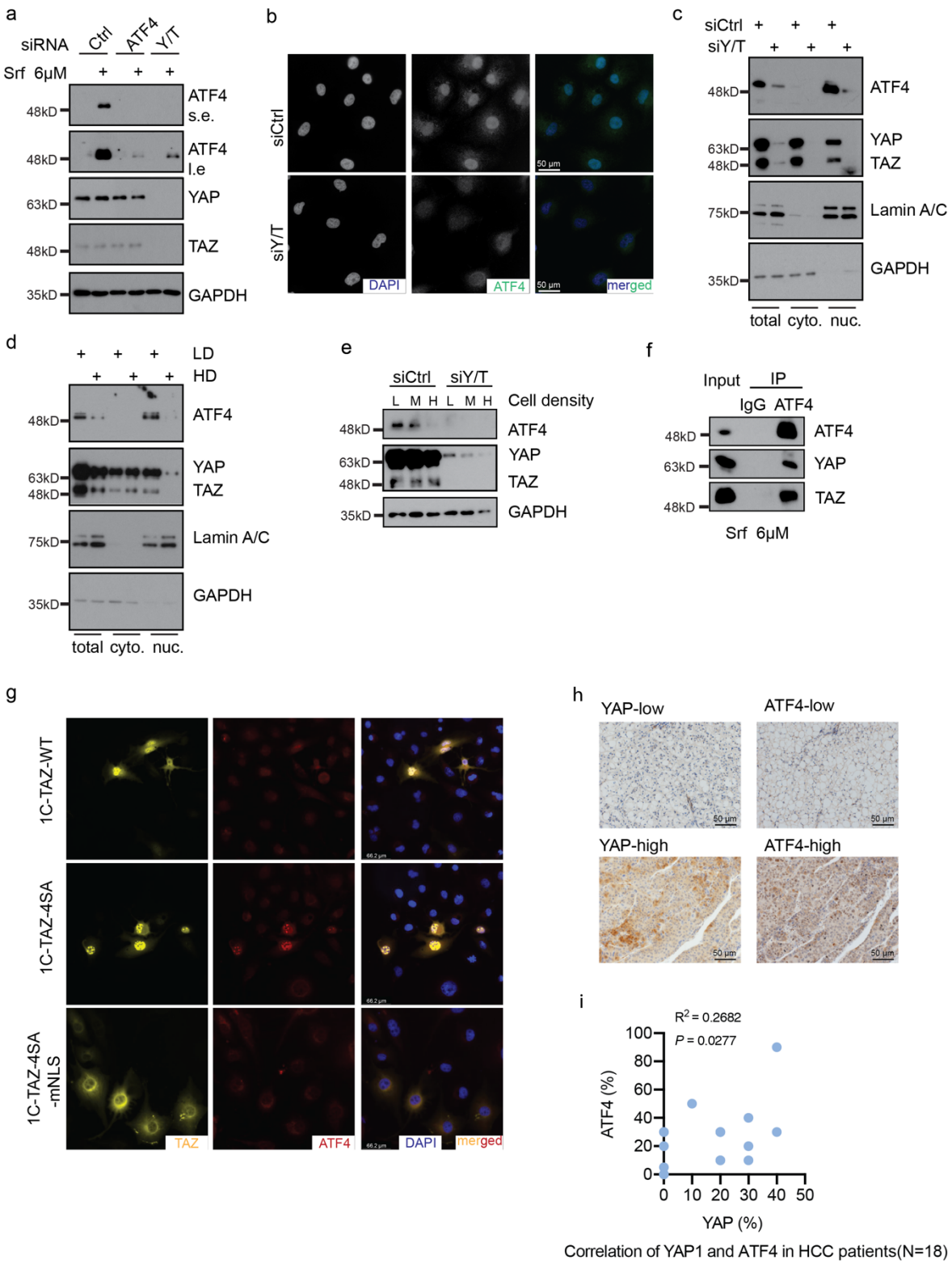

Figure 4. YAP/TAZ stabilize ATF4 protein and direct it into the nucleus.

(a) YAP/TAZ deficiency repressed Sorafenib-induced expression of ATF4, whereas ATF4 depletion had no effect on YAP/TAZ protein levels. HLE cells were transfected with siCtrl or siATF4 or siY/T and treated with 6μM Sorafenib or not for 18 hours. ATF4 and YAP/TAZ protein levels were analyzed by immunoblotting. GAPDH served as loading control. Results represent three independent experiments. **(b)** YAP/TAZ deficiency induced a reduction of ATF4

protein level and nuclear localization. HLE cells were transfected with siCtrl or siY/T, and ATF4 and YAP/TAZ were visualized by immunofluorescence microscopy. DAPI visualized nuclei. Scale bar, 50μm. Results represent three independent experiments. **(c)** Cellular fractionation revealed that YAP/TAZ deficiency ATF4 nuclear localization. HLE cells were transfected with siCtrl or siY/T, and cell lysates were separated into cytoplasmic and nuclear fractions and analyzed by immunoblotting for ATF4 and YAP/TAZ. GAPDH served as loading control of total lysate and cytoplasmic fractions, Lamin A/C served as loading control for nuclear proteins. Results represent three independent experiments. **(d)** Cellular fractionation revealed that high cell density, and with it, lower YAP/TAZ activity reduced the levels of nuclear ATF4. HLE cells were seeded at different cell numbers, and cell lysates of high cell density cells (HD) and low cell density (LD) were fractionated into cytoplasmic and nuclear fractions and analyzed for ATF4 and YAP/TAZ by immunoblotting. GAPDH served as loading control for total lysate and cytoplasmic proteins, Lamin A/C served as loading control for nuclear proteins. Results represent three independent experiments. **(e)** Increasing cell density declined YAP/TAZ stability and led to a reduction of ATF4. HLE cells were seeded to reach low (L), medium (M) and high (H) cell density and transfected with siCtrl or siY/T. Protein levels of ATF4 and YAP/TAZ were determined by immunoblotting blotting. GAPDH served as loading control. Results represent three independent experiments. **(f)** YAP/TAZ physically interacted with ATF4. HLE cells were cultured with 6μM Sorafenib for 18 hours and ATF4 was immunoprecipitated and precipitated YAP, TAZ and ATF4 were visualized by immunoblotting. Unrelated IgG was used as control for immunoprecipitation. Input represents cell lysates directly analyzed by immunoblotting. Results represent three independent experiments. **(g)** YAP/TAZ direct the nuclear localization of ATF4. HLE cell were transfected with plasmid constructs coding for wild-type TAZ (1C-TAZ-WT), constitutive-active TAZ (1C-TAZ- 4SA) or constitutive-active TAZ lacking a nuclear localization signal (NLS) (1C-TAZ-mNLS) and analyzed TAZ and ATF4 by immunofluorescence microscopy. DAPI visualized nuclei. Scale bar, 66.2μm. Results represent three independent experiments. **(h)** Representative images of immuno-histochemical staining of ATF4 and YAP proteins in HCC samples from patients. Scale bar, 50μm.**(i)** Quantification of the immunohistochemical stainings in (j) showed a positive correlation of ATF4 and YAP expression, N=18. Statistical significance was calculated using Pearson correlation analysis.

3.2.3.6 YAP/TAZ and ATF4 collaboratively regulate SLC7A11 expression

Since YAP/TAZ appeared to regulate ATF4 nuclear activity and together they induced SLC7A11 expression, we next asked whether and how YAP/TAZ and ATF4 act globally in response to Sorafenib. We first compared the expression of genes affected in the presence of Sorafenib by siRNA-mediated ablation of either YAP/TAZ or ATF4 by RNA sequencing. 262 genes were found co-regulated by YAP/TAZ and ATF4, among which were well-known ATF4 targets, such as ATF3, CHAC1 and SLC7A11 (**Figure 5a; Suppl. Table V**). Quantitative RT-PCR further confirmed that these gene were co-regulated by YAP/TAZ and ATF4 (**Figure 5b**). We next assessed whether ATF4 directly regulated their expression via canonical amino acid responsive element (AARE) motifs. ChIP-qPCR analysis revealed that ATF4 indeed bound to the AARE regions of the ATF3 and SLC7A11 gene promoters (**Figure 5c**).

Our previous results demonstrated that YAP/TAZ regulates SLC7A11 expression via a TEAD binding motif on its gene promoter. Given that a fraction of

YAP/TAZ targets was found co-regulated by ATF4, we further investigated an alternative regulation of SLC7A11 by YAP/TAZ, such as via the AARE motif in the SLC7A11 promoter. Indeed, ChIP-qPCR analysis revealed that YAP/TAZ was also able to bind to the AARE motif in the SLC7A11 gene promoter (**Figure 5d, e**). Given that YAP/TAZ physically interacted with ATF4 and that YAP/TAZ and ATF4 bound to the AARE motif in the SLC7A11 gene promoter, ATF4 might mediate the indirect binding of YAP/TAZ to the AARE motif. To test this, a tandem-ChIP assay was performed with a 1st round of anti-ATF4 ChIP followed by a 2nd round of anti-YAP/TAZ ChIP. Indeed, we found that the AARE motif in the SLC7A11 gene promoter was significantly enriched by YAP/TAZ in the 2nd round ChIP (**Figure 5f, g**), indicating that YAP/TAZ bound to the AARE motif in the SLC7A11 gene promoter via binding to ATF4. To further demonstrate this, a YAP/TAZ ChIP assay was performed in ATF4 deficient cells. Strikingly, while the YAP/TAZ localized to the classical *Cyr61* promoter, the binding of YAP/TAZ to the AARE motif on the promoter of SLC7A11 was decreased upon ATF4 deficiency, suggesting that ATF4 indeed mediated the binding of YAP/TAZ to the AARE motif (**Figure 5h**).

Together, the results suggest that YAP/TAZ and ATF4 collaboratively regulate SLC7A11 expression in HCC cells.

Figure 5. Gao et al

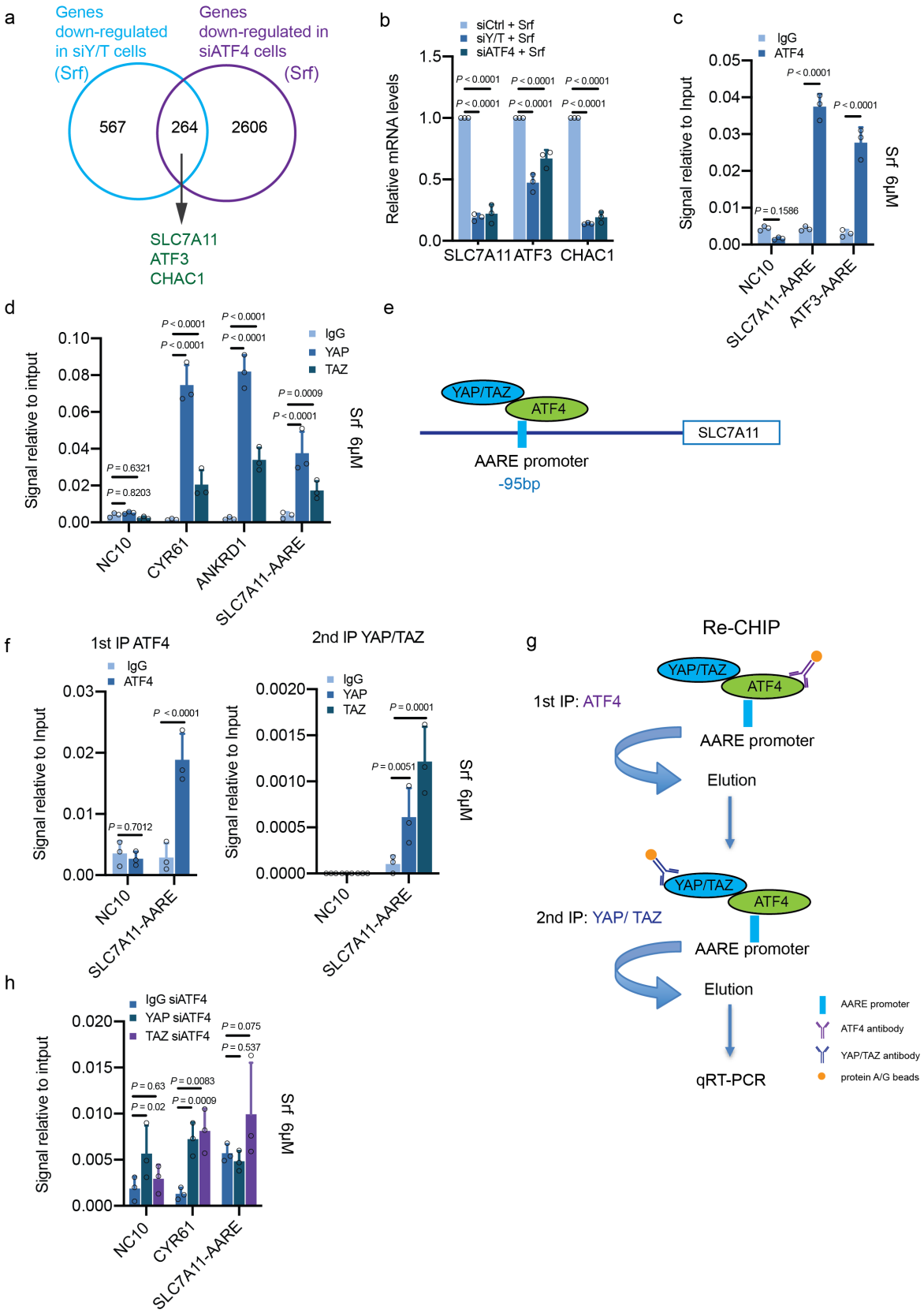

Figure 5. YAP/TAZ-ATF4 collaboratively regulate *SLC7A11* expression.

(a) 264 common genes were identified down-regulated by both deficiency for YAP/TAZ and deficiency for ATF4, among which were known ATF4 targets, such as SLC7A11, ATF3 and CHAC1. HLE cells were transfected with siCtrl, siYAP/TAZ or siATF4 and cultured with 6μM Sorafenib for 18 hours and RNA was subjected to next generation RNA sequencing. Venn diagram analysis was conducted with VENNY 2.1.0. **(b)** Quantitative RT-PCR analysis verified that depletion of YAP/TAZ or ATF4 declined the expression levels of *SLC7A11*, *ATF*3 and *CHAC1*. HLE cells were transfected with siCtrl, siY/T or siATF4 and cultured with 6μM Sorafenib for 18 hours. Quantitative RT-PCR was conducted to determine SLC7A11, ATF3 and CHAC1 mRNA levels. Statistical significance was calculated using one-way ANOVA. **(c)** Binding of ATF4 to the AARE binding motif in the promoters of *SLC7A11* and *ATF*3. ChIP was performed on HLE cell lysate with antibodies against ATF4 and rabbit IgG as control. DNA fragments were amplified using the primers specific for AARE binding motif in the *SLC7A11* and the ATF3 promoter regions. The non-coding region NC10 served as negative control. Statistical significance was calculated using one-way ANOVA. **(d)** Binding of YAP and TAZ to the AARE binding motif in the *SLC7A11* promoter. ChIP was performed on HLE cell lysate with antibodies against YAP and TAZ and rabbit IgG as control. DNA fragments were amplified using the primers specific for AARE binding motif in the *SLC7A11* promoter region. The non-coding region NC10 served as negative control, and the bona fide TEAD target genes *CYR61* and *ANKRD1* served as positive controls. Statistical significance was calculated using one-way ANOVA. **(e)** Schematic representation of the ATF4 binding motif AARE located at – 95bp of the *SLC7A11* promoter region. YAP/TAZ were predicted to interact with ATF4 binding to the AARE binding motif in the promoter of *SLC7A11*. **(f**) YAP/TAZ bind to the AARE binding motif within the *SLC7A11* promoter via ATF4. HLE cells were cultured with 6μM Sorafenib for 18 hours before harvest. In a 1st round ChIP ATF4 was immunoprecipitated with antibody against ATF4, rabbit IgG was used as control. DNA-protein immunocomplexes were eluted and in a 2nd round ChIP antibody against YAP/TAZ was used to precipitate DNA fragments which were then amplified and analyzed by quantitative PCR for the AARE motif in the *SLC7A11* promoter. NC10 served as negative PCR control. Statistical significance was calculated using one-way ANOVA. **(g)** Schematic representation of the ChIP-ReChIP strategy to test whether YAP/TAZ bind to the AARE binding motif within the *SLC7A11* promoter via binding to ATF4. **(h)**YAP/TAZ ChIP assay with the deficiency of ATF4, the binding of YAP/TAZ to the SLC7A11-AARE promoter was undermined with the depletion of ATF4, but ATF4 deficiency has no effect on the YAP/TAZ binding to the CYR61 promoter: HLE cells were transfected with siATF4 , cells were cultured with 6μM Sorafenib for 18 hours before harvest, ChIP-grade antibodies of YAP and TAZ were used to pull down YAP or TAZ, Rabbit IgG was used as a control, DNA fragments which were pulled down together with YAP/TAZ were amplified and analyzed by ChIP-qPCR. CYR61 is served as the positive control to ensure the pulling down of YAP/TAZ, NC10 is served as a negative control. Statistical significance was calculated using one-way ANOVA.

3.2.3.7 Targeting ferroptosis overcomes Sorafenib resistance

Our results suggested that YAP/TAZ and ATF4 promoted Sorafenib resistance by upregulation of SLC7A11 gene expression and thus antagonizing ferroptosis. We next investigated the therapeutic effect of targeting YAP/TAZ in combination with Sorafenib in HCC. To this end, we established highly tumorigenic SNU398 cells expressing either a shRNA against luciferase (SNU398-shLuc) as control or a shRNA against YAP and TAZ (SNU398-shY/T) (**Figure 6a**). These cells were then implanted into the flanks of NSG immunocompromised mice, and the mice were then treated with vehicle

control or with Sorafenib (20mg/kg). In line with the in vitro colony formation assays described above, YAP/TAZ deficiency resulted in an increased sensitivity to Sorafenib treatment in vivo, as reflected by decreased tumor growth rates as well as by smaller tumor masses at end point analysis (**Figure 6b-d**).

We further examined the potential therapeutic efficacy of targeting ferroptosis in order to overcome Sorafenib resistance. SNU398 cells were implanted into the flanks of NSG immunodeficient mice, and the mice were then treated with sulfasalazine (SSA) [241,242], a pharmacological inhibitor of SLC7A11, or with Buthionine Sulfoximine (BSO) [243], a glutathione depletion reagent. Importantly, the combination therapy of Sorafenib with either compound led to delayed tumor growth (**Figure 6e**), suggesting that co-targeting ferroptosis can efficiently sensitize tumors to Sorafenib therapy. Histochemical analysis of the tumors by 4-hydroxynonenal staining confirmed an increase of lipid peroxidation in the inhibitor-treated tumors, while tumor cell proliferation as determined by Ki67 staining was not significantly affected (**Figure 6 f, g**).

Taken together, our studies demonstrate that blocking YAP/TAZ or ATF4, or their transcriptional target gene product SLC7A11 and its induction of the glutathione synthesis pathway can efficiently sensitize HCC tumors to Sorafenib therapy by unleashing ferroptosis to promote cell death.

Figure 6. Gao et al

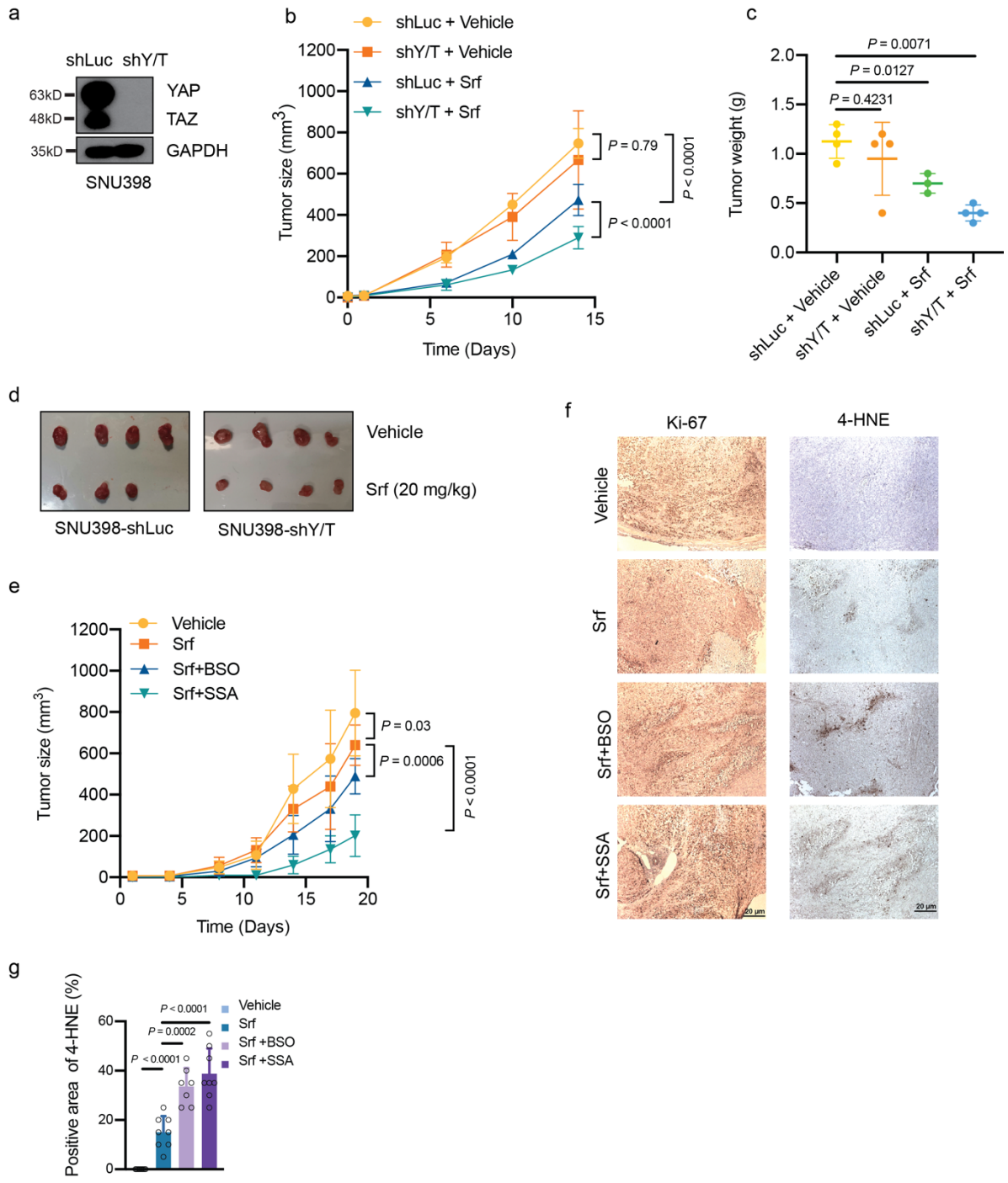

Figure 6. Targeting ferroptosis overcomes Sorafenib resistance.

(a) Establishment of a YAP/TAZ-deficient SNU398 cell line. SNU398 cells were infected with lentivirus to stably express either shLuc as control or shYAP/TAZ. Immunoblotting illustrated the loss of YAP/TAZ expression. GAPDH served as loading control. **(b,c,d)** Combination of YAP/TAZ deficiency and Sorafenib treatment suppressed tumor growth in a HCC xenograft model. SNU398-shLuc or SNU398-shYAP/TAZ (shY/T) cells were transplanted into the flanks of immunodeficient NSG mice. Once the tumors were palpable, mice were treated with 20mg/kg Sorafenib or vehicle control, and tumor sizes were measured twice a week (b). Tumor weights and sizes were also recorded after sacrifice of the mice (c,d). Statistical significance was calculated using Two-way ANOVA

analysis. **(e)** Pharmacological inhibition of glutathione synthesis and function sensitizes HCC tumors to Sorafenib therapy. SNU398 cells were transplanted into the flanks of immunodeficient NSG mice. Once the tumors were palpable, mice were treated with vehicle control or with 20mg/kg Sorafenib alone, or with 20mg/kg Sorafenib and 20mM BSO or 120mg/kg SSA. Tumor sizes were measured twice a week. Statistical significance was calculated using Two-way ANOVA analysis. **(f)** Representative pictures of immunohistochemical staining of Ki67 and 4-HNE in tissue sections taken from HCC tumors of the mice treated as described in (e). Ki67 is a marker for cell proliferation, while 4-HNE is a marker of ferroptosis and lipid peroxidation. Scale bars, 50μm.**(g)** Quantification of 4-HNE-positive cells of the immunohistochemical stainings described in (f). Statistical significance was calculated using one-way ANOVA.

Figure 7. Gao et al

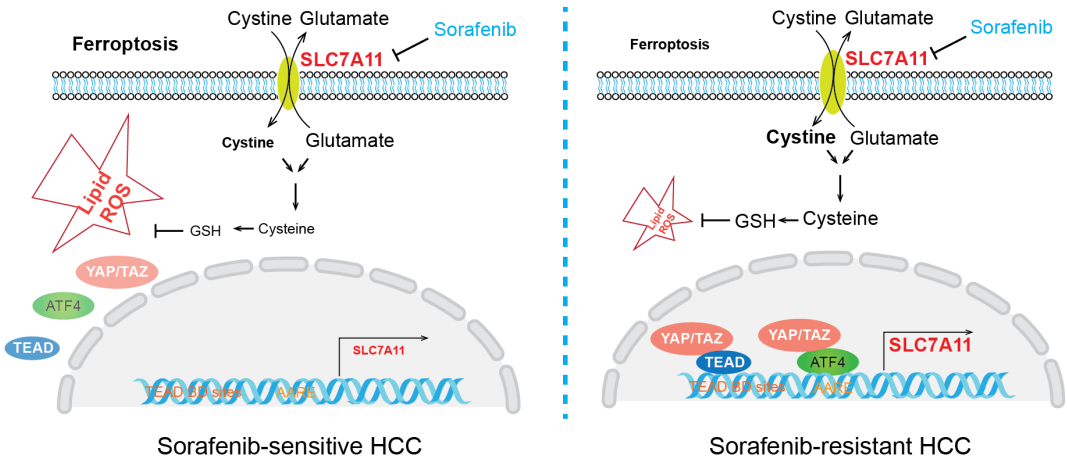

Figure 7. Working model of how YAP/TAZ and ATF4 repress ferroptosis in Sorafenib-resistant HCC cells. In Sorafenib-sensitive cells, YAP/TAZ and ATF4 are not localized to the nucleus and not activated. As a consequence, the expression of anti-oxidant genes, such as *SLC7A11*, is not induced, and glutathione (GSH) levels are low. ROS levels then increase and ferroptosis can ensue, even more so in the presence of Sorafenib. In Sorafenib-resistant cell, YAP/TAZ and ATF4 are activated in the nucleus and induce the expression of *SLC7A11* which increases GSH levels. ROS levels are thus reduced, ferroptosis is repressed, and HCC cells survive even in the presence of Sorafenib.

3.2.4 Discussion

The development of therapy resistance is a general and sobering clinical challenge observed in a variety of therapeutic approaches, including newest molecularly targeted therapies. Sorafenib, a standard-of-care treatment for advanced HCC, targets cancer cells by blocking intracellular protein kinase cascades [244]. Further studies have uncovered that the cystine-glutamate antiporter SLC7A11, a key antagonist of ferroptosis, is also inhibited by Sorafenib [235]. As such, the mode-of-action of Sorafenib relies on its multiple roles in blocking proliferation and in inducing cell death. In our study, we have aimed at delineating the molecular drivers of

Sorafenib resistance by combining a genome-wide synthetic lethality screen with transcriptomic analysis. These combined approaches identified YAP/TAZ, well known transducers of the Hippo signaling pathway, as key factors in mediating Sorafenib resistance. One major mechanism relies on YAP/TAZ's ability to restrain therapy-induced ferroptosis by promoting *SLC7A11* gene expression via both TEAD-dependent and ATF4-dependent transcriptional activities (**Figure 7**).

Previous studies have suggested that *SLC7A11* can be transcriptionally regulated by a set of key oncogenic transcription factors, including mutant p53 [245], NRF2 [236] and ATF4 [237]. We here report that YAP/TAZ, as transcriptional co-activators, form complexes with TEADs and thus indirectly bind to the TEAD motif in the *SLC7A11* gene promoter and thus induce the expression of SLC7A11. In line with previous report that ATF4 binds to AARE motif in the *SLC7A11* promoter[246], we observed that YAP/TAZ can bind to ATF4 and thus to the AARE motif in the *SLC7A11* gene promoter, suggesting that ATF4 serves as a novel transcriptional partner of YAP/TAZ. In fact, in addition to *SLC7A11*, global transcriptomic analysis revealed that YAP/TAZ and ATF4 share a substantial number of common direct and indirect transcriptional targets. While our current study focuses on *SLC7A11*, the functional contribution of ATF4 as an additional DNA binding partner of YAP/TAZ in physiological and pathophysiological processes warrants further investigation. Moreover, we have found that YAP/TAZ can form complexes with ATF4. The interaction of YAP/TAZ with ATF4 appears to promote the nuclear localization of ATF4 and thus its transcriptional activity and to stabilize ATF4 protein by preventing its cytoplasmic ubiquitylation and proteasomal degradation. Moreover, while TEADS have been previously shown to be critical for the nuclear import of YAP/TAZ [240], we here show that TEADs via YAP/TAZ are also required to direct ATF4 to the nucleus. Hence, our study suggests YAP/TAZ, and indirectly TEADs, as key chaperones for ATF4 during stress responses, such as in response to Sorafenib.

YAP/TAZ have been previously implicated in the development of resistance to targeted therapies as well as in epithelial tumor progression via regulating ferroptosis [247]. In contrast, in breast tumors YAP has been shown to promote ferroptosis. Under cell-cell contact conditions, E-cadherin suppresses ferroptosis by activating NF2 and the Hippo signaling pathway [232]. Further, YAP transcriptionally up-regulates key ferroptosis genes, such as ACSL4 and TFRC [232]. Likewise, TAZ has been shown to promote ferroptosis in renal and ovarian tumors by upregulating EMP1-NOX4 [231]

and ANGPTL4-NOX2 [247], respectively. Therefore, the role(s) of YAP/TAZ in ferroptosis regulation appears to be highly context-dependent. Detailed investigations are warranted to molecularly segregate the promoting and inhibitory roles of Hippo signaling in ferroptosis and the consequences for physiological and pathophysiological processes.

Our studies have identified a novel role of YAP/TAZ in restraining ferroptosis during the development of resistance against Sorafenib therapy in HCC. In its sum, the work raises the possibility, and provides first proof-of-concept, that targeting YAP/TAZ can be an efficient way to overcome therapy resistance. In fact, small inhibitors targeting YAP/TAZ have been and are being explored as anti-cancer agents at a pre-clinical and clinical stage. Notably, a vast majority of inventions aim to disrupt TEAD-dependent YAP/TAZ function in tumor progression, such as blocking TEAD palmitoylation. Our observations of ATF4-dependent YAP/TAZ activities, together with previous findings of and interaction of YAP/TAZ and β-catenin and SMADs, suggest that targeting YAP/TAZ themselves, such as via a PROTAC approach, might represent a most efficient approach in clinics. Finally, in the context of Sorafenib resistance as a major clinical challenge in the therapy of HCC, we report first pre-clinical proof that the specific targeting of enzymes and transporters involved in glutathione synthesis and homeostasis may offer attractive opportunities to overcome Sorafenib and potentially other therapy resistance.

3.2.5 Materials and Methods

DNA Constructs, siRNAs and antibodies

1C-TAZ-WT, 1C-TAZ-4SA, 1C-TAZ-4SA-mNLS were kind gifts from Andras Kapus. pcDNA3-HA-YAP1-5SA was a kind gift from Alex Hergovich. pLenti-CMV-SLC7A11-sh926R-FLAG-IRES-Hygro was purchased from Addgene (# 118702), To get pSuper-retro-puro-shYAP/TAZ construct, oligo of 5'---3' TGTGGATGAGATGGATACA which targets both YAP and TAZ mRNAs was cloned into pSuper-retro-puro-vector. To get pGL4.10-SLC7A11, -1000 bp to + 200 bp promoter fragment of SLC7A11 was cloned into pGL4.10-Vector.

On-target siRNAs were purchased from Horizon Discovery are listed at Suppl. Table VI, antibodies used are listed in Suppl. Table VII, and oligonucleotides are listed in Suppl. Table VIII.

Cell culture, transfection, reagents and stable cell lines generation

HEK-293T, SNU398 cells were obtained from American Type Culture Collection (ATCC), Huh7, HLE, Hep3B were gifts from Luca Quagliata. All cell lines used in this study were tested for the absence of Mycoplasma contamination every two weeks. Plasmids transfection into HEK293T cells were carried out by using PEI (Polyethylenimine, Linear, MW 25000, Polysciences Catalog No. 23966-1), plasmids transfection into HCC cell lines were carried out with Lipofectamine 3000 (Invitrogen). siRNA transfections were carried out with Lipofectamine RNAiMAX (Invitrogen) according to the manufacturer's instructions.

To establish SLC7A11-stable overexpression cell lines, lentivirus was produced by transfection on HEK-293T cells with pLenti-CMV-SLC7A11-sh926R-FLAG-IRES-Hygro, infections were performed using 8μg/ml polybrene (Sigma #107689), Hygromycin B (Invivogene, # ant-hg-1) was used for the selection. To establish YAP/TAZ-stable knock-down cell lines, retrovirus was produced by transfection on Platinium-A cells (Cell Biolabs) with pSuper-retro-puro-shYAP/TAZ, infections were performed using 8μg/ml Polybrene (Sigma #107689), Puromycin (Invivogen, # ant-pr-5b) was used for the selection.

Dual-Luciferase report assay

Cells were seeded into 24-well plates, siRNAs were transfected once cell confluence had reached 60%. Medium was changed after 6 hours. 24 hours later, pGL4.10-SLC7A11 and pRL-CMV were transfected together into cells with a 10:1 mass ratio, and medium was changed after 6 hours. Cells were washed with PBS twice, and *Firefly* luminescence and *Renilla* luminescence were measured using Dual-Luciferase report Assay Kit (Promega E1980) and a bioluminescence plate reader (Berthold Centro LB 960).

Intercellular GSH assay

Cells were seeded into 96-well pates (5000 cells per well), treated with DMSO or 6μM Sorafenib, respectively, 18 hours later cells were washed with PBS twice and harvested by trypsinization. Cell numbers were counted with a cell counter. Intracellular GSH levels were measured with GSH-Glo Glutathione Assay kit (Promega V6911/V6912) and a Berthold luminometer (Berthold Centro LB 960), results were normalized to cell numbers.

Colony formation assay

Cells were seeded into 12-well plates (5000 cells per well) and cultured for 2 weeks, siRNAs were transfected every other day, culture medium with either DMSO or Sorafenib was exchanged every 24 hours. 2 weeks later cells washed with PBS and fixed with 4% paraformaldehyde for 30 min at room temperature, washed with PBS again and stained with crystal violet (1mg/ml dissolved into 10% ethanol) for 30 min at room temperature. After washing with PBS, plates were left to dry and cells stained with crystal violet were counted using Fiji (NIH Image).

Cystine uptake measurement

Cells were seeded into 60mm dishes with 10^6 cells. 24 hours later, cells were transfected with siRNAs and fresh medium were changed 6 hours after the transfection. 24 hours after the transfection, cells were treated with DMSO, Sorafenib or Erastin for 18 hours. Cystine-FITC (BioTracker Cystine-FITC Live Cell Dye, Sigma SCT047) was diluted in medium at a concentration of 5μM and added to cells to incubate at 37°C for 30 minutes. Cells were washed with PBS and harvested by trypsinization. Resuspend cells in PBS and filter cells with a 40μM strainer. Intracellular Cystine-FITC levels were measured by the Flow cytometry (Beckman Coulter Cytoflex LX) with a 488nm laser, Data were collected and analyzed with the Flow Jo (Ashland, Oregon-based FlowJo LLC).

Cellular lipid measurement

Cells were seeded into 60mm dishes with 10^6 cells. 24 hours later, cells were transfected with siRNAs and fresh medium were changed 6 hours after the transfection. 24 hours after the transfection, cells were treated with DMSO, Sorafenib for 18 hours. C11-BODIPY 581/591 (Thermo Fisher Scientific, D3861) was used to stain the cells for 30 min at 37°C and harvested by trypsinization. Cells were resuspended in PBS and filtered by a 40μM strainer. Flow cytometry (Beckman Coulter Cytoflex LX) with 488nm and 561nm lasers were used for the excitation. Data were collected and analyzed with the Flow Jo (Ashland, Oregon-based FlowJo LLC).

Cellular Reactive Oxygen Species (ROS) measurement

Cells were seeded into 60mm dishes with 10^6 cells. 24 hours later, cells were transfected with siRNAs and fresh medium were changed 6 hours after the transfection. 24 hours after the transfection, cells were treated with DMSO, Sorafenib or Erastin for 18 hours. CellROX™ Green Flow Cytometry Assay Kit (Thermo Fisher Scientific, C10492) was used to stain the cells for 30 min at 37 °C and harvested by trypsinization. Cells were resuspended in PBS and filtered by a 40μM strainer. Flow cytometry (Beckman Coulter Cytoflex LX) with 488nm laser was used for the excitation. Data were collected and analyzed with the Flow Jo (Ashland, Oregon-based FlowJo LLC).

Chromatin immunoprecipitation

Cells were washed with cold PBS twice, crosslinking was conducted with 1% formaldehyde and EGS (Thermo Fisher #21565), afterwards, glycine was used to quench reaction, cells were rinsed three times with cold PBS and scraped off from dishes for centrifuge. Crosslinked protein-bound DNA cells were lysed with CHIP lysis buffer and sonicated (Bioruptor, Diagenode) to achieve 100-500 bps chromatin fragments, sonication efficacy was validated by running 1% agarose gel. Prepare 150μg chromatin in 600μl CHIP dilution buffer, save 1% for input samples, rest of the chromatin were incubated with 5μg normal rabbit IgG antibody (Cell Signaling Technology, 2729) or anti-YAP1 antibody (Cell Signaling Technology, 4912), anti-TAZ (V386) antibody (Cell Signaling Technology, 4883), anti-ATF-4 (D4B8) antibody (Cell Signaling Technology, 11815) at 4°C for overnight. Immunocomplexes were incubated with 30μl pre-locked Sepharose Protein A beads (Affi-Prep Protein A Support, Bio-Rad; 1560006) at 4°C, 2 hours later, centrifuge the immunocomplexes at 10000 rpm for 1 minute and discard the supernatant, the beads were washed with CHIP wash buffer. Immunocomplexes were eluted from the beads, for Re-CHIP experiment, after the first step elution, half of the samples were incubated with another antibody and pre-locked Sepharose Protein A beads for the secondary immunoprecipitation. Afterwards, input and IP samples were all de-crosslinked together. De-crosslinked samples were purified with the QIAquick Gel Extraction kit (Qiagen, #28704) and eluted DNA samples were analyzed by the quantitative real-time PCR. Fold enrichments for specific *SLC7A11* promoter regions were calculated by IP over input samples and normalized to isotype-specific IgG as the negative control. Enrichments

of *CYR61* promoter was used as a positive control. Primers used in the ChIP experiment are listed in Supplementary Table VIII.

Tumor transplantation

SNU398-parental cells, SNU398-shLuc or SNU398-shYAP/TAZ cells (1*10^6 in 100µl PBS) were implanted into the left flanks of immuno-deficient NOD/SCID; common γ receptor-/- (NSG) mice. When tumors were palpable, Sorafenib (LC Laboratories, S-8502) was applied with 20mg/kg daily via gavage, SSA (Sulfasalazine, Sigma, S0883) was given at 120mg/kg via intraperitoneal injection daily, 20mM BSO (L-Buthionine-sulfoximine, Sigma, B2515) was given via drinking water for 3 weeks. Tumor width and length were measured twice a week, tumor volumes were calculated using the formulation of volume = length * width^2*0.52. All animal experiments were performed according the Swiss Federal Animal Welfare Law under approval number 2839 by the Veterinary Office of the Canton Basel Stadt.

Protein lysis, immunoprecipitation, ubiquitination assay

For immunoblotting analysis, cells were washed with 1x PBS twice and lysed with RIPA lysis buffer (Sigma R0278). Cell lysates were centrifuged and the pellets were removed before protein concentration measurement and immunoblotting analysis.

For immunoprecipitation, cells were washed with 1x PBS twice and lysed with CST lysis buffer (CST9803) supplemented with protease inhibitors (Sigma P2714) at 4°C, then centrifuged at 13000rpm for 10 minutes, and pellets were removed. 1/10 of the cell lysate was taken as input, the rest of the cell lysate were incubated with specific antibodies and protein A/G-Sepharose overnight at 4°C. After 5 times washing with CST lysis buffer, the precipitated proteins were eluted with SDS-loading buffer and analyzed by immunoblotting.

For the ubiquitination assay, cells transfected with plasmids were lysed with RIPA buffer supplemented with additional 0.1% SDS to a final concentration of 0.2% SDS, followed by standard immunoprecipitation protocols.

For immunoblotting analysis, protein samples were fractionated by SDS-PAGE gels and transferred to PVDF membranes, then membranes were blocked with 5% skimmed milk in TBST, and antibodies were incubated with the membranes overnight at 4 °C. Membranes were washed with TBST 3x10 min and incubated with the

secondary antibodies for 2 hours at room temperature, then washed for 3x10 min with TBST. Chemiluminescence was detected with X-Ray films (FUJIFILM) or Fusion machine (Analis) once the membranes were incubated with chemiluminescent HRP substrate (Millipore WBKLS0500). Fiji software was used to quantify the immunoblots by densitometry (NIH Image). Information on the antibodies used is presented in Suppl. Table VII.

RNA extraction and quantitative RT-PCR

RNA samples were extracted with TRIZOL reagent (Sigma T9424), reverse transcription PCR was performed with Reverse Transcriptase kit (Promega A3803), real-time PCR was performed using Powerup SYBR Green PCR master mix (A25743) and a Step-One Plus real-time PCR machine (Applied Biosystems). Human RPL19 expression was used for normalization. Sequences of primers are list at Suppl. Table VIII.

Immunofluorescence

Cells were cultured on coverslips, washed with PBS twice and fixed with 4% Paraformaldehyde for 10 min, and then washed twice with PBS. Cells were permeabilized with 0.1% Triton (DAPI was also diluted into Triton at 100ng/ml to stain the nucleus) on ice for 10 min. After three times wash with PBS, cells were blocked with 5% goat serum for 1 hour at room temperature, then incubated with diluted antibodies (in 5% goat serum) overnight at 4°C. Cells were washed with PBS three times then incubated with secondary antibody (1:200 dilution) at room temperature for 1 hour. Then cells were washed with PBS three times, and mounting medium was added to mount coverslips to glass slides. Immunofluorescence staining was visualized on Leica DMI 4000/6000 microscope.

Immunohistochemistry

Tumor sections were deparaffinized with 3x10 min Roticlear, 2x5 min 100% EtOH, 1x10 min 90% EtOH, 1x5 min 80% EtOH, 1x5 min 70% EtOH, 1x5 min 30% EtOH, 3x10 min PBS. Antigen-retrieval was performed in 10mM pH6.0 citrate buffer in a pressure-cooker, then washed 3x10 min with 0.3% Trition-100 in PBS. Peroxidase was quenched with 3% H_2O_2 for 10 min, washed with PBS 3x10 min, then blocked with 2.5% goat serum for 30 min at room temperature. Incubation with primary

antibody (diluted into 2.5% goat serum) was at 4°C overnight, followed by washing 3x10 min with PBS, incubation with secondary antibody (Vector MP-7541-50) at room temperature for 30 min, washing 3x10 min with PBS, incubation with peroxidase substrate (Vector SK-4105) at room temperature for 5 min and washing with water for 5 min. Counterstaining with Hematoxylin was done for 1 min to stain nuclei, followed by washing with water for 5 min, and dehydration with 50% EtOH, 70% EtOH and 95% EtOH for 5 min each, then 2x10 min 100% EtOH, and clearing with 2x10 minu xylene. Coverslip were mounted with 2 to 3 drops mounting media (Thermo Fisher Scientific Cytoseal™ XYL mounting media 8312-4) and let dry overnight. Slides were imaged with a Zeiss brightfield microscope (Zeiss Axioskop 2 Plus) and analyzed with Fiji (NIH Image).

Immunohistochemistry of Patient Samples

Immunohistochemical staining of SLC7A11 was assessed on a TMA of an independent cohort of 233 HCCs, 119 cirrhotic tissues and 19 normal liver samples, as previously described [248]. Additionally, SLC7A11 and YAP staining were performed in 10 HCC patients using whole serial tissue slides. Similarly, YAP and ATF4 staining were performed in a cohort of 18 HCC patients using whole serial tissue slides. Staining was performed on a Leica Bond III immunohistochemistry staining system (Muttenz, Switzerland) using DAB as chromogen as previously described [249]. Antigen retrieval was performed using HIER 2 solution. Primary antibodies were used at the following concentration: anti-SLC7A11 (1:50, Cell Signaling clone 12691S), YAP (1:500, abcam ab52771) and ATF4 (1:100, Abcam ab221791).

Synthetic lethality screening

The barcoded shRNA library which targets 6317 mRNAs (50467 shRNA) involved in signaling pathways (Human genome-wide pooled lentiviral shRNA library module 1, Vector: pRSI16cb, Cellecta) was introduced to Sorafenib-resistant cells by lentiviral transduction with a MOI=0.5, 2μg/mL Puromycin were treated on cells to select the successfully infected cells. Cells were cultured with 7μM Sorafenib and the medium was refreshed three times a week for 4 weeks to generate enough cell numbers. Genomic DNA was extracted with the QIAGEN QIAamp DNA Micro Kit (QIAGEN, #56304). shRNA barcodes were amplified with the NGS Prep Kit (For shRNA Libraries

in pRSI16cb (KOHGW), Biocat, # LNGS-120-CT). PCR products were purified with the QIAquick PCR purification kit (QIAGEN, #28106) and separated by electrophoresis in 3.5% agarose gel, exact bands were cut out and purified with the QIAquick gel extraction kit (QIAGEN, #28706), DNA concentrations were measured and adjusted to 10nM, Next-Generation Sequencing (NGS) of pooled amplified barcodes were performed on Illumina's HiSeq.

RNA sequencing analysis

RNA was extracted in biological triplicates using miRNeasy Mini kit (Qiagen) according to the manufacturer's instructions. RNA quality control was performed using a fragment analyser and the standard or high-sensitivity RNA analysis kits (Labgene; DNF-471-0500 or DNF-472-0500). RNA concentrations were measured using the Quanti-iTTM RiboGreen RNA assay Kit (Life Technologies/Thermo Fisher Scientific). A total of 200ng of RNA was utilized for library preparation with the TruSeq stranded total RNA LT sample prep Kit (Illumina). Poly-A + RNA was sequenced with HiSeq SBS Kit v4 (Illumina) on an Illumina HiSeq 2500 using protocols defined by the manufacturer.

Single-end RNA-seq reads (81-mers) were mapped to the human genome assembly, version hg19 (GRCh37.75), with RNA-STAR [250], with default parameters except for allowing only unique hits to genome (outFilterMultimapNmax=1) and filtering reads without evidence in spliced junction table (outFilterType="BySJout"). Expression levels per gene (counts over exons) for the RefSeq mRNA coordinates from UCSC (genome.ucsc.edu, downloaded in December 2015) were quantified using qCount function from QuasR package (version 1.12.0). The differentially expressed genes were identified using the edgeR package (version 3.14.0). Genes with p-values smaller than 0.05 and minimum log2-fold changes of +/-0.58 were considered as differentially regulated and were used for downstream functional and pathway enrichment analysis.

Functional enrichment analysis

We performed functional enrichment analysis of differentially expressed genes for biological processes or pathways in R using several publicly available Bioconductor resources, including org.Hs.eg.db (version 3.3.0), GO.db (version 3.4.1), GOstats (version 2.42.0) [251], KEGG.db (version 3.2.3) and ReactomePA (version 1.16.2)

[252]. The significance of each biological processes or pathways identified was calculated using the hypergeometric test (equivalent to Fisher's exact test) and those with p values ≤0.05 were considered significant.

Gene set enrichment analysis (GSEA)

The GSEA analysis was performed using the JAVA application of the Broad Institute version 3.0 (http://www.broadinstitute.org/gsea). The gene sets used for the analysis were derived from gene ontology annotations, and pathways were obtained from the Kyoto Encyclopedia of Genes and Genomes (KEGG) (http://www.genome.jp/kegg/) databases.

Patient material and ethics

All relevant ethical regulations were strictly followed in this study. All the analysis using human tissue samples reported in this study were approved by the ethics commission of Northwestern Switzerland (EKNZ, approval No.361/12).

Re-analysis of transcriptomic profiling data

RNA-sequencing gene expression values were retrieved from om TCGA Liver dataset [253] using the cbioportal (http://www.cbioportal.org, accessed 05/12/2017) website [254]. The dataset included 364 and 314 HCCs with overall survival and disease-free survival information, respectively. Survival analyses were performed using the Kaplan-Meier method and the log-rank test. The cut-off was defined as previously described [255].

Statistical analysis

All statistical tests were two-sided. Data are presented as mean. Bar plots with error bars represent mean ± standard derivation (SD). All analyses were performed using Prism 8.0 (Graphpad Software, Inc., La Jolla, CA) as indicated in the figure legend.

3.2.6 Supplementary Information

Supplementary Figures

Suppl Figure 1. Gao et al

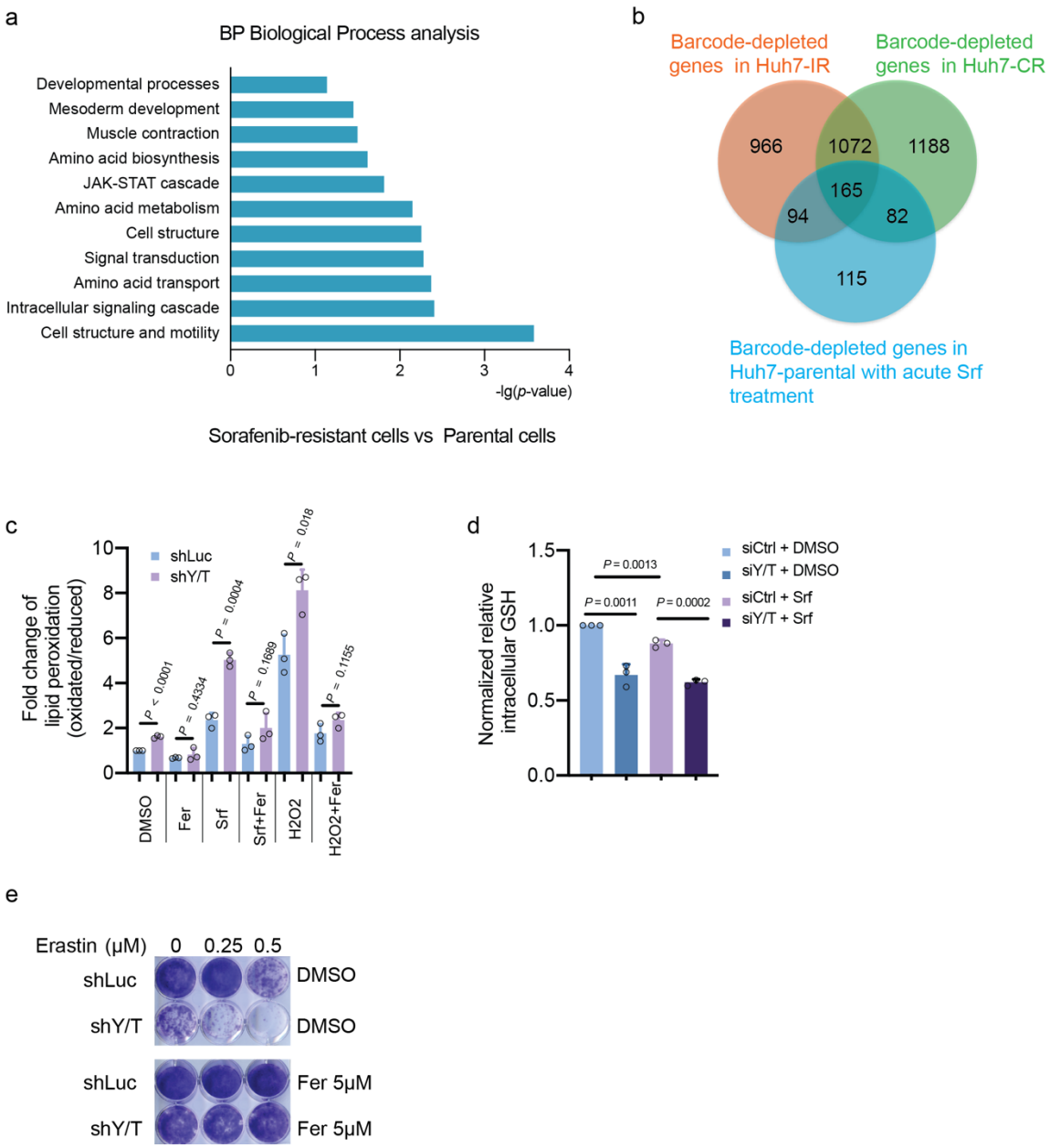

Supplementary Figure 1. YAP/TAZ are key drivers of Sorafenib resistance through inhibition of lipid peroxidation.

(a) Biological process analysis of the gene expression profiles of Sorafenib-resistant cells revealed a significant shift in amino acid metabolism, among other signaling pathways and regulatory networks. **(b)** Overlapping Barcode-depleted genes in Huh7-IR/CR and Huh7-parental with acute Sorafenib treatment. 1072 barcode-depleted genes were identified to maintain Sorafenib resistance after subtracting the 165 barcode-depleted genes in acute Sorafenib-treated Huh7-parental cells. **(c)** Lipid peroxidation levels increased upon depletion of YAP/TAZ, in particular in combination with Sorafenib (Srf) or H2O2. This increase could be repressed by the ferroptosis inhibitor Ferrostatin-1 (Fer). HLE-shLuc and HLE-shY/T cells were treated as indicated and stained with C11-BODIPY

581/591. Reduced-Bodipy was measured by flow cytometry with a 488 nm laser and oxidized-Bodipy was measured using a 561 nm laser. Ratios of oxidized/reduced represent the fold-change of lipid peroxidation. Statistical significance was calculated using one-way ANOVA. **(d)** Intracellular GSH levels declined with the depletion of YAP/TAZ either with or without Sorafenib treatment. HLE-shLuc and HLE-shY/T cells were cultured with DMSO or 6μM Sorafenib for 18 hours, and intracellular GSH levels were measured using the GSH-Glo Glutathione Assay kit. Statistical significance was calculated using one-way ANOVA. **(e)** Erastin-induced cell death of YAP/TAZ-depleted HCC cells was prevented by Ferrostatin-1. HLE-shLuc and HLE-shY/T cells were treated with different concentrations of Erastin (0, 0.25, 0.5μM) plus DMSO or Ferrostatin-1 (Fer; 5μM) for 2 weeks. Results represent three independent experiments.

Suppl Figure 2. Gao et al

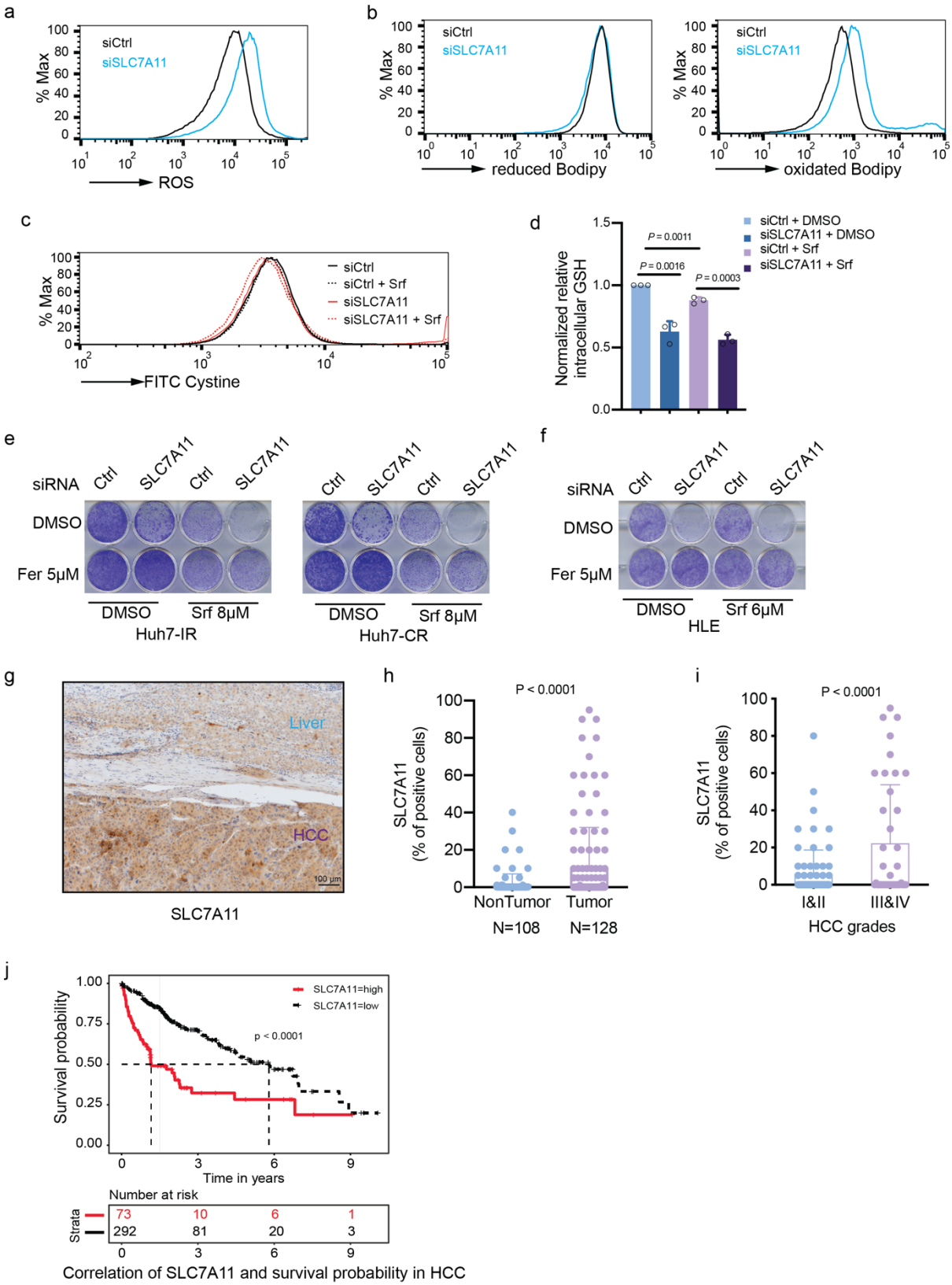

Supplementary Figure 2. SLC7A11 is a regulator of ferroptosis in HCC cells.

Results

(a) Basal reactive oxygen (ROS) levels increased upon loss of SLC7A11. HLE cells were transfected with siCtrl or siSLC7A11 and cultured for 36 hours were stained with CellROX™ Green Flow Cytometry Assay Kit, ROS levels were measured by flow cytometry using a 488 nm laser. Results represent three independent experiments. **(b)** Basal lipid peroxidation levels increased with the loss of SLC7A11. HLE cells were transfected with siCtrl or siSLC7A11 and cultured for 36 hours were stained with C11-BODIPY 581/591. Reduced-Bodipy was measured by flow cytometry using a 488 nm laser, and oxidized-Bodipy was measured with a 561 nm laser. A significant shift of oxidized-Bodipy occurred upon depletion of SLC7A11. Results represent three independent experiments. **(c)** SLC7A11 deficiency impaired cystine uptake by HCC cells either with or without Sorafenib treatment. HLE cells were transfected with siCtrl or siSLC7A11 were treated for 18 hours with DMSO or 6μM Sorafenib. Cystine-FITC was added to the cells for 30 minutes at 37ºC, and intracellular Cystine-FITC levels were determined by flow cytometry with a 488 nm laser. Results represent three independent experiments. **(d)** Intracellular GSH levels declined with the depletion of SLC7A11 either with or without Sorafenib treatment. HLE cells were transfected with siCtrl or siSLC7A11 were treated with DMSO or 6μM Sorafenib for 18 hours, and intracellular GSH levels were measured using the GSH-Glo Glutathione Assay kit. Statistical significance was calculated using one-way ANOVA. **(e)** Colony formation assay demonstrating that the ferroptosis inhibitor Ferrostatin-1 (Fer) could reverse Sorafenib-induced cell death in SLC7A11-deficient HCC cells. Huh7-IR and Huh7-CR cells were transfected with siCtrl or siSLC7A11 and treated with Sorafenib (8μM) or DMSO plus either DMSO or Ferrostatin-1 (Fer; 5μM) for 2 weeks. Results represent three independent experiments. **(f)** Colony formation assay showing that the ferroptosis inhibitor Ferrostatin-1 (Fer) could reverse Sorafenib-induced cell death in SLC7A11-deficient HCC cells. HLE cells transfected with siCtrl or siSLC7A11 were treated with Sorafenib (6μM) or DMSO plus either DMSO or Ferrostatin-1 (Fer; 5μM) for 2 weeks. Results represent three independent experiments. **(g)** Immunohistochemical staining of SLC7A11 in HCC and adjacent non-neoplastic areas from patients. Tumor tissues showed a higher expression of SLC7A11. Scale bar, 100μm. **(h)** Quantification of SLC7A11-positive cells in tumor and non-tumor samples showed that HCC tumors present higher SLC7A11 levels. Statistical significance was calculated using unpaired t-test. **(i)** SLC7A11 protein correlated with aggressiveness of HCC samples as assessed by Edmonson grade III and IV samples. Statistical significance was calculated using unpaired t-test. **(k)** Kaplan-Meyer analysis of the TCGA database revealed that high SLC7A11 expression in HCC of patients significantly correlated with poor clinical outcome. Statistical significance was calculated using log-rank (Mantel-Cox) test.

Suppl Figure 3. Gao et al

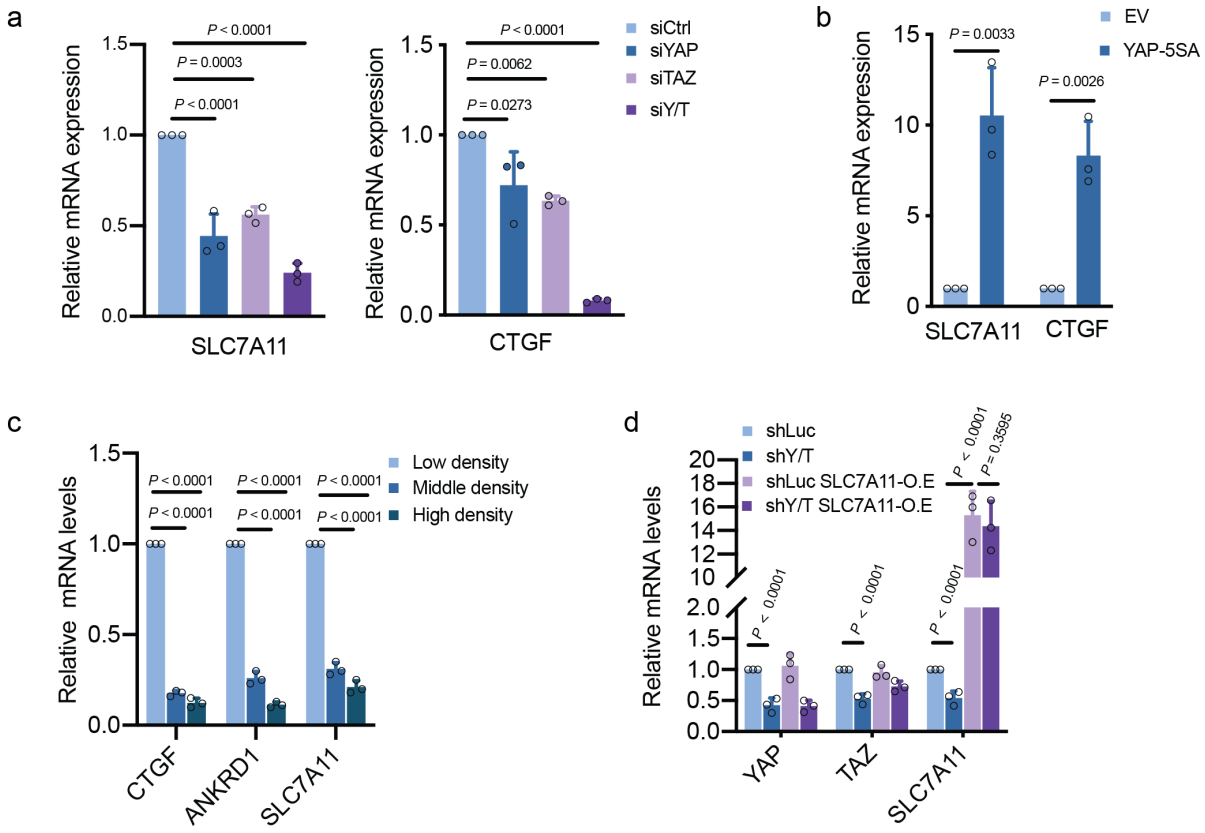

Supplementary Figure 3. YAP/TAZ transcriptionally upregulate *SLC7A11* expression.

(a) Either YAP or TAZ deficiency, and most effectively their combinatorial depletion, reduced SLC7A11 mRNA levels. HLE cells were transfected with siCtrl, siYAP, siTAZ or siY/T as indicated, and mRNA levels were determined by quantitative RT-PCR. The YAP/TAZ transcriptional target CTGF served as positive control. Statistical significance was calculated using one-way ANOVA. **(b)** The forced expression of a constitutive-active form of YAP (YAP-5SA) upregulated SLC7A11 expression. HLE cells were transfected with empty vector (EV) or a vector coding for YAP-5SA, and SCL7A11 mRNA levels were determined by quantitative RT-PCR. CTGF served as positive control. Statistical significance was calculated using one-way ANOVA. **(c)** High cell density reduced the SLC7A11 mRNA levels. HLE cells were seeded at different cell numbers to obtain low, medium and high cell densities. SCL7A11 mRNA levels were determined by quantitative RT-PCR. CTGF and ANKRD1 served as positive controls. Statistical significance was calculated using one-way ANOVA. **(d)** Validation of shRNA-mediated depletion of YAP and TAZ expression and of the forced expression of SLC7A11. The efficiency of shRNA-mediated knockdown of YAP/TAZ (shY/T) and of the forced expression of SLC7A11 (SLC7A11-OE) was determined by quantitative RT-PCR. Statistical significance was calculated using one-way ANOVA.

Suppl Figure 4. Gao et al

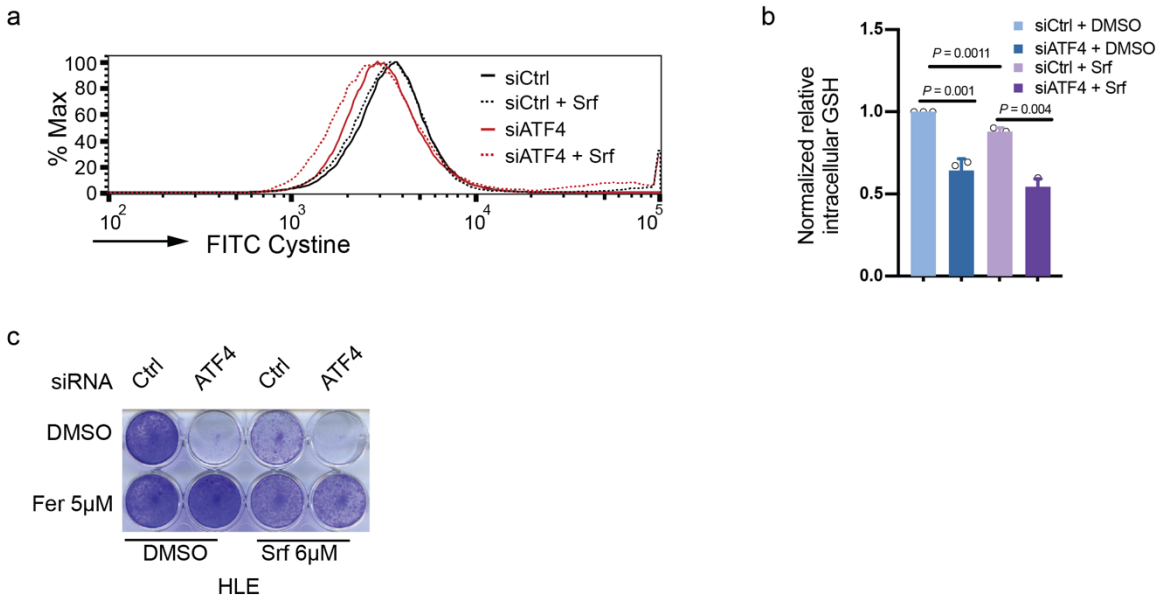

Supplementary Figure 4. ATF4 regulates ferroptosis.

(a) Depletion of ATF4 impaired cystine uptake in the presence or absence of Sorafenib. HLE cells transfected with siCtrl or siATF4 were treated with DMSO or 6μM Sorafenib for 18 hours. Cystine-FITC was added to the for 30 minutes ay 37ºC, and the intracellular Cystine-FITC levels were determined by flow cytometry with a 488 nm laser. Results represent three independent experiments. **(b)** Intracellular GSH levels declined with the depletion of ATF4 either with or without Sorafenib treatment. HLE cells were transfected with siCtrl or siATF4 were treated with DMSO or 6μM Sorafenib for 18 hours, and intracellular GSH levels were measured using the GSH-Glo Glutathione Assay kit. Statistical significance was calculated using one-way ANOVA. **(c)** Colony formation assay showing that the ferroptosis inhibitor Ferrostatin-1 (Fer) could reverse Sorafenib-induced cell death in ATF4-deficient HCC cells. HLE cells transfected with siCtrl or siATF4 were treated with Sorafenib (6μM) or DMSO plus either DMSO or Ferrostatin-1 (Fer; 5μM) for 2 weeks. Results represent three independent experiments.

Suppl Figure 5. Gao et al

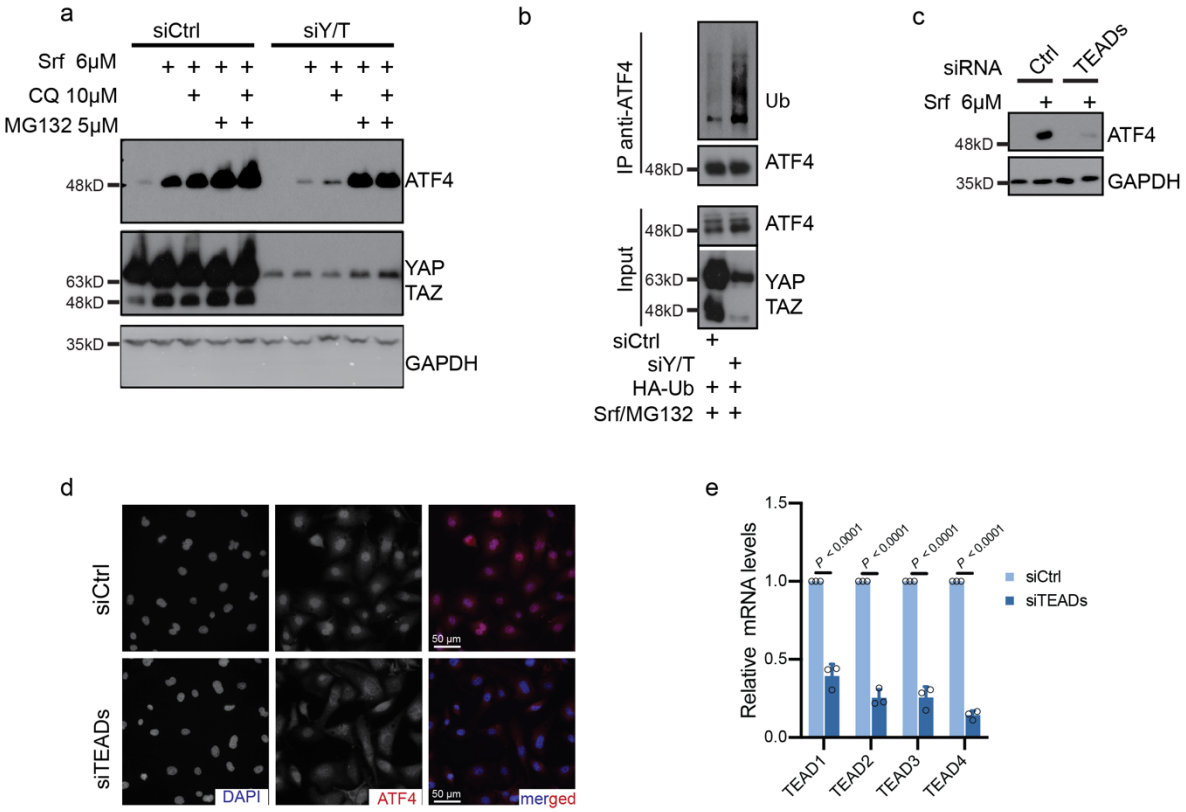

Supplementary Figure 5. YAP/TAZ and TEADs stabilize ATF4 protein.

(a) YAP/TAZ protected ATF4 from proteasome-mediated degradation but not autophagy. HLE cells were transfected with siCtrl or siYAP/TAZ (siY/T) and treated with Sorafenib and the autophagy inhibitor chloroquine (CQ) or the proteasome inhibitor MG132 for 18 hours, as indicated. Immunoblotting showed that YAP/TAZ deficiency declined Sorafenib induced ATF4 protein levels which was blocked by MG132 but not by CQ. GAPDH served as loading control. Results represent three independent experiments. **(b**) YAP/TAZ deficiency promoted ubiquitylation of ATF4. HLE cells were treated with Sorafenib and MG132 for 18 hours, before ATF4 was immunoprecipitated, and the immunoprecipitates were analyzed by immunoblotting for ATF4 and ubiquitylation of ATF4 (Ub) and for ATF4 and YAP/TAZ in the input samples. Results represent three independent experiments. **(c)** TEAD deficiency reduced ATF4 expression. HLE cells were transfected with siCtrl or siTEADs (siTEAD1 + siTEAD2 + siTEAD3 + siTEAD4) and treated with 6μM Sorafenib. Immunoblotting visualized the levels of ATF4. GAPDH served as loading control. Results represent three independent experiments. **(d)** TEADs direct the nuclear localization of ATF4. HLE cell were transfected with siCtrl or siTEADs, and the nuclear localization of ATF4 was analyzed by immunofluorescence microscopy. DAPI visualized nuclei. Scale bar, 50μm. **(e)** Validation of the knockdown efficiency of siTEAD-transfected HLE cells as determined by quantitative RT-PCR for TEAD1, TEAD2, TEAD3 and TEAD4. Statistical significance was calculated using one-way ANOVA.

Supplementary Tables

Suppl. Table I. Biological process analysis of gene expression in Sorafenib-resistant cells (Excel file).

Suppl. Table II. Barcode-depleted genes in Huh7-IR/CR cells subtracted with depleted genes in acute Sorafenib-treated Huh7-Parental cells (Excel file).

Suppl. Table III. Overlapping elements of barcode-depleted genes and genes up-regulated in expression in Sorafenib-resistant cells (Excel file).

Suppl. Table IV. Overlapping elements of genes down-regulated in expression in siYAP/TAZ-transfected HLE cells and genes up-regulated in Sorafenib-resistant cells Excel file).

Suppl. Table V. Overlapping elements of genes down-regulated in expression in both siATF4 and siYAP/TAZ-transfected HLE cells upon Sorafenib treatment (Excel file).

Suppl. Table VI. siRNAs used in the study.

	Catalog ID (Horizon discovery)
siCtrl	ON-TARGET plus non-targeting pool (D-001810-10-20)
siYAP1	ON-TARGET plus Human YAP1 (L-012200-00-0005)
siTAZ	ON-TARGET plus Human TAZ (L-009608-00-0005)
siATF4	ON-TARGET plus Human ATF4 (L-005125-00-0005)
siSLC7A11	ON-TARGET plus Human SLC7A11 (L-007612-01-0005)
siNRF2	ON-TARGET plus Human NFE2L2 siRNA (L-003755-00-0005)

Suppl. Table VII. Antibodies used in the study.

Antibodies	SOURCE	IDENTIFIER
YAP	CST	4912
YAP	Abcam	Ab52771
TAZ(V386)	CST	4883
YAP/TAZ (63.7)	Santa Cruz	Sc-101199
GAPDH	Abcam	ab9485
ATF-4 (D4B8)	CST	11815
ATF-4	Abcam	Ab221791

SLC7A11 (D2M7A)	CST	12691S
4-HNE	Abcam	ab46545
NRF2 (EP1808Y)	Abcam	ab62352
Lamin A/C	Santa Cruz	Sc-6215
Cleaved-caspase3	CST	9661
Ki67	Abcam	ab833
Ubiquitin	CST	3933

Suppl. Table VIII. Oligonucleotides used in the study.

Oligonucleotides	5' --- 3'
hRPL19, forward primer	GATGCCGGAAAAACACCTTG
hPRL19, reverse primer	CAGGGCAGTGATCTCCTTCTG
YAP, forward primer	CCTTCTTCAAGCCGCCGGAG
YAP, reverse primer	CAGTGTCCCAGGAGAAACAGC
TAZ, forward primer	TATCCCAGCCAAATCTCGTG
TAZ, reverse primer	TTCTGCTGGCTCAGGGTACT
ATF4, forward primer	CCCTTCACCTTCTTACAACCTC
ATF4, reverse primer	TGCCCAGCTCTAAACTAAAGGA
CTGF, forward primer	AGGAGTGGGTGTGTGACGA
CTGF, reverse primer	CCAGGCAGTTGGCTCTAATC
CYR61, forward primer	AGCCTCGCATCCTATACAACC
CYR61, reverse primer	TTCTTTCACAAGGCGGCACTC
SLC7A11, forward primer	TCTCCAAAGGAGGTTACCTGC
SLC7A11, reverse primer	AGACTCCCCTCAGTAAAGTGAC
ANKRD1, forward primer	AGTAGAGGAACTGGTCACTGG
ANKRD1, reverse primer	TGGGCTAGAAGTGTCTTCAGA
ATF3, forward primer	CGCTGGAATCAGTCACTGTCAG
ATF3, reverse primer	CTTGTTTCGGCACTTTGCAGCTG
CHAC1, forward primer	GTGGTGACGCTCCTTGAAGATC
CHAC1, reverse primer	GAAGGTGACCTCCTTGGTATCG
NRF2, forward primer	CACATCCAGTCAGAAACCAGTGG
NRF2, reverse primer	GGAATGTCTGCGCCAAAAGCTG

CYR61-CHIP-F	CCCTTGGCTGTTATGAGGAA
CYR61-CHIP-R	CCTTGCATTCCTTTGCATTT
ATF3-AARE-CHIP-F	GGCTCCGGTCCTGATAT G
ATF3-AARE-CHIP-R	CACTGGTGATGCAAGTTCGG
SLC7A11-AARE-CHIP-F	TTGAGCAACAAGCTCCTCCT
SLC7A11-AARE-CHIP -R	CAAACCAGCTCAGCTTCCTC
SLC7A11-CHIP-P1-F	GTAGCTTTAGGATACATTCTACTCACA
SLC7A11-CHIP-P1-R	GCAACTCGTAGTGAGCAACA
SLC7A11-CHIP-P2-F	TTGGATTTGACTGTATTGCCTT
SLC7A11-CHIP-P2-R	TTGTGAGTAGAATGTATCCTAAAGC
Negative control Chr10 (NC10)-F	ACCAACACTCTTCCCTCAGC
Negative control Chr10 (NC10)-R	TTATTTTGGTTCAGGTGGTTGA

3.2.7 Acknowledgements

We thank Prof. Andras Kapus, Prof. Boyi Gan and Dr. Alexander Hergovich for their support with plasmids. We thank C. Beisel and the Genomics Facility Basel for RNA-sequencing. E. Panoussis, U. Schmieder and the DBM animal core facility for the support with animal experiments, P. Lorentz and the DBM microscopy facility for imaging, Mike N. Hall and Jan Tchorz for constructive suggestions. We thank the tissue biobank of the Institute of Pathology at the University Hospital of Basel for providing slides of the Tissue microarray.

3.2.8 Author contributions

F.T. and G.C conceived this study. R.G. and F.T. designed and performed the experiments, analyzed the data and wrote the manuscript. G.C. designed the experiments and wrote the manuscript. D.B and F.T. established the cell lines. R.G and F.T. performed the synthetic lethal screening, S.S. helped to conduct ChIP-qPCR. R.K.R.K analyzed the RNA-sequencing data. M.C.-L., C.E. and S.P. performed the histopathological analysis.

References

1. Tang, A., et al., *Epidemiology of hepatocellular carcinoma: target population for surveillance and diagnosis.* 2018. **43**(1): p. 13-25.
2. Ahmed, I. and D.N.J.S. Lobo, *Malignant tumours of the liver.* 2009. **27**(1): p. 30-37.
3. Forner, A., M. Reig, and J.J.T.L. Bruix, *Hepatocellular carcinoma.* 2018. **391**(10127): p. 1301-1314.
4. Hajarizadeh, B., et al., *Epidemiology and natural history of HCV infection.* 2013. **10**(9): p. 553.
5. Heidelbauch, J. and M. Bruderly, *Cirrhosis and chronic liver failure: part I diagnosis and evaluation.* 2006.
6. Kudo, M.J.L.C., *Management of hepatocellular carcinoma in Japan as a world-leading model.* 2018. **7**(2): p. 134-147.
7. Yang, J.D., et al., *Hepatocellular carcinoma occurs at an earlier age in Africans, particularly in association with chronic hepatitis B.* 2015. **110**(11): p. 1629-1631.
8. Yang, J.D., L.R.J.N.r.G. Roberts, and hepatology, *Hepatocellular carcinoma: a global view.* 2010. **7**(8): p. 448.
9. Macek Jilkova, Z., K. Kurma, and T.J.C. Decaens, *Animal models of hepatocellular carcinoma: the role of immune system and tumor microenvironment.* 2019. **11**(10): p. 1487.
10. Thomas, M.B. and A.X.J.J.o.C.O. Zhu, *Hepatocellular carcinoma: the need for progress.* 2005. **23**(13): p. 2892-2899.
11. Cheng, A.-L., et al., *Efficacy and safety of sorafenib in patients in the Asia-Pacific region with advanced hepatocellular carcinoma: a phase III randomised, double-blind, placebo-controlled trial.* 2009. **10**(1): p. 25-34.
12. El-Serag, H.B.J.G., *Epidemiology of viral hepatitis and hepatocellular carcinoma.* 2012. **142**(6): p. 1264-1273. e1.
13. Llovet, J.M., C. Brú, and J. Bruix. *Prognosis of hepatocellular carcinoma: the BCLC staging classification*. in *Seminars in liver disease*. 1999. © 1999 by Thieme Medical Publishers, Inc.
14. Park, J.W., et al., *Global patterns of hepatocellular carcinoma management from diagnosis to death: the BRIDGE Study.* 2015. **35**(9): p. 2155-2166.
15. Sanoff, H.K., et al., *Everolimus and pasireotide for advanced and metastatic hepatocellular carcinoma.* 2015. **33**(2): p. 505-509.
16. Wilhelm, S., et al., *Discovery and development of sorafenib: a multikinase inhibitor for treating cancer.* 2006. **5**(10): p. 835-844.
17. Llovet, J.M., et al., *Sorafenib in advanced hepatocellular carcinoma.* 2008. **359**(4): p. 378-390.
18. Kudo, M., et al., *Lenvatinib versus sorafenib in first-line treatment of patients with unresectable hepatocellular carcinoma: a randomised phase 3 non-inferiority trial.* 2018. **391**(10126): p. 1163-1173.
19. Kudo, M.J.O., *Systemic therapy for hepatocellular carcinoma: 2017 update.* 2017. **93**(Suppl. 1): p. 135-146.
20. Finn, R.S., et al., *Atezolizumab plus bevacizumab in unresectable hepatocellular carcinoma.* 2020. **382**(20): p. 1894-1905.
21. Llovet, J.M., et al., *A molecular signature to discriminate dysplastic nodules from early hepatocellular carcinoma in HCV cirrhosis.* 2006. **131**(6): p. 1758-1767.

22. Calado, R.T., et al., *Constitutional telomerase mutations are genetic risk factors for cirrhosis.* 2011. **53**(5): p. 1600-1607.
23. Amaddeo, G., et al., *Integration of tumour and viral genomic characterisations in HBV-related hepatocellular carcinomas.* 2015. **64**(5): p. 820-829.
24. Bruix, J. and M.J.H. Sherman, *Management of hepatocellular carcinoma.* 2005. **42**(5): p. 1208-1236.
25. Bruix, J. and M.J.H. Sherman, *Management of hepatocellular carcinoma: an update.* 2011. **53**(3): p. 1020.
26. Guichard, C., et al., *Integrated analysis of somatic mutations and focal copy-number changes identifies key genes and pathways in hepatocellular carcinoma.* 2012. **44**(6): p. 694.
27. Hartmann, D., et al., *Telomerase gene mutations are associated with cirrhosis formation.* 2011. **53**(5): p. 1608-1617.
28. Kotoula, V., et al., *Expression of human telomerase reverse transcriptase in regenerative and precancerous lesions of cirrhotic livers.* 2002. **22**(1): p. 57-69.
29. Nault, J.C., et al., *High frequency of telomerase reverse-transcriptase promoter somatic mutations in hepatocellular carcinoma and preneoplastic lesions.* 2013. **4**(1): p. 1-7.
30. Bressac, B., et al., *Selective G to T mutations of p53 gene in hepatocellular carcinoma from southern Africa.* 1991. **350**(6317): p. 429-431.
31. Wang, J., et al., *Hepatitis B virus integration in a cyclin A gene in a hepatocellular carcinoma.* 1990. **343**(6258): p. 555-557.
32. Audard, V., et al., *Cholestasis is a marker for hepatocellular carcinomas displaying β-catenin mutations.* 2007. **212**(3): p. 345-352.
33. de La Coste, A., et al., *Somatic mutations of the β-catenin gene are frequent in mouse and human hepatocellular carcinomas.* 1998. **95**(15): p. 8847-8851.
34. Totoki, Y., et al., *Trans-ancestry mutational landscape of hepatocellular carcinoma genomes.* 2014. **46**(12): p. 1267.
35. Hsu, I., et al., *Mutational hot spot in the p53 gene in human hepatocellular carcinomas.* 1991. **350**(6317): p. 427-428.
36. Hindupur, S.K., et al., *The protein histidine phosphatase LHPP is a tumour suppressor.* 2018. **555**(7698): p. 678-682.
37. Ahn, S.M., et al., *Genomic portrait of resectable hepatocellular carcinomas: implications of RB1 and FGF19 aberrations for patient stratification.* 2014. **60**(6): p. 1972-1982.
38. Sawey, E.T., et al., *Identification of a therapeutic strategy targeting amplified FGF19 in liver cancer by Oncogenomic screening.* 2011. **19**(3): p. 347-358.
39. Chiang, D.Y., et al., *Focal gains of VEGFA and molecular classification of hepatocellular carcinoma.* 2008. **68**(16): p. 6779-6788.
40. Craig, A.J., et al., *Tumour evolution in hepatocellular carcinoma.* 2020. **17**(3): p. 139-152.
41. Lowinger, T.B., et al., *Design and discovery of small molecules targeting raf-1 kinase.* 2002. **8**(25): p. 2269-2278.
42. Carlomagno, F., et al., *BAY 43-9006 inhibition of oncogenic RET mutants.* 2006. **98**(5): p. 326-334.
43. Liu, L., Y. Cao, and C.J.P.p.A.A.C.R.N.C.I.E.O.R.T.C. Chen, *Sorafenib (BAY 43-9006) inhibits the Raf/MEK/ERK pathway in hepatocellular carcinoma (HCC) cells and produces robust efficacy against PLC/PRF/5 HCC tumors in mice.* 2005.

44. Wilhelm, S.M., et al., *BAY 43-9006 exhibits broad spectrum oral antitumor activity and targets the RAF/MEK/ERK pathway and receptor tyrosine kinases involved in tumor progression and angiogenesis.* 2004. **64**(19): p. 7099-7109.
45. Rahmani, M., et al., *Apoptosis induced by the kinase inhibitor BAY 43-9006 in human leukemia cells involves down-regulation of Mcl-1 through inhibition of translation.* 2005. **280**(42): p. 35217-35227.
46. Yu, C., et al., *The role of Mcl-1 downregulation in the proapoptotic activity of the multikinase inhibitor BAY 43-9006.* 2005. **24**(46): p. 6861-6869.
47. Dixon, S.J., et al., *Pharmacological inhibition of cystine–glutamate exchange induces endoplasmic reticulum stress and ferroptosis.* 2014. **3**: p. e02523.
48. Louandre, C., et al., *Iron-dependent cell death of hepatocellular carcinoma cells exposed to sorafenib.* 2013. **133**(7): p. 1732-1742.
49. Lachaier, E., et al., *Sorafenib induces ferroptosis in human cancer cell lines originating from different solid tumors.* 2014. **34**(11): p. 6417-6422.
50. Zucman-Rossi, J., et al., *Genetic landscape and biomarkers of hepatocellular carcinoma.* 2015. **149**(5): p. 1226-1239. e4.
51. Trédan, O., et al., *Drug resistance and the solid tumor microenvironment.* 2007. **99**(19): p. 1441-1454.
52. van Malenstein, H., et al., *Long-term exposure to sorafenib of liver cancer cells induces resistance with epithelial-to-mesenchymal transition, increased invasion and risk of rebound growth.* 2013. **329**(1): p. 74-83.
53. Maheswaran, T., S.M.J.J.o.g. Rushbrook, and hepatology, *Epithelial–mesenchymal transition and the liver: Role in hepatocellular carcinoma and liver fibrosis.* 2012. **27**(3): p. 418-420.
54. Xiao, Q., Y. Zhou, and V.M.J.H.G. Lauschke, *Ethnogeographic and inter-individual variability of human ABC transporters.* 2020: p. 1-24.
55. Hoffmann, K., et al., *Sorafenib modulates the gene expression of multi-drug resistance mediating ATP-binding cassette proteins in experimental hepatocellular carcinoma.* 2010. **30**(11): p. 4503-4508.
56. Meier, Y., et al., *Interindividual variability of canalicular ATP-binding-cassette (ABC)–transporter expression in human liver.* 2006. **44**(1): p. 62-74.
57. Al-Abdulla, R., et al., *Epigenetic events involved in organic cation transporter 1-dependent impaired response of hepatocellular carcinoma to sorafenib.* 2019. **176**(6): p. 787-800.
58. Huang, W.-C., et al., *BCRP/ABCG2 inhibition sensitizes hepatocellular carcinoma cells to sorafenib.* 2013. **8**(12): p. e83627.
59. Herraez, E., et al., *Expression of SLC22A1 variants may affect the response of hepatocellular carcinoma and cholangiocarcinoma to sorafenib.* 2013. **58**(3): p. 1065-1073.
60. Zhao, Q., et al., *Increased expression of SLC46A3 to oppose the progression of hepatocellular carcinoma and its effect on sorafenib therapy.* 2019. **114**: p. 108864.
61. Morgensztern, D. and H.L.J.A.-c.d. McLeod, *PI3K/Akt/mTOR pathway as a target for cancer therapy.* 2005. **16**(8): p. 797-803.
62. Chen, K.-F., et al., *Blockade of STAT3 activation by sorafenib derivatives through enhancing SHP-1 phosphatase activity.* 2012. **55**: p. 220-227.
63. Tsujimoto, Y., S.J.C.D. Shimizu, and Differentiation, *Another way to die: autophagic programmed cell death.* 2005. **12**(2): p. 1528-1534.

64. Kalluri, R. and R.A.J.T.J.o.c.i. Weinberg, *The basics of epithelial-mesenchymal transition.* 2009. **119**(6): p. 1420-1428.
65. Liu, L.-p., et al., *Sorafenib inhibits hypoxia-inducible factor-1α synthesis: implications for antiangiogenic activity in hepatocellular carcinoma.* 2012. **18**(20): p. 5662-5671.
66. Tak, E., et al., *Human carbonyl reductase 1 upregulated by hypoxia renders resistance to apoptosis in hepatocellular carcinoma cells.* 2011. **54**(2): p. 328-339.
67. Powis, G. and L.J.M.c.t. Kirkpatrick, *Hypoxia inducible factor-1α as a cancer drug target.* 2004. **3**(5): p. 647-654.
68. Maxwell, P., et al., *Hypoxia-inducible factor-1 modulates gene expression in solid tumors and influences both angiogenesis and tumor growth.* 1997. **94**(15): p. 8104-8109.
69. Bertout, J.A., S.A. Patel, and M.C.J.N.R.C. Simon, *The impact of O 2 availability on human cancer.* 2008. **8**(12): p. 967-975.
70. Jiang, B.-H., et al., *Hypoxia-inducible factor 1 levels vary exponentially over a physiologically relevant range of O2 tension.* 1996. **271**(4): p. C1172-C1180.
71. Semenza, G.L.J.A.R.o.P.M.o.D., *Oxygen sensing, hypoxia-inducible factors, and disease pathophysiology.* 2014. **9**: p. 47-71.
72. Semenza, G.L.J.T.i.p.s., *Hypoxia-inducible factors: mediators of cancer progression and targets for cancer therapy.* 2012. **33**(4): p. 207-214.
73. Semenza, G.L.J.O., *Defining the role of hypoxia-inducible factor 1 in cancer biology and therapeutics.* 2010. **29**(5): p. 625-634.
74. Hu, C.-J., et al., *The N-terminal transactivation domain confers target gene specificity of hypoxia-inducible factors HIF-1α and HIF-2α.* 2007. **18**(11): p. 4528-4542.
75. Hu, C.-J., et al., *Differential roles of hypoxia-inducible factor 1α (HIF-1α) and HIF-2α in hypoxic gene regulation.* 2003. **23**(24): p. 9361-9374.
76. Chen, C., et al., *Regulation of glut1 mRNA by hypoxia-inducible factor-1 Interaction between H-ras and hypoxia.* 2001. **276**(12): p. 9519-9525.
77. Gordan, J.D., C.B. Thompson, and M.C.J.C.c. Simon, *HIF and c-Myc: sibling rivals for control of cancer cell metabolism and proliferation.* 2007. **12**(2): p. 108-113.
78. Rey, S. and G.L.J.C.r. Semenza, *Hypoxia-inducible factor-1-dependent mechanisms of vascularization and vascular remodelling.* 2010. **86**(2): p. 236-242.
79. Lappi-Blanco, E., et al., *VEGF and bFGF are highly expressed in intraluminal fibromyxoid lesions in bronchiolitis obliterans organizing pneumonia.* 2002. **196**(2): p. 220-227.
80. Forsythe, J.A., et al., *Activation of vascular endothelial growth factor gene transcription by hypoxia-inducible factor 1.* 1996. **16**(9): p. 4604-4613.
81. Dewhirst, M.W., Y. Cao, and B.J.N.R.C. Moeller, *Cycling hypoxia and free radicals regulate angiogenesis and radiotherapy response.* 2008. **8**(6): p. 425-437.
82. Lee, Y.J., P.M.J.M. Corry, and c. biochemistry, *Hypoxia-induced bFGF gene expression is mediated through the JNK signal transduction pathway.* 1999. **202**(1-2): p. 1-8.
83. Finger, E.C., A.J.J.C. Giaccia, and M. Reviews, *Hypoxia, inflammation, and the tumor microenvironment in metastatic disease.* 2010. **29**(2): p. 285-293.

84. Krishnamachary, B., et al., *Hypoxia-inducible factor-1-dependent repression of E-cadherin in von Hippel-Lindau tumor suppressor–null renal cell carcinoma mediated by TCF3, ZFHX1A, and ZFHX1B.* 2006. **66**(5): p. 2725-2731.
85. Yang, M.-H., et al., *Direct regulation of TWIST by HIF-1α promotes metastasis.* 2008. **10**(3): p. 295-305.
86. Imai, T., et al., *Hypoxia attenuates the expression of E-cadherin via up-regulation of SNAIL in ovarian carcinoma cells.* 2003. **163**(4): p. 1437-1447.
87. Erler, J.T., et al., *Lysyl oxidase is essential for hypoxia-induced metastasis.* 2006. **440**(7088): p. 1222-1226.
88. Comerford, K.M., et al., *Hypoxia-inducible factor-1-dependent regulation of the multidrug resistance (MDR1) gene.* 2002. **62**(12): p. 3387-3394.
89. Erler, J.T., et al., *Hypoxia-mediated down-regulation of Bid and Bax in tumors occurs via hypoxia-inducible factor 1-dependent and-independent mechanisms and contributes to drug resistance.* 2004. **24**(7): p. 2875-2889.
90. Bruick, R.K.J.P.o.t.N.A.o.S., *Expression of the gene encoding the proapoptotic Nip3 protein is induced by hypoxia.* 2000. **97**(16): p. 9082-9087.
91. Hao, J., et al., *Effects of lentivirus-mediated HIF-1α knockdown on hypoxia-related cisplatin resistance and their dependence on p53 status in fibrosarcoma cells.* 2008. **15**(7): p. 449-455.
92. Luo, D., et al., *The role of hypoxia inducible factor-1 in hepatocellular carcinoma.* 2014. **2014**.
93. Albadari, N., S. Deng, and W.J.E.o.o.d.d. Li, *The transcriptional factors HIF-1 and HIF-2 and their novel inhibitors in cancer therapy.* 2019. **14**(7): p. 667-682.
94. Liang, Y., et al., *Hypoxia-mediated sorafenib resistance can be overcome by EF24 through Von Hippel-Lindau tumor suppressor-dependent HIF-1α inhibition in hepatocellular carcinoma.* 2013. **57**(5): p. 1847-1857.
95. Li, S., et al., *Genistein suppresses aerobic glycolysis and induces hepatocellular carcinoma cell death.* 2017. **117**(10): p. 1518-1528.
96. Wu, F.-Q., et al., *ADRB2 signaling promotes HCC progression and sorafenib resistance by inhibiting autophagic degradation of HIF1α.* 2016. **65**(2): p. 314-324.
97. Zhao, D., et al., *Upregulation of HIF-2α induced by sorafenib contributes to the resistance by activating the TGF-α/EGFR pathway in hepatocellular carcinoma cells.* 2014. **26**(5): p. 1030-1039.
98. Wang, G.L., et al., *Hypoxia-inducible factor 1 is a basic-helix-loop-helix-PAS heterodimer regulated by cellular O2 tension.* 1995. **92**(12): p. 5510-5514.
99. Zundel, W., et al., *Loss of PTEN facilitates HIF-1-mediated gene expression.* 2000. **14**(4): p. 391-396.
100. Sang, N., et al., *MAPK signaling up-regulates the activity of hypoxia-inducible factors by its effects on p300.* 2003. **278**(16): p. 14013-14019.
101. Bruick, R.K. and S.L.J.S. McKnight, *A conserved family of prolyl-4-hydroxylases that modify HIF.* 2001. **294**(5545): p. 1337-1340.
102. Ivan, M., et al., *HIFα targeted for VHL-mediated destruction by proline hydroxylation: implications for O2 sensing.* 2001. **292**(5516): p. 464-468.
103. Jaakkola, P., et al., *Targeting of HIF-α to the von Hippel-Lindau ubiquitylation complex by O2-regulated prolyl hydroxylation.* 2001. **292**(5516): p. 468-472.
104. Kondo, K., et al., *Inhibition of HIF is necessary for tumor suppression by the von Hippel-Lindau protein.* 2002. **1**(3): p. 237-246.

105. Flügel, D., A. Görlach, and T.J.B. Kietzmann, *GSK-3β regulates cell growth, migration, and angiogenesis via Fbw7 and USP28-dependent degradation of HIF-1α.* 2012. **119**(5): p. 1292-1301.
106. Goto, Y., et al., *UCHL1 provides diagnostic and antimetastatic strategies due to its deubiquitinating effect on HIF-1α.* 2015. **6**(1): p. 1-13.
107. Troilo, A., et al., *HIF1α deubiquitination by USP8 is essential for ciliogenesis in normoxia.* 2014. **15**(1): p. 77-85.
108. Denko, N.C.J.N.R.C., *Hypoxia, HIF1 and glucose metabolism in the solid tumour.* 2008. **8**(9): p. 705-713.
109. Dirac, A.M. and R.J.M.C.R. Bernards, *The deubiquitinating enzyme USP26 is a regulator of androgen receptor signaling.* 2010. **8**(6): p. 844-854.
110. Pan, J., et al., *USP37 directly deubiquitinates and stabilizes c-Myc in lung cancer.* 2015. **34**(30): p. 3957-3967.
111. Martin, Y., et al., *USP29 controls the stability of checkpoint adaptor Claspin by deubiquitination.* 2015. **34**(8): p. 1058-1063.
112. Qian, W., et al., *Deubiquitinase USP29 promotes gastric cancer cell migration by cooperating with phosphatase SCP1 to stabilize Snail protein.* 2020. **39**(44): p. 6802-6815.
113. Wu, Y., et al., *USP29 enhances chemotherapy-induced stemness in non-small cell lung cancer via stabilizing Snail1 in response to oxidative stress.* 2020. **11**(9): p. 1-14.
114. Justice, R.W., et al., *The Drosophila tumor suppressor gene warts encodes a homolog of human myotonic dystrophy kinase and is required for the control of cell shape and proliferation.* 1995. **9**(5): p. 534-546.
115. Tapon, N., et al., *salvador Promotes both cell cycle exit and apoptosis in Drosophila and is mutated in human cancer cell lines.* 2002. **110**(4): p. 467-478.
116. Xu, T., et al., *Identifying tumor suppressors in genetic mosaics: the Drosophila lats gene encodes a putative protein kinase.* 1995. **121**(4): p. 1053-1063.
117. Harvey, K.F., C.M. Pfleger, and I.K.J.C. Hariharan, *The Drosophila Mst ortholog, hippo, restricts growth and cell proliferation and promotes apoptosis.* 2003. **114**(4): p. 457-467.
118. Udan, R.S., et al., *Hippo promotes proliferation arrest and apoptosis in the Salvador/Warts pathway.* 2003. **5**(10): p. 914-920.
119. Pantalacci, S., N. Tapon, and P.J.N.c.b. Léopold, *The Salvador partner Hippo promotes apoptosis and cell-cycle exit in Drosophila.* 2003. **5**(10): p. 921-927.
120. Wu, S., et al., *hippo encodes a Ste-20 family protein kinase that restricts cell proliferation and promotes apoptosis in conjunction with salvador and warts.* 2003. **114**(4): p. 445-456.
121. Dong, J., et al., *Elucidation of a universal size-control mechanism in Drosophila and mammals.* 2007. **130**(6): p. 1120-1133.
122. Huang, J., et al., *The Hippo signaling pathway coordinately regulates cell proliferation and apoptosis by inactivating Yorkie, the Drosophila Homolog of YAP.* 2005. **122**(3): p. 421-434.
123. Zhao, B., et al., *Inactivation of YAP oncoprotein by the Hippo pathway is involved in cell contact inhibition and tissue growth control.* 2007. **21**(21): p. 2747-2761.
124. Hong, W. and K.-L. Guan. *The YAP and TAZ transcription co-activators: key downstream effectors of the mammalian Hippo pathway*. in *Seminars in cell & developmental biology*. 2012. Elsevier.

125. Liu, C.-Y., et al., *The hippo tumor pathway promotes TAZ degradation by phosphorylating a phosphodegron and recruiting the SCFβ-TrCP E3 ligase.* 2010. **285**(48): p. 37159-37169.
126. Zhao, B., et al., *A coordinated phosphorylation by Lats and CK1 regulates YAP stability through SCFβ-TRCP.* 2010. **24**(1): p. 72-85.
127. Zhao, B., et al., *TEAD mediates YAP-dependent gene induction and growth control.* 2008. **22**(14): p. 1962-1971.
128. Lai, D., et al., *Taxol resistance in breast cancer cells is mediated by the hippo pathway component TAZ and its downstream transcriptional targets Cyr61 and CTGF.* 2011. **71**(7): p. 2728-2738.
129. Ghiso, E., et al., *YAP-dependent AXL overexpression mediates resistance to EGFR inhibitors in NSCLC.* 2017. **19**(12): p. 1012-1021.
130. Zhang, N., et al., *The Merlin/NF2 tumor suppressor functions through the YAP oncoprotein to regulate tissue homeostasis in mammals.* 2010. **19**(1): p. 27-38.
131. Ibar, C. and K.D.J.D.C. Irvine, *Integration of hippo-YAP signaling with metabolism.* 2020. **54**(2): p. 256-267.
132. Zanconato, F., M. Cordenonsi, and S.J.C.c. Piccolo, *YAP/TAZ at the roots of cancer.* 2016. **29**(6): p. 783-803.
133. Fan, R., N.-G. Kim, and B.M.J.P.o.t.N.A.o.S. Gumbiner, *Regulation of Hippo pathway by mitogenic growth factors via phosphoinositide 3-kinase and phosphoinositide-dependent kinase-1.* 2013. **110**(7): p. 2569-2574.
134. García-Escudero, R., et al., *Overexpression of PIK3CA in head and neck squamous cell carcinoma is associated with poor outcome and activation of the YAP pathway.* 2018. **79**: p. 55-63.
135. Zanconato, F., et al., *YAP/TAZ as therapeutic targets in cancer.* 2016. **29**: p. 26-33.
136. Yang, S., et al., *CDK1 phosphorylation of YAP promotes mitotic defects and cell motility and is essential for neoplastic transformation.* 2013. **73**(22): p. 6722-6733.
137. Liang, K., et al., *Expression of hippo pathway in colorectal cancer.* 2014. **20**(3): p. 188.
138. Zhou, G.-X., et al., *Effects of the hippo signaling pathway in human gastric cancer.* 2013. **14**(9): p. 5199-5205.
139. Chen, K.H., et al., *Methylation-associated inactivation of LATS1 and its effect on demethylation or overexpression on YAP and cell biological function in human renal cell carcinoma.* 2014. **45**(6): p. 2511-2521.
140. Dubois, F., et al., *RASSF1A Suppresses the Invasion and Metastatic Potential of Human Non–Small Cell Lung Cancer Cells by Inhibiting YAP Activation through the GEF-H1/RhoB Pathway.* 2016. **76**(6): p. 1627-1640.
141. Wang, J., et al., *ABL kinases promote breast cancer osteolytic metastasis by modulating tumor-bone interactions through TAZ and STAT5 signaling.* 2016. **9**(413): p. ra12-ra12.
142. Lin, C., X.J.B. Xu, and Pharmacotherapy, *YAP1-TEAD1-Glut1 axis dictates the oncogenic phenotypes of breast cancer cells by modulating glycolysis.* 2017. **95**: p. 789-794.
143. Cosset, É., et al., *Glut3 addiction is a druggable vulnerability for a molecularly defined subpopulation of glioblastoma.* 2017. **32**(6): p. 856-868. e5.
144. Zheng, X., et al., *Lnc RNA wires up Hippo and Hedgehog signaling to reprogramme glucose metabolism.* 2017. **36**(22): p. 3325-3335.

145. Jeong, S.-H., et al., *Hippo-mediated suppression of IRS2/AKT signaling prevents hepatic steatosis and liver cancer.* 2018. **128**(3): p. 1010-1025.
146. Kapoor, A., et al., *Yap1 activation enables bypass of oncogenic Kras addiction in pancreatic cancer.* 2014. **158**(1): p. 185-197.
147. Lin, L., et al., *The Hippo effector YAP promotes resistance to RAF-and MEK-targeted cancer therapies.* 2015. **47**(3): p. 250-256.
148. Zhou, T.-y., et al., *Inactivation of hypoxia-induced YAP by statins overcomes hypoxic resistance tosorafenib in hepatocellular carcinoma cells.* 2016. **6**: p. 30483.
149. Zhou, D., et al., *Mst1 and Mst2 maintain hepatocyte quiescence and suppress hepatocellular carcinoma development through inactivation of the Yap1 oncogene.* 2009. **16**(5): p. 425-438.
150. Urtasun, R., et al., *Connective tissue growth factor autocriny in human hepatocellular carcinoma: Oncogenic role and regulation by epidermal growth factor receptor/yes‐associated protein–mediated activation.* 2011. **54**(6): p. 2149-2158.
151. Juric, V., et al., *Fas-mediated apoptosis is regulated by the extracellular matrix protein CCN1 (CYR61) in vitro and in vivo.* 2009. **29**(12): p. 3266-3279.
152. Yuan, W.-C., et al., *NUAK2 is a critical YAP target in liver cancer.* 2018. **9**(1): p. 1-12.
153. Gao, J., et al., *Cirrhotic stiffness affects the migration of hepatocellular carcinoma cells and induces sorafenib resistance through YAP.* 2019. **234**(3): p. 2639-2648.
154. Liu-Chittenden, Y., et al., *Genetic and pharmacological disruption of the TEAD–YAP complex suppresses the oncogenic activity of YAP.* 2012. **26**(12): p. 1300-1305.
155. Gavini, J., et al., *Verteporfin-induced lysosomal compartment dysregulation potentiates the effect of sorafenib in hepatocellular carcinoma.* 2019. **10**(10): p. 1-17.
156. Tang, F., et al., *LATS1 but not LATS2 represses autophagy by a kinase-independent scaffold function.* 2019. **10**(1): p. 1-17.
157. Dixon, S.J., et al., *Ferroptosis: an iron-dependent form of nonapoptotic cell death.* 2012. **149**(5): p. 1060-1072.
158. Gao, M., et al., *Glutaminolysis and transferrin regulate ferroptosis.* 2015. **59**(2): p. 298-308.
159. Hayano, M., et al., *Loss of cysteinyl-tRNA synthetase (CARS) induces the transsulfuration pathway and inhibits ferroptosis induced by cystine deprivation.* 2016. **23**(2): p. 270-278.
160. Jiang, L., et al., *Ferroptosis as a p53-mediated activity during tumour suppression.* 2015. **520**(7545): p. 57-62.
161. Gao, M., et al., *Ferroptosis is an autophagic cell death process.* 2016. **26**(9): p. 1021-1032.
162. Feng, H., et al., *Transferrin Receptor Is a Specific Ferroptosis Marker.* 2020. **30**(10): p. 3411-3423. e7.
163. Nishizawa, H., et al., *Ferroptosis is controlled by the coordinated transcriptional regulation of glutathione and labile iron metabolism by the transcription factor BACH1.* 2020. **295**(1): p. 69-82.
164. Dixon, S.J., et al., *Human haploid cell genetics reveals roles for lipid metabolism genes in nonapoptotic cell death.* 2015. **10**(7): p. 1604-1609.

165. Yang, W.S., et al., *Peroxidation of polyunsaturated fatty acids by lipoxygenases drives ferroptosis.* 2016. **113**(34): p. E4966-E4975.
166. Doll, S., et al., *ACSL4 dictates ferroptosis sensitivity by shaping cellular lipid composition.* 2017. **13**(1): p. 91-98.
167. Kagan, V.E., et al., *Oxidized arachidonic and adrenic PEs navigate cells to ferroptosis.* 2017. **13**(1): p. 81-90.
168. Shimada, K., et al., *Global survey of cell death mechanisms reveals metabolic regulation of ferroptosis.* 2016. **12**(7): p. 497-503.
169. Sun, X., et al., *Activation of the p62-Keap1-NRF2 pathway protects against ferroptosis in hepatocellular carcinoma cells.* 2016. **63**(1): p. 173-184.
170. Chen, D., et al., *ATF4 promotes angiogenesis and neuronal cell death and confers ferroptosis in a xCT-dependent manner.* 2017. **36**(40): p. 5593-5608.
171. Zhu, S., et al., *HSPA5 regulates ferroptotic cell death in cancer cells.* 2017. **77**(8): p. 2064-2077.
172. Yang, W.S., et al., *Regulation of ferroptotic cancer cell death by GPX4.* 2014. **156**(1-2): p. 317-331.
173. Zhang, Y., et al., *Imidazole ketone erastin induces ferroptosis and slows tumor growth in a mouse lymphoma model.* 2019. **26**(5): p. 623-633. e9.
174. Sleire, L., et al., *Drug repurposing: sulfasalazine sensitizes gliomas to gamma knife radiosurgery by blocking cystine uptake through system Xc−, leading to glutathione depletion.* 2015. **34**(49): p. 5951-5959.
175. Yang, W.S. and B.R.J.T.i.c.b. Stockwell, *Ferroptosis: death by lipid peroxidation.* 2016. **26**(3): p. 165-176.
176. Wenz, C., et al., *t-BuOOH induces ferroptosis in human and murine cell lines.* 2018. **92**(2): p. 759-775.
177. Gaschler, M.M., et al., *FINO 2 initiates ferroptosis through GPX4 inactivation and iron oxidation.* 2018. **14**(5): p. 507-515.
178. Angeli, J.P.F., et al., *Inactivation of the ferroptosis regulator Gpx4 triggers acute renal failure in mice.* 2014. **16**(12): p. 1180-1191.
179. Wu, Z., et al., *Chaperone-mediated autophagy is involved in the execution of ferroptosis.* 2019. **116**(8): p. 2996-3005.
180. Alvarez, S.W., et al., *NFS1 undergoes positive selection in lung tumours and protects cells from ferroptosis.* 2017. **551**(7682): p. 639-643.
181. Xie, Y., et al., *The tumor suppressor p53 limits ferroptosis by blocking DPP4 activity.* 2017. **20**(7): p. 1692-1704.
182. Toyokuni, S., et al., *Iron and thiol redox signaling in cancer: an exquisite balance to escape ferroptosis.* 2017. **108**: p. 610-626.
183. Miess, H., et al., *The glutathione redox system is essential to prevent ferroptosis caused by impaired lipid metabolism in clear cell renal cell carcinoma.* 2018. **37**(40): p. 5435-5450.
184. Bai, T., et al., *Sigma-1 receptor protects against ferroptosis in hepatocellular carcinoma cells.* 2019. **23**(11): p. 7349-7359.
185. Sun, X., et al., *Metallothionein-1G facilitates sorafenib resistance through inhibition of ferroptosis.* 2016. **64**(2): p. 488-500.
186. Louandre, C., et al., *The retinoblastoma (Rb) protein regulates ferroptosis induced by sorafenib in human hepatocellular carcinoma cells.* 2015. **356**(2): p. 971-977.
187. Llovet, J., et al., *Hepatocellular carcinoma. Nature reviews Disease primers. 2016; 2: 16018*. 2016, Epub 2016/05/10. PubMed PMID: 27158749. doi: 10.1038/nrdp.

188. Semenza, G.L.J.N.r.c., *Targeting HIF-1 for cancer therapy.* 2003. **3**(10): p. 721-732.
189. Méndez-Blanco, C., et al., *Sorafenib resistance in hepatocarcinoma: role of hypoxia-inducible factors.* 2018. **50**(10): p. 1-9.
190. Semenza, G.L.J.S.s.S., *Hypoxia-inducible factor 1 (HIF-1) pathway.* 2007. **2007**(407): p. cm8-cm8.
191. Berra, E., A. Ginouves, and J. Pouyssegur, *The hypoxia-inducible-factor hydroxylases bring fresh air into hypoxia signalling.* EMBO Rep, 2006. **7**(1): p. 41-5.
192. Gossage, L., T. Eisen, and E.R. Maher, *VHL, the story of a tumour suppressor gene.* Nat Rev Cancer, 2015. **15**(1): p. 55-64.
193. Kaelin, W.G., Jr. and P.J. Ratcliffe, *Oxygen sensing by metazoans: the central role of the HIF hydroxylase pathway.* Mol Cell, 2008. **30**(4): p. 393-402.
194. Ivan, M. and W.G. Kaelin, Jr., *The EGLN-HIF O2-Sensing System: Multiple Inputs and Feedbacks.* Mol Cell, 2017. **66**(6): p. 772-779.
195. Koppenol, W.H., P.L. Bounds, and C.V.J.N.R.C. Dang, *Otto Warburg's contributions to current concepts of cancer metabolism.* 2011. **11**(5): p. 325-337.
196. Shen, Y., et al., *Activating oxidative phosphorylation by a pyruvate dehydrogenase kinase inhibitor overcomes sorafenib resistance of hepatocellular carcinoma.* 2013. **108**(1): p. 72-81.
197. Zhang, H.-L., et al., *Blocking preferential glucose uptake sensitizes liver tumor-initiating cells to glucose restriction and sorafenib treatment.* 2017. **388**: p. 1-11.
198. Icard, P., et al., *How the Warburg effect supports aggressiveness and drug resistance of cancer cells?* Drug Resist Updat, 2018. **38**: p. 1-11.
199. Morandi, A. and S. Indraccolo, *Linking metabolic reprogramming to therapy resistance in cancer.* Biochim Biophys Acta Rev Cancer, 2017. **1868**(1): p. 1-6.
200. Parkin, D.M., et al., *Global cancer statistics, 2002.* 2005. **55**(2): p. 74-108.
201. Chang, Y.S., et al., *Sorafenib (BAY 43-9006) inhibits tumor growth and vascularization and induces tumor apoptosis and hypoxia in RCC xenograft models.* 2007. **59**(5): p. 561-574.
202. Zhu, Y.-j., et al., *New knowledge of the mechanisms of sorafenib resistance in liver cancer.* 2017. **38**(5): p. 614-622.
203. Wang, C., et al., *Phospho-ERK is a biomarker of response to a synthetic lethal drug combination of sorafenib and MEK inhibition in liver cancer.* 2018. **69**(5): p. 1057-1065.
204. van Oosterwijk, J.G., et al., *Hypoxia-induced upregulation of BMX kinase mediates therapeutic resistance in acute myeloid leukemia.* 2018. **128**(1): p. 369-380.
205. Zhao, C.-X., C.-L. Luo, and X.-H.J.M.o. Wu, *Hypoxia promotes 786-O cells invasiveness and resistance to sorafenib via HIF-2α/COX-2.* 2015. **32**(1): p. 419.
206. Wu, F.Q., et al., *ADRB2 signaling promotes HCC progression and sorafenib resistance by inhibiting autophagic degradation of HIF1alpha.* J Hepatol, 2016. **65**(2): p. 314-24.
207. Wilkinson, K.D.J.J.o.c.s., *DUBs at a glance.* 2009. **122**(14): p. 2325-2329.
208. Popov, N., et al., *The ubiquitin-specific protease USP28 is required for MYC stability.* 2007. **9**(7): p. 765-774.
209. Sun, X.-X., et al., *The nucleolar ubiquitin-specific protease USP36 deubiquitinates and stabilizes c-Myc.* 2015. **112**(12): p. 3734-3739.

210. Song, M.S., et al., *The deubiquitinylation and localization of PTEN are regulated by a HAUSP–PML network.* 2008. **455**(7214): p. 813-817.
211. Cummins, J.M., et al., *Tumour suppression: disruption of HAUSP gene stabilizes p53.* Nature, 2004. **428**(6982): p. 1 p following 486.
212. Byun, S., et al., *USP8 is a novel target for overcoming gefitinib resistance in lung cancer.* 2013. **19**(14): p. 3894-3904.
213. Yuan, T., et al., *Deubiquitinating enzyme USP10 promotes hepatocellular carcinoma metastasis through deubiquitinating and stabilizing Smad4 protein.* Mol Oncol, 2020. **14**(1): p. 197-210.
214. Zhu, H., et al., *USP10 Promotes Proliferation of Hepatocellular Carcinoma by Deubiquitinating and Stabilizing YAP/TAZ.* Cancer Res, 2020. **80**(11): p. 2204-2216.
215. Chauhan, D., et al., *A small molecule inhibitor of ubiquitin-specific protease-7 induces apoptosis in multiple myeloma cells and overcomes bortezomib resistance.* 2012. **22**(3): p. 345-358.
216. Tian, Z., et al., *A novel small molecule inhibitor of deubiquitylating enzyme USP14 and UCHL5 induces apoptosis in multiple myeloma and overcomes bortezomib resistance.* 2014. **123**(5): p. 706-716.
217. Wang, L., et al., *The combination of the glycolysis inhibitor 2-DG and sorafenib can be effective against sorafenib-tolerant persister cancer cells.* 2019. **12**: p. 5359.
218. Tesori, V., et al., *The multikinase inhibitor Sorafenib enhances glycolysis and synergizes with glycolysis blockade for cancer cell killing.* 2015. **5**: p. 9149.
219. Pisarsky, L., et al., *Targeting Metabolic Symbiosis to Overcome Resistance to Anti-angiogenic Therapy.* Cell Rep, 2016. **15**(6): p. 1161-74.
220. Dobin, A., et al., *STAR: ultrafast universal RNA-seq aligner.* Bioinformatics, 2013. **29**(1): p. 15-21.
221. Falcon, S. and R. Gentleman, *Using GOstats to test gene lists for GO term association.* Bioinformatics, 2007. **23**(2): p. 257-258.
222. Yu, G. and Q.-Y. He, *ReactomePA: an R/Bioconductor package for reactome pathway analysis and visualization.* Molecular BioSystems, 2016. **12**(2): p. 477-479.
223. Llovet, J.M., et al., *Sorafenib in advanced hepatocellular carcinoma.* New England journal of medicine, 2008. **359**(4): p. 378-390.
224. Kudo, M., et al., *Lenvatinib versus sorafenib in first-line treatment of patients with unresectable hepatocellular carcinoma: a randomised phase 3 non-inferiority trial.* The Lancet, 2018. **391**(10126): p. 1163-1173.
225. Lee, M.S., et al., *Atezolizumab with or without bevacizumab in unresectable hepatocellular carcinoma (GO30140): an open-label, multicentre, phase 1b study.* The Lancet Oncology, 2020. **21**(6): p. 808-820.
226. Dixon, S.J., et al., *Ferroptosis: an iron-dependent form of nonapoptotic cell death.* Cell, 2012. **149**(5): p. 1060-1072.
227. Jiang, X., B.R. Stockwell, and M.J.N.R.M.C.B. Conrad, *Ferroptosis: mechanisms, biology and role in disease.* Nature Reviews Molecular Cell Biology, 2021: p. 1-17.
228. Lachaier, E., et al., *Sorafenib induces ferroptosis in human cancer cell lines originating from different solid tumors.* Anticancer research, 2014. **34**(11): p. 6417-6422.
229. Pan, D.J.D.c., *The hippo signaling pathway in development and cancer.* Developmental cell, 2010. **19**(4): p. 491-505.

230. Harvey, K.F., X. Zhang, and D.M.J.N.R.C. Thomas, *The Hippo pathway and human cancer.* Nature Reviews Cancer, 2013. **13**(4): p. 246-257.
231. Yang, W.-H., et al., *The Hippo pathway effector TAZ regulates ferroptosis in renal cell carcinoma.* Cell reports, 2019. **28**(10): p. 2501-2508. e4.
232. Wu, J., et al., *Intercellular interaction dictates cancer cell ferroptosis via NF2–YAP signalling.* Nature, 2019. **572**(7769): p. 402-406.
233. Tang, F., et al., *LATS1 but not LATS2 represses autophagy by a kinase-independent scaffold function.* Nature communications, 2019. **10**(1): p. 1-17.
234. Totaro, A., T. Panciera, and S.J.N.c.b. Piccolo, *YAP/TAZ upstream signals and downstream responses.* Nature cell biology, 2018. **20**(8): p. 888-899.
235. Dixon, S.J., et al., *Pharmacological inhibition of cystine–glutamate exchange induces endoplasmic reticulum stress and ferroptosis.* Elife, 2014. **3**: p. e02523.
236. Sun, X., et al., *Activation of the p62-Keap1-NRF2 pathway protects against ferroptosis in hepatocellular carcinoma cells.* Hepatology, 2016. **63**(1): p. 173-184.
237. Chen, D., et al., *ATF4 promotes angiogenesis and neuronal cell death and confers ferroptosis in a xCT-dependent manner.* Oncogene, 2017. **36**(40): p. 5593-5608.
238. Kim, Y.-S., et al., *Sorafenib induces apoptotic cell death in human non-small cell lung cancer cells by down-regulating mammalian target of rapamycin (mTOR)-dependent survivin expression.* Biochemical pharmacology, 2011. **82**(3): p. 216-226.
239. Heallen, T., et al., *Hippo pathway inhibits Wnt signaling to restrain cardiomyocyte proliferation and heart size.* Science, 2011. **332**(6028): p. 458-461.
240. Diepenbruck, M., et al., *Tead2 expression levels control the subcellular distribution of Yap and Taz, zyxin expression and epithelial–mesenchymal transition.* Journal of cell science, 2014. **127**(7): p. 1523-1536.
241. Gout, P., et al., *Sulfasalazine, a potent suppressor of lymphoma growth by inhibition of the xc− cystine transporter: a new action for an old drug.* Leukemia, 2001. **15**(10): p. 1633-1640.
242. Wang, W., et al., *CD8+ T cells regulate tumour ferroptosis during cancer immunotherapy.* Nature, 2019. **569**(7755): p. 270-274.
243. Watanabe, T., et al., *A novel model of continuous depletion of glutathione in mice treated with L-buthionine (S, R)-sulfoximine.* The Journal of toxicological sciences, 2003. **28**(5): p. 455-469.
244. Wilhelm, S., et al., *Discovery and development of sorafenib: a multikinase inhibitor for treating cancer.* Nature reviews Drug discovery, 2006. **5**(10): p. 835-844.
245. Jiang, L., et al., *Ferroptosis as a p53-mediated activity during tumour suppression.* Nature, 2015. **520**(7545): p. 57-62.
246. Sato, H., et al., *Transcriptional control of cystine/glutamate transporter gene by amino acid deprivation.* Biochemical and biophysical research communications, 2004. **325**(1): p. 109-116.
247. Yang, W.-H., et al., *A TAZ–ANGPTL4–NOX2 Axis regulates ferroptotic cell death and chemoresistance in epithelial ovarian cancer.* Molecular Cancer Research, 2020. **18**(1): p. 79-90.
248. Andreozzi, M., et al., *HMGA1 expression in human hepatocellular carcinoma correlates with poor prognosis and promotes tumor growth and migration in in vitro models.* Neoplasia, 2016. **18**(12): p. 724-731.

249. Coto-Llerena, M., et al., *High expression of FAP in colorectal cancer is associated with angiogenesis and immunoregulation processes.* Frontiers in oncology, 2020. **10**: p. 979.
250. Dobin, A., et al., *STAR: ultrafast universal RNA-seq aligner.* Bioinformatics, 2013. **29**(1): p. 15-21.
251. Falcon, S. and R.J.B. Gentleman, *Using GOstats to test gene lists for GO term association.* Bioinformatics, 2007. **23**(2): p. 257-258.
252. Yu, G. and Q.-Y.J.M.B. He, *ReactomePA: an R/Bioconductor package for reactome pathway analysis and visualization.* Molecular BioSystems, 2016. **12**(2): p. 477-479.
253. Ally, A., et al., *Comprehensive and integrative genomic characterization of hepatocellular carcinoma.* Cell, 2017. **169**(7): p. 1327-1341. e23.
254. Gao, J., et al., *Integrative analysis of complex cancer genomics and clinical profiles using the cBioPortal.* Science signaling, 2013. **6**(269): p. pl1-pl1.
255. Budczies, J., et al., *Cutoff Finder: a comprehensive and straightforward Web application enabling rapid biomarker cutoff optimization.* PloS one, 2012. **7**(12): p. e51862.

Contribution to other projects

In addition to my lead roles in the two PhD thesis projects described above, I had the opportunity to contribute to the following research project in the laboratory:

Tang, Fengyuan, Ruize Gao, Beena Jeevan-Raj, Christof B. Wyss, Ravi KR Kalathur, Salvatore Piscuoglio, Charlotte KY Ng et al. "LATS1 but not LATS2 represses autophagy by a kinase-independent scaffold function." Nature communications 10, no. 1 (2019): 1-17.

Acknowledgements

First of all, I would like to express my sincere gratitude to Prof. Dr. Gerhard M. Christofori for providing me an opportunity to work and study in Basel. I feel so lucky to work in this laboratory that Gerhard gave me the freedom to pursue my own ideas and provided us the powerful support to the projects.

Furthermore, I would like to extend my gratitude to my committee members Prof. Michael N. Hall, Prof. Matthias P. Wymann, Prof. Matthias Peter and Prof. Jan Tchorz for their helpful suggestions on my Ph.D. study.

Appreciations to Dr. Fengyuan Tang, for his guides on my work and life at the beginning of my Ph.D. study. We also made great teamwork during the past four years. Moreover, I would also like to thank Dr. Ravi Kiran Reddy Kalathur, Dr. David Büchel, Dr. Marco Morini, Dr. Fabiana Lüönd, Dr. Nami Sugiyama, Dr. Stefanie Tiede, Dr. Meera Saxena and Agathe Morand for their advices on my projects. I owe many thanks to Eleni Panoussis, Ursula Schmieder for their kind help on mice experiments. I would also like to thank Prof. Dr. Salvatore Piscuoglio, Prof. Dr. Markus H. Heim and their groups for the help on my projects.

Special thanks to Erika Visscher and Julia Leykauf, their work helped me to focus on research. I am also very thankful to Angelika Offinger and Lisa Schneider for helping with the mice experiments.

Most importantly, I am extremely thankful to my family and friends for their support and understanding. Especially, I would like to express my deepest love to my wife, Renxuan Dong, her support, love and encouragement provide me power to reach here.

nature COMMUNICATIONS

ARTICLE

https://doi.org/10.1038/s41467-019-13591-7 OPEN

LATS1 but not LATS2 represses autophagy by a kinase-independent scaffold function

Fengyuan Tang[1*], Ruize Gao[1], Beena Jeevan-Raj[1], Christof B. Wyss[1], Ravi K.R. Kalathur[1], Salvatore Piscuoglio[2], Charlotte K.Y. Ng[2], Sravanth K. Hindupur[3], Sandro Nuciforo[1], Eva Dazert[3], Thomas Bock[3], Shuang Song[4], David Buechel[1], Marco F. Morini[1], Alexander Hergovich[5], Patrick Matthias[4], Dae-Sik Lim[6], Luigi M. Terracciano[2], Markus H. Heim[1], Michael N. Hall[3] & Gerhard Christofori[1*]

Autophagy perturbation represents an emerging therapeutic strategy in cancer. Although LATS1 and LATS2 kinases, core components of the mammalian Hippo pathway, have been shown to exert tumor suppressive activities, here we report a pro-survival role of LATS1 but not LATS2 in hepatocellular carcinoma (HCC) cells. Specifically, LATS1 restricts lethal autophagy in HCC cells induced by sorafenib, the standard of care for advanced HCC patients. Notably, autophagy regulation by LATS1 is independent of its kinase activity. Instead, LATS1 stabilizes the autophagy core-machinery component Beclin-1 by promoting K27-linked ubiquitination at lysine residues K32 and K263 on Beclin-1. Consequently, ubiquitination of Beclin-1 negatively regulates autophagy by promoting inactive dimer formation of Beclin-1. Our study highlights a functional diversity between LATS1 and LATS2, and uncovers a scaffolding role of LATS1 in mediating a cross-talk between the Hippo signaling pathway and autophagy.

[1] Department of Biomedicine, University of Basel, Basel, Switzerland. [2] Institute of Pathology, University Hospital Basel, Basel, Switzerland. [3] Biozentrum, University of Basel, Basel, Switzerland. [4] Friedrich Miescher Institute for Biomedical Research, Basel, Switzerland. [5] UCL Cancer Institute, University College London, London WC1E 6BT, UK. [6] Korea Advanced Institute of Science and Technology, Daejeon 34141, Republic of Korea. *email: fengyuan.tang@unibas.ch; gerhard.christofori@unibas.ch

Liver cancer is the second leading cause of cancer-related mortality with hepatocellular carcinoma (HCC), representing about 90% of all cases of primary liver cancer[1]. Viral infections (hepatitis B or C), alcohol abuse, and metabolism-induced non-alcoholic fatty liver disease are major risk factors for HCC incidence[1]. Unlike other malignancies, HCC is often diagnosed only at advanced stages, where liver transplantation, surgical therapies, and resection are not available. Sorafenib (Srf), a multi-kinase inhibitor, is the standard-of-care treatment and the only effective systemic option for late-stage HCC, however, only with an average increased overall patient survival of ~3 months[2]. Apparently, HCC cells acquire resistance to Srf therapy. Therefore, understanding how HCC cells respond to Srf is important to improve the efficacy of Srf-based therapy in HCC patients; notably, to overcome the development of evasive resistance to Srf therapy.

Macroautophagy (hereafter referred to as autophagy) is a self-digestion process that targets the cytoplasmic components to the lysosomes for nutrient recycling in response to cellular stress and starvation[3]. Autophagy has been shown to play dual roles in tumor initiation and tumor progression[4,5]. Autophagy deficiency promotes tumor initiation but represses malignant tumor progression and, as a consequence, autophagy plays a conflicting role in cancer therapy, including the treatment of HCC with Srf[6]. Although acute treatment of HCC cells with Srf induces a lethal version of autophagy[7–9], a survival version of autophagy is likely to mediate the adaptive response to Srf and promotes cell viability in Srf-resistant cells[10,11]. Thus, the biological consequence of autophagy activation in response to therapy is context-dependent and the mechanistic understanding of how autophagy is regulated in cancer appears of great importance to optimize therapeutic interventions.

The Hippo signaling pathway has emerged as a major growth control network regulating cell death, proliferation, and differentiation[12,13]. Activated Hippo or MAP4Ks phosphorylate and activate the downstream kinases Large Tumor Suppressor 1 and 2 (LATS 1 and 2), which in turn phosphorylate and inactivate the Hippo signaling transducers YAP and TAZ[14]. In short, Hippo signaling critically relies on a variety of protein kinase activities and protein phosphorylation events.

Here we report a kinase activity-independent role of LATS1, but not LATS2, in regulating therapy-induced autophagy in HCC cells. The results indicate that this scaffolding function of LATS1 plays a critical role in the regulation of autophagy and in therapy response of HCC cells and potentially other cancer type cells.

Results

Repression of Srf-induced cell death by LATS1. The mammalian Hippo pathway has been linked to tumorigenesis and therapy resistance[15–17]. While examining the role of the Hippo signaling pathway in the response of HCC cells to Srf treatment, we discovered an unexpected cell survival role of LATS1. Small interfering RNA (siRNA)-mediated ablation of LATS1, but not of LATS2, resulted in an increase of Srf-induced apoptotic cell death and a statistically significant reduction of viability in different HCC cell lines (Fig. 1a and Supplementary Fig. 1a, b), indicating a potential functional diversity between LATS1 and LATS2 in HCC. The pro-survival function of LATS1 in Srf-treated HCC cells was further validated by stable short hairpin RNA (shRNA)-mediated depletion of LATS1 expression (Fig. 1b and Supplementary Fig. 1c–e). Moreover, although shRNA-mediated loss of LATS1 did not affect primary tumor growth of HCC cells in xenotransplanted immunodeficient mice, it significantly reduced tumor growth under Srf treatment (Fig. 1c and Supplementary Fig. 1f). Furthermore, we confirmed a pro-survival role of LATS1 in HCC patient-derived ex vivo organoid lines[18] (Fig. 1d).

To further examine the role of LATS1 in Srf resistance in HCC, we established Srf-resistant Huh7 cells by (1) step-wise increasing the concentration of Srf to induce resistance (Huh7-IR cells) or (2) by adding a consistent high concentration of Srf to induce resistance (Huh7-CR cells) (Fig. 1e and Supplementary Fig. 1g, h). Analysis of LATS1 protein expression revealed an upregulation in these resistant cells in comparation to the parental line (Fig. 1f). More importantly, knockdown of the upregulated LATS1 in resistant cells led to a reduction of cell viability with decreased number of cell colonies (Fig. 1g).

We next investigated the clinical significance of these observations. Expression of the LATS1 and LATS2 tumor suppressors has been reported to be deregulated in several types of cancers[19]. We first analyzed the expression of LATS1/2 in HCC patient samples in comparison with healthy liver tissues in The Cancer Genome Atlas (TCGA) database[20]. Surprisingly, LATS1 messenger RNA levels were found to be significantly higher, whereas LATS2 mRNA levels were rather lower in HCC patient samples as compared with normal liver controls (Fig. 1h, i). Prognostic analysis of the HCC patient data in the TCGA liver HCC database further supported the notion of a pro-tumorigenic role of LATS1; high levels of LATS1 mRNA correlated with poor overall and disease-free HCC patient survival (Fig. 1j, k). Strikingly, the opposite trend was observed with LATS2, where high LATS2 mRNA levels correlated with better survival in HCC patients, although with marginal significance (Supplementary Fig. 1i, j). Finally, the correlation between LATS1 mRNA expression and Srf response was explored in a local patient cohort where serial and paired tumor and non-tumor biopsies were taken and analyzed before and during Srf therapy. Although not with significance, a trend of higher LATS1 mRNA expression was found in pre-treatment tumor tissues in patients not responding to Srf therapy as compared with Srf therapy responders (Fig. 1l, left panel). Most important, significantly higher LATS1 mRNA expression was found in Srf non-responders as compared with Srf responders after Srf treatment (Fig. 1l, right panel), suggesting that LATS1 mRNA levels may represent a new biomarker to predict Srf response in HCC patients.

Together, these findings demonstrate a role of LATS1, but not LATS2, in therapy response of HCC. Notably, they identify an unexpected HCC cell survival function of the tumor suppressor kinase LATS1 in response to Srf treatment.

Kinase activity-independent regulation of autophagy by LATS1. LATS1 and LATS2 kinases are known to redundantly mediate the phosphorylation-induced inactivation of the transcription factors YAP/TAZ[21]. Our results indicate a functional diversity between LATS1 and LATS2 in regulating Srf resistance. We thus assessed whether LATS1's canonical kinase activity was required for its role in cell viability. Analysis of partial resistant HCC cells[22] forced to express either a wild-type (WT) or a kinase-dead (KD) version of LATS1 revealed a reduction of cell death in cells overexpressing both forms of LATS1 (Supplementary Fig. 1k). Moreover, a similar effect was observed with siRNA-resistant cDNAs mediating the re-expression of a WT or a KD version of LATS1 in LATS1-knockdown cells (Supplementary Fig. 1l, m). Analysis of the activity status of the Hippo transducer YAP confirmed RNA interference (RNAi)-mediated ablation of LATS1 and/or LATS2 resulted into an increase of total YAP protein levels and potentially YAP activity, as monitored by immunoblotting and phos-tag gel electrophoresis (Supplementary

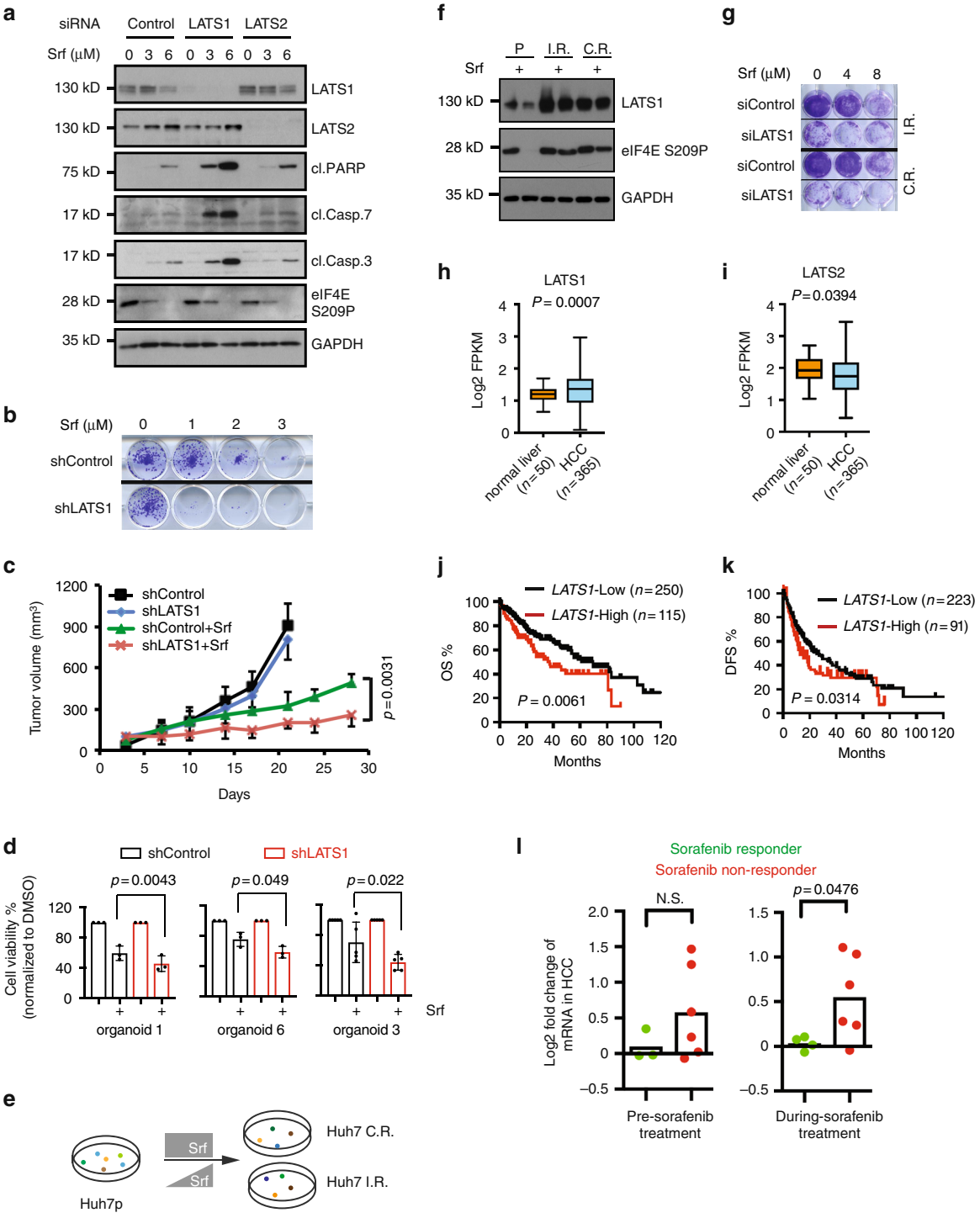

Fig. 1n). Together, these results indicate that the pro-survival role of LATS1 is independent of its kinase activity.

To uncover the molecular mechanism underlying the pro-survival function of LATS1 in HCC, we performed transcriptomic analysis by RNA sequencing (RNA-seq) of the HCC cell line Huh7 in response to Srf and siRNA-mediated ablation of LATS1 or LATS2 expression. In line with a specific role of LATS1 in regulating Srf-induced cell death, LATS1 deficiency led to a dramatic change in global transcription as compared to the loss of LATS2 (Supplementary Fig. 2a). Pathways analysis identified phagosomal pathways highly expressed in LATS1-deficient cells (Supplementary Fig. 2b). Gene set enrichment analysis (GSEA) revealed that the changes in gene expression caused by the loss of LATS1 correlated positively with the regulation of autophagy in the Gene Ontology (GO) and Kyoto Encyclopedia of Genes and Genomes (KEGG) databases (Supplementary Fig. 2c), and also in a dataset derived from *Lats1/2*-deficient murine hepatoblasts (Supplementary Fig. 2d).

Srf is well-known to promote autophagy induction and autophagic flux[9]. Thus, we investigated the effect of LATS1 on autophagy induction in HCC cells upon Srf treatment. Indeed, siRNA-mediated knockdown of LATS1, but not LATS2, resulted in a significant increase of LC3B puncta at both basal level and upon Srf stimulation in HCC cells (Fig. 2a, b and Supplementary

Fig. 1 A pro-survival role of LATS1 in HCC cells in response to sorafenib treatment. a Huh7 cells were transfected with indicated siControl and treated with DMSO vehicle or sorafenib (Srf) for 72 h. Cell death was analyzed by immunoblotting with indicated antibodies. Results represent three independent experiments. **b** Colony formation was determined in Huh7 cells expressing either shControl (shRNA targeting LacZ) or a shRNA against LATS1 and exposed to sorafenib. Results represent three independent experiments. **c** Huh7 cells either expressing shControlor sh LATS1 were implanted into the flank of NSG mice. The mice were treated with placebo or sorafenib and tumor volumes were measured. $n = 7$–9 for each treatment cohort. Statistical significance was calculated using the R package compareGrowthCurves. **d** Loss of LATS1 expression results in impaired viability of HCC organoid lines in response to sorafenib (Srf). Results were pooled from three to five independent experiments. Statistical significance was calculated using two-tailed, paired *t*-test. **e** Schematic illustration of establishment of sorafenib-resistant cells by (1) step-wise increasing sorafenib concentration (Huh7-IR cells) and (2) consistent high concentration (Huh7-CR cells). **f** Analysis of LATS1 protein expression in sorafenib-resistant cells. Parental (Huh7p) and IR/CR cells were treated with Sorafenib (5 μM) for24 h. Cells were analyzed by immunoblotting with indicated antibodies. Results represent three independent experiments. **g** siRNA-mediated loss of LATS1 expression results in impaired colony formation of sorafenib-resistant Huh7 cells in response to sorafenib (Srf). Results represent three independent experiments. **h**, **i** The expression of LATS1 (**h**) and LATS2 (**i**) was determined in the TCGA database. Expression values were log2-transformed. Statistical analysis was calculated using two-tailed, unpaired Welch's *t*-test. **j**, **k** Kaplan–Meier analysis of the TCGA database for the expression of LATS1. Overall survival (OS) (**j**) and disease-free survival (DFS) (**k**) of high and low patients are shown. Statistical significance was calculated using log-rank (Mantel–Cox) test. **l** LATS1 expression was determined by RNA sequencing of needle biopsies from patients before sorafenib treatment and during sorafenib treatment. mRNA levels of tumor biopsies were normalized to corresponding adjacent non-neoplastic tissue for each individual patient. Each dot represents one patient (Pre-sorafenib: $n = 3$ for responders and $n = 6$ for non-responders; On-sorafenib: $n = 4$ for responders and $n = 6$ for non-responders). Data represents log2 fold changes. Statistical significance was determined by Komogorov–Smirnov *t*-test.

Fig. 3a, b). Increased LC3B puncta could result from either enhanced autophagy induction or impaired autophagic flux. To discriminate between these possibilities, we first quantified the LC3B puncta number upon treatment with the lysosomal inhibitor bafilomycin A1 (Baf) and with Srf. LC3B puncta numbers were found higher in LATS1-deficient, but not in LATS2-deficient cells, as compared with siControl-transfected cells (Fig. 2a, b and Supplementary Fig. 3a, b), indicating that the loss of LATS1 efficiently promoted autophagy induction.

Furthermore, we analyzed the effect of LATS1 in autophagic flux. Immunoblotting for p62, also known as SQSTM1 and a marker for autophagic flux, revealed a significant reduction of its levels upon loss of LATS1 but not LATS2, indicating that the specific loss of LATS1 also induced a higher autophagic flux activity (Supplementary Fig. 3c). Blocking autophagic flux by chloroquine (CQ) prevented the reduction of p62 upon LATS1 deficiency, indicating that LATS1-mediated p62 downregulation occurred via the activation of autophagic flux (Supplementary Fig. 3d). Conversely, the forced expression of LATS1 inhibited Srf-induced degradation of p62, suggesting a restrictive role of LATS1 in autophagic flux (Fig. 2c and Supplementary Fig. 3e). These results suggest that LATS1, but not LATS2, represses autophagy induction and autophagic flux in HCC cells at baseline and in response to Srf treatment.

Given the notable difference between the functional contribution of LATS1 and LATS2 to autophagy regulation described above, we addressed whether the functional contribution of LATS1 to autophagy regulation depended on its kinase activity. Strikingly, overexpression of both WT and a KD version of LATS1 inhibited Srf-induced p62 degradation, indicating a kinase activity-independent role of LATS1 in autophagy regulation (Fig. 2c). Likewise, exogenously expressed siRNA-refractory WT and KD LATS1 prevented p62 degradation induced by the loss of endogenous LATS1 expression (Fig. 2d, e). Together, the data indicate that LATS1, but not LATS2, represses autophagy in HCC cells by a kinase-independent mechanism.

We next assessed whether the LATS1-mediated prevention of Srf-induced autophagy in HCC cells was specific for Srf treatment or represents a generic effect in response to other molecularly targeted therapies. Indeed, we observed a similar effect of LATS1 on regulation of autophagy and cell death in response to cabozantinib and sunitinib, where knockdown of LATS1 resulted in higher autophagic flux as monitored by p62 degradation and increased cell death (Supplementary Fig. 3f). As we observed a general trend of downregulation of endogenous LATS1 in response to targeted therapies in HCC (Figs. 1a and 2c, and Supplementary Fig. 3e, f), we further investigated potential degradation pathways of LATS1 under these stresses. Interestingly, blockade of autophagy as well as the proteasomal degradation pathway stabilized LATS1 protein, suggesting that Srf treatment can induce autophagic and proteasomal degradation of LATS1 (Supplementary Fig. 3g), and highlighting a potential feedback loop between LATS1 and autophagy regulation.

Next, we determined the direct impact of enhanced autophagy on reduced cell viability in the context of loss of LATS1 expression. We first tested whether the genetic inhibition of autophagy could overcome the enhanced cell death promoted by the loss of LATS1 expression. Repression of autophagy by siRNA-mediated ablation of ATG5 expression, a factor essential for autophagy initiation[23] (Supplementary Fig. 4a), efficiently prevented cell death and decreased cell viability induced by siRNA or shRNA-induced ablation of LATS1 expression and Srf exposure (Supplementary Fig. 4b–d). Next, we pharmacologically blocked autophagy by CQ and found that CQ could partially revert the reduced colony formation upon loss of LATS1, supporting a death-promoting role of LATS1 deficiency-induced autophagy in response to Srf (Supplementary Fig. 4e, f).

In addition to many tyrosine kinase receptors, Srf also targets RAF kinases. Given a direct LATS1-RAF cross-talk[24] and a potential crucial role of the mitogen-activated protein kinase (MAPK) signaling pathway in autophagy[25], we further examined the role of RAF-MAPK signaling in LATS1-mediated Srf response using the MEK inhibitor PD0325901. Although MEK inhibition alone did not have a significant impact on autophagy and cell death, its combination with Srf resulted in increased autophagy and cell death upon RNAi-mediated ablation of LATS1 expression (Supplementary Fig. 4g).

Together, the results demonstrate a kinase activity-independent role of LATS1, but not LATS2, in restricting autophagy and consequently preventing Srf-induced cell death in HCC cells.

A general role of LATS1-mediated inhibition of autophagy. Increased autophagy has been broadly implicated in cancer therapy, especially in targeted therapy[6]. To assess whether LATS1-mediated autophagy repression exerts a general function in various types of cancer therapy, we analyzed vemurafenib-mediated BRAF inhibition (BRAFi) in BRAFV600E-mutant A2058 melanoma cells. Interestingly, similar patterns of

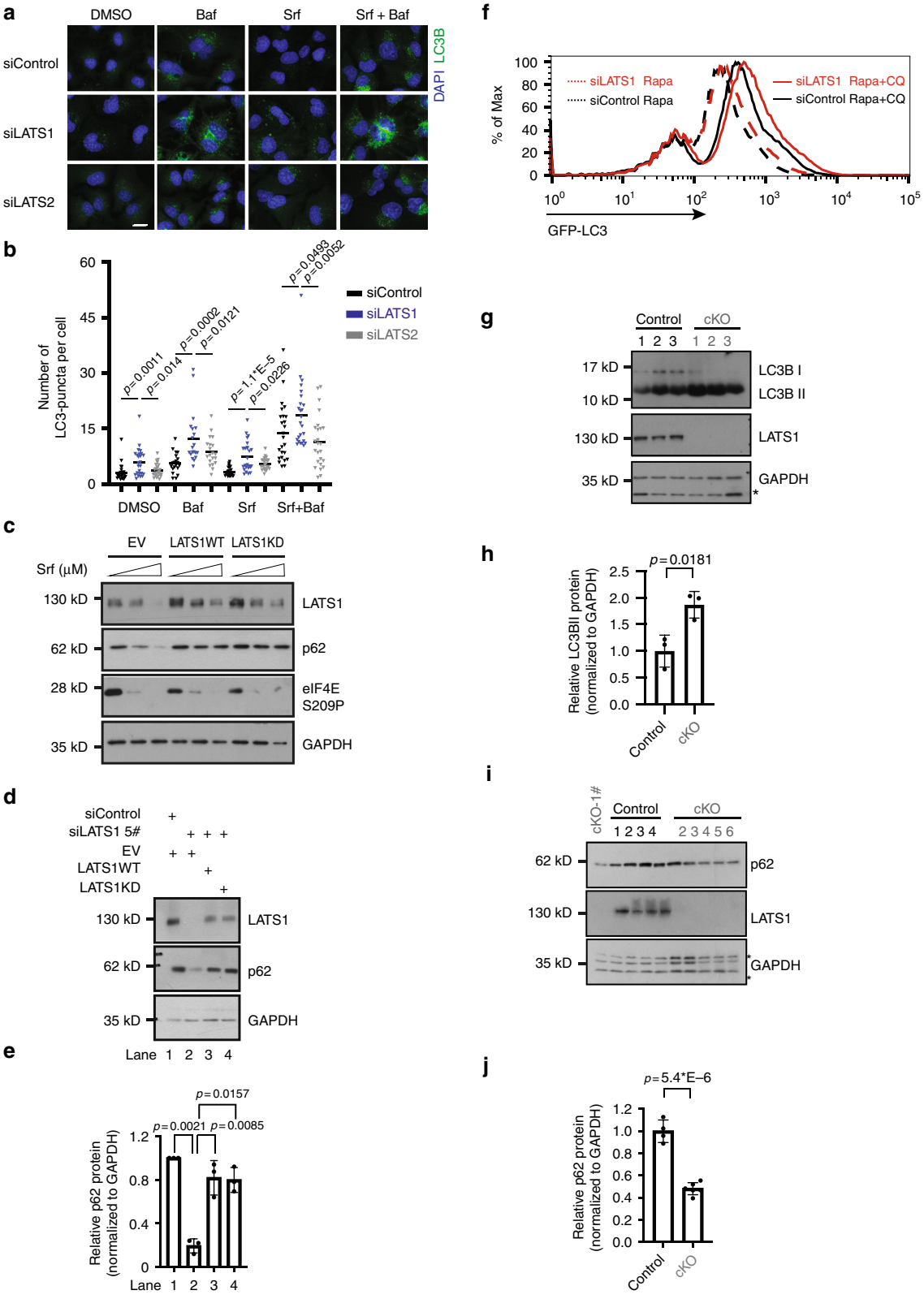

increased LC3B puncta were observed in response to BRAFi in LATS1, but not LATS2, knockdown cells, which were further enhanced upon CQ treatment (Supplementary Fig. 5a, b), suggesting that BRAFi-induced autophagy induction was increased upon loss of LATS1. Analysis of autophagic flux indicated that the loss of LATS1 enhanced vemurafenib-induced p62 degradation (Supplementary Fig. 5c). Increased p62 degradation upon loss of LATS1 could be prevented by the autophagic flux inhibitor CQ, confirming an enhanced autophagic flux (Supplementary Fig. 5d). These results show that LATS1 can also restrict BRAF inhibitor-induced autophagy in melanoma cells.

Autophagy is a cellular response to many stresses and is best characterized under conditions of mammalian target of rapamycin inhibition[26]. We thus assessed the functional role of LATS1 in

Fig. 2 LATS1 restricts autophagy in a kinase activity-independent manner. a, **b** Immunofluorescence analysis of LC3B puncta in Huh7 cells in response to sorafenib (Srf) treatment. Cells transfected with indicated siRNAs were treated with DMSO or sorafenib (6 μM for Huh7) for 40 h and bafilomycin A1 (Baf; 0.1 μM) for 2 h. Representative images (**a**) and quantification of LC3B puncta numbers (**b**) from three independent experiments are shown. Statistical analysis was calculated by one-way ANOVA. Scale bars, 25 μm. **c** The forced expression of both wild-type (WT) LATS1 and a kinase-dead (KD D846A) version of LATS1 blocks sorafenib-induced autophagic flux in Hep3B cells. Results represent three independent experiments. **d**, **e** Huh7 cells transfected with either siControl or siRNA against LATS1 were in addition transfected with empty vector (EV) or a vector encoding siRNA-refractory wild-type (WT) or a kinase-dead (KD D846A) version of LATS1, as indicated. Representative immunoblots (**d**) and quantification of the relative p62 levels (**e**) (normalized to GAPDH, fold change) from three independent experiments are shown. Statistical significance was calculated using one-way ANOVA. **f** Flow cytometry analysis of autophagy induction in U2OS-GFP-LC3 cells. Cells were transfected with indicated siRNAs and then treated with rapamycin (100 nM) for 16 h and additional chloroquine (10 μM) for 2 h. Results represent for three independent experiments. **g**, **h** Control mice (*Lats1*$^{fl/fl}$; Control) or mice with a hepatocyte-specific depletion of Lats1 (*Alb-Cre;Lats1*$^{fl/fl}$; cKO) were treated with chloroquine (30 mg/kg) for 4 h. Liver samples were collected and lysed for immunoblotting analysis. An immunoblot (**g**) and quantification of the relative LC3BII levels (**h**) (normalized to GAPDH, fold change) from $n = 3$ mice per cohort are shown. Statistical significance was calculated using two tailed, unpaired *t*-test. **i**, **j** Control mice (*Lats1*$^{fl/fl}$; Control) or mice with a hepatocyte-specific depletion of Lats1 (*Alb-Cre;Lats1*$^{fl/fl}$; cKO) were treated with rapamycin (2 mg/kg, twice within 24 h) followed with being fasted for 12 h. Liver samples were collected and lysed for immunoblotting analysis. An immunoblot (**i**) and quantification of the relative p62 levels (**j**) (normalized to GAPDH, fold change) in livers of $n = 4$ for control and $n = 6$ for cKO mice. Statistical significance was calculated using two-tailed unpaired *t*-test.

rapamycin-induced autophagy in standard cellular models, such as U2OS sarcoma cells. Indeed, immunofluorescence microscopy analysis revealed an increased number of LC3B puncta upon LATS1 knockdown in U2OS cells, which was further increased upon CQ treatment (Supplementary Fig. 5e, f), indicating rapamycin-induced autophagy induction was attenuated by LATS1. The analysis of global autophagy induction by flow cytometry analysis of LC3 signal intensity[27] revealed an increase of LC3 upon LATS1 knockdown, confirming a specific restrictive role of LATS1, but not LATS2, in rapamycin-induced autophagy (Fig. 2f and Supplementary Fig. 5g). In line with decreased p62 protein levels upon rapamycin treatment in LATS1-knockdown cells, cleavage of a green fluorescent protein (GFP)-fused form of LC3, a frequently used alternative assay for autophagic flux activity[28,29], was also increased upon loss of LATS1, which further supported the notion that LATS1 restricted autophagic flux (Supplementary Fig. 5h). To further validate LATS1-mediated autophagy regulation, we assessed the autophagosome and autolysosome dynamics in U2OS cells stably expressing a fusion RPF-GFP-LC3 construct. Analysis of the numbers of autophagosome (yellow) and of autolysosome (red) in response to rapamycin or CQ or a combination of both confirmed that LATS1 restricted rapamycin-induced autophagy induction as well as autophagic flux activity (Supplementary Fig. 6a–c).

We next investigated the autophagy regulatory role of LATS1 in vivo by comparing liver-specific *Lats1* conditional knockout mice (*Lats*$^{fl/fl}$; *Alb-cre*; cKO) to control mice (*Lats*$^{fl/fl}$; Control). To investigate the role of Lats1 in autophagy induction of hepatocytes, we treated the mice with CQ and found that loss of Lats1 resulted in higher lipidated LC3BII (Fig. 2g, h), indicating that Lats1 efficiently inhibited autophagy induction in vivo. To study the role of Lats1 in autophagic flux, we treated the mice with rapamycin followed by overnight starvation. Immunoblotting for p62 in the livers of the different genotype mice revealed lower amounts of p62 in cKO mice compared to Control mice (Fig. 2i, j), suggesting that Lats1 also inhibited autophagic flux in vivo.

Together, the observations demonstrate a general inhibitory role of LATS1 in autophagy regulation, either under physiological conditions or in response to targeted therapy or rapamycin-induced cell stress.

LATS1 interacts with and stabilizes Beclin-1. To delineate the molecular mechanisms underlying autophagy regulation by LATS1, we assessed whether LATS1 directly or indirectly affected any autophagy core-machinery proteins. Beclin-1 exerts a central role in autophagy induction and execution by orchestrating different autophagy complexes via direct binding to a variety of co-factors, but also by forming inactive homo-dimers[30]. Given that the LATS family kinase NDR can interact with Beclin-1[31], we first tested a potential physical interaction between LATS1 and Beclin-1. Strikingly, LATS1 formed a complex with Beclin-1 in a kinase activity-independent manner, as both KD and constitutively active (PIF) versions of LATS1 interacted with Beclin-1 to a comparable extent as WT LATS1 (Fig. 3a). By comparing LATS1 and NDR1 on Beclin-1 interaction and Srf-induced autophagy, we found that LAST1 interacted with Beclin-1 with much higher affinity (Supplementary Fig. 7a). Although RNAi-mediated ablation of LATS1 increased Srf-induced autophagic cell death, loss of NDR1 barely had any effect Srf-induced autophagy (Supplementary Fig. 7b). The LATS1-Beclin-1 protein interaction was also observed with endogenous proteins (Fig. 3b). Importantly, an increased interaction between LATS1 and Beclin-1 was observed in response to Srf treatment, as well as in Srf-resistant cells, indicating a potential Srf stress-induced specific LATS1-Beclin-1 interaction (Fig. 3c, d). Notably, the LATS1-Beclin-1 interaction substantially promoted an upregulation of Beclin-1 protein in a LATS1 dosage-dependent manner (Fig. 3e). In striking contrast, LATS2 barely had any effect on Beclin-1 protein stability (Supplementary Fig. 7c). Various versions of kinase-inactive LATS1 as well as the constitutively active LATS1 PIF-mutant stabilized Beclin-1 comparable to WT LATS1 (Supplementary Fig. 7d). The use of different protein tags, either at the C- or N-terminal end of LATS1, confirmed the impact of LATS1 on Beclin-1 stabilization (Supplementary Fig. 7e).

We next determined whether LATS1 promoted Beclin-1 upregulation at the mRNA or protein level. Analysis of Beclin-1 mRNA revealed no difference between control and LATS1-knockdown cells (Supplementary Fig. 7f), yet a cycloheximide pulse-chase experiment revealed that overexpressed LATS1 stabilized Beclin-1 at the protein level (Fig. 3f, g). This stabilizing effect was further confirmed at the endogenous level, where ablation of LATS1, but not LATS2, resulted in decreased Beclin-1 protein levels in response to the cap-dependent protein synthesis blockade induced by Srf (Fig. 3h). Furthermore, aging-induced downregulation of Beclin-1 was further enhanced upon Lats1 deficiency in mouse livers in vivo, indicating a specific Lats1-mediated Beclin-1 stabilization during aging (Fig. 3i). These findings suggested that LATS1 stabilized Beclin-1 at the protein level.

Taken together, these results indicate that LATS1 interacts with and stabilizes Beclin-1 protein.

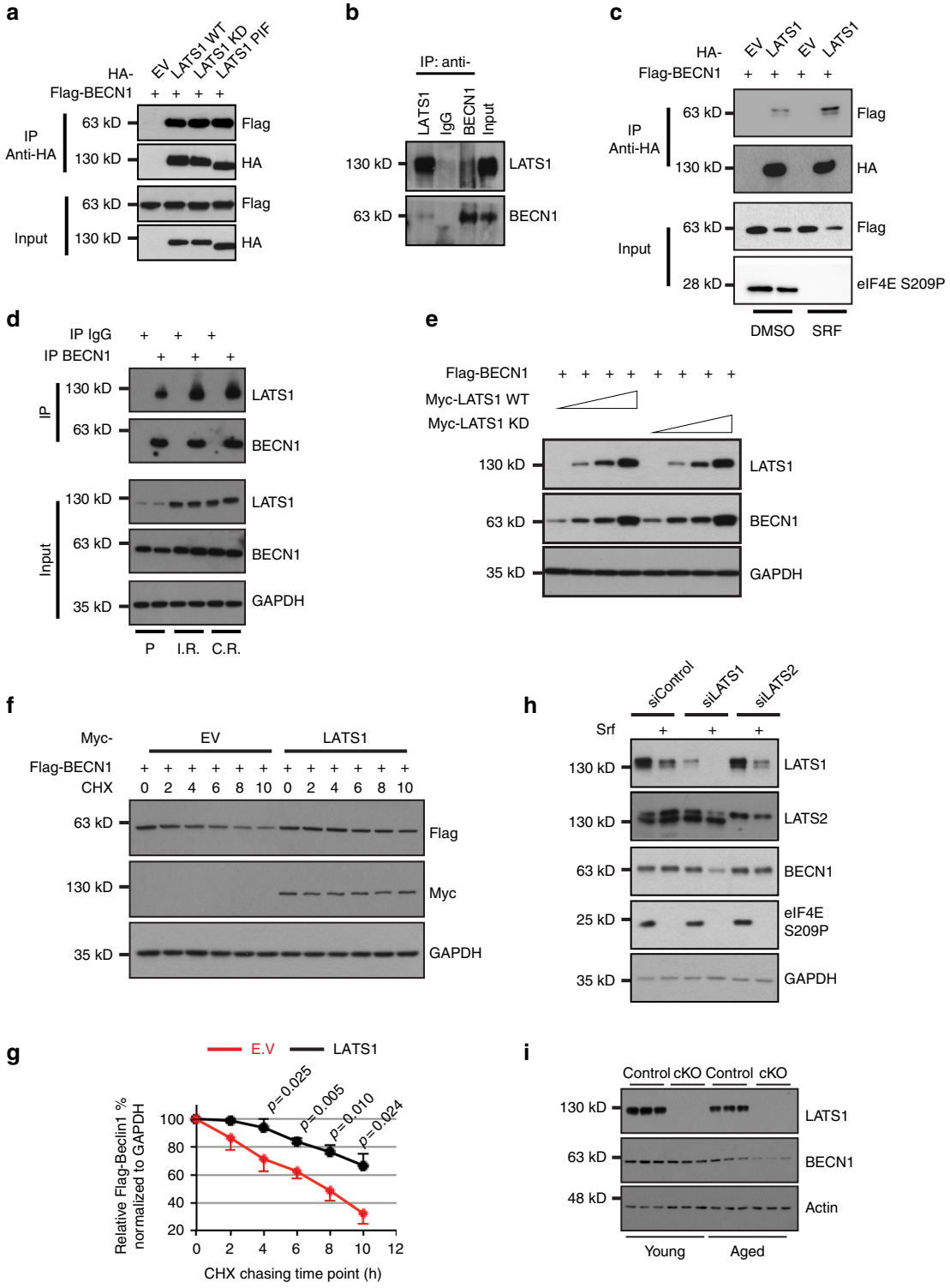

Identification of the functional diversity between LATS1 and LATS2. Our findings revealed a surprising functional diversity between LATS1 and LATS2 in regulating autophagy and Beclin-1 protein stability. We thus sought to identify the molecular difference underlying these divergent functions of LATS1 and LATS2. Using the stabilization of Beclin-1 by interacting with LATS1 but not LATS2, we mapped the essential domain of LATS1 required for interacting with and stabilizing Beclin-1 between amino acids 167 and 523 (Fig. 4a and Supplementary Fig. 7g, h). Of note, sequence alignment between LATS1 and LATS2 showed that a major part of this domain represented the most diverse amino acid sequences between LATS1 and LATS2 (amino acids 151–554 in LATS1 and amino acids 149–513 in LATS2, respectively). In contrast, the LATS1 kinase domain did not seem essential. This notion was functionally confirmed by using a construct containing only the LATS1 kinase domain but not the essential domain; the kinase domain alone failed to repress Srf-induced autophagy (Supplementary Fig. 7i).

We examined the importance of the essential domain by replacing this variable area of LATS2 with the comparable area

Fig. 3 LATS1 interacts with and stabilizes Beclin-1 in a kinase activity-independent manner. a HEK293T/17 cells were transfected with indicated plasmids. Seventy-two hours later, cell lysates were immunoprecipitated with anti-HA antibody followed by immunoblotting with indicated antibodies. Input represents lysates directly immunoblotted without immunoprecipitation. Results represent three independent experiments. **b** Huh7 cells were lysed for immunoprecipitation with indicated antibodies followed by immunoblotting analysis for Beclin-1 and LATS1. Input represents lysates before immunoprecipitation. Results represent three independent experiments. **c** HEK293T/17 cells transfected with indicated plasmids were treated with sorafenib (SRF; 10 μM, 2 h) followed by immunoprecipitation with indicated antibody. Results represent three independent experiments. **d** Huh7p or IR or CR cells were lysed for immunoprecipitation with indicated antibodies followed by immunoblotting analysis for Beclin-1 and LATS1. Input represents lysates before immunoprecipitation. Results represent three independent experiments. **e** LATS1 promotes Beclin-1 stability in a dosage-dependent manner. HEK293T/17 cells were transfected with same amount of vector encoding for Flag-tagged Beclin-1 together with increased amounts of vectors encoding for Myc-tagged wild-type LATS1 or kinase-dead mutant LATS1 (KD D846A) as indicated. Seventy-two hours later, cells were lysed and analyzed by immunoblotting for the expression of Beclin-1 (Flag) and LATS1 (Myc). Results represent three independent experiments. **f**, **g** HEK293T/17 cells transfected with indicated plasmids were treated with cycloheximide (CHX; 40 μg/mL) for the indicated times. Representative Immunoblots was shown in **f** and quantification **g** of band intensity was pooled from three independent experiments. Statistical significance was done using one-way ANOVA. $^{**}P < 0.01$. Note: to achieve equal amount of Beclin-1 protein level at time point 0, amounts of Flag-Beclin-1 plasmid transfected between empty vector and LATS1 were 3:1. **h** Huh7 cells transfected with indicated siRNAs were treated with DMSO or sorafenib (Srf; 10 μM) for 48 h. Cell lysates were analyzed by immunoblotting with indicated antibodies. A representative immunoblot from three independent experiments is shown. **i** Liver tissues from Control mice (*Lats1*$^{fl/fl}$; Control; $n = 3$) or mice with a hepatocyte-specific depletion of Lats1 (*Alb-Cre;Lats1*$^{fl/fl}$; cKO; $n = 3$) were collected at young adult age (12–16 weeks) or at old age (55–65 weeks) and lysed for immunoblotting analysis.

from LATS1, generating a LATS2 chimera protein, which contained unchanged domains of LATS2 at the N and C termini but with a middle domain derived from LATS1 (Fig. 4b). Interestingly, the LATS2 chimera stabilized Beclin-1 to a comparable extent as WT LATS1, whereas WT LATS2 had no effect (Fig. 4c). The LATS2-chimeric protein could also restore the p62 levels that were reduced by the siRNA-mediated ablation of LATS1 expression (Fig. 4d, e).

These data show that a small protein domain present in LATS1 but not in LATS2 is sufficient to mediate the stabilization of Beclin-1 and, thus, to repress autophagy. Since current knowledge suggests a redundant function of LATS1 and LATS2, these results are unexpected and identify a diverse function of the two closely related kinases at the molecular level.

LATS1 promotes K27-ubiquitination of Beclin-1 on lysines K32 and K263. Stabilization of proteins is frequently triggered by their post-translational modification, for example by ubiquitination. Beclin-1 is tightly regulated at the post-translational level by phosphorylation, acetylation and ubiquitination[30,32–34]. Ubiquitination of Beclin-1 generally leads either to its proteasomal degradation or stabilization or to its activation, depending on the specific ubiquitin linkage[35].

Thus, we assessed whether LATS1 had any effect on Beclin-1 ubiquitination. Surprisingly, although LATS1 stabilized Beclin-1 protein, we found that LATS1, but not LATS2, substantially promoted Beclin-1 ubiquitination, notably without requiring its kinase activity (Fig. 5a). Furthermore, endogenous LATS1 also promoted Beclin-1 ubiquitination as knockdown of LATS1 resulted in decreased ubiquitination of endogenous Beclin-1 (Fig. 5b). Consistent with its ability to stabilize Beclin-1, the hybrid LATS2 chimera potently increased ubiquitination of Beclin-1 (Supplementary Fig. 8a). The use of a large number of lysine mutant versions of ubiquitin revealed that both exogenous and endogenous LATS1-induced ubiquitination of Beclin-1 involved a lysine 27-mediated linkage of ubiquitin molecules (Fig. 5b, c and Supplementary Fig. 8b, c, d).

To further delineate the functional role of LATS1-induced Beclin-1 ubiquitination, we first analyzed which protein domain of Beclin-1 was ubiquitinated in a LATS1-dependent manner. Co-expression of various GFP-fused domains of Beclin-1 with LATS1 and ubiquitin identified the N terminus and central coiled-coil domain of Beclin-1 as most susceptible to LATS1-induced ubiquitination (Fig. 5d and Supplementary Fig. 8e). Next, we sought to map the LATS1-induced ubiquitination sites via mass spectrometry (MS) analysis. Indeed, lysine residues 32 and 263, which locate inside the N-terminal intrinsic disordered domain and central coiled-coil domain, respectively, were predominantly detected with increased levels of ubiquitination by LATS1 (Fig. 5e and Supplementary Fig. 8f). Sequence alignment of lysine residues K32 and K263 across different species revealed that K263 was more conserved (Supplementary Fig. 8g), indicating that K263 ubiquitination induced by LATS1 or homolog genes might be a more common event.

To validate whether these two lysine residues were bona fide sites on Beclin-1, we mutated these two lysine (K32/263) residues to arginine (R). Strikingly, while WT Beclin-1 was efficiently ubiquitinated in dependence on LATS1, this ubiquitination was greatly diminished with the K32/263R mutant version of Beclin-1 (Fig. 5f).

K27 linkage represents a largely unexplored, non-canonical form of ubiquitination. The HECT family E3 ligase NEDD4 has been previously reported to mediate K6, K11, and K27-linked polyubiquitination and consequently influence the stability of Beclin-1[36,37]. We thus assessed whether NEDD4 play a role in LATS1-mediated K27-linked ubiquitination on Beclin-1. First, we confirmed that the forced expression of NEDD4 stabilized Beclin-1 protein in a dose-dependent manner (Supplementary Fig. 9a). This NEDD4-mediated stabilization of Beclin-1 was accompanied by its increased K27-linked ubiquitination (Supplementary Fig. 9b). Although LATS2 interacts with Beclin-1 at a visible lower affinity in comparison with LATS1 (Supplementary Fig. 9c), LATS2 did not have any effect on Beclin-1 ubiquitination (Fig. 5a, c) and stability (Supplementary Fig. 7a, b). We next assessed whether NEDD4 interaction can distinguish LATS1 and LATS2. In line with a previous report[36,38], LATS1 was also found to physically interact with NEDD4 (Supplementary Fig. 9d). Importantly, the interaction between LATS1 and NEDD4 was independent of its kinase activity, but required its unique domain not present in LATS2 (Supplementary Fig. 9d, e). Consequently, LATS1, but not LATS2, promoted NEDD4 stability (Supplementary Fig. 9f, g). Conversely, NEDD4-LATS1 interaction led to the degradation of LATS1 but not LATS2 (Supplementary Fig. 9g, h). To assess whether NEDD4 directly affected LATS1-induced Beclin-1 ubiquitination on K32/263, we analyzed the potential NEDD4-mediated K27-ubiquitination of Beclin-1. Strikingly, while NEDD4 potently induced K27-linked polyubiquitination of WT Beclin-1, it failed to do so in the K32/263R mutant (Supplementary Fig. 9i), identifying NEDD4 as a potential E3 ligase for K27-linked polyubiquitination at K32/263 of Beclin-1.

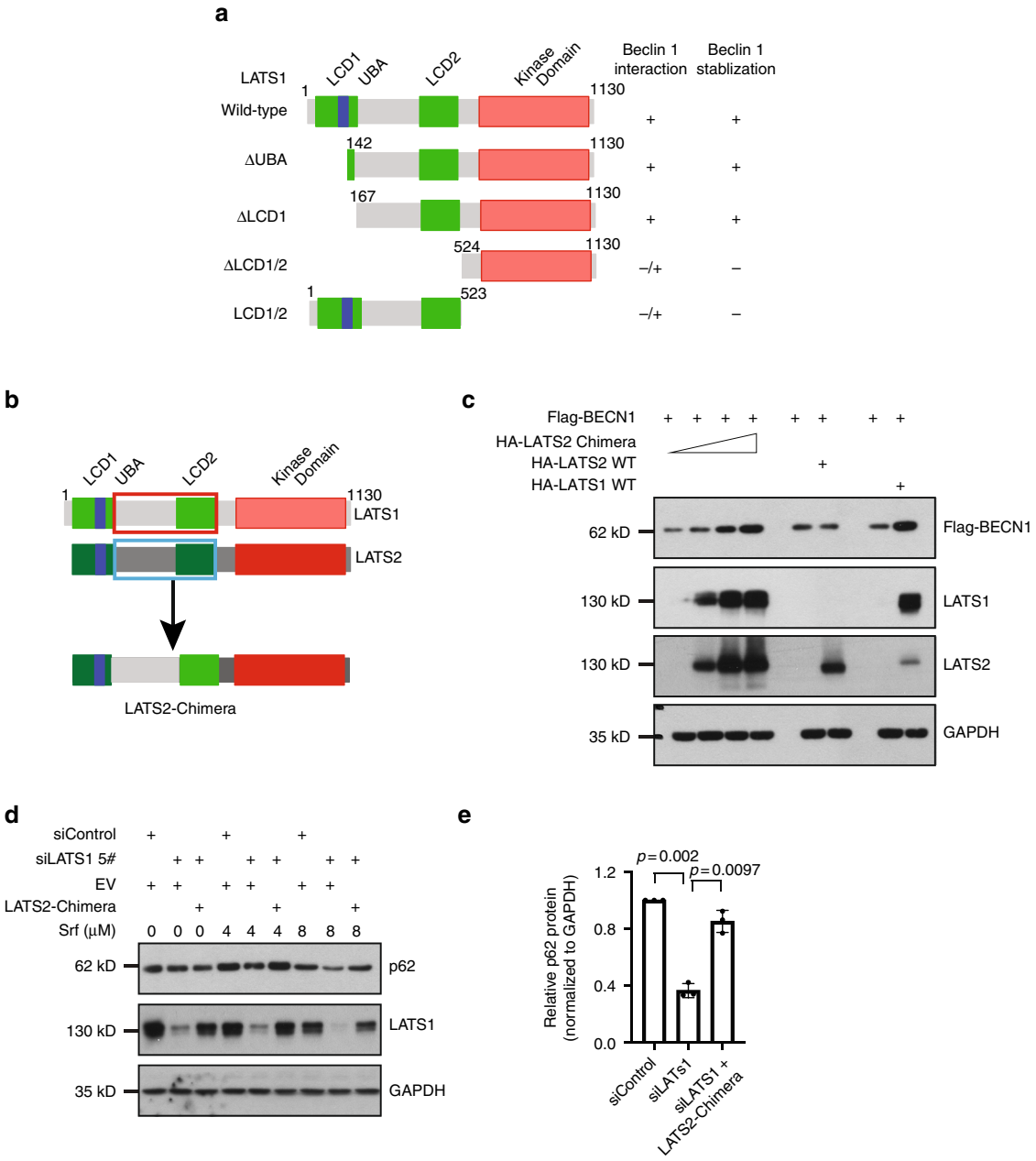

Fig. 4 Functional characterization of the divergence between LATS1 and LATS2. a Schematic representation of the protein domain structure and truncated mutants of LATS1 used for mapping the LATS1 protein domain required for Beclin-1 interaction and stabilization. **b** Schematic illustration of the generation of a LATS2-LATS1 chimeric protein by replacing the center domain of LATS2 (blue bracket) with the analogous domain of LATS1 (red bracket; amino acids 151–554) inserted between the wild-type LATS2 N-terminal (amino acids 1–147) and C-terminal (amino acids 514–1088) domains. **c** Functional validation of the LATS2 chimera protein in Beclin-1 stabilization. HEK293T/17 cells were transfected with the same amount of vectors encoding for Flag-tagged Beclin-1 (Flag-BECN1) together with HA-tagged wild-type LATS1 or LATS2, or increasing amounts of vector encoding the HA-tagged LATS2-chimeric protein as indicated. Cells were collected 72 h after transfection and analyzed by immunoblotting for Flag-BECN1, LATS1, and LATS2. Immunoblotting for GAPDH was used as loading control. Results represent three independent experiments. **d**, **e** LATS2 chimera protein can fully rescue autophagic flux (p62) in endogenous LATS1-knockdown Huh7 cells in response to sorafenib. Huh7 cells transfected with siControl or siLATS1 were in addition transfected with empty vector (EV) or a vector encoding for LATS2 chimera. Cells were lysed 72 h after transfection and p62 and LATS1 protein levels were analyzed by immunoblotting. GAPDH was used as loading control. A representative immunoblot (**d**) and quantification of the relative p62 levels (**e**) (sorafenib 8 μM condition, normalized to GAPDH) from three independent experiments are shown. Statistical significance was calculated using one-way ANOVA.

Together, the results suggest that LATS1 specifically promotes a K27-linked ubiquitination of Beclin-1 at lysine residues 32 and 263, most likely via the E3 ligase NEDD4.

Beclin-1 K32/263 ubiquitination is required for LATS1 effect. Our observations suggest that LATS1 induces Beclin-1 stabilization and K27-linked ubiquitination at K32/263 of Beclin-1. To determine whether this Beclin-1 ubiquitination affects its protein stability, we directly tested the LATS1-mediated stabilization of WT and mutant Beclin-1. Interestingly, while WT Beclin-1 was potently stabilized, LATS1-mediated stabilization was significantly impaired with the K32/263R mutant (Fig. 6a, b).

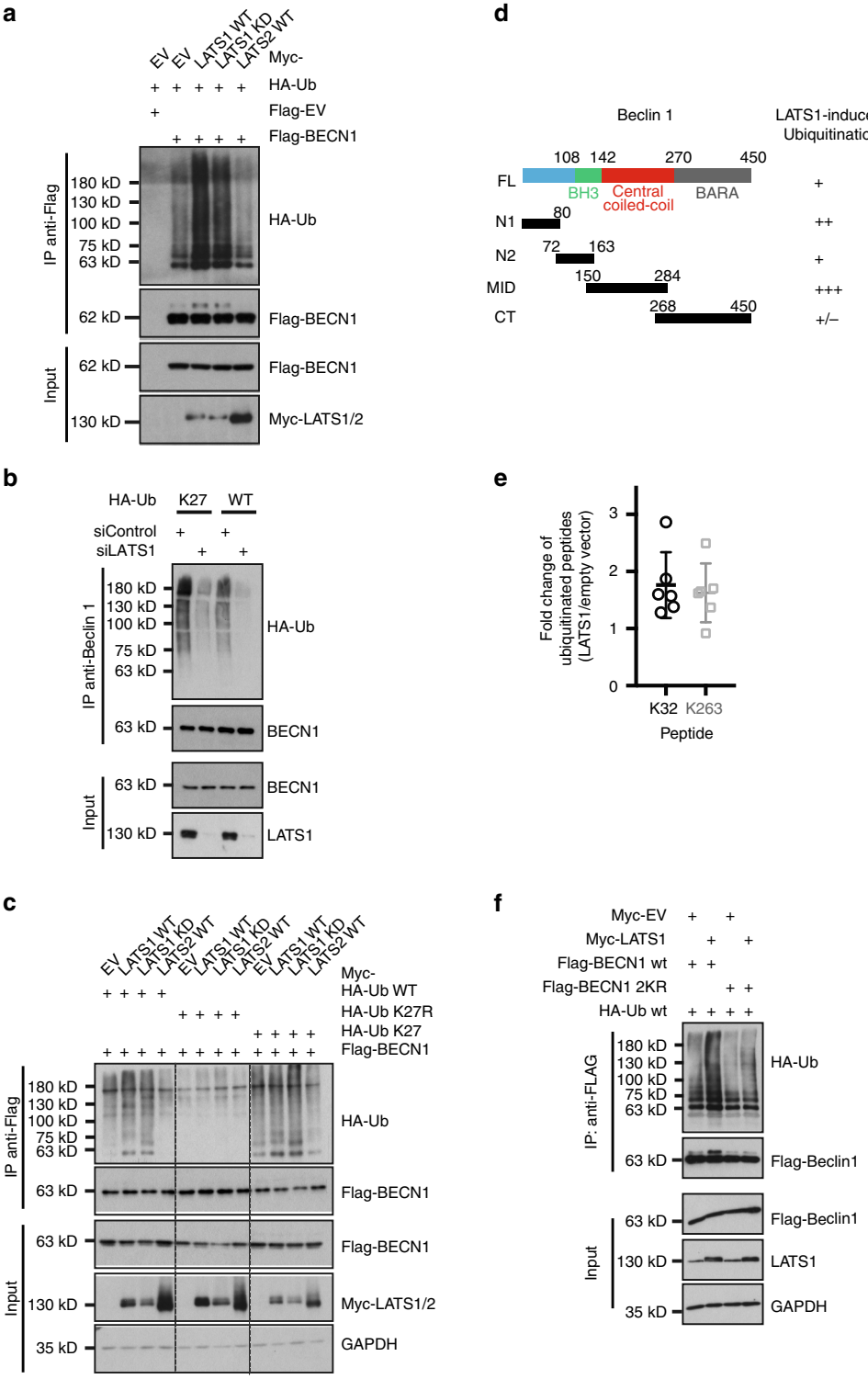

These results indicate that K27-linked ubiquitination of Beclin-1 on K32/263 is relevant for Beclin-1 stability.

To assess whether LATS1-induced ubiquitination of Beclin-1 had a causal role in autophagy regulation, we re-introduced siRNA-refractory versions of either WT Beclin-1 or its K32/263R mutant into Beclin-1 knockdown cells (Fig. 6c) and assessed autophagy induction by Srf in HCC cells and by rapamycin in U2OS cells. Interestingly, we observed an enhanced autophagy induction, as reflected by an increased number of LC3B puncta upon immunofluorescence staining (Fig. 6d, e) or a higher LC3 signal by flow cytometry (Fig. 6f) in the Beclin-1 K32/263R mutant as compared with WT Beclin-1. Next, we determined autophagic flux in cells expressing either WT or K32/263R mutant Beclin-1 by analyzing p62 protein degradation in response to Srf treatment. In line with an increased autophagy induction, we observed higher autophagic flux (Fig. 6g, h).

Although Beclin-1 generally represented an essential gene for cell viability (Supplementary Fig. 10a), we further analyzed the biological effects of LATS1-medated ubiquitination of Beclin-1. In agreement with a restrictive role in autophagy, we found that

Fig. 5 LATS1 promotes Beclin-1 ubiquitination at lysine residues K32 and K263. a HEK293T/17 cells transfected with indicated plasmids were collected 72 h later for immunoprecipitation with anti-Flag antibody and then immunoblotted for HA and Flag-tagged proteins and for LATS1/2. Input represents analysis of cell lysates before immunoprecipitation. Immunoblots represents three independent experiments. **b** HEK293T/17 cells were transfected with indicated siRNAs followed by transfection with HA-tagged wild-type or K27 (all lysins were mutated to arginine except K27) ubiquitin constructs. Seventy-two hours later, cell lysates were prepared and immunoprecipitated with Beclin-1 antibody and immunoblotted with antibodies against Beclin-1 and HA (HA-Ub). Input represents immunoblotting of cell lysates for Beclin-1 and LATS1 before immunoprecipitation. Immunoblots represent three independent experiments. **c** HEK293T/17 cells transfected with indicated plasmids. Seventy-two hours later, cell lysates were prepared and immunoprecipitated with anti-Flag antibody and immunoblotted with antibodies against HA and Flag-tagged proteins and LATS1/2. Input represents analysis of cell lysates before immunoprecipitation. GAPDH was used as loading control. Immunoblots represent three independent experiments. **d** Schematic representation of LATS1-mediated ubiquitination levels in the different domains of Beclin-1. Note that the MID construct containing the central coiled-coil domain is the minimal recipient domain for ubiquitination. **e** Mass spectrometric identification of ubiquitination sites in Beclin-1 induced by LATS1. HEK293T/17 cells were transfected with vectors encoding for HA-tagged wild-type ubiquitin, Flag-tagged-Beclin-1 with vectors encoding for empty vector and Myc-tagged LATS1. After immunoprecipitation with antibodies against Flag, samples were eluted for ubiquitination site identification by mass spectrometry. Related fold change of ubiquitinated peptide (ratio of LATS1/empty vector) is presented. Results were pooled from five independent experiments. **f** Mutation of lysine residues K32/263 blocks LATS1-induced ubiquitination of Beclin-1. Beclin-1 lysine K32 and K263 were mutated to arginine via site-directed mutagenesis. HEK293T/17 cells were transfected with indicated plasmids. Cells were collected 72 h later for immunoprecipitation with anti-Flag antibody and then immunoblotted for HA, Flag tagged proteins and LATS1/2. Input represents analysis of cell lysates before immunoprecipitation. Immunoblots represents three independent experiments. Note that the different proteins have been analyzed on different membranes.

ubiquitination deficiency in Beclin-1 resulted in increased cell death and decreased long-term cell viability (Fig. 6i, j).

The results indicate that LATS1-induced ubiquitination of Beclin-1 functionally results in Beclin-1 stabilization and, with it, into a repression of autophagic cell death.

LATS1 induces inactive Beclin-1 dimerization. Our results suggest a LATS1-specific role in restricting autophagy via modulating Beclin-1 protein through K27-linkage ubiquitination. K27-linked ubiquitin bestows some unique features, which lead to stabilization and/or dimerization/aggregation of targeted proteins[39–42]. We thus addressed how LATS1-induced Beclin-1 ubiquitination may affect autophagy. Notably, K32 and K263 on Beclin-1, which are ubiquitylated by NEDD4/LATS1, locate within the N-terminal intrinsic disordered domain and coiled-coil domain, respectively (Fig. 4d). Although the intrinsic disordered domain is structurally unexplored, the coiled-coil domain has been reported essential for Beclin-1 to form activating autophagy regulatory complexes as well as inactive Beclin-1 self-dimers[43]. Remarkably, an anti-parallel coiled-coil structure within a Beclin-1 homo-dimer involves most of their coiled-coil domains (aa 175–263), where the C termini of the coiled-coil domains (aa 248–265) are critical for stabilization of the homo-dimer[44]. Crystal structural studies suggest that lysine 263 is the last amino acid of alpha helix[45]. Based on the stabilizing effect of LATS1 on Beclin-1, the potential effect of K27-linked ubiquitination on protein aggregation, and the unique position of K263 within the C terminus of the coiled-coil domain, we assessed whether LATS1 promoted Beclin-1 self-dimerization. Indeed, LATS1 significantly promoted Beclin-1 self-dimer formation in a kinase-independent manner (Fig. 7a, b). Consistent with Beclin-1 stabilization reported above, LATS2 failed, whereas the hybrid LATS2 chimera efficiently induced Beclin-1 self-dimerization (Fig. 7c, d). Finally, LATS1-induced Beclin-1 homo-dimer formation was found reduced with the Beclin-1 K263R mutant (Fig. 7e, f), indicating that ubiquitylation on lysine 263 is functionally essential to mediate the role of LATS1 in promoting Beclin-1 homo-dimer formation and thus in preventing autophagy. Consistent with this notion, LATS1 also repressed the formation of an active autophagy initiation complex (Beclin-1/ATG14L/VPS34) (Supplementary Fig. 10b).

Together, the data demonstrate that LATS1 promotes the formation of inactivated Beclin-1 homo-dimers to prevent it from forming pro-autophagic (Beclin-1/ATG14L/VPS34) complexes. Thus, we report a kinase-independent function for LATS1, but not LATS2, in preventing autophagy under physiological conditions and in response to therapy stress and thus regulating therapy response in HCC cells (Fig. 7g). Such pro-tumorigenic activity is certainly an unexpected function of the well-studied tumor suppressor LATS1, an insight that may open new avenues to overcome therapy resistance.

Discussion

LATS1 and LATS2 kinases are evolutionarily conserved tumor suppressors, which share ~50% and 85% amino acid sequence identity between the full proteins and the kinase domains, respectively. In most cellular contexts, LATS1 and LATS2 act in a redundant manner as effector kinases of the Hippo signaling pathway by phosphorylating and inactivating the transcription factors YAP and TAZ[21]. We here report a functional divergence between LATS1 and LATS2 by the identification of a kinase activity-independent scaffolding function of LATS1, but not LATS2, in the regulation of autophagy. Although LATS1 promotes cell viability in response to Srf treatment of HCC cells, LATS2 has no effect. Analysis of autophagy modulation by LATS1 and LATS2 further confirms our observation of a specific role of LATS1 in restricting Srf-induced lethal autophagy in HCC cells. Subsequent mechanistic studies reveals a unique role of LATS1, but not LATS2, in stabilizing the autophagy core-machinery protein Beclin-1 via K27-linked ubiquitination and self-dimerization. The distinct role between LATS1 and LATS2 in autophagy regulation is exerted by a protein domain of LATS1 located between amino acids 167 and 524, a domain that also represents the most divergent part between LATS1 and LATS2.

The major function of LATS kinases in Hippo signaling is to phosphorylate the transcription factors YAP and TAZ, which earmarks them for nuclear export, deactivation, and degradation. On the other hand, the kinase activity-independent roles of LATS kinases have just started to be addressed. For instance, LATS2 restricts WNT signaling activity by disrupting the BCL9/β-catenin complex, which is dependent on its N-terminal domain but not on its kinase domain[46]. Likewise, the N-terminal domains of LATS1 and LATS2 are required to target ERα for DCAF-1-mediated degradation during mammary gland lineage commitment[47]. Interestingly, LATS1 is reported to interact with NF2[48], $CRL4^{DCAF1}$ [49], and CDK2[50]. Although the kinase domain is required to interact with $CRL4^{DCAF1}$ (aa 598–1130)[49], the N-terminal domain of LATS1 has been identified to mediate its interaction with NF2 (AIxEIxxSL, aa 72–89 of LATS1)[48], CDK20 (aa 1–200 of LATS1)[50], and Beclin-1 (aa 154–554 of LATS1) (this

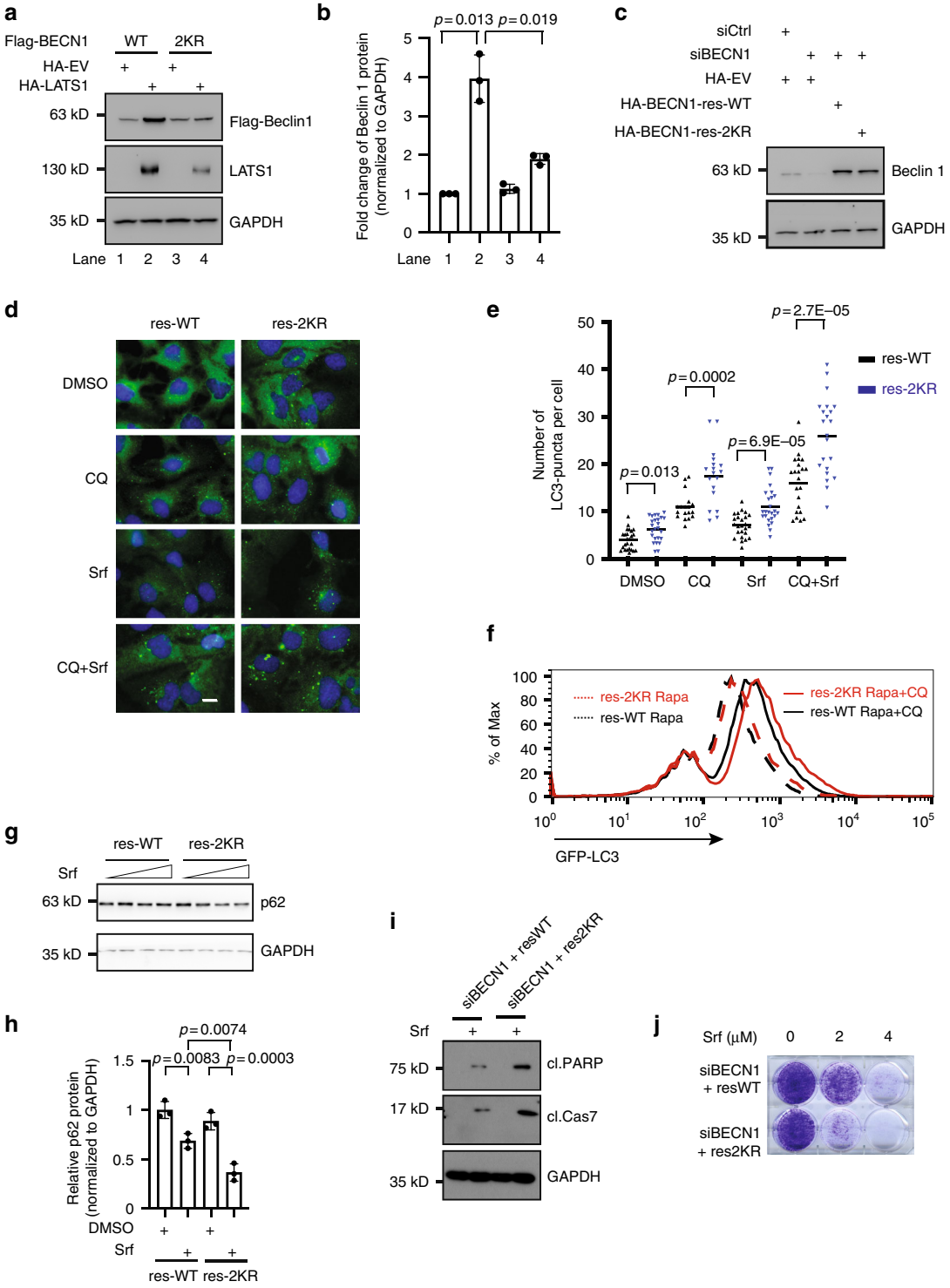

report). These results indicate different but unique interaction interfaces among these LATS1 complexes. Whether and how conformation changes of LATS1 induced by its interaction with specific binding partner affects the binding to other partners certainly merits further biochemical investigation.

On the other hand, an interplay between the Hippo signaling pathway and autophagy has been identified by mainly focusing on the activity of MST kinases, the upstream regulators of LATS activity. For instance, MST kinases regulate autophagy by directly phosphorylating BCL2, BCL-X_L and LC3B proteins[51–53]. LATS1 also interacts with BAG3[54], a BCL family member implicated in tension-induced autophagy[55]. However, a direct functional contribution of LATS1 to BAG3-mediated autophagy remains open. A role of the LATS1 homolog warts (wts) in autophagy has been described in *Drosophila* and *Caenorhabditis elegans*. Although *wts* mutation leads to attenuated autophagy in the salivary glands of the fly, RNAi-mediated depletion of wts leads to degradation of p62 in the worm[56,57]. These results suggest a a potential cellular context-dependent role of wts in autophagy regulation.

Our study has used an unbiased bioinformatics analysis to identify a restrictive role of LATS1, but not LATS2, in Srf-induced autophagy in HCC and other cancer types and normal liver

Fig. 6 LATS1-induced Beclin-1 ubiquitination is required for Beclin-1 stabilization and autophagy regulation. a, **b** Mutation of lysine residues K32/263 in Beclin-1 blocks LATS1-induced Beclin-1 stabilization. HEK293T/17 cells were transfected with the same amount of vector encoding for Flag-tagged wild-type or K32/263R lysine mutant Beclin-1 together with a vector encoding for HA-tagged LATS1 or empty vector as indicated. Seventy-two hours later cells were analyzed by immunoblotting with indicated antibodies. Representative immunoblots (**a**) and quantification of the relative Flag-tagged Beclin-1 (**b**) (normalized to GAPDH) from three independent experiments are shown. Statistical significance was calculated using one-way ANOVA. **c** Huh7 cells were transfected with indicated siRNAs followed by transfection with HA-tagged siRNA-refractory wild-type or K32/263R lysine mutant Beclin-1 cDNAs. Cells were analyzed by immunoblotting with indicated antibodies. Results represent three independent experiments. **d**, **e** Huh7 cells were transfected with indicated siRNAs followed with siRNA-refractory wild-type or K32/263R mutant Beclin-1 cDNAs. Cells were then treated with DMSO or sorafenib (Srf; 6 μM for Huh7) for 24 h and/or in combination with chloroquine (CQ; 20 μM) for 2 h before fixation. Representative images (**d**) and quantification of LC3B-puncta numbers (**e**) pooled from three independent experiments are shown. Statistical analysis was calculated by one-way ANOVA. Scale bars, 25 μm. **f** U2OS-GFP-LC3 Cells were transfected with indicated siRNAs followed with siRNA-refractory wild-type or K32/263R lysine mutant Beclin-1 cDNAs. Cells were then treated with rapamycin (Rapa; 100 nM) for 16 h and/or in combination with chloroquine (CQ; 10 μM) for 2 h before analysis. Results represent three independent experiments. **g**, **h** Huh7 cells were transfected with indicated siRNAs followed with siRNA-refractory wild-type or K32/263R lysine mutant Beclin-1 cDNAs. Cells were then treated with sorafenib for 24 h. Cells were analyzed by immunoblotting. Representative images (**g**) and quantification of relative p62 levels (**h**, treated with DMSO or 6 μM sorafenib) pooled from three independent experiments are shown. Statistical analysis was calculated by one-way ANOVA. Scale bars, 25 μm. **i, j** Cells were transfected with indicated siRNAs followed with siRNA-refractory wild-type or K32/263R mutant Beclin-1 cDNAs. **i** Cells then treated with sorafenib (Srf; 6 μM) for 48 h for immunoblotting (**i**) or for 7–10 days for colony formation assays (**j**). Results represent three independent experiments.

in vivo. Importantly, this distinct function of LATS1, but not LATS2, in autophagy appears independent of its kinase activity. Our data rather indicate that LATS1 acts as a scaffold to bind Beclin-1 and to promote K27-linked ubiquitination of Beclin-1 at lysine residues K32 and K263 in its N-terminal intrinsic disordered domain and coiled-coil domain, respectively. Consequently, K27-linked ubiquitination of Beclin-1 on K32 and K263 promotes Beclin-1 stabilization, its self-dimerization, and autophagy inhibition. Although increased at the protein level, in its self-dimerized form Beclin-1 is inactivated and can no more contribute to the execution of autophagy[43], as for instance induced by Srf treatment of HCC cells (Fig. 7g). It is noted that NEDD4 functions as a potential ubiquitin E3 ligase in regulating LATS1-induced ubiquitination of Beclin-1. Sequence alignment across different species of Beclin-1 lysine residue K32 and K263 suggests that K263 might represent evolutionary conserved regulatory mechanism of LATS1/wts towards Beclin-1. Interestingly, invertebrate genomes encode one wts kinase, whereas vertebrate genomes encode two wts homolog kinases (LATS1 and LATS2). Beclin-1, on the other hand, functions as a platform to orchestrate diverse autophagy regulatory complexes[29,30]. Notably, the central coiled-coil domain plays a key role in shifting Beclin-1 to different sub-complexes, such as Beclin-1/UVRAG, Beclin-1/ATG14, or its inactive homo-dimer. In line with previous findings of an important input of the C terminus of the coiled-coil domain to homo-dimer formation[44], our results demonstrate that lysine residue K263 is critical for Beclin-1 homo-dimer formation, which functionally mediates the regulatory role of LATS1 in autophagy.

In contrast to its tumor suppressive role in the Hippo signaling pathway, we report that LATS1 exerts a pro-survival function in HCC cells in response to Srf treatment, i.e., an oncogenic activity. Indeed, RNAi-mediated ablation of LATS1 expression results in an increase of Srf-induced apoptosis and a reduction of cell viability in vitro and a decrease of tumor growth in vivo. Moreover, gene expression analysis of HCC patient samples indicates a poor survival of patients with high expression of LATS1 in their tumors, further supporting the notion of a pro-oncogenic role of LATS1 in HCC cells. Most importantly, a significant higher expression of LATS1 is observed in patients not responding to Srf as compared with patients responding to Srf therapy, suggesting LATS1 as a clinically relevant biomarker for Srf sensitivity.

The therapeutic targeting of the Hippo signaling pathway is currently under intense investigation in basic and pharmaceutical research laboratories. Here we have identified a non-redundant function of LATS in HCC. We have delineated the mechanistic details of a kinase activity-independent function of LATS1 in autophagy regulation and in tumorigenesis, thus raising a note of caution on the therapeutic targeting of LATS kinases. Their pro-tumorigenic and tumor suppressive roles, their non-redundant distinct activities and their kinase activity-dependent and independent functions need to be considered to efficiently interfere with tumor progression and therapy resistance and to avoid undesired consequences.

Methods

DNA plasmids, siRNA, and shRNA sequences and antibodies. DNA plasmids and sequences of siRNAs used in this study are listed in Supplementary Dataset 1. Additional information on antibodies is provided in Supplementary Dataset 2.

Cell culture, transfection, and reagents. HEK293T/17, Huh7, Hep3B, SNU423, and SNU398 were obtained from American Type Culture Collection. Hep40 cell line was a kind gift from Brian Carr. U2OS cell line stably expressing GFP-LC3 was a kind gift from Carine Joffre. All the cell lines in this study were regularly confirmed for the absence of *Mycoplasma* contamination. Transfection of plasmids into HEK293T/17 and HCC cells were carried out using jetPEI (polyPlus Transfections) and Lipofectamine 3000 (Invitrogen) according to the manufacturers' instructions, respectively. Lipofectamine RNAiMAX (Invitrogen) was used to transfect siRNAs. To establish stable knockdown or overexpression cell lines, retrovirus were produced by transfection of Platinium-A cells (Cell Biolabs) with pBabe-retro-puro or pSuper-retro-puro constructs, respectively. Control or gene-specific siRNAs were from Dharmacon as ON-TARGET plus SMARTpools or Set of 4 upgrade products.

Srf was from Selleckchem (in vitro study) and LC Laboratories (in vivo study). Baf and CQ were from Sigma.

HCC patient-derived ex vivo organoid lines. The stable HCC organoid lines used in this study have been reported previously[18]. Briefly, ultrasound-guided tumor biopsies were obtained from patients undergoing diagnostic liver biopsy at the University Hospital Basel. Written informed consent was obtained from all patients and the study was approved by the ethics committee of the northwestern part of Switzerland (Protocol Number EKNZ 2014-099). Tumor needle biopsy tissue was rapidly transferred to the lab, minced, and digested with 2.5 mg/mL collagenase IV (Sigma), 0.1 mg/mL DNase (Sigma) at 37 °C for 5 min. Digested biopsy/cell clusters were then seeded into reduced growth factor BME2 (Basement Membrane Extract, Type 2; Amsbio). After polymerization of BME2, expansion medium was added to the BME2 droplets. The composition of the medium is: advanced Dulbecco's modified Eagle's medium (DMEM)/F-12 (GIBCO) supplemented with 1:50 B-27 (GIBCO), 1:100 N-2 (GIBCO), 10 mM nicotinamide (Sigma), 1.25 mM *N*-acetyl-L-cysteine (Sigma), 10 nM [Leu15]-gastrin (Sigma), 10 mM forskolin (Tocris), 5 mM A83-01 (Tocris), 50 ng/mL EGF (PeproTech), 100 ng/mL FGF10 (PeproTech), 25 ng/mL HGF (PeproTech), and 10% RSpo1-conditioned medium (homemade). Tumor organoids were passaged by dissociation with 0.25% Trypsin-EDTA (GIBCO).

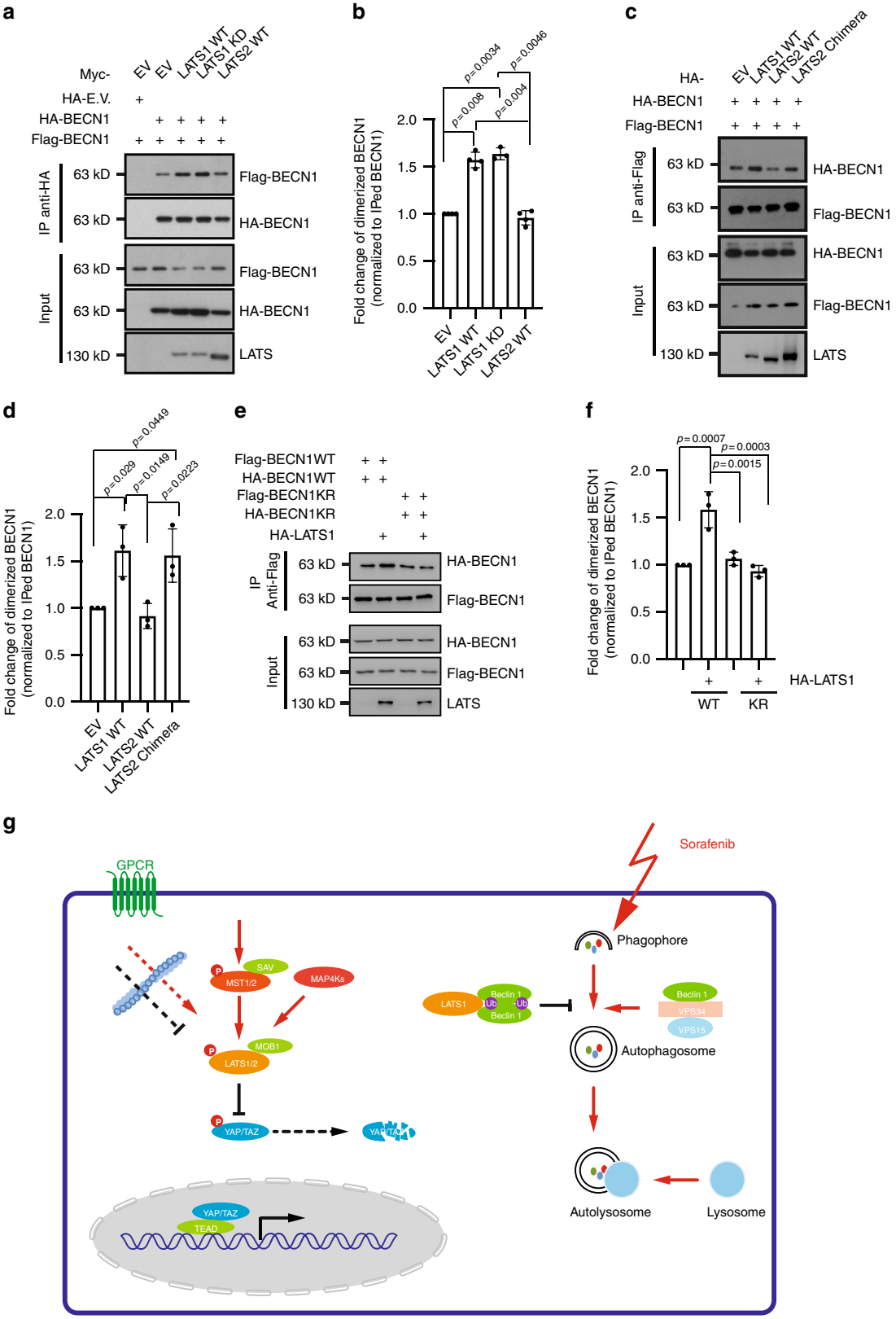

Srf treatment of tumor organoids. One thousand cells per well were seeded in a 384-well plate and Srf added 24 h later. After 6 days of drug treatment, cell viability was assessed with CellTiterGlo 3D according to the manufacturer's instructions.

Autophagy study in vivo. Mice carrying floxed alleles of Lats1 (*Lats1*$^{fl/fl}$) were kindly provided by Randy L. Johnson (M.D. Anderson Cancer Center) via Georg Halder (VIB-KU Leuven Center for Cancer Biology). Mice expressing liver-specific-cre recombinase (Alb-cre) driven by the albumin promoter (JAX stock #003574) was kindly provided by Markus H. Heim. *Lats1* conditional knock mice (*Lats1*$^{fl/fl}$, Alb-cre) were generated by crossing *Lats1*$^{fl/fl}$ mice with Alb-cre mice in a C57BL/6J background. Mice were bred and maintained under specific and opportunistic pathogen-free (SOPF) facility with food and water ad libitum. All in vivo experiments were performed under approval number 2839 within the Swiss Federal Animal Welfare Law.

Fig. 7 LATS1 induces inactive Beclin-1 self-dimerization. a LATS1, but not LATS2, promotes Beclin-1 self-dimerization in a kinase activity-independent manner. HEK293T/17 cells were transfected with indicated plasmids. Cells were collected 72 h later for immunoprecipitation with anti-HA antibody and then immunoblotted for HA, Flag-tagged Beclin-1, and LATS1/2. Input represents analysis of cell lysates before immunoprecipitation. Immunoblots represent three independent experiments. **b** Quantification of dimerized Beclin-1 (BECN1) protein abundancy pooled from four independent experiments described in (**a**). Statistical significance was calculated using one-way ANOVA. ***$P < 0.001$. **c** LATS2 chimera maintains the ability to promote Beclin-1 self-dimerization. HEK293T/17 cells were transfected with Flag-tagged (Flag-BECN1) and with HA-tagged (HA-BECN1) Beclin-1 and with empty vector (EV) or with vectors encoding for wild-type (WT) LATS1 or LATS2, or LATS2 chimera, as indicated. Cells were collected 72 h later for immunoprecipitation with anti-Flag antibody and then immunoblotted for HA, Flag-tagged Beclin-1, and LATS1/2. Input represents analysis of cell lysates before immunoprecipitation. Immunoblots represent three independent experiments. **d** Quantification of dimerized Beclin-1 (BECN1) protein abundancy pooled from four independent experiments described in **c**. Statistical significance was calculated using one-way ANOVA. *$P < 0.05$. **e** LATS1-induced ubiquitination at lysine 263 is essential for LATS1-mediated promotion of Beclin-1 self-dimerization. HEK293T/17 cells were transfected with indicated plasmids. Cells were collected 72 h later for immunoprecipitation with anti-Flag antibody and then immunoblotted for HA, Flag-tagged Beclin-1, and LATS1. Input represents analysis of cell lysates before immunoprecipitation. Immunoblots represent three independent experiments. **f** Quantification of dimerized Beclin-1 (BECN1) protein abundancy pooled from three independent experiments described in **e**. Statistical significance was calculated using one-way ANOVA. ***$P < 0.001$, *$P < 0.05$. **g** Schematic representation of the role of LATS1 in canonical Hippo signaling (left side) and of its non-canonical role in repressing sorafenib-induced autophagy (right side). LATS1-induced K27-linked ubiquitination of Beclin-1 on K32 and K263 results into its inactivation by self-dimerization and thus to an inhibition of autophagy.

To block autophagic flux, mice were intraperitoneally (i.p.) injected with CQ (30 mg/kg in phosphate-buffered saline, PBS) and liver tissues were collected for analysis 4 h after injection. To induce autophagic flux, mice were i.p. injected with rapamycin (2 mg/kg in PBS containing 5% PEG400/5% Tween-80/4% ethanol) twice a day (0600 and 1800 h) followed by fasting for 12 h and extraction of liver tissue for analysis.

Cloning. To establish the hybrid LATS2 chimera construct, the LATS2 N terminus (amino acids 1–148), LATS1 domain (amino acids 151–554), and LATS2 C terminus (amino acids 514–1088) were PCR-amplified and assembled into pcDNA3-derived vectors using NEB Builder HiFi kit (NEB).

Cell viability and colony formation assays. Short-term cell viability was measured using CellTiter-Fluor cell viability assay (Promega) with a SpectraMAX plate reader according to the manufacturer's instructions. Viability of ex vivo organoid lines in response to Srf was determined according to the protocol described in ref. [18]. Long-term cell viability and proliferation was performed using colony formation assays. Briefly, 200–1000 cells seeded in triplicate on 12-well plates were cultured for 2–3 weeks. Completed culture medium supplemented with Srf or DMSO (dimethyl sulfoxide) was refreshed every 3 days for the first week and every 2 days from the second week onwards. To visualize differences in cell growth, crystal violet staining was performed. Briefly, cells were fixed with 4% paraformaldehyde for 20 min at room temperature, washed twice with H_2O, and stained with crystal violet (1 mg/mL dissolved in 10% ethanol) for 20 min. After washing with H_2O, plates were left to dry at room temperature. The cell stained crystal violet was retrieved with 10% acetic acid and absorbance at 595 nm was measured using a SpectraMAX plate reader.

Tumor transplantation and Srf therapy. NSG mice were maintained in SOPF facility with food and water ad libitum. Huh7 cells (5×10^5 in 200 µL DMEM: Matrigel (1:1 ratio)) were implanted into the left flanks. When tumors were palpable, mice were randomly grouped into vehicle or Srf treatment cohorts. When tumor volumes reached 100 mm^3, Srf (30 mg/kg) or vehicle control was administrated daily via oral gavage for 4 weeks. Tumor diameters were measured twice a week using a caliper, and tumor volumes were calculated as follows: volume $= d^2{*}D/2$, where d and D is the shorter and longer tumor diameter, respectively. All in vivo experiments were performed under approval number 2839 within the Swiss Federal Animal Welfare Law.

Analysis of autophagy. For LC3B staining, cells were transfected and seeded on glass coverslips. After treatment, cells were washed in PBS and fixed with ice-cold methanol for 20 min. After PBS washes, fixed cells were incubated in 0.1% Triton X-100 in PBS for 5 min, followed by blocking with 0.1% Trition X-100 in 3% bovine serum albumin (BSA) for 1 h. Endogenous LC3B were detected by incubation of fixed cells with anti-LC3B antibody (CST3868, 1:200) overnight, followed with anti-rabbit Alexa 488 secondary antibody (Invitrogen 1:300). After 4′,6-diamidino-2-phenylindole (DAPI) staining, cells were washed and mounted in fluorescence mounting medium (Dako S3023). Images were acquired on a Leica DMI 4000 microscope. For quantifications, more than 5 fields (at least 100 cells in total) were randomly selected based on DAPI staining and the number of LC3B dots per cell was quantified using ImageJ software.

Autophagy detection using flow cytometry was performed according to the protocol described in ref. [27]. Briefly, U2OS-GFP-LC3 cells were trypsinized and incubated with 0.5% saporin in PBS for 5 min. Cells were washed and suspended for analysis using a BD FACS Canto II flow cytometer. Data were analyzed with Flowjo software.

Protein lysis, immunoprecipitation, ubiquitination, and immunoblot analysis. Cells were lysed with RIPA buffer (Sigma R0278) supplemented with additional 2% NP-40. Cell lysates were sonicated before protein concentration determination (BCA protein assay kit, Pierce 23225). Equal amount of protein was fractionated by SDS-polyacrylamide gel eletrophoresis and transferred onto a polyvinylidene difluoride membrane, which was blocked with 5% milk in Tris-buffered saline (TBS) followed with desired antibodies in 5% BSA-TBS. The protocol for co-immunoprecipitation has been described previously[58]. Briefly, cells were lysed with Cell Signaling Technology (CST) lysis buffer (CST9803) supplemented with 1 mM phenylmethylsulfonyl fluoride and incubated with specific antibodies with protein A/G-Sepharose overnight. After three times washing with CST lysis, the precipitated proteins were eluted with SDS-loading buffer and analyzed by immunoblotting. For the ubiquitination assay, cells transfected with plasmids were lysed with RIPA buffer supplemented with additional 0.1% SDS to a final concentration of 0.2% SDS, followed by standard immunoprecipitation protocols. Chemiluminescence was detected with X-Ray films or Fusion FX (Analis). Image J software was used to quantify the immunoblots by densitometry. Information on the antibodies used is presented in Supplementary Dataset 2.

Identification of ubiquitination sites by mass spectrometry. MS analysis was performed in the proteomics core facility of the Biozentrum, University of Basel. Briefly, HEK cells were transfected with Flag-tagged Beclin-1 and HA-tagged ubiquitin together with either empty vector or vector encoding LATS1. After lysis and immunoprecipitation, proteins were eluted with 600 µl 100 mM trimethylamine, pH 11. The eluate was dried in a SpeedVac and fully resuspended in 100 µL of 50 mM Tris-HCl (pH 7.5) with sonication. Samples were heated up for 10 min and cooled down followed by incubated with chloroacetamide (1 µL per samples). Proteins were subjected to endoproteinase LysC (1:100 (w/w), Wako) digestion at 37 °C for 4 h, then subjected to trypsin digestion (0.5 µg/µL; 1:50; w/w) at 37 °C overnight. The samples were then subjected to liquid chromatography–tandem MS (LC-MS/MS).

The acquired raw-files were imported into the Progenesis QI software (v2.0, Nonlinear Dynamics Limited), which was used to extract peptide precursor ion intensities across all samples applying the default parameters. The generated mgf-files were searched using MASCOT (Version: 2.4.1) against a decoy database containing normal and reverse sequences of the predicted SwissProt entries of Homo sapiens (www.ebi.ac.uk, release date 2016/25/05) and commonly observed contaminants (in total 41,170 sequences for Homo sapiens) generated using the SequenceReverser tool from the MaxQuant software (Version 1.0.13.13). The search criteria were set as follows: semi tryptic specificity was required (cleavage after lysine or arginine residues, unless followed by proline); four missed cleavages were allowed; carbamidomethylation (C) was set as fixed modification; oxidation (M) and GlyGly (K) were applied as variable modifications; mass tolerance of 10 p.p.m. (precursor) and 0.02 Da (fragments). The database search results were filtered using the ion score to set the false discovery rate (FDR) to 1% on the peptide and protein level, respectively, based on the number of reverse protein sequence hits in the datasets. The relative quantitative data obtained were normalized and statistically analyzed using our in-house script as above[59]. In addition, Scaffold (version Scaffold_4.8.7, Proteome Software Inc., Portland, OR) was used to validate MS/MS based peptide and protein identifications. Peptide identifications were accepted if they could be established at greater than 93.0% probability by the Scaffold Local FDR algorithm. Protein identifications were accepted if they could be established at greater than 98.0% probability to achieve an FDR < 1.0% and contained at least two identified peptides. Protein probabilities were assigned by the Protein Prophet algorithm[60]. Proteins that contained similar peptides and could not be differentiated based on MS/MS analysis alone were grouped to satisfy the principles of parsimony.

RNA extraction and sequencing analysis. RNA from siRNA-transfected and Srf-treated cells was extracted in biological triplicates using miRNeasy Mini kit (Qiagen) according to the manufacturer's instructions. RNA quality control was performed using a fragment analyser and the standard or high-sensitivity RNA analysis kits (Labgene; DNF-471-0500 or DNF-472-0500). RNA concentrations were measured using the Quanti-iTTM RiboGreen RNA assay Kit (Life Technologies/Thermo Fisher Scientific). A total of 200 ng of RNA was utilized for library preparation with the TruSeq stranded total RNA LT sample prep Kit (Illumina). Poly-A+ RNA was sequenced with HiSeq SBS Kit v4 (Illumina) on an Illumina HiSeq 2500 using protocols defined by the manufacturer.

Single-end RNA-seq reads (81-mers) were mapped to the human genome assembly, version hg19 (GRCh37.75), with RNA-STAR[61], with default parameters except for allowing only unique hits to genome (outFilterMultimapNmax = 1) and filtering reads without evidence in spliced junction table (outFilterType = "BySJout"). Expression levels per gene (counts over exons) for the RefSeq mRNA coordinates from UCSC (genome.ucsc.edu, downloaded in December 2015) were quantified using qCount function from QuasR package (version 1.12.0). The differentially expressed genes were identified using the edgeR package (version 3.14.0). Genes with p-values smaller than 0.05 and minimum log2 fold changes of ±0.58 were considered as differentially regulated and were used for downstream functional and pathway enrichment analysis.

Functional enrichment analysis. We performed functional enrichment analysis of differentially expressed genes for biological processes or pathways in R using several publicly available Bioconductor resources including org.Hs.eg.db (version 3.3.0), GO.db (version 3.4.1), GOstats (version 2.42.0)[62], KEGG.db (version 3.2.3), and ReactomePA (version 1.16.2)[63]. The significance of each biological processes or pathways identified was calculated using the hypergeometric test (equivalent to Fisher's exact test) and those with p-values ≤ 0.05 were considered significant.

Gene set enrichment analysis. The GSE A analysis was performed using the JAVA application of the Broad Institute version 3.0 (http://www.broadinstitute.org/gsea). The gene sets used for the analysis were derived from GO annotations, and pathways were obtained from the GO (http://www.geneontology.org/) and KEGG (http://www.genome.jp/kegg/) databases.

Patient material and ethics. All relevant ethical regulations were strictly followed in this study. All the analysis using human tissue samples reported in this study were approved by the ethics commission of Northwestern Switzerland (EKNZ, approval number 361/12).

Re-analysis of transcriptomic profiling data. RNA-seq gene expression values were retrieved from om TCGA Liver dataset[64] using the cbioportal (http://www.cbioportal.org, accessed 12/05/2017) website[65]. The dataset included 364 and 314 HCCs with overall survival and disease-free survival information, respectively. Survival analyses were performed using the Kaplan–Meier method and the log-rank test. The cut-off was defined as previously described[66].

Statistical analysis. All statistical tests were two-sided. Specific details on the statistical method are provided in each figure legend. Data are presented as mean. Bar plots with error bars represent mean ± SD. Statistical significance was defined as $*P < 0.05$, $**P < 0.01$, $***P < 0.001$. All analyses were performed using Excel or Graphpad Prism 6.0 (Graphpad Software, Inc., La Jolla, CA) or SPSS v.20 (Endicott, New York, NY).

Reporting summary. Further information on research design is available in the Nature Research Reporting Summary linked to this article.

Data availability

The mass spectrometry proteomics data have been deposited to the ProteomeXchange Consortium via the PRIDE partner repository with the dataset identifier PXD013159 and 10.6019/PXD013159. The RNA-seq files are deposited on GEO database with an accession number GSE117116. Data sets with accession numbers GSE71873 and Uniprot access numbers

Q14457 for human,
O8859 for Mouse,
F1RCP1 for Fish,
Q4A1L3 for Frog,
Q22592 for Worm,
Q9VCE1 for fly,
Q02948 for yeast,
and TCGA Liver datasets have been used in the study.

The source data underlying Figs. 1a, c-d, f, i, 2b-e and g-h, 3a-i, 4c-e, 5a-c and e-f, 6a-c, e and g-i, 7a-f, and Supplementary Figs. 1a-c, e-g, k and l-n, 3b-g, 4a-e and g, 5b-d, f, h, 6c, 7a-i, 8a-d and f, 9a-i, and 10c are provided in Source Data file.

Received: 1 May 2019; Accepted: 14 November 2019;
Published online: 17 December 2019

References

1. Llovet, J. M. et al. Hepatocellular carcinoma. *Nat. Rev. Dis. Prim.* **2**, 16018 (2016).
2. Llovet, J. M. et al. Sorafenib in advanced hepatocellular carcinoma. *N. Engl. J. Med.* **359**, 378–390 (2008).
3. Levine, B. & Klionsky, D. J. Development by self-digestion: molecular mechanisms and biological functions of autophagy. *Dev. Cell* **6**, 463–477 (2004).
4. White, E. Deconvoluting the context-dependent role for autophagy in cancer. *Nat. Rev. Cancer* **12**, 401 (2012).
5. Dikic, I. & Elazar, Z. Mechanism and medical implications of mammalian autophagy. *Nat. Rev. Mol. Cell Biol.* **19**, 349–364 (2018).
6. Rubinsztein, D. C., Codogno, P. & Levine, B. Autophagy modulation as a potential therapeutic target for diverse diseases. *Nat. Rev. Drug Discov.* **11**, 709 (2012).
7. Li, J. et al. Rage induces hepatocellular carcinoma proliferation and sorafenib resistance by modulating autophagy. *Cell Death Dis.* **9**, 225 (2018).
8. Wu, F.-Q. et al. ADRB2 signaling promotes HCC progression and sorafenib resistance by inhibiting autophagic degradation of HIF1α. *J. Hepatol.* **65**, 314–324 (2016).
9. Tai, W. T. et al. Mcl-1-dependent activation of Beclin 1 mediates autophagic cell death induced by sorafenib and SC-59 in hepatocellular carcinoma cells. *Cell Death Dis.* **4**, e485 (2013).
10. Shi, Y.-H. et al. Targeting autophagy enhances sorafenib lethality for hepatocellular carcinoma via ER stress-related apoptosis. *Autophagy* **7**, 1159–1172 (2011).
11. Satoshi, S. et al. Inhibition of autophagy potentiates the antitumor effect of the multikinase inhibitor sorafenib in hepatocellular carcinoma. *Int. J. Cancer* **131**, 548–557 (2012).
12. Pan, D. The Hippo signaling pathway in development and cancer. *Dev. Cell* **19**, 491–505 (2010).
13. Harvey, K. F., Zhang, X. & Thomas, D. M. The Hippo pathway and human cancer. *Nat. Rev. Cancer* **13**, 246 (2013).
14. Meng, Z., Moroishi, T. & Guan, K.-L. Mechanisms of Hippo pathway regulation. *Genes Dev.* **30**, 1–17 (2016).
15. Kim, M. H. et al. Actin remodeling confers BRAF inhibitor resistance to melanoma cells through YAP/TAZ activation. *EMBO J.* **35**, 462–478 (2016).
16. Lin, L. et al. The Hippo effector YAP promotes resistance to RAF- and MEK-targeted cancer therapies. *Nat. Genet.* **47**, 250 (2015).
17. Zanconato, F., Battilana, G., Cordenonsi, M. & Piccolo, S. YAP/TAZ as therapeutic targets in cancer. *Curr. Opin. Pharmacol.* **29**, 26–33 (2016).
18. Nuciforo, S. et al. Organoid models of human liver cancers derived from tumor needle biopsies. *Cell Rep.* **24**, 1363–1376 (2018).
19. Sharif, A. A. D. & Hergovich, A. The NDR/LATS protein kinases in immunology and cancer biology. *Semin. Cancer Biol.* **48**, 104–114 (2018).
20. Cancer Genome Atlas Research Network. Comprehensive and Integrative Genomic Characterization of Hepatocellular Carcinoma. *Cell* **169**, 1327–1341 e1323 (2017).
21. Furth, N. & Aylon, Y. The LATS1 and LATS2 tumor suppressors: beyond the Hippo pathway. *Cell Death Differ.* **24**, 1488 (2017).
22. Chen, K.-F. et al. Sorafenib overcomes TRAIL resistance of hepatocellular carcinoma cells through the inhibition of STAT3. *Clin. Cancer Res.* **16**, 5189–5199 (2010).
23. Mizushima, N. et al. A protein conjugation system essential for autophagy. *Nature* **395**, 395 (1998).
24. Romano, D. et al. Protein interaction switches coordinate Raf-1 and MST2/Hippo signalling. *Nat. Cell Biol.* **16**, 673 (2014).
25. Kinsey, C. G. et al. Protective autophagy elicited by RAF→MEK→ERK inhibition suggests a treatment strategy for RAS-driven cancers. *Nat. Med.* **25**, 620–627 (2019).
26. Levine, B. & Kroemer, G. Autophagy in the pathogenesis of disease. *Cell* **132**, 27–42 (2008).
27. Eng, K. E., Panas, M. D., Hedestam, G. B. K. & McInerney, G. M. A novel quantitative flow cytometry-based assay for autophagy. *Autophagy* **6**, 634–641 (2010).
28. Klionsky, D. J. et al. Guidelines for the use and interpretation of assays for monitoring autophagy. *Autophagy* 12, 1–222 (2016).
29. Mizushima, N., Yoshimori, T. & Levine, B. Methods in mammalian autophagy research. *Cell* **140**, 313–326 (2010).
30. Kang, R., Zeh, H. J., Lotze, M. T. & Tang, D. The Beclin 1 network regulates autophagy and apoptosis. *Cell Death Differ.* **18**, 571 (2011).

31. Joffre, C. et al. The pro-apoptotic STK38 kinase is a new Beclin1 partner positively regulating autophagy. *Curr. Biol.* **25**, 2479–2492 (2015).
32. Russell, R. C. et al. ULK1 induces autophagy by phosphorylating Beclin-1 and activating VPS34 lipid kinase. *Nat. Cell Biol.* **15**, 741 (2013).
33. Sun, T. et al. Acetylation of Beclin 1 inhibits autophagosome maturation and promotes tumour growth. *Nat. Commun.* **6**, 7215 (2015).
34. Shi, C.-S. & Kehrl, J. H. TRAF6 and A20 regulate lysine 63–linked ubiquitination of Beclin-1 to control TLR4-induced autophagy. *Sci. Signal.* **3**, ra42–ra42 (2010).
35. Grumati, P. & Dikic, I. Ubiquitin signaling and autophagy. *J. Biol. Chem.* **293**, 5404–5413 (2018).
36. Salah, Z., Cohen, S., Itzhaki, E. & Aqeilan, R. NEDD4 E3 ligase inhibits the activity of the Hippo pathway by targeting LATS1 for degradation. *Cell Cycle* **12**, 3817–3823 (2013).
37. Pei, G. et al. The E3 ubiquitin ligase NEDD4 enhances killing of membrane-perturbing intracellular bacteria by promoting autophagy. *Autophagy* **13**, 2041–2055 (2017).
38. Bae, S. J. et al. NEDD4 controls intestinal stem cell homeostasis by regulating the Hippo signalling pathway. *Nat. Commun.* **6**, 6314 (2015).
39. Nucifora, F. C. Jr et al. Ubiquitination via K27 and K29 chains signals aggregation and neuronal protection of LRRK2 by WSB1. *Nat. Commun.* **7**, 11792 (2016).
40. Zucchelli, S. et al. TRAF6 promotes atypical ubiquitination of mutant DJ-1 and alpha-synuclein and is localized to Lewy bodies in sporadic Parkinson's disease brains. *Hum. Mol. Genet.* **19**, 3759–3770 (2010).
41. Birsa N., et al. K27 ubiquitination of the mitochondrial transport protein Miro is dependent on serine 65 of the Parkin ubiquitin ligase. *J. Biol. Chem.* **289**, 14569–14582 (2014).
42. Castañeda Carlos, A. et al. Linkage via K27 bestows ubiquitin chains with unique properties among oolyubiquitins. *Structure* **24**, 423–436 (2016).
43. Li, X. et al. Imperfect interface of Beclin1 coiled-coil domain regulates homodimer and heterodimer formation with Atg14L and UVRAG. *Nat. Commun.* **3**, 662 (2012).
44. Ranaghan, M. J. et al. The autophagy-related Beclin-1 protein requires the coiled-coil and BARA domains to form a homodimer with submicromolar affinity. *Biochemistry* **56**, 6639–6651 (2017).
45. Huang, W. et al. Crystal structure and biochemical analyses reveal Beclin 1 as a novel membrane binding protein. *Cell Res.* **22**, 473 (2012).
46. Li, J. et al. LATS2 suppresses oncogenic Wnt signaling by disrupting b-catenin/BCL9. *Interact. Cell Rep.* **5**, 1650–1663 (2013).
47. Britschgi, A. et al. The Hippo kinases LATS1 and 2 control human breast cell fate via crosstalk with ERα. *Nature* **541**, 541 (2017).
48. Yin, F. et al. Spatial organization of Hippo signaling at the plasma membrane mediated by the tumor suppressor Merlin/NF2. *Cell* **154**, 1342–1355 (2013).
49. Li, W. et al. Merlin/NF2 loss-driven tumorigenesis linked to CRL4DCAF1-mediated inhibition of the Hippo pathway kinases Lats1 and 2 in the nucleus. *Cancer Cell* **26**, 48–60 (2014).
50. Pefani, D.-E. et al. RASSF1A–LATS1 signalling stabilizes replication forks by restricting CDK2-mediated phosphorylation of BRCA2. *Nat. Cell Biol.* **16**, 962 (2014).
51. Maejima, Y. et al. Mst1 inhibits autophagy by promoting the interaction between Beclin1 and Bcl-2. *Nat. Med.* **19**, 1478 (2013).
52. Nakamura M., Zhai P., Del Re D. P., Maejima Y., Sadoshima J. Mst1-mediated phosphorylation of Bcl-xL is required for myocardial reperfusion injury. *JCI Insight* **1**, pii: e86217 (2016).
53. Wilkinson Deepti, S. et al. Phosphorylation of LC3 by the Hippo kinases STK3/STK4 is essential for autophagy. *Mol. Cell* **57**, 55–68 (2015).
54. Ulbricht, A. et al. Cellular mechanotransduction relies on tension-induced and chaperone-assisted autophagy. *Curr. Biol.* **23**, 430–435 (2013).
55. Klimek, C., Kathage, B., Wördehoff, J. & Höhfeld, J. BAG3-mediated proteostasis at a glance. *J. Cell Sci.* **130**, 2781–2788 (2017).
56. Dutta, S. & Baehrecke, E. H. Warts is required for PI3K-regulated growth arrest, autophagy, and autophagic cell death in *Drosophila*. *Curr. Biol.* **18**, 1466–1475 (2008).
57. Guo, B. et al. Genome-wide screen identifies signaling pathways that regulate autophagy during *Caenorhabditis elegans* development. *EMBO Rep.* **15**, 705–713 (2014).
58. Tang, F. et al. The kinases NDR1/2 act downstream of the Hippo homolog MST1 to mediate both egress of thymocytes from the thymus and lymphocyte motility. *Sci. Signal.* **8**, ra100–ra100 (2015).
59. Ahrné, E. et al. Evaluation and improvement of quantification accuracy in isobaric mass Tag-based protein quantification experiments. *J. Proteome Res.* **15**, 2537–2547 (2016).
60. Nesvizhskii, A. I., Keller, A., Kolker, E. & Aebersold, R. A statistical model for identifying proteins by tandem mass spectrometry. *Anal. Chem.* **75**, 4646–4658 (2003).
61. Dobin, A. et al. STAR: ultrafast universal RNA-seq aligner. *Bioinformatics* 29, 15–21 (2013).
62. Falcon, S. & Gentleman, R. Using GOstats to test gene lists for GO term association. *Bioinformatics* **23**, 257–258 (2007).
63. Yu, G. & He, Q.-Y. ReactomePA: an R/Bioconductor package for reactome pathway analysis and visualization. *Mol. Biosyst.* **12**, 477–479 (2016).
64. TCGA. Comprehensive and integrative genomic characterization of hepatocellular carcinoma. *Cell* **169**, 1327–1341.e1323 (2017).
65. Gao, J. et al. Integrative analysis of complex cancer genomics and clinical profiles using the cBioPortal. *Sci. Signal.* **6**, pl1–pl1 (2013).
66. Budczies, J. et al. Cutoff Finder: a comprehensive and straightforward web application enabling rapid biomarker cutoff optimization. *PLoS ONE* **7**, e51862 (2012).

Acknowledgements

We thank Christian Beisel and the Genomics Facility Basel for RNA-sequencing; Thomas Bürglin for FACS sorting, analysis, and discussion for evolution; Helena Antoniadis, Ursula Schmieder, and animal facility for their support with animal experiments; the DBM microscopy facility for imaging; Carine Jorffre for U2OS-GFP-LC3 cell line; Jacques Camonis for help with image analysis; Daniel Hess for helpful discussions; Georg Halder and Randy Johnson for transgenic line, Alexander Schmidt for help with Mass Spectrometry. This work has been supported by the Swiss National Science Foundation (310030B_163471 to G.C.), the SystemsX.ch MTD MERiC (to G.C., M.N.H. and M.H.H.), and the European Research Council (ERC) Synergy Grant MERiC (to G.C., M.N.H. and M.H.H.), the Swiss Cancer League (Oncosuisse) KLS-3639-02-2015 to L.M.T. and KFS-3995-08-2016 to S.P. F.T. was supported by University of Basel Junior Researcher Fund (DBM-2181). S.P. is an Ambizione Fellow of the Swiss National Science Foundation (PZ200P3_168165). A.H was a Wellcome Trust Research Career Development fellow (090090/Z/09/Z).

Author contributions

F.T. and G.C. conceived this study. F.T. designed and performed the experiments, analyzed the data and wrote the manuscript. G.C. designed the experiments and wrote the manuscript. R.G. performed the experiments and analyzed the data. B.J.-R. and C.B.W. performed the immunofluorescence and analyzed the data. S.P., C.K.Y.N. and R.K.R.K. analyzed public databases for gene expression and patient survival. S.K.H. and T.B. performed mass spectrometry analysis. S.N. performed the organoid study and analyzed the data. E.D. and C.K.Y.N. analyzed gene expression in patients. S.S., D.B. and M.F.M. assisted with the experiments. A.H., P.M. and D.-S.L. provided critical reagents. L.M.T., M.H.H and M.N.H provided access to patient samples.

Competing interests

The authors declare no competing interests.

Additional information

Supplementary information is available for this paper at https://doi.org/10.1038/s41467-019-13591-7.

Correspondence and requests for materials should be addressed to F.T. or G.C.

Peer review information *Nature Communication* thanks Wanjin Hong, Eric O'Neill, and other, anonymous, reviewers for their contributions to the peer review of this work. Peer review reports are available.

Reprints and permission information is available at http://www.nature.com/reprints

Publisher's note Springer Nature remains neutral with regard to jurisdictional claims in published maps and institutional affiliations.